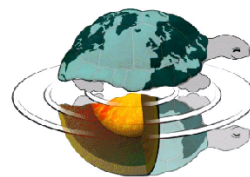




UNIVERSITÀ DEGLI STUDI DI MILANO

DOTTORATO DI RICERCA IN SCIENZE DELLA TERRA



Ciclo XXXII

DIPARTIMENTO DI SCIENZE DELLA TERRA

TESI DI DOTTORATO DI RICERCA

Calcareous nannofossil biostratigraphy and
taxonomy across the Early Toarcian Oceanic
Anoxic Event: a comparison between Tethyan
and Boreal sections

GEO/01 04/A2

DOTTORANDO
STEFANO VISENTIN

TUTOR

Prof.ssa ELISABETTA ERBA

COORDINATORE DEL DOTTORATO

Prof. FERNANDO CAMARA ARTIGAS

“...For the stratigrapher the Jurassic is the very well and fountain of his subject. It was on the Jurassic rocks that William Smith, Father of Historical Geology, founded the science of stratigraphy, enunciated the law of superposition, identified fossils with particular strata, and named the classic formations. It was on Jurassic rocks that Oppel founded modern zonal stratigraphy and named the classic zones. It was for Jurassic rocks that d’Orbigny introduced the first scheme of stages. All these concepts became part of the fabric of stratigraphical geology the world over...”

Arkell, 1956

Contents

1. Introduction.....	1
2. The Early Toarcian Oceanic Anoxic Event.....	3
2.1 – General characters of Oceanic Anoxic Events.....	3
2.2 – The T-OAE	6
2.3 – Calcareous nannofossils.....	8
2.4 – Calcareous nannofossils across the T-OAE.....	10
3. Early Jurassic calcareous nannofossils.....	19
3.1 – Biozonation schemes	19
3.2 – Biostratigraphies of previous authors.....	27
4. Studied sections	45
4.1 – The Sogno Core	45
4.2 – The L1 and Schandelah Cores.....	52
5. Materials and methods.....	57
5.1 – Sample preparation techniques	57
5.2 – Nannofossil preservation and abundance analysis	59
6. Taxonomic notes.....	61
6.1 – General taxonomic observations	61
6.2 – Taxonomic revision of genus <i>Carinolithus</i>	62
7. Results.....	81
7.1 – Sogno Core	81
7.2 – L1 and Schandelah Cores	88
8. Discussion	97
8.1 – Sogno Core	97
8.2 – L1 and Schandelah Cores	103
8.3 – Synthesis of calcareous nannofossil events in the uppermost Pliensbachian/Lower Toarcian interval.....	109
8.4 – Biostratigraphic constraints of the T-OAE	114
9. Conclusion	121
References.....	123
Appendix list.....	137
A – Taxonomic list	
B – Table of studied papers	
C – Morphometry of genus <i>Carinolithus</i>	
D – Range chart of the Sogno Core	
E – Range chart of the L1 and Schandelah Cores	
F – Erba et al. (2019a)	

G – Erba et al. (2019b)

H – Abstracts presented at international congresses

Acknowledgements

Abstract

The Early Toarcian Oceanic Anoxic Event (T-OAE), in the Early Jurassic Period, was associated with one of the largest perturbations of the carbon cycle in the past 250 Ma. This dramatic episode of ecosystem adjustments, global warming, oceanic anoxia and altered chemistry occurred during a crucial time for calcareous nannoplankton diversification as a major speciation episode took place in the Late Pliensbachian – Early Toarcian time interval. New genera and species appeared and quickly evolved allowing a high-resolution biostratigraphy of the onset and the termination of the T-OAE based on first and last occurrences. Moreover, drastic drops in abundance of some taxa are associated to the paleoenvironmental perturbations recorded across the T-OAE.

In this PhD thesis I present a high-resolution calcareous nannofossil biostratigraphy of three cores drilled in the Lombardy Basin (Sogno Core) and in the Lower Saxony Basin (L1 and Schandelah Cores), covering the lithological expression of the T-OAE in the Tethyan and Boreal realms. Events recognized across the Sogno Core allow the detection of three biozones (NJT5a, NJT5b and NJT6) whereas those recognized in the L1 and Schandelah Cores result in the identification of three zone/subzones (NJ5b, NJ6 and NJ7). These results are integrated with data from literature in order to derive a solid framework of primary and secondary events characterizing the upper Pliensbachian/lower Toarcian interval with a special focus on the Pliensbachian/Toarcian boundary and the characterization of the T-OAE in the Tethyan and Boreal realms.

For the Tethyan sections (Italy, South-East Spain, South France, Greece and Hungary) the primary events include the FOs of *Lotharingius sigillatus*, *Carinolithus poulabronei*, *Lotharingius crucicentralis*, *Carinolithus superbus sceptrum*, *Watznaueria* sp. 1, *Discorhabdus striatus*, *Schizosphaerella crisis* and LO of *Mitrolithus jansae* while the FOs of *Lotharingius velatus* and *Discorhabdus ignotus* are considered within the secondary ones. Likewise, for the Boreal Realm (sections in Central-North France, England and Germany), my synthesis resulted in the separation of primary events including the FOs of *Crepidolithus impotus*, *L. sigillatus*, *C. superbus sceptrum*, *D. striatus* and LOs of *Crucirhabdus primulus* and *Biscutum finchii* from the secondary ones comprising the FOs of *L. crucicentralis*, *L. velatus*, *D. ignotus*, *C. poulabronei*, *Watznaueria* sp. 1, *Schizosphaerella crisis* and LOs of *Crepidolithus granulatus*, *Parhabdolithus liasicus* and *Biscutum grandis*.

My study revealed that the FO of *C. superbus sceptrum* is the only event reproducible at a supraregional level and confirmed that the Pliensbachian/Toarcian boundary is approximated by the FOs of *L. sigillatus* (slightly below) and *C. poulabronei* (slightly above) in the Tethyan Realm and by the LO of *C. primulus* in the Boreal.

At lower latitudes (sections in Italy, South-East Spain, South France, Greece and Hungary), my study revealed that the T-OAE is well constrained by the FOs of *C. superbus sceptrum* and the “*Schizosphaerella* crisis” at the onset and by the LO of *M. jansae* at its termination. These events are reproducible in Portugal, with the addition of the FCO of *D. ignotus* marking the termination of the event.

At higher latitudes (sections in Central-North France, North Spain, England and Germany) my study confirms that the onset of the T-OAE is constrained by the FO of *C. superbus sceptrum*. Secondary events, not reproducible in North Spain, are the “*Schizosphaerella* crisis” at the onset of the T-OAE and the LOs of *C. granulatus*, *B. finchii*, *P. liasicus* and *B. grandis* within the carbon isotope excursion characterizing the T-OAE.

Morphometric analyses conducted on *Carinolithus superbus* and *Carinolithus magharensis* specimens allow to clarify taxonomic discrepancies regarding the two taxa. Qualitative investigations performed on *Carinolithus cantaluppii* revealed that this taxon is a diagenetic artefact of the genus and, therefore, that this species must be rejected. Implications for biostratigraphy and evolutionary trends are discussed.

Chapter 1

Introduction

The Early Toarcian Oceanic Anoxic Event (T-OAE) is recognized as one of the most intense and geographically extensive events of oceanic anoxia and organic-carbon burial in the Mesozoic era (Jenkyns, 1985; 1988). This dramatic episode is marked by major changes in global geochemical cycles, with a relatively rapid negative shift up to - 7% in bulk marine and terrestrial organic carbon isotope records and a typically smaller (3-6%) negative excursion in carbonate archives and specific organic compounds (Hesselbo et al. 2000; Sørensen et al. 2000; Jenkyns et al. 2002; Kemp et al. 2005; Hesselbo et al. 2007; Hermoso et al. 2009; French et al. 2014; Suan et al. 2015). The T-OAE perturbations have been linked to volcanism of the Karoo-Ferrar large igneous province and associated release of volcanogenic CO₂, and/or thermogenic methane (CH₄) from sill intrusion into Gondwanan coals, and/or biogenic methane from dissociation of sub-seafloor clathrates (Hesselbo et al. 2000; Kemp et al. 2005; Duncan et al. 1997; McElwain et al. 2005, Svensen et al. 2007). The reconstructed elevated atmospheric CO₂ induced climatic and environmental change (Jenkyns et al. 2002; McElwain et al. 2005; Dera et al. 2011; Ulmann et al. 2014; Brazier et al. 2010) by accelerating the global hydrological cycle and increasing silicate weathering, thereby increasing delivering of riverine nutrients to the oceans and potentially also to large inland lakes (Jenkyns, 2010). In the marine realm, the consequential increase in primary productivity and carbon flux to the seafloor is credited with enhanced burial of planktonic material in relatively deep continental-marginal sites, whereas in shallower water semi-restricted marine basins, chemical and physical water-column stratification probably aided the burial of organic matter (Jenkyns, 2010; Xu et al. 2017).

Calcareous nannofossils are extremely useful tools for biostratigraphy and paleoceanography to improve dating and understanding of the marine ecosystem and biological processes such as photosynthesis (biological pump) and mineralization (carbonate pump) that affect the organic and inorganic carbon cycle, as well as adsorption of atmospheric CO₂ in the oceans. In the last three decades much attention has been devoted to Early Jurassic calcareous nannofossils as stratigraphic tool for correlations at regional to global scale. The Late Pliensbachian-Early Toarcian interval, including the T-OAE, was a crucial time for calcareous nannofossils evolution, as a major speciation episode took place and some of the most common Jurassic and Cretaceous genera (*Biscutum*, *Lotharingius*, *Discorhabdus* and *Watznaueria*) appeared and rapidly evolved (Bown, 1987b; Mattioli and Erba,

1999; Bown et al. 2004; Erba, 2004, 2006; Casellato and Erba, 2015). As a result, the high number of biohorizons characterizing the Late Pliensbachian to Early Toarcian time interval offers the opportunity to biostratigraphically constrain the T-OAE. Several studies focused on Lower Jurassic calcareous nannofossil assemblages and biostratigraphy, with the large majority being dedicated to the T-OAE. Two palaeogeographic provinces are recognized in the European Jurassic, namely the Boreal and Tethyan Realms (Arkell, 1956) characterized by differences in faunas and floras. Consequently, two main biozonation schemes were proposed: the one of Bown (1987b) and then revised by Bown et al. (1988) and Bown and Cooper (1998) for the Boreal Realm (United Kingdom, Germany, The Netherlands, North France) and the biozonation of Mattioli and Erba (1999) established for Tethyan settings (Italy, Western Portugal, South East Spain, South France, Hungary, Greece). Recently, two additional biozonation schemes were proposed: Fraguas et al. (2015) proposed a zonation for the Cantabrian Range (Northern Spain) and Ferreira et al. (2019) published a comprehensive synthesis based on sections from the Lusitanian Basin (Portugal).

The purposes of this study are:

- high-resolution calcareous nannofossil biostratigraphy of the Upper Pliensbachian-Lower Toarcian interval, including the T-OAE, recovered in three cores: the Sogno Core (Lombardy Basin, Northern Italy) in a Tethyan setting and the L1 and Schandelah Cores (Lower Saxony Basin, Northern Germany) in the Boreal Realm;
- Integration of the results obtained for the three cores with the available literature to derive an updated biostratigraphic framework of primary and secondary calcareous nannofossil events for the uppermost Pliensbachian-Lower Toarcian interval with a special focus on the Pliensbachian/Toarcian boundary and the characterization of the T-OAE;
- Comparison of events at lower and higher latitudes to assess their reproducibility and reliability;
- Revised taxonomy of the genus *Carinolithus* through morphometric investigations of selected parameters for the *C. superbus* and *C. magharensis* groups. Also, morphometry is intended to evaluate the role of diagenesis on the species *C. cantaluppii*. Implications for biostratigraphic resolution of the Toarcian-Aalenian interval are foreseen.

Chapter 2

The Early Toarcian Oceanic Anoxic Event

2.1. General characters of Oceanic Anoxic Events

The following description is taken from the papers by Erba et al. (2019a) and Erba et al. (2019b) reported in Appendix F and G.

The early phase of the Deep-Sea Drilling Project provided evidence of extensive occurrence of Cretaceous black shales from previously unsampled oceanic basins. As on-land, stratigraphies of pelagic successions showed that organic carbon-rich lithologies are confined to specific geologically short intervals suggesting a global rather than local to regional oxygen-depletion of bottom waters.

The term “Oceanic Anoxic Event” (OAE) was coined by Schlanger and Jenkyns (1976) after the recovery of mid-Cretaceous black shales at sites drilled in the Pacific Ocean. Such lithologic units were recognized as equivalent and coeval of well-known lithostratigraphic markers previously described in the Tethys and Atlantic Oceans. The term OAE was originally defined to signify time intervals during which black shale deposition was prevalent at a global scale. The original definition was, therefore, based on lithologic criteria and applied to two-time intervals, namely the Aptian-Albian (OAE1) and the Cenomanian-Turonian (OAE2). Additional investigations on land and in the oceans pointed out the occurrence of the Coniacian–Santonian OAE3 (Arthur and Schlanger, 1979; Jenkyns, 1980) and of the Toarcian OAE (Jenkyns, 1985; 1988). Based on integrated and higher resolution stratigraphy, Arthur et al. (1990) subdivided OAE1 into discrete events OAE1a, OAE1b, OAE1c and OAE1d, still using the sedimentary record of organic C-rich black shales.

With the rapid development of chemostratigraphy, and specifically of C and O stable isotopic investigations, it became clear that the T-OAE, OAE1a and OAE2 are associated with negative and positive anomalies of carbon-isotope curves obtained from carbonate and/or organic matter, caused by major perturbations of the global carbon cycle (Jenkyns, 2010). The original definition of OAEs (Schlanger & Jenkyns, 1976) has become somehow misleading for various reasons: a) anoxia is rarely reached; b) terrestrial successions also record the global C cycle anomalies; c) anomalies are of long to short duration; d) black shale intervals were proved to be diachronous in many cases.

High-resolution integrated stratigraphy of marine and terrestrial records has produced a solid time framework for OAEs (Robinson et al. 2017) (Fig. 2.1), and $\delta^{13}\text{C}$ chemostratigraphy has grown as a prominent basic tool for identifying, characterizing and correlating OAEs (e.g. Erba, 2004; Tsikos et al. 2004; Weissert and Erba, 2004; Jenkyns, 2010). In fact, although a black marker bed is not present

in Lower Cretaceous pelagic successions, a discrete C isotope excursion of Late Valanginian age was identified in the Maiolica Formation from the Southern Alps (Weissert, 1989; Lini et al., 1992). Such an anomaly was constrained by bio-magnetostratigraphy (Channell et al., 1993) and used by Erba et al. (2004) to formalize the Valanginian event as the “Weissert OAE”. Global anoxia has not been documented, but discrete black shale levels enriched in organic matter are described from the Tethys and Pacific Oceans in the early phase of the Weissert-OAE (Erba et al., 2004).

In the past four decades OAEs have been recognized in oceanic and terrestrial sequences, highlighting local variations in depositional conditions, various types and degrees of diagenesis, and preservation of organic matter. As summarized by Jenkyns (2010), equivalents of the Bonarelli, Selli, Weissert and Toarcian events have been recognized in a variety of sedimentary basins, and a number of geochemical anomalies have been detected in addition to C isotopic excursions. Yet, a lively debate about causes and consequences of OAEs and their influence on biota continues to involve experts from various disciplines within geosciences. The original hypotheses of Schlanger and Jenkyns (1976) are still discussed to discern and discriminate the role of productivity from that of organic matter preservation under anoxic conditions.

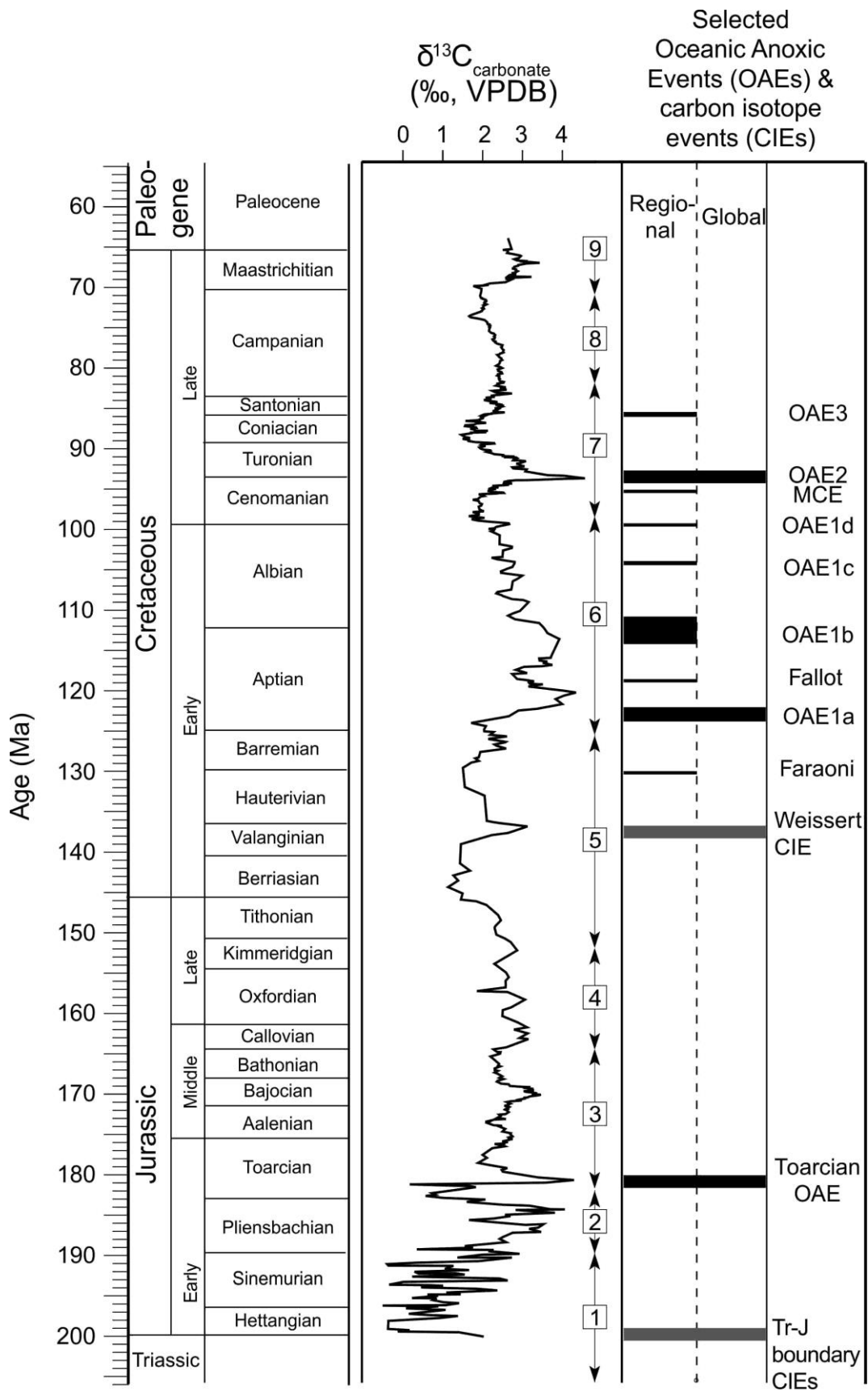


Fig. 2.1 - Bulk carbonate carbon isotope ($\delta^{13}\text{C}_{\text{carb}}$) stratigraphy and OAEs of the Jurassic and Cretaceous interval (modified after Robinson et al. 2017).

Pelagic successions containing OAEs are crucial to understand the biotic variations in marine planktonic communities associated with such global perturbations of the ocean/atmosphere system. In marine ecosystems, coccolithophores are part of phytoplankton responsible for primary productivity, energy transfer to higher trophic levels, export of biogenic particles to the seafloors and exchanges between the surface ocean and the atmosphere. In Jurassic and Cretaceous oceans, calcareous nannoplankton was already the most efficient rock-forming group (e.g. Erba, 2006). Indeed, Jurassic and Cretaceous pelagic micrites mainly consist of coccoliths and nannoliths, in addition to variable amounts of diagenetic calcite. Consequently, pelagic carbonates offer the opportunity of characterizing variations in abundance and composition of calcareous nannofloras across OAEs to quantify their resilience to extreme conditions.

2.2. The Toarcian Oceanic Anoxic Event (T-OAE)

The early Toarcian Oceanic Anoxic Event (T-OAE) is the oldest Mesozoic case of global anoxia with widespread deposition of organic matter-rich sediments in a variety of depositional settings from continental to shallow- and deep-marine (Jenkyns, 1985, 1988, 2010).

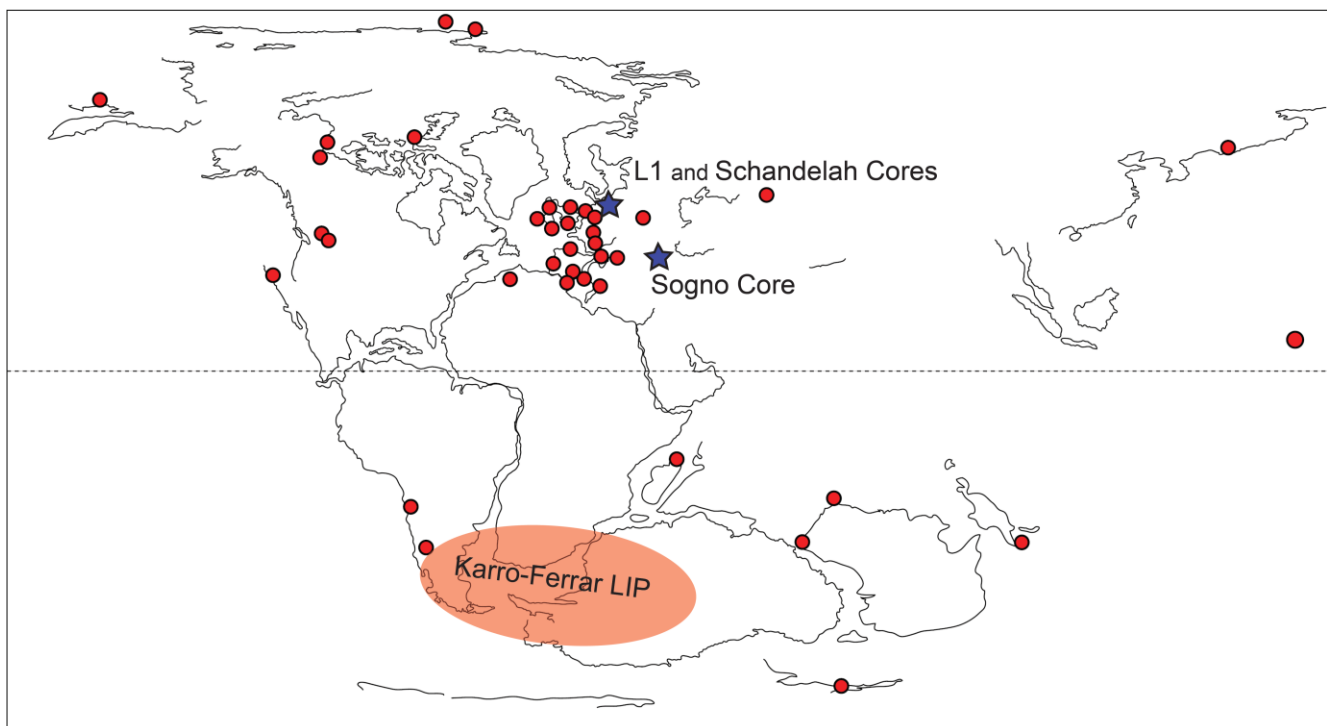


Fig. 2.2 – Map showing the distribution of localities presenting black shales and sediments containing more than 1% total organic carbon associated with the T-OAE (red dots). The location of the L1 and Schandelah Cores (Lower Saxony Basin), the Sogno Core (Lombardy Basin) (blue stars) and the Karoo-Ferrar Large Igneous Province (LIP) emplacement (orange area) are reported (modified from Robinson et al. 2017).

Available evidence suggests that ~183 Ma the atmosphere and oceans experienced excess CO₂ possibly due to degassing of lava fields in the Karoo-Ferrar large igneous province and/or from dissociation and oxidation of methane hydrates in continental-margin sediments (Jenkyns, 2010). High atmospheric carbon dioxide possibly initiated greenhouse conditions that accelerated weathering and the hydrological cycle, increasing nutrient recycling into the oceans. Fig. 2.2 displays the distribution of localities presenting black shales and organic rich sediments associated with the T-OAE together with the location of the investigated cores in this thesis (i.e. L1 and Schandelah Cores and Sogno Core).

The T-OAE is associated with a major negative carbon isotope excursion (Jenkyns and Clayton, 1986; Hesselbo et al. 2000; 2007; Schouten et al. 2000; Jenkyns et al. 2002; Van Breugel et al. 2006; Al-Suwaidi et al. 2010; Caruthers et al., 2011; Izumi et al. 2012; Kafousia et al. 2014; Reolid et al. 2014; Xu et al. 2017) (Fig. 2.3), Os anomaly (Cohen et al. 2004), biocalcification crisis (Erba 2004; Mattioli et al. 2004; Casellato and Erba, 2015; Erba et al. 2019a), increased primary productivity (Erba 2004; Jenkyns 2010) and ocean acidification (Erba, 2004; Trecalli et al. 2012; Casellato and Erba, 2015; Posenato et al. 2018), which occurred during an exceptional warming phase (Dera et al., 2011; Korte and Hesselbo, 2011) and a major transgression (e.g. Haq et al., 1987; Hardenbol et al., 1998).

The T-OAE is considered a natural Earth system experiment, which allows to: (a) detect and quantify processes associated with emissions of greenhouse gases and natural atmospheric pollutants, (b) understand the role of greenhouse gases on climate dynamics and its influence on the hydrological cycle; (c) characterize changes in ocean and atmospheric chemistry and their interactions; (d) assess changes in biodiversity and dynamics of ecosystems, and understand the functioning of biotic sinks; (e) quantify biosphere-geosphere-atmosphere interactions and their timings/rates.

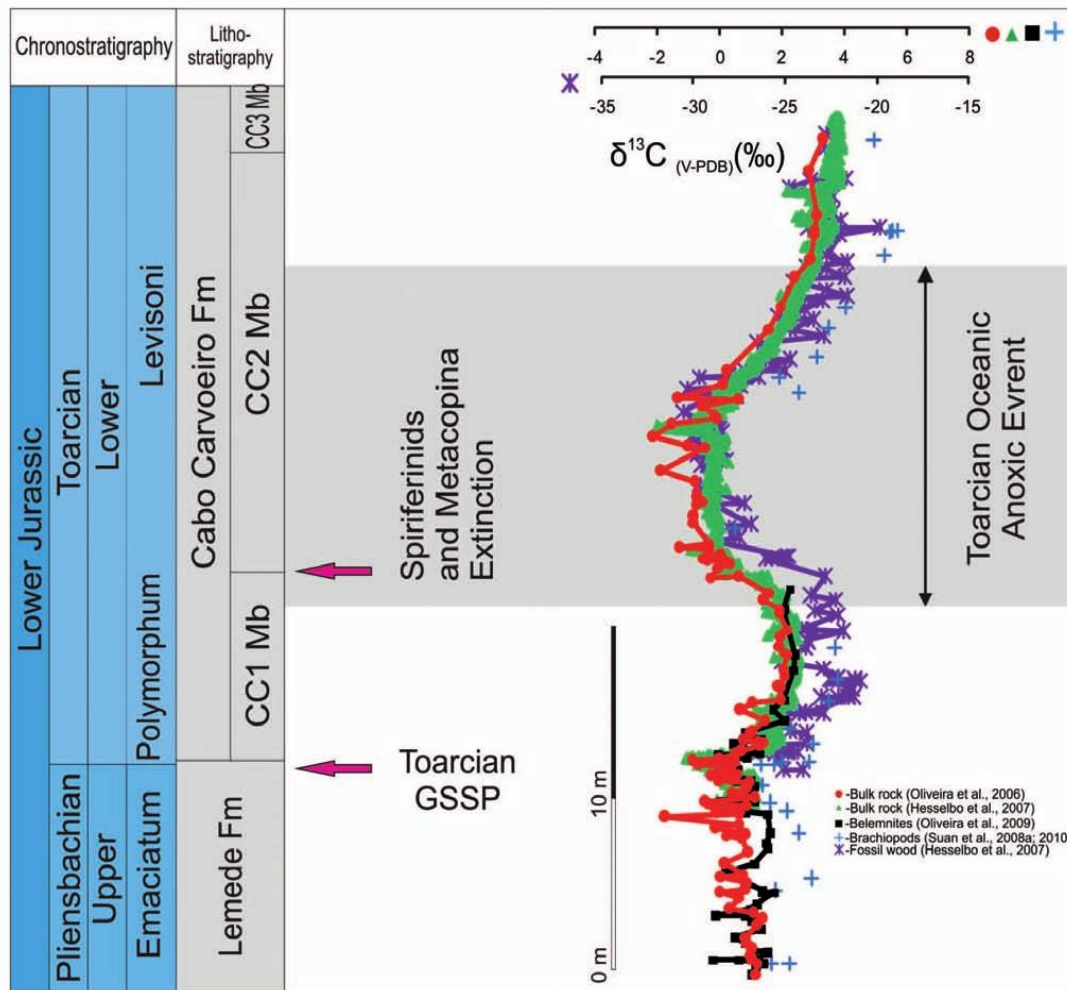


Fig. 2.3 - Carbon isotope stratigraphy across the Upper Pliensbachian / Lower Toarcian succession, with a special focus on the T-OAE, cropping out in the Peniche section (after Duarte et al., 2017).

The T-OAE in Italy

At the beginning of the XX century, Dal Piaz (1907) described Toarcian organic-rich facies in pelagic Jurassic successions of the Alpi Feltrine in the Southern Alps, similarly to other occurrences in Germany and Switzerland (Posidonienschiefer), England (Jet Rock and Bituminous Shales) and France (Schistes Cartons). Dal Piaz's perception of black shales as geological archives of major environmental changes was by far innovative and a precursor of modern paleoceanography. A few decades later Gaetani and Poliani (1978) described a lower Toarcian black shale interval, named "*Livello a Pesci*" (Fish Level), in the pelagic succession of the Lombardy Basin. In the 80s, Jenkyns (1985; 1988) labelled these black shale intervals as the Toarcian OAE (T-OAE).

2.3. Calcareous nannofossils

Calcareous nannofossils are the fossil remains of coccolithophores that are photoautotrophic single-celled algae, which live in the photic zone (upper 50 to 200 m). They are one of the most abundant primary producers, contributing to the productivity of the oceans (Bown, 1987b; 1988; Bown and Copper, 1998; Rost and Riebesell, 2004; Erba, 2006). The term calcareous nanoplankton was originally introduced by Lohman (1909) for planktonic organisms smaller than 63 μm , and in general between 0.25 to 30 μm in size comprising a diverse range of organisms, such as coccoliths, ascidian spicules, calcispheres (calcareous dinoflagellates) or juvenile foraminifera. This term is now used for golden-brown algae coccolithophores (phylum Haptophyta) secreting tiny calcite crystals to build coccoliths and ultimately coccospheres.

Coccolithophores may produce two types of coccoliths: a) holococcoliths, which are formed by numerous minute euhedral calcite crystals, and b) heterococcoliths consisting of variably shaped calcite crystal units (Bown, 1998; Baumann et al. 2005). Nannoliths are biogenic calcitic structures often of uncertain affinity, which have a different biomineralization process to either holococcoliths or heterococcoliths (Young et al. 1999), although several modern nannoliths are undoubtedly produced by coccolithophore algae. Calcareous nannofossils include the fossil remains of coccolithophores, namely coccoliths and coccospheres as well as associate nannoliths. A synthesis of coccolith structure based on the rim morphologies is provided by Bown and Cooper (1998) and in this thesis reported in Fig 2.4. The global occurrence of calcareous nanoplankton, their talent in producing calcite plates and ability to temporarily bloom in coastal and oceanic waters makes this phytoplanktonic group the most effective producers of calcite on Earth (Erba, 2006). The oldest calcareous nannofossils have been recorded from the Late Triassic (Bown and Copper, 1998). During the extinction event at the Triassic/Jurassic boundary, all but one species disappeared. Nanofossils were re-established in the earliest Jurassic and they inhabited all marine environments, reaching a steady increase in diversity throughout the Jurassic and the Cretaceous. Their maximum diversity was reached in the Late Cretaceous (Bown et al. 2004; Mutterlose et al. 2005; Erba, 2006). At the Cretaceous/Paleogene boundary approximately 90 % of calcareous nannofossil taxa became extinct. At the beginning of the Paleocene new species had a considerable increase, reaching a maximal diversification of coccolith families and nannolith groups during the Cenozoic.

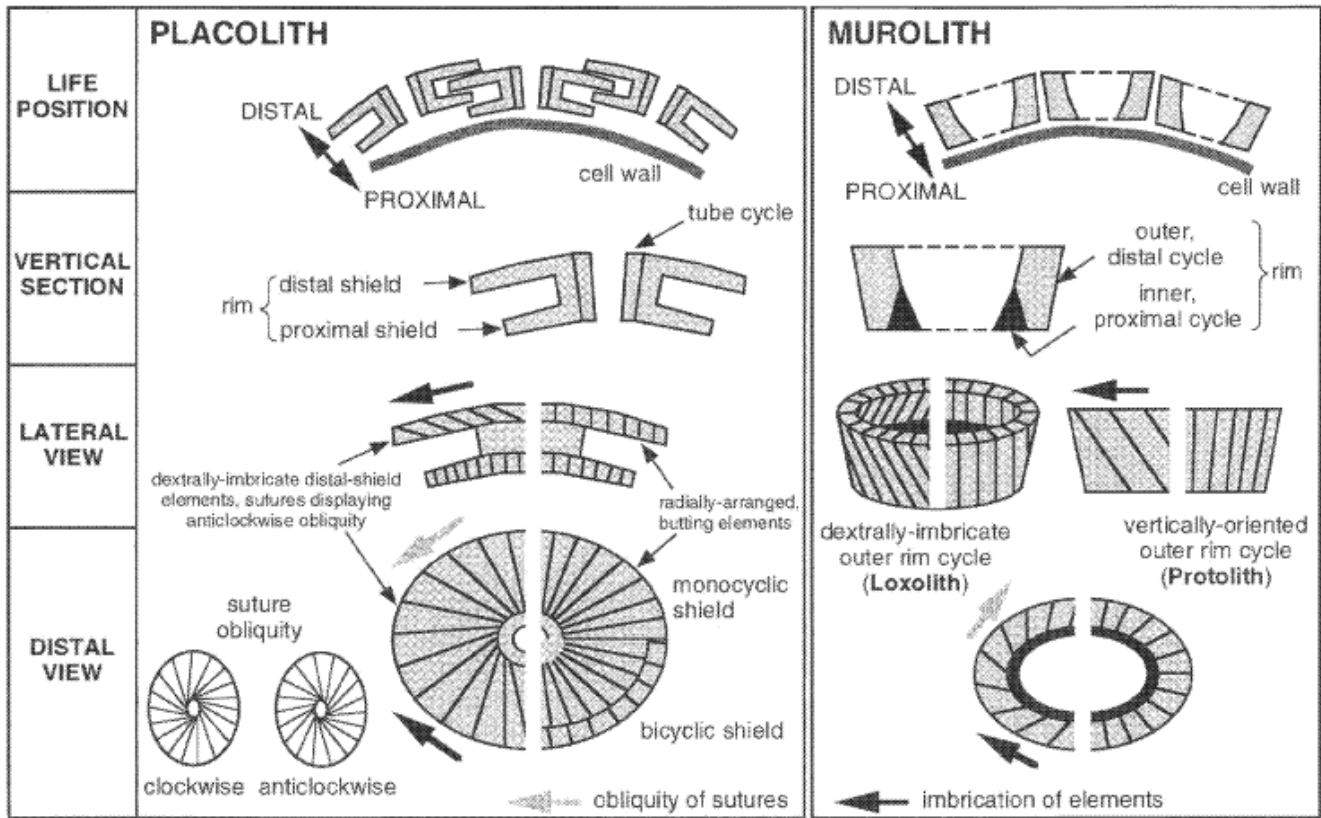


Fig. 2.4 - Coccolith rim morphologies (after Bown and Cooper, 1998)

2.4. Calcareous nannofossils across the T-OAE

General paleoecology

Calcareous nannofossils have been extensively studied for both biostratigraphy and paleoecology-based paleoceanography. For the Early Jurassic, the focus has been devoted to the T-OAE, in order to better constrain and derive the causes of this dramatic event. Although much research, paleoecological affinities of Early Jurassic are still not well understood and sometimes controversial (Casellato and Erba, 2015). A synthesis of calcareous nanoplankton paleoecology taking into consideration previous works is provided by Casellato and Erba (2015) and in this thesis reported in fig. 2.5.

Some authors (i.e. Claps et al., 1995; Erba, 2004) considered the taxon *S. punctulata* (a probable dinoflagellate cyst) as deep dweller based on its size and mass. This taxon was associated to a deep chlorophyll maximum that flourishes in oceanic stable conditions, when the nutricline is deep and surface waters are characterized by enhanced oligotrophy. Other authors (i.e. Mattioli, 1997; Mattioli and Pittet, 2004; Reggiani et al. 2010a) interpreted *S. punctulata* as shallow-dweller preferring relatively high nutrients in unstable surface waters, especially in proximal setting. The temperature affinity of this taxon is still controversial, being interpreted as a warmer (Tremolada et al. 2006) or colder water form (Fraguas et al. 2012).

The genus *Crepidolithus* was considered a deep dweller taxon (Bucefalo Palliani et al. 1998; Bour et al. 2007) with oligotrophic affinity (Bour et al. 2007). Only in one case *Crepidolithus* spp. (*C. cavus* and *C. aff. C. ocellatus*) was interpreted as preferring higher latitudes (Mattioli et al. 2008). Different interpretations have been associated to the ecology of the species *C. crassus*: most authors indicate this taxon as deep dweller (Tremolada et al. 2005; Mattioli et al. 2008; Reggiani et al. 2010b) and oligotrophic form (Mattioli & Pittet, 2004; Aguado et al. 2008; Mattioli et al. 2008). Moreover, some authors reconstructed preferences for distal or proximal settings (i.e. Mattioli and Pittet, 2004, Reggiani et al. 2010a) including affinities for lower or higher latitudes (Reggiani et al. 2010b). Walsworth-Bell (2001) considered *C. crassus* an opportunistic taxon. As far as the taxon *M. jansae* is concerned, it was mainly interpreted as deep (Bucefalo Palliani et al. 1998; Mattioli and Pittet, 2004; Mattioli et al. 2008; Reggiani et al. 2010b; Reolid et al. 2014) to intermediate (Erba, 2004; Tremolada et al. 2005) dweller, widespread especially at lower latitudes (Bucefalo Palliani et al. 2002; Mattioli et al. 2008; Reggiani et al. 2010b) and in colder temperature (Fraguas et al. 2012; Clémence et al. 2015). An oligotrophic affinity was pointed out by Tremolada et al. (2005).

Fig. 2.5. - Paleoecological affinities of selected Early Jurassic nannoplankton taxa, as reconstructed in previous works (after Casellato and Erba, 2015).

TAXON	PALEOECOLOGICAL AFFINITY	PCA	AUTHORS	
<i>S. punctulata</i>	oligotrophic		Claps et al. 1995 Cobianchi & Picotti 2001 Pittet & Mattioli 2002 Olivier et al. 2004 Mattioli & Pittet 2004 Erba 2004	
		x	Tremolada et al. 2005	
		x	Tremolada et al. 2006	
		x	Aguado et al. 2008	
	mesotrophic	(x)	Reggiani et al. 2010b	
	mesotrophic		Mattioli 1997	
	deep-dweller		Claps et al. 1995 Erba 2004	
	shallow-dweller		Mattioli 1997 Mattioli & Pittet 2004 Reggiani et al. 2010a	
proximal	(x)	Mattioli & Pittet 2004		
warmer temperature	x	Tremolada et al. 2006		
colder temperature	x	Fraguas et al. 2012		
genus <i>Crepidolithus</i>	oligotrophic	x	Bour et al. 2007	
	deep-dweller	x	Bucefalo Palliani et al. 1998 Bour et al. 2007	
	oligotrophic	x	Fraguas et al. 2012	
	deep-dweller	x	Fraguas et al. 2012	
	higher latitudes	x	Mattioli et al. 2008	
	<i>C. crassus</i>	oligotrophic	x	Mattioli & Pittet 2004 Aguado et al. 2008
		opportunistic	x	Mattioli et al. 2008 Walsworth-Bell 2001
		deep-dweller	x	Tremolada et al. 2005 Mattioli et al. 2008 Reggiani et al. 2010b
		proximal		Mattioli & Pittet 2004
		distal		Reggiani et al. 2010a
higher latitudes	x	Reggiani et al. 2010b		
<i>M. jansae</i>	oligotrophic		Tremolada et al. 2005	
	intermediate-dweller		Erba 2004 Tremolada et al. 2005	
	deep-dweller	x	Bucefalo Palliani et al. 1998 Mattioli & Pittet 2004 Mattioli et al. 2008 Reggiani et al. 2010b Reolid et al. 2014	
	lower latitudes	x	Bucefalo Palliani et al. 2002 Mattioli et al. 2008 Reggiani et al. 2010b	
		x	Fraguas et al. 2012	
	colder temperature	x	Clémence et al. 2015	
genus <i>Biscutum</i>	mesotrophic		Mattioli 1997 Bucefalo Palliani & Mattioli 1995 Mattioli & Pittet 2004 Erba 2004 Bour et al. 2007 Reolid et al. 2014	
	mesotrophic	x	Tremolada et al. 2005	
	mesotrophic	x	Tremolada et al. 2006	
	colder temperature	x	Tremolada et al. 2006	
	warmer temperature	x	Fraguas et al. 2012	
	<i>B. novum</i>	mesotrophic	x	Mailliot et al. 2009 Mattioli et al. 2008
		warmer temperature	x	Clémence et al. 2015
		colder temperature	x	Mattioli et al. 2008
		stress tolerant to anoxia and low salinities	x	Clémence et al. 2015
	<i>B. finchii</i>	mesotrophic	x	Bucefalo Palliani et al. 2002 Mailliot et al. 2009 Mattioli et al. 2008
		colder temperature	x	Mattioli et al. 2008 Clémence et al. 2015
	<i>B. dubium</i>	mesotrophic	x	Bucefalo Palliani et al. 2002 Aguado et al. 2008
<i>B. intermedium</i>	mesotrophic	x	Aguado et al. 2008	
genus <i>Lotharingius</i>	mesotrophic		Mattioli & Pittet 2004 Bucefalo Palliani et al. 2002 Reolid et al. 2014	
	shallow-dweller		Mattioli & Pittet 2004 Reolid et al. 2014	
	mesotrophic		Tremolada et al. 2005	
	mesotrophic	x	Mattioli et al. 2008	
	shallow-dweller	x	Mattioli et al. 2008	
	shallow-dweller	x	Fraguas et al. 2012	
	<i>L. hauffii</i>	mesotrophic		Pittet & Mattioli 2002 Olivier et al. 2004 Clémence et al. 2015
		mesotrophic	x	Clémence et al. 2015
	<i>L. sigillatus</i>	warmer temperature	x	Clémence et al. 2015 Fraguas et al. 2012
		warmer temperature	x	Fraguas et al. 2012
<i>L. crucicentralis</i>	warmer temperature	x	Fraguas et al. 2012	
<i>Calyculus</i>	mesotrophic	x	Mattioli & Pittet 2004 Bour et al. 2007	
	shallow-dweller	x	Mattioli et al. 2008 Mattioli et al. 2009	
	intermediate-dweller		Erba 2004	
	deep-dweller		Bucefalo Palliani & Mattioli 1995	
	low salinity	x	Mattioli et al. 2008 Mailliot et al. 2009	
	warmer temperature	x	Fraguas et al. 2012	
stress tolerant to anoxia and low salinities	x	Clémence et al. 2015		
<i>Carinolithus</i>	stress tolerant to anoxia and low salinities	x	Clémence et al. 2015	

Based on paleoecological preferences reconstructed for the Cretaceous (see Mutterlose et al. 2005 for a synthesis), the genus *Biscutum* was also considered a higher fertility indicator. A common preference for mesotrophic conditions was derived for *B. novum* (Mattioli et al. 2008; Mailliot et al. 2009), *B. finchii* (Bucefalo Palliani et al. 2002; Mattioli et al. 2008; Mailliot et al. 2009), *B. dubium* (Bucefalo Palliani et al. 2002; Aguado et al. 2008) and *B. intermedium* (Aguado et al. 2008). Furthermore, proliferation of genus *Biscutum* seems linked to surface water temperature. This is the case of *B. novum*, although affinity for both warmer and colder conditions was proposed. Some preference for colder water was suggested for *B. finchii* (Mattioli et al. 2008; Clémence et al. 2015). In addition, *B. novum* was interpreted as tolerant to anoxia and low salinities (Clémence et al. 2015).

The genus *Lotharingius* was interpreted as a shallow dweller (Mattioli and Pittet, 2004; Reolid et al. 2014; Ferreira et al. 2017) and higher fertility taxon, usually associated to *Biscutum*. *L. hauffii* and *L. sigillatus* were found to be favored by mesotrophic conditions (Tremolada et al. 2005; Mattioli et al. 2008) whereas *L. sigillatus* and *L. crucicentralis* were associated to warmer temperature (Fraguas et al. 2012; Clémence et al. 2015).

As far as genus *Calyculus* is concerned, paleoecological reconstructions proposed a mesotrophic affinity possibly adapted to lower salinity (Mattioli and Pittet, 2004; Bour et al. 2007). Clémence et al. (2015) considered genera *Calyculus* and *Carinolithus* tolerant to anoxia and low salinities. Figure. 2.6 illustrates a possible distribution of *Lotharingius*, *Biscutum*, *Calyculus*, *Carinolithus*, *Crepidolithus*, *M. jansae* and *S. punctulata* relative to their depth within the photic zone in areas of stability (thermocline and deep nutricline) and instability (surface nutricline) (after Casellato and Erba, 2015).

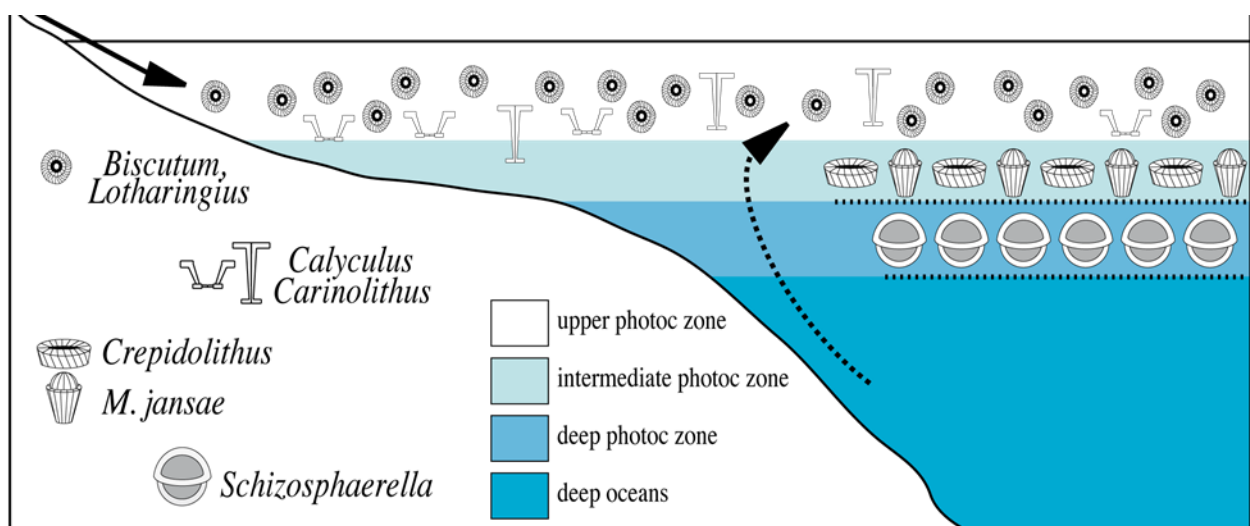


Fig. 2.6 – Inferred position of some Early Toarcian nannoplankton taxa within the photic zone. Arrows indicate nutrient fluxes via run-off (solid line) and upwelling (dotted line) (after Casellato and Erba, 2015).

Reconstructions across the T-OAE based on calcareous nannofossil assemblages

Calcareous nannofossils are extremely useful to improve our understanding of the marine ecosystem and biological processes such as photosynthesis (biological pump) and mineralization (carbonate pump) that affect the organic and inorganic carbon cycle, including adsorption of atmospheric CO₂ in the oceans.

As proposed by Tremolada et al. (2005), during the latest Pliensbachian (Fig. 2.7.a) stable oligotrophic conditions promoted the proliferation of deep dwelling and highly calcified *S. punctulata* and *M. jansae*. The Late Pliensbachian was possibly characterized by lower CO₂ concentrations (e.g. Hesselbo et al. 2000), icehouse conditions (Van de Schootbrugge et al. 2005), low run-off intensity (Cohen et al. 2004) and general high carbonate production.

At the beginning of the Toarcian (Fig. 2.7.b) enhanced continental run-off is evidenced by a significant increase of terrigenous input. A decreased light penetration penalized the deep dweller *S. punctulata* (“*Schizosphaerella* decline”) favoring the intermediate dweller *M. jansae*. At the same time, accelerated run-off induced lower salinity and brought an increase of *Calyculus* (Casellato and Erba, 2015). Major nannofossil changes started in this period with a speciation episode and increase in diversity. The reorganization of calcareous nannoplankton communities correlates with the early phase of the Karoo-Ferrar Large Igneous Province (LIP) (Palfy and Smith, 2000) potentially introducing large amounts of CO₂ in the atmosphere/ocean system, leading to climate change and increased run-off.

The onset of the T-OAE (Fig. 2.7.c) corresponds to higher concentration of nutrients, possibly associated with lower salinity and perhaps warmer waters stimulating the proliferation of shallow, mesotrophic coccolith-producers (especially *Biscutum* and *Lotharingius*) and favoring *Calyculus*, but hampering deep to intermediate-dwelling, oligotrophic forms such as *S. punctulata*, *M. jansae* and *Crepidolithus* (Casellato and Erba, 2015). The greenhouse conditions led to an abrupt increase in temperature that affected surface, intermediate and bottom waters and may have led to the release of methane hydrates modifying water alkalinity (Hesselbo et al. 2000; Beerling et al. 2002; Jenkyns, 2003). The rapid drop in abundance of *S. punctulata* (“*Schizosphaerella* crisis”) and the increase in percentages of r-selected taxa may indicate a slight rise of the nutricline, caused by the input of nutrients from continents, to the intermediate and then upper photic zone (Casellato and Erba, 2015). Changes in calcareous nannofossil assemblages, such as the deep-dweller crisis, shortly but clearly precede the deposition of anoxic sediments (Erba, 2004; Tremolada et al., 2005) indicating that phytoplanktonic communities reacted to the early changes in trophic and climatic conditions. The decrease in both abundance and size of *S. punctulata* documented in several sections (i.e. Claps et al.

1995; Mattioli and Pittet, 2002; Erba, 2004; Suan et al. 2008; 2010; Mailliot, 2009; Reolid et al. 2014; Clémence et al. 2015; Casellato and Erba, 2015; Peti and Thibault, 2017) and the decrease in abundance of *M. jansae* (Casellato and Erba, 2015) could have been triggered by a combination of high CO₂ levels, a very shallow nutricline, and, perhaps, the disruption of the thermocline (Erba, 2004; Tremolada et al. 2005; Casellato and Erba, 2015). Fraguas and Young (2011) and Ferreira et al. (2017) observed a drastic decrease in size also for the mesotrophic genus *Lotharingius* during the T-OAE. The latter authors pointed out that under unstable environmental conditions (T-OAE) likely fast reproduction rates occurred, favoring the production of small coccoliths. Small *Lotharingius* specimens, likely better adapted to fluctuating environmental conditions displayed their highest relative abundance in this period, whereas during the Middle-Late Toarcian, ecological stability likely supported either a faster or a longer coccolith growth and the occurrence of larger coccoliths is observed (Ferreira et al., 2017).

After the T-OAE, paleoceanographic conditions, at least as far as the photic zone is concerned, only partly and gradually returned to a pre-perturbation state suggesting that the deepening of the nutricline and re-establishment of stability required a long period after anoxia terminated (Casellato & Erba, 2015).

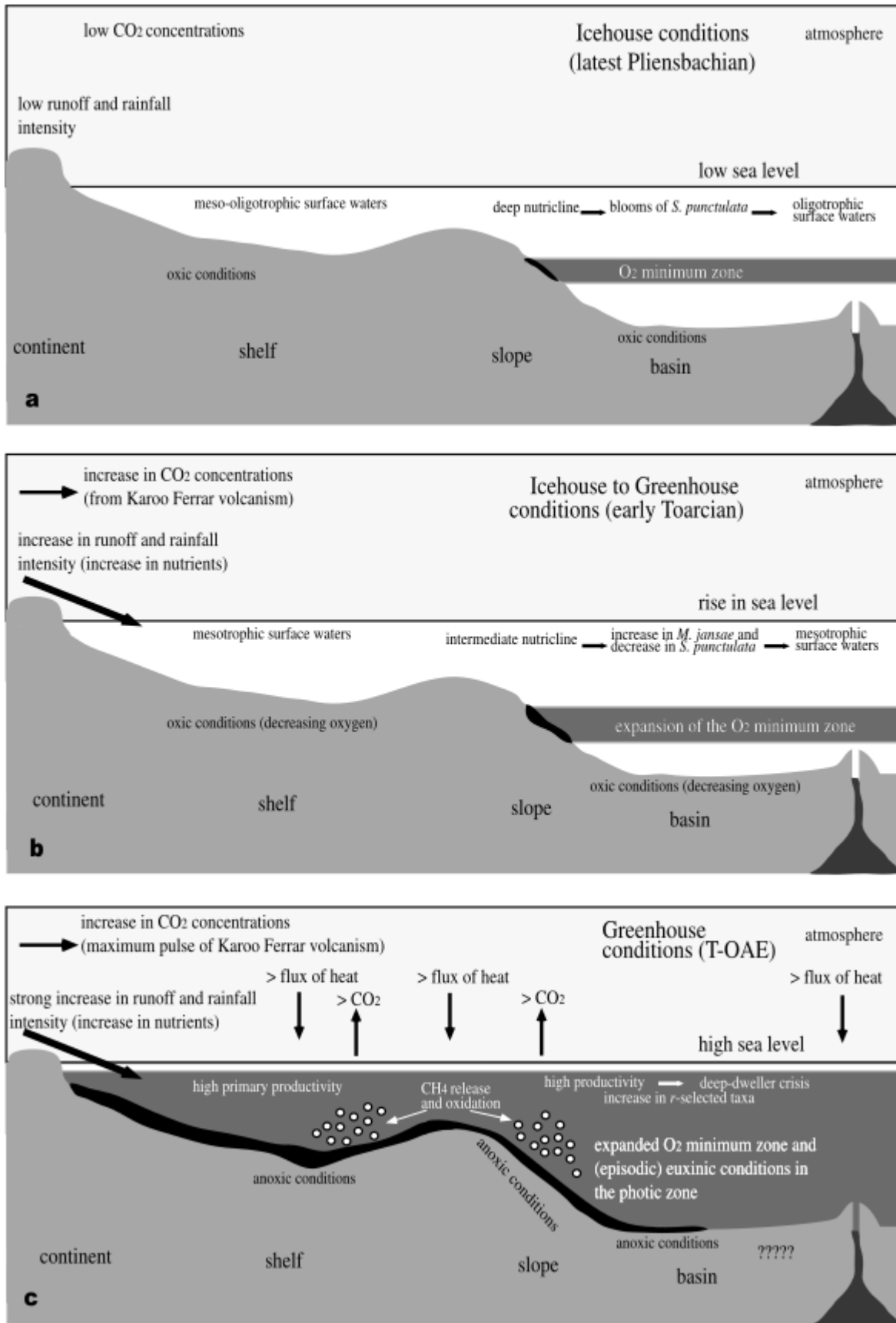


Fig. 2.7 – Paleoceanographic model proposed for the: (a) Latest Pliensbachian, (b) Early Toarcian, (c) Toarcian OAE (after Tremolada et al., 2005).

Multidisciplinary studies performed by Suan et al. (2008) reveal that the Early Toarcian paleoenvironmental crisis occurred during two episodes of maximum stress: the first crisis is recorded in the earliest Toarcian while the most severe changes are recorded during the T-OAE (Fig. 2.7). The two episodes coincide with two carbonate production crises that affected both platform-derived and nannofossil carbonate and may have been directly related to CO₂-induced changes in seawater chemistry. This fact is supported by a dramatic reduction in size of *Schizosphaerella* recorded in the Peniche section across the two successive C isotope negative.

High-precision radiometric dating indicates that the emplacement of the Karoo-Ferrar province, one of the largest igneous provinces of the Phanerozoic Eon, was contemporaneous with these events (Palfy and Smith, 2000). Two successive, time-spaced events of isotopically light carbon release are not only conformable with the episodic nature of flood basalt volcanism (Lin and Van Keken, 2005) but are also compatible with evidence of brief and volumetrically important events of magmatism in the Karoo province (Jourdan et al. 2007) suggesting that these major paleoenvironmental perturbations were directly or indirectly linked to paroxysmal phases of intense of subaerial vulcanism (Suan et al. 2008). A large source of “light” carbon may have been provided indirectly by the thermal metamorphism of organic-rich sediments in the Karro-Ferrar province (McElwain et al. 2005; Svensen et al. 2007). Moreover, elevated levels of greenhouse gases and input of “light” carbon during the T-OAE may have been reinforced by several pulses of astronomically driven gas hydrate dissociation, as suggested by the orbital pacing of large shifts to lower $\delta^{13}\text{C}$ values identified in Yorkshire by Kemp et al. (2005). These events should have been accompanied by rapid increases of atmospheric CO₂ levels and may have induced rapid events of “ocean acidification” (Kemp et al. 2005; Beerling and Brentnall, 2007).

Four phases were reconstructed by Suan et al. (2008) (Fig. 2.8). The average diameter of *Schizosphaerella* reached the highest values during the Late Pliensbachian (phase a) and during the early *polymorphum* Ammonite Zone (AZ) (phase c) that were likely characterized by low CO₂ levels and possibly icehouse conditions. High and moderate production and export of platform ooze and relative low sea level further characterize these time intervals. The average diameter of *Schizosphaerella* reached the smallest values during the onset of the *polymorphum* AZ (phase b) and the early *levisoni* AZ (phase d). High rates of continental runoff, increase of nutrient input and reduced salinity as well as an increased atmospheric CO₂ and elevated temperatures during phases b and d triggered dramatic changes in ocean chemistry and trophic conditions that affected the calcification potential of both *Schizosphaerella* and platforms.

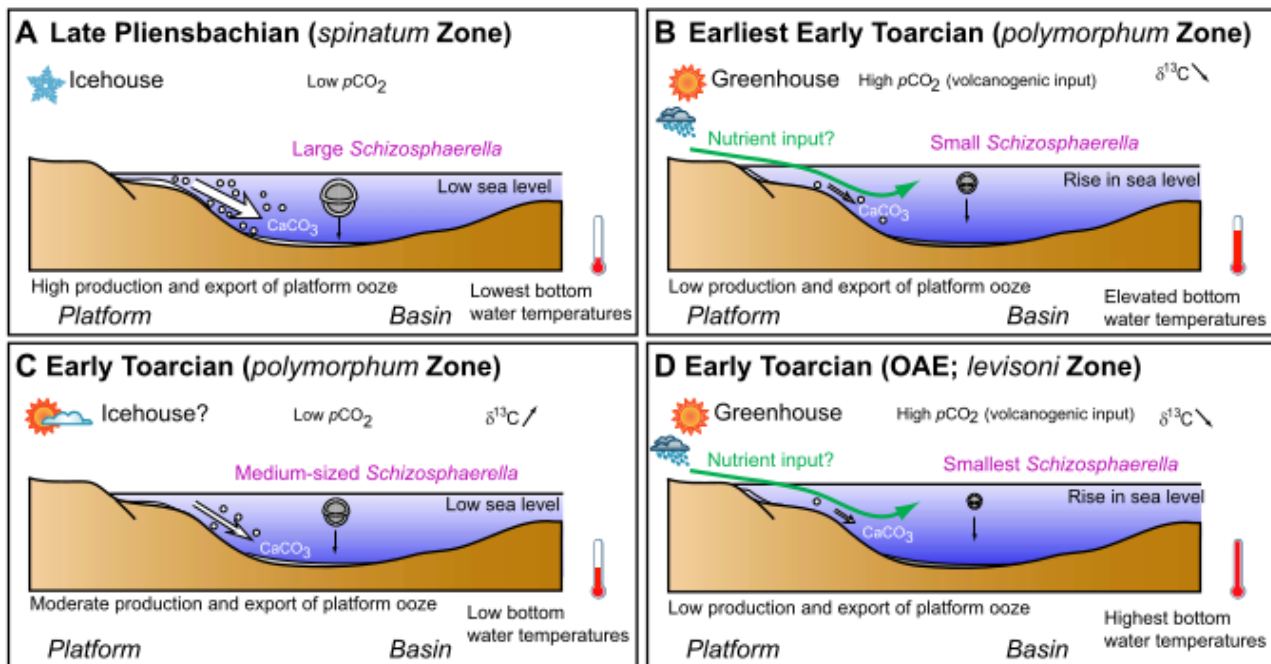


Fig. 2.8 – Schematic paleoceanographic model for the (a) Late Pliensbachian; (b) lowermost Early Toarcian; (c) Early Toarcian (middle *polymorphum* zone), (c) Early Toarcian (middle *polymorphum* zone), (d) lower part of the *levisoni* zone (T-OAE) (after Suan et al. 2008).

Chapter 3

Early Jurassic calcareous nannofossils

3.1. Biozonation schemes

Calcareous nannofossil biostratigraphy is a powerful tool that allows effective dating and correlation of land outcrops and offshore wells. For the Lower and Middle Jurassic, biostratigraphic potential of calcareous nannofossils is quite high due to their rapid evolutionary rates, as well as common and continuous occurrence in sediments (Mattioli et al. 2013). Although diagenesis modifies calcareous nannofloras and strong etching and/or overgrowth can partially or totally destroy the most delicate taxa (Mattioli, 1993,1997, Mattioli and Erba, 1999), the common occurrence of diagenesis-resistant forms provides a good stratigraphic resolution. Two palaeogeographic provinces are recognized in the European Jurassic, namely the Tethyan and Boreal Realms (Arkell, 1956) characterized by differences in faunas and floras. Benthic and planktonic organisms including calcareous nannoplankton, show a clear differentiation in the two areas (Bown, 1987b; Bown, 1992; Bown and Cooper, 1998; Baldanza et al. 1995; Mattioli and Erba, 1999). Consequently, two biozonation schemes were proposed: the one originally proposed by Bown (1987b) and then revised by Bown et al. (1988) and Bown and Cooper (1998) for the Boreal Realm (United Kingdom, Germany, The Netherlands, North France, North Spain) and the biozonation of Mattioli and Erba (1999) established for Tethyan settings (Italy, Western Portugal, South East Spain, South France, Hungary, Greece). Later, two additional biozonation schemes were proposed: that of Fraguas et al. (2015) for the Cantabrian Range (Northern Spain) and the one of Ferreira et al. (2019) as a comprehensive synthesis based on sections from the Lusitanian Basin (Portugal).

The zonal scheme proposed by Bown et al. (1988) (Fig. 3.1) is a synthesis of the nannofossil events detected in several sections and boreholes from northern and western Europe. Calcareous nannofossil biohorizons were directly calibrated with ammonite zonation. A total of seventeen zones, defined as NJ – Nannofossil Jurassic (NJ1 to NJ17) spanning the Upper Triassic (Norian) to the Upper Jurassic (Portlandian / Volgian) were identified. Some zones were defined for the first time by Bown et al. (1988) whereas other biozones derive from previous zonal schemes (i.e. Stradner, 1963; Prins, 1969; Barnard and Hay, 1974; Medd, 1982; Roth et al. 1983; Bown, 1987b; Lord et al. 1987). Subsequently Bown and Cooper (1998) modified some of the Upper Jurassic Boreal zones (NJ15b to NJ18) following a detailed study of the Kimmeridgian Upper Volgian section at Gorodische (Russia).

For the Late Pliensbachian to Early Toarcian time interval, including the T-OAE, three biozones were proposed and coded NJ5, NJ6 and NJ7. The original definition of these biozones is reported below.

- **NJ5 *Lotharingius hauffii* Zone**

Author: Bown (1987b)

Definition: from the FO of *Lotharingius hauffii* to the FO of *Carinolithus superbus*

Range: Upper Pliensbachian (*margaritatus* AZ) to Lower Toarcian (*falciferum* AZ).

Remarks: This zone displays an important nannofloras turnover, with many murolith-coccoliths becoming extinct and new placolith groups diversifying and becoming more abundant. In particular, the *Lotharingius* group begins to dominate the assemblages. The zone is also characterized by the near-total range of *B. finchii*. (Bown and Cooper, 1998).

- **NJ5a *Biscutum finchii* Subzone**

Author: Bown (1987b)

Definition: from the FO of *Lotharingius hauffii* to the FO of *Crepidolithus impontus*

Range: Upper Pliensbachian (*margaritatus* to *spinatum* AZs)

Remarks: The FO of *B. finchii* also approximates the base of this zone (Bown and Cooper, 1998).

- **NJ5b *Crepidolithus impontus* Subzone**

Author: Bown (1987b), emended by Bown and Cooper (1998).

Definition: from the FO of *Crepidolithus impontus* to the FO of *Carinolithus superbus*

Range: Upper Pliensbachian (*spinatum* AZ) to Lower Toarcian (*falciferum* AZ).

Remarks: As discussed by Bown and Cooper (1998), the nominate taxon (previously called *Crepidolithus cavus*) is given an alternative name, *C. impontus*, to avoid the confusion which has arisen over the identification of earlier *Crepidolithus* coccoliths which have a central-area bar. *C. impontus* has a wide central area spanned by a delicate, narrow bar, and is quite distinct from *C. cavus* which was described by Rood et al. (1973) from the Lower Pliensbachian. Many new species have FOs, or first occur consistently, in this subzone, (i.e. *A. atavus*, *B. grandis*, *B. prinsii*, *Calyculus* spp., *L. sigillatus*, *S. arctus*, *Z. erectus*). The LOs of murolith taxa, such as *P. liasicus*, *C. primulus* and *M. elegans*, have been variably reported in the literature. This may be due to increasing rarity in the highest parts of their ranges. Bown and Cooper (1998) reported as reliable events only the **FO of *L. sigillatus*** and **LO of *C. primulus*** within this Subzone. The evolutionary transition from *Calyculus* to *Carinolithus* is also observed through this Subzone.

- **NJ6 *Carinolithus superbus* Zone**

Author: Bown (1987b)

Definition: from the FO of *Carinolithus superbis* to the FO of *Discorhabdus striatus*

Range: Lower Toarcian (*falciferum* AZ).

Remarks: The LOs of *B. finchii*, *B. grandis* and *O. hamiltoniae* are recorded in this Zone. Bown and Cooper (1998) reported as reliable events only the **LOs of *B. finchii*** and ***O. hamiltoniae*** within this Zone.

- **NJ7 *Discorhabdus striatus* Zone**

Author: Bown (1987b)

Definition: from the FO of *Discorhabdus striatus* to the FO of *Retecapsa incompta*

Range: Lower Toarcian (*falciferum* AZ) to Upper Toarcian (*levesquei* AZ).

Remarks: Few FOs and LOs are observed through this interval. The FO of *D. criotus* may be useful in dividing the zone. Assemblages are dominated by *Lotharingius* (Bown and Cooper, 1998).

Italy/S France Mattioli et al., in prep.	Portugal Bergen, in prep.	BOREAL NF ZONES Bown et al., 1988	NANNOFOSSIL EVENTS		BOREAL AMM. ZONES	AGE
			Secondary events	Zonal events		
	S. hexum	NJ12	↕	S. hexum T. shawensis	discus	BATHONIAN
	H. cuvillieri	NJ12a	↕		aspidoides hodsoni	
	T. shawensis	NJ11	↕	H. cuvillieri, T. shawensis, C. margerellii, S. spec. octum	morrissi subcontractus progracilis tenuiplicatus	
	S. spec. octum		↕		zigzag	
	D. striatus acmé		↕		parkinsoni garantiana subfurcatum	
	C. superbus	NJ10	↕	C. superbus D. constans	humphriesianum sauzei	
	S. speciosum	NJ9	↕		laeviuscula	
	D. constans		↕		discites	
	T. tiziense	NJ8	↕	P. grassei	concauum	AALENIAN
	W. britannica		↕		murchisonae	
	W. britannica acmé	NJ8b	↕	B. prinsii, C. imponentis	opalinum	
	D. constans		↕		levesquei	
	T. sullivanii	NJ8a	↕	Trisc. sp., B. intermedium	thouarsense	TOARCIAN
	T. tiziense		↕		variabilis	
	B. prinsii	NJ7	↕	L. hauffii acmé D. criotus	bifrons	
	R. incompta		↕		falciferum	
	L. hauffii acmé	NJ7	↕	O. hamiltoniae	tenuicostatum	PLIENSBACH.
	D. striatus		↕		spinatum	
	C. superbus	NJ6	↕	B. finchii	margaritatus	SINEMURIAN
	C. primulus	NJ5	↕	C. primulus L. sigillatus	daevoei	
	L. hauffii		NJ5a	↕	L. hauffii	
	B. novum	NJ4	↕	B. finchii	jamesoni	HETTANGIAN
	L. ?barozii		NJ4b	↕	C. pliensbachensis	
	C. pliensbach.	NJ3	↕	C. pliensbachensis	oxyonyum	
	B. aff. B. dubium		NJ3a	↕	S. cruciululus	obtutum
	C. granulatus	NJ2	↕	O. hamiltoniae	turneri	
	?C. pliensbachensis		NJ2b	↕	P. robustus	semicostatum
		NJ1	↕	C. robustus	bucklandi	
	C. pliensbach. M. jansae M. elegans		NJ1a	↕	C. pliensbachensis M. elegans	angulata
	P. liasicus	NJ1	↕	P. liasicus	liasicus	
			NJ1	↕	S. punctulata	planorbis

Fig. 3.1 – Hettangian to Bathonian biostratigraphic zones and events of the Boreal biozonation scheme (after Bown and Cooper, 1998)

The zonal scheme proposed by Mattioli and Erba (1999) (Fig. 3.2) is a synthesis of the nannofossil events recognized in several Lower and Middle Jurassic sections belonging to the Mediterranean Province-Tethys Ocean and spanning the Hettangian to Callovian interval. Several sections are ammonite-rich and allow a direct calibration of nannofossil biohorizons. The large dataset allowed estimates of reliability and reproducibility of single events. A total of eleven zones and fifteen subzones, defined as NJT – Nannofossil Jurassic Tethys (NJT1 to NJT11) were proposed for the Hettangian to Callovian interval. The authors decided to use as much as possible events and zones previously established in older zonal schemes (i.e. Bown 1987b; Bown et al., 1988), however, new events and zones were also introduced. Forty-seven biohorizons based on diagenesis-resistant and common taxa were proposed as main events; additional seventeen events, based on rare but ubiquitous taxa, were described as rare events; additional twelve potential events requiring further investigations due to taxonomic problems and sporadic occurrence were also introduced.

For the Late Pliensbachian to Early Toarcian time interval, including the T-OAE, three biozones were proposed and coded NJT5, NJT6 and NJT7. The original definition of these biozones is reported below.

- **NJT5 *Lotharingius hauffii* Zone**

Author: originally Bown, (1987b); then emended as NJT5 by Mattioli and Erba (1999)

Definition: from the FO of *Lotharingius hauffii* to the FO of *Carinolithus superbus*

Range: Late Pliensbachian to Early Toarcian

Remarks: A progressive increase in abundance and species richness marks the Pliensbachian/Toarcian boundary (Mattioli and Erba, 1999).

- **NJT5a *Biscutum finchii* Subzone**

Author: Mattioli and Erba (1999)

Definition: from the FO of *Lotharingius hauffii* to the FO of *Lotharingius sigillatus*

Range: Late Pliensbachian to earliest Toarcian

Remarks: This subzone corresponds to the NJ5a and part of the NJ5b Subzones of Bown (1987b). *L. umbriensis*, *L. frodoi*, *L. barozii*, *B. prinsii*, *B. leufuensis*, *S. lowei* and *Calyculus* spp. first occur in this subzone. Subzone NJT5a roughly corresponds to the spinatum AZ (Mattioli and Erba, 1999).

- **NJT5b *Lotharingius sigillatus* Subzone**

Author: Mattioli and Erba (1999)

Definition: from the FO of *Lotharingius sigillatus* to the FO of *Carinolithus superbus*

Range: Early Toarcian (*tenuicostatum* AZ)

Remarks: This subzone corresponds to the upper part of the NJ5b ASz and the base of the NJ6 zone of Bown (1987b). *L. crucicentralis* first appears in the Early Toarcian. In this subzone also the first

appearance of the genus *Carinolithus* is observed with *C. poulabronei* and *C. cantaluppii*. The assemblages become richer and more diversified (Mattioli and Erba, 1999).

- **NJT6 *Carinolithus superbis* Zone**

Author: originally Bown, (1987b); then emended as NJT6 by Mattioli and Erba (1999)

Definition: from the FO of *Carinolithus superbis* to the FO of *Discorhabdus striatus*

Range: Lower Toarcian (*tenuicostatum* to *serpentinus* AZs).

Remarks: This zone is correlative of the NJ6 zone of Bown (1987b). *L. velatus*, *D. ignotus*, *W. colacicchi* and *W. fossacincta* (*Watznaueria* sp. 1) first occur in this zone. Conversely, some typical representatives of Early Jurassic assemblages, such as *M. jansae*, disappear. *Calyculus* spp. is a characteristic constituent of this zone, whereas *C. superbis* is still quite rare (Mattioli and Erba, 1999).

- **NJT7 *Discorhabdus striatus* Zone**

Author: originally Bown, (1987b); then emended as NJT7 by Mattioli and Erba (1999)

Definition: from the FO of *Discorhabdus striatus* to the FO of *Retecapsa incompta*

Range: Early Toarcian (*serpentinus* AZ) to Late Toarcian (*meneghinii* AZ).

Remarks: In this zone *C. superbis* becomes common and *D. criotus*, *B. depravatus* and *T. sullivanii* first occur. *C. cantaluppii*, *M. lenticularis* and small specimens of *Calyculus* spp. disappear (Mattioli and Erba, 1999).

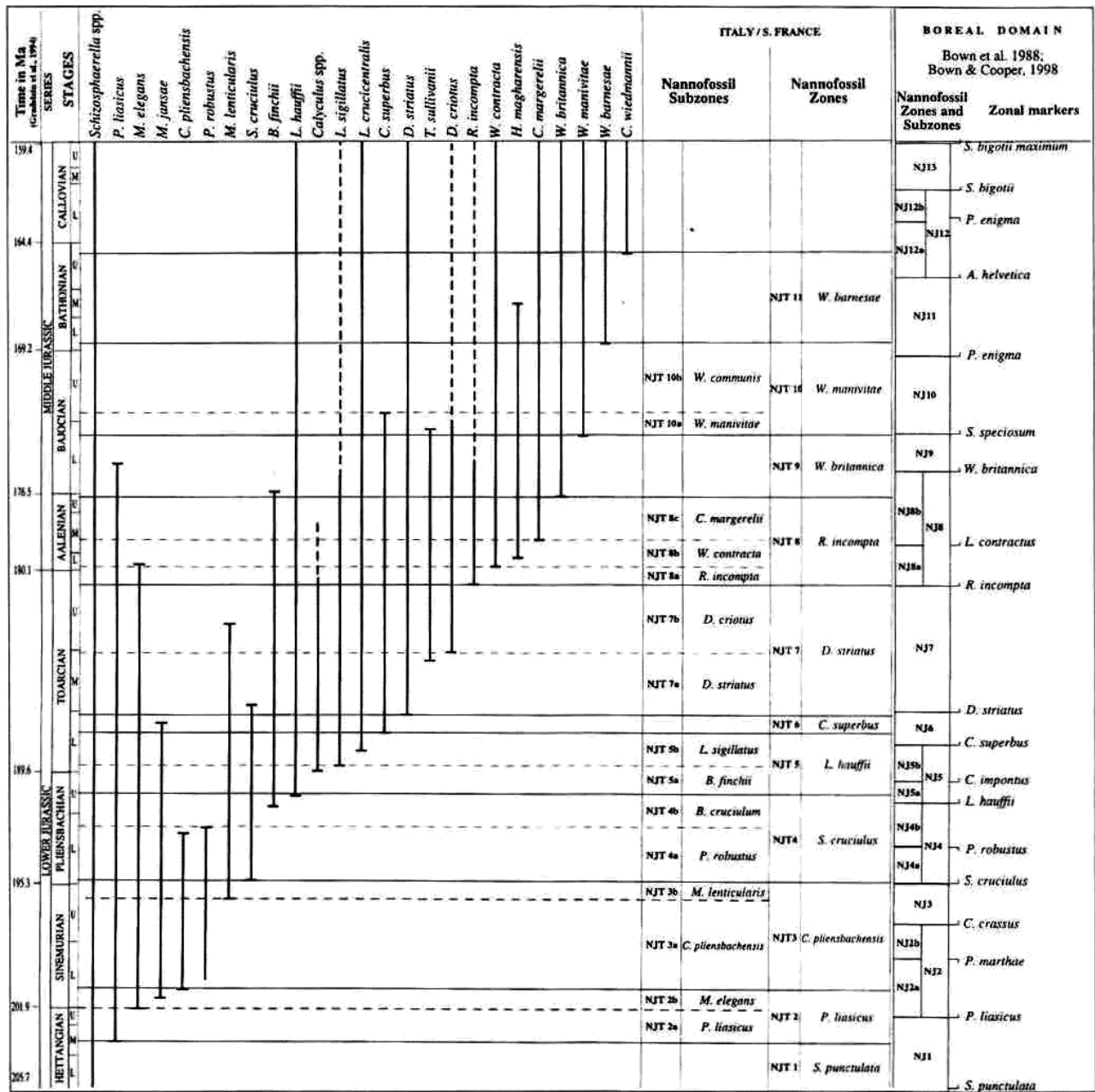


Fig. 3.2 – Hettangian to Callovian biostratigraphic zones and events of the Tethys biozonation scheme. The comparison with the zonal scheme of Bown and Cooper (1998) is reported on the right side (after Mattioli and Erba, 1999).

The zonal scheme of Fraguas et al. (2015) (Fig. 3.3) provided a synthesis of the Upper Sinemurian-Lower Toarcian calcareous nannofossil biostratigraphy for the Cantabrian Range (Northern Spain), based on four sections from the Basque-Cantabrian Basin (i.e. Camino, San Andrés, Tudanca and Santotis) and one section from Asturias (i.e. West Rodiles). The authors decided to use as much as possible events and zones previously established in older zonal schemes (e.g. Bown and Cooper, 1998; Mattioli and Erba, 1999); unpublished data were also considered. Calcareous nannofossil main and secondary events were calibrated with ammonite zonations established for the studied areas. A total of five main events, five secondary events, four calcareous nannofossil zones, two subzones and one emended zone were proposed. The zones were defined as NJ – Nannofossil Jurassic (NJ3 to NJ6) which is the same acronym adopted in the zonal scheme of Bown and Cooper (1998). For the Late Pliensbachian to Early Toarcian time interval, two biozones were proposed and coded NJ5 and NJ6. The original definition of these biozones is reported below.

- **NJ5 *Lotharingius hauffii* Zone**

Author: Bown, (1987b).

Definition: from the FO of *Lotharingius hauffii* to the FO of *Carinolithus superbis*

Remarks: Bown, (1987b) and Bown and Cooper (1998) proposed that the time interval spanned by this zone coincides with the stratigraphic distribution of *B. finchii*. (Fraguas et al. 2015).

Associated species: *B. finchii*, *C. jansae*, *C. crassus*, *L. hauffii*, *L. sigillatus*, *O. hamiltoniae*, *P. l. liasicus*, *Schizosphaerella* sp., *S. cruciulus* and *T. patulus* dominate the calcareous nannofossil assemblages, displaying a continuous record throughout all the studied sections. The species *B. grande*, *B. novum*, *B. prinsii*, *Calyculus* spp., *C. cantabriensis*, *C. cavus*, *C. crucifer*, *C. granulatus*, *C. primulus*, *L. barozii*, *M. elegans*, *P.l. distinctus*, *S. avitum* and *S. orbiculus* are rare and show a discontinuous record in the Cantabrian Range. *B. dubium*, *B. intermedium* and *L. umbriensis* have been identified in the Reinosa area (Basque-Cantabrian Basin) and in West Rodiles section (Asturias) with relative low abundances and discontinuous records. *L. crucicentralis* has only been recognized in Asturias with a high relative abundance and a continuous range. (Fraguas et al. 2015).

- **NJ5a *Biscutum finchii* Subzone**

Author: originally Bown, (1987b); then emended by Fraguas et al. (2015)

Definition: from the FO of *Lotharingius hauffii* to the FO of *Lotharingius sigillatus*

Associated species: *B. finchii*, *C. jansae*, *C. crassus*, *O. hamiltoniae*, *P. l. liasicus*, *Schizosphaerella* sp., *S. cruciulus* and *T. patulus* dominate the calcareous nannofossil assemblages, showing a continuous record. (Fraguas et al. 2015).

- **NJ5b *Lotharingius sigillatus* Subzone**

Author: originally Mattioli and Erba (1999); then emended by Fraguas et al. (2015)

Definition: from the FO of *Lotharingius sigillatus* to the FO of *Carinolithus superbus*

Associated species: *C. jansae*, *C. crassus*, *L. hauffii*, *L. sigillatus*, *O. hamiltoniae*, *Schizosphaerella* sp. and *T. patulus* are dominant and display a continuous record. (Fraguas et al. 2015).

- **NJ6 *Carinolithus superbus* Zone**

Author: Bown (1987b)

Definition: from the FO of *Carinolithus superbus* to the FO of *Discorhabdus striatus*

Range: The upper boundary of this zone has not been identified since it is located above the last studied sample in the West Rodile section. Its lower boundary lies within the *tenuicostatum* AZ. (Fraguas et al. 2015).

Associated species: *C. superbus*, *C. crassus*, *L. crucicentralis*, *L. hauffii*, *L. sigillatus*, *O. hamiltoniae*, *Schizosphaerella* sp. and *T. patulus* dominate the calcareous nannofossil assemblages and show continuous records throughout the West Rodiles section (Asturias). The species *B. novum*, *B. prinsii*, *Calyculus* spp., *C. cantabriensis*, *C. crucifer*, *L. barozii*, *L. umbriensis*, *P.l. distinctus* and *P.l. liasicus* are rare and show a continuous record in Asturias, whilst *C. cantaluppi*, *C. poul nabronei*, *B. dubium*, *B. finchii*, *B. grande*, *B. intermedium*, *C. cavus*, *C. granulatus*, *C. primulus*, *M. elegans*, *S. avitum* are very rare and display discontinuous ranges. (Fraguas et al. 2015).

Stage	Substage	Present work; N Spain					Bown and Cooper (1998); NW Europe				
		Amm.	Calcareous nannofossils				Amm.	Calcareous nannofossils			
		AZs	CNZs	CNSzs	Main events	Secondary events	AZs	CNZs	CNSzs	Main events	Secondary events
Toarcian	Lower	Sr	NJ6 <i>C. superbus</i>		<i>C. superbus</i>		Fa	NJ6 <i>C. superbus</i>		<i>C. superbus</i>	<i>B. finchii</i>
	Upper	Te	NJ5 <i>L. hauffii</i>	NJ5b <i>L. sigillatus</i>	<i>L. sigillatus</i>	FCO <i>L. hauffii</i>	Te	NJ5 <i>L. hauffii</i>	NJ5b <i>C. imponentus</i>	<i>C. imponentus</i>	<i>C. primulus</i>
Upper	Sp	NJ5a <i>B. finchii</i>		<i>L. hauffii</i>	Sp		NJ5a <i>B. finchii</i>		<i>L. sigillatus</i>		
Pliensbachian	Upper	Mr	NJ4 <i>S. cruciulus</i>	NJ4b <i>B. novum</i>	<i>B. novum</i>	FCO <i>L. barozii</i> <i>C. jansae</i> <i>B. finchii</i> <i>B. grande</i>	Mr	NJ4 <i>S. cruciulus</i>	NJ4b <i>C. granulatus</i>	<i>L. hauffii</i>	<i>B. finchii</i>
	Upper	St		NJ4a <i>C. cantabriensis</i>	<i>S. cruciulus</i>		St		NJ4a <i>C. ptiensbachensis</i>		<i>P. robustus</i>
	Lower	Da	NJ3 <i>C. crassus</i>			Da	NJ3 <i>C. crassus</i>				
	Lower	lb				lb					
	Lower	Ja				Ja					
Sinemurian	Upper	Ra				Ra					

Fig. 3.3 – Upper Sinemurian to Lower Toarcian biostratigraphic zones and events of the Cantabrian Range biozonation scheme (left side) compared with the zonal scheme of Bown and Cooper (1998) (right side) (after Fraguas et al. 2015).

Recently, Ferreira et al. (2019) (Fig. 3.4) provided a comprehensive biostratigraphic scheme for the Early and Middle Jurassic epochs based on sections from the Lusitanian Basin (i.e. São Pedro Moel, Peniche, Rabaçal, Brenha, Cabo Mondego). The authors focussed their attention exclusively on this basin since it was located at the strategic intersection of important Jurassic water masses during a period of drastic environmental changes and conveyed mixed phytoplanktonic communities in its surface waters. The authors decided to use as much as possible events and zones previously established in older zonal schemes (e.g. Bown and Cooper, 1998; Mattioli and Erba, 1999) and to improve the resolution where possible. A total of one hundred events, eleven zones and twenty-nine subzones calibrated with a solid ammonite zonation were provided and defined as NJT - Nannofossil Jurassic Tethys (NJT3 to NJT10) which is the same acronym adopted in Mattioli and Erba (1999). For the Late Pliensbachian to Early Toarcian time interval, three biozones were proposed and coded NJT5, NJT6 and NJT7. Author, definition and range of these biozones are reported below (see Ferreira et al. 2019 for remarks).

- **NJT5 *Lotharingius hauffii* Zone**

Author: originally Bown (1987b); then emended as NJT5 by Mattioli and Erba (1999)

Definition: from the FO of *Lotharingius hauffii* to the FO of *Carinolithus superbus*

Range: Late Pliensbachian to earliest Toarcian, from part of the *margaritatus* AZ up to part of the *polymorphum* AZ.

- **NJT5a *Similiscutum finchii* Subzone**

Author: Mattioli and Erba (1999); then emended by Ferreira et al. (2019)

Definition: from the FO of *Lotharingius hauffii* to the FO of *Lotharingius crucicentralis*

Range: Late Pliensbachian, from part of the *margaritatus* AZ to the basal *emaciatum* AZ

- **NJT5b *Lotharingius sigillatus* Subzone**

Author: Mattioli and Erba (1999); then emended by Ferreira et al. (2019)

Definition: from the FO of *Lotharingius crucicentralis* to the FO of *Zeughrabdotus erectus*

Range: topmost Pliensbachian, within almost the totality of the *emaciatum* AZ.

- **NJT5c *Zeughrabdotus erectus* Subzone**

Author: Ferreira et al. (2019)

Definition: from the FO of *Zeughrabdotus erectus* to the FO of *Carinolithus superbus*

Range: Early Toarcian, within the *polymorphum* AZ

- **NJT6 *Carinolithus superbus* Zone**

Author: Bown (1987b), emended as NJT6 by Mattioli and Erba (1999)

Definition: from the FO of *Carinolithus superbus* to the FO of *Discorhabdus striatus*

Range: Early Toarcian, from part of the *polymorphum* AZ up to part of the *levisoni* AZ.

- **NJT6a *Carinolithus superbis* Subzone**

Author: Ferreira et al. (2019)

Definition: from the FO of *Carinolithus superbis* to the LO of *Mitrolithus jansae*

Range: Early Toarcian, from part of the *polymorphum* AZ up to part of the *levisoni* AZ

- **NJT6b *Mitrolithus jansae* Subzone**

Author: Ferreira et al. (2019)

Definition: from the LO of *Mitrolithus jansae* to the FO of *Discorhabdus striatus*

Range: Early Toarcian, within the *levisoni* AZ

- **NJT7 *Discorhabdus striatus* Zone**

Author: Bown (1987b), emended as NJT7 by Mattioli and Erba (1999)

Definition: from the FO of *Discorhabdus striatus* to the FO of *Retecapsa incompta*

Range: Early and Middle Toarcian, from the top of the *levisoni* AZ to the basal *gradata* AZ.

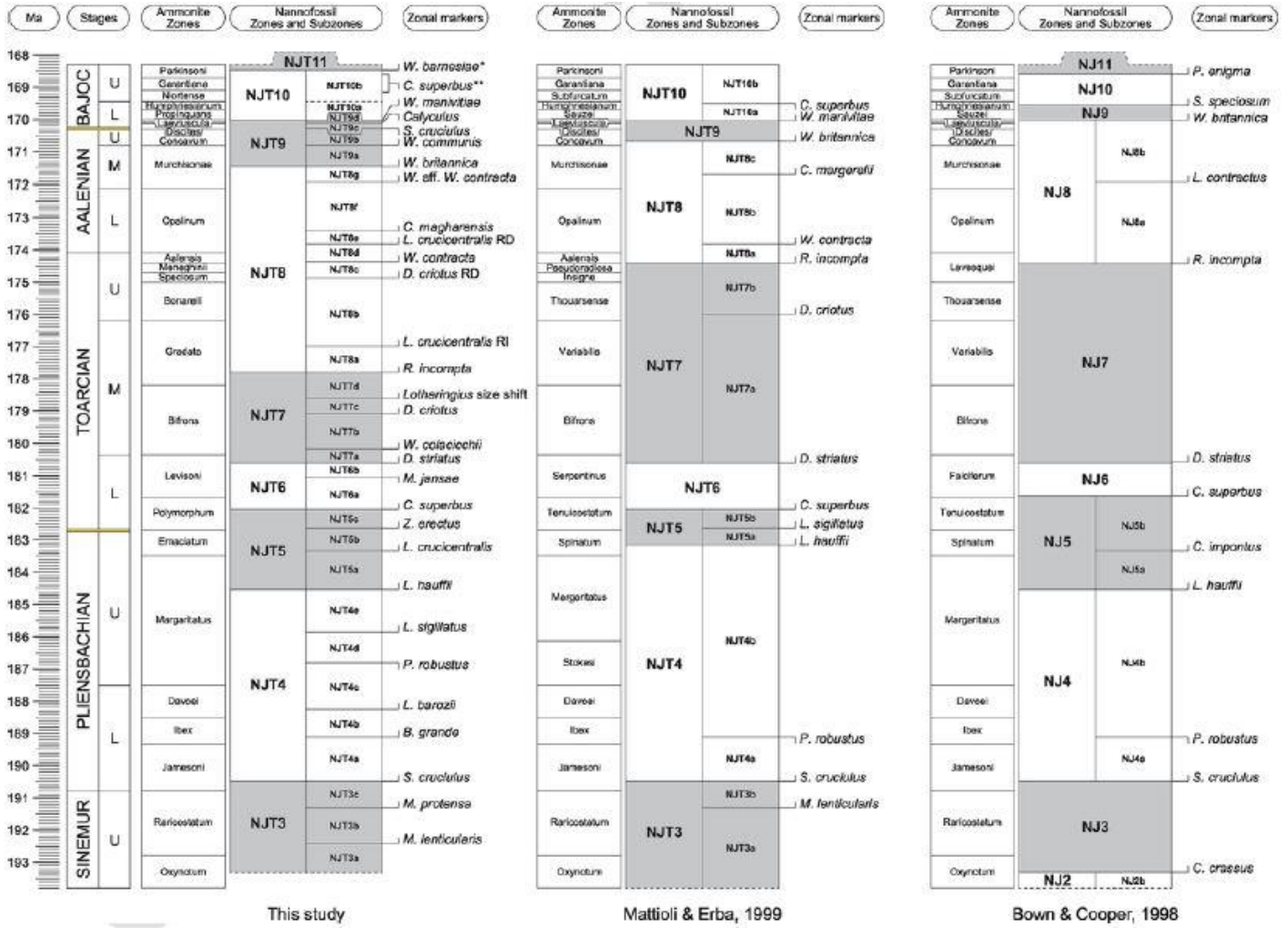


Fig. 3.4 - Upper Sinemurian to Lower Toarcian biostratigraphic zones and events of the biozonation scheme of Ferreira et al. (2019) (left side) compared with the zonal scheme of Mattioli and Erba (1999) (middle) and Bown and Cooper (1998) (right side) (after Ferreira et al. 2019).

3.2. Biostratigraphies of previous authors

In the last three decades much attention has been devoted to Early Jurassic calcareous nannofossils to explore their potential as stratigraphic tool for correlations at regional to global scale. The Late Pliensbachian-Early Toarcian interval was a crucial time for calcareous nannoplankton evolution as a major speciation episode took place and some of the most common Jurassic and Cretaceous genera (*Biscutum*, *Lotharingius*, *Discorhabdus* and *Watznaueria*) appeared and rapidly evolved (Bown, 1987b; Mattioli and Erba, 1999; Bown et al. 2004; Erba, 2004; 2006; Casellato and Erba, 2015). As a consequence, the high number of biohorizons characterizing the Late Pliensbachian to Early Toarcian time interval offers the opportunity to biostratigraphically constrain the T-OAE. Several studies focused on Lower Jurassic calcareous nannofossil assemblages and biostratigraphy in both Tethys and Boreal Realms, with the large majority being dedicated to the Pliensbachian/Toarcian boundary and the T-OAE. Papers documenting Pliensbachian-Toarcian calcareous nannofossils are reported in Appendix B. They are organized following the publication date and for each paper the following data are listed: a) investigated realm; b) investigated basin/area; c) investigated section/s; d) time interval studied; e) methodology applied; f) taxonomy; g) biostratigraphy; h) plates; i) range chart; j) biozonation; k) ammonite stratigraphy; l) oxygen and/or carbon isotopic stratigraphy; m) magnetostratigraphy; n) ciclostratigraphy; o) paleoceanographic reconstructions; p) paleoecological investigations; q) morphometric investigations; r) principal component analyses investigations; s) cluster analyses.

In Appendix B, papers dealing with calcareous nannofossil biostratigraphy are highlighted in yellow and red. Those in red were published after Casellato and Erba (2015).

Following Mattioli and Erba (1999), Casellato and Erba (2015) compared nannofossil biohorizons comprised between the FOs of *Calyculus* and *Watznaueria* against ammonite biozones for the latest Pliensbachian to Early Toarcian time interval (Fig. 3.6) and carbon isotope anomaly across the T-OAE (Fig. 3.7) as documented in manuscripts reported in appendix B and highlighted in yellow. In this PhD thesis I completed the synthesis with manuscripts published after Casellato and Erba (2015).

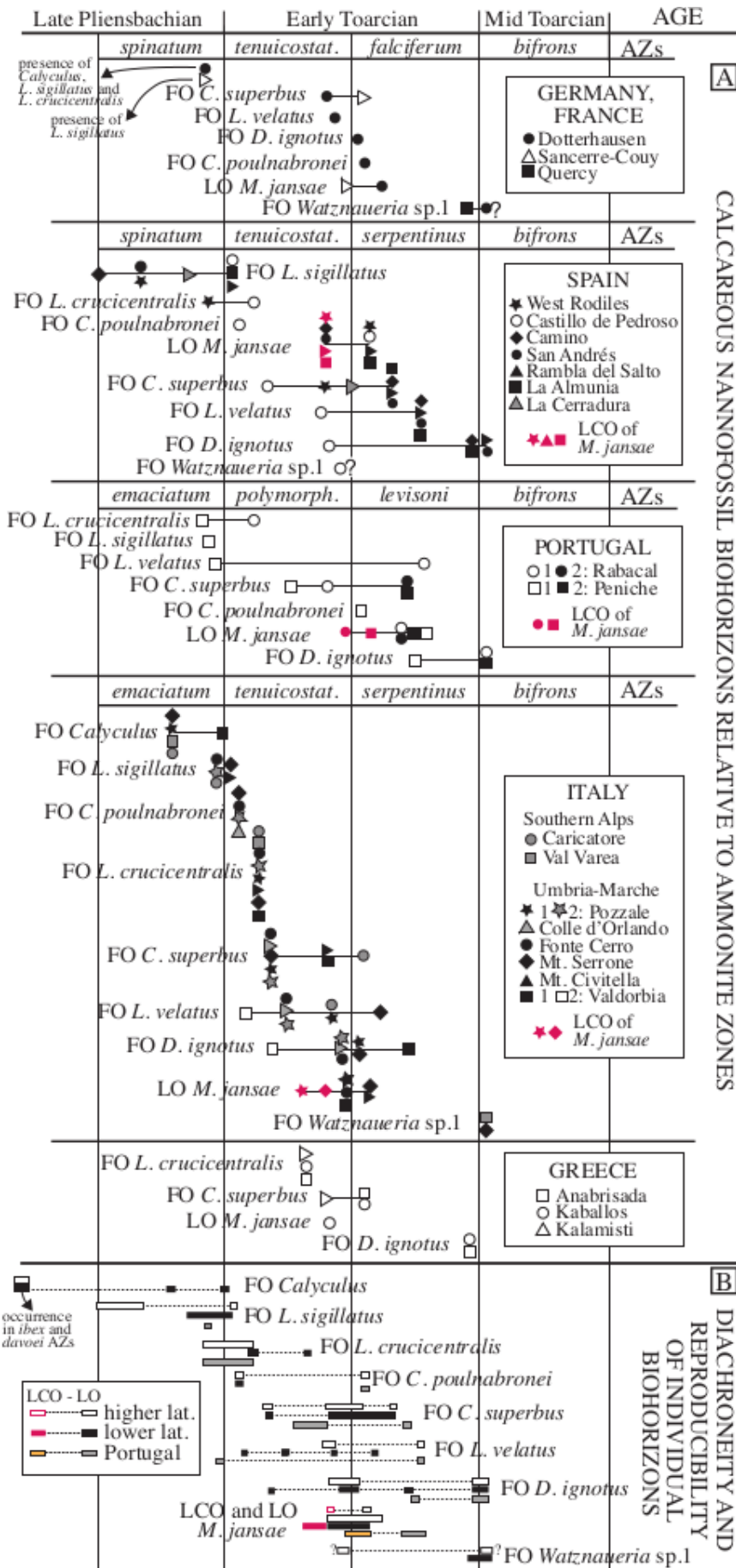


Fig. 3.6 – A) Calcareous nannofossil biohorizons plotted against Ammonite Zones from higher and lower latitudes. Solid symbols identify data derived from published range charts; empty ones refer to works without range chart. B) Diachroneity and reproducibility of individual biohorizons based on ammonite dating (after Casellato & Erba, 2015).

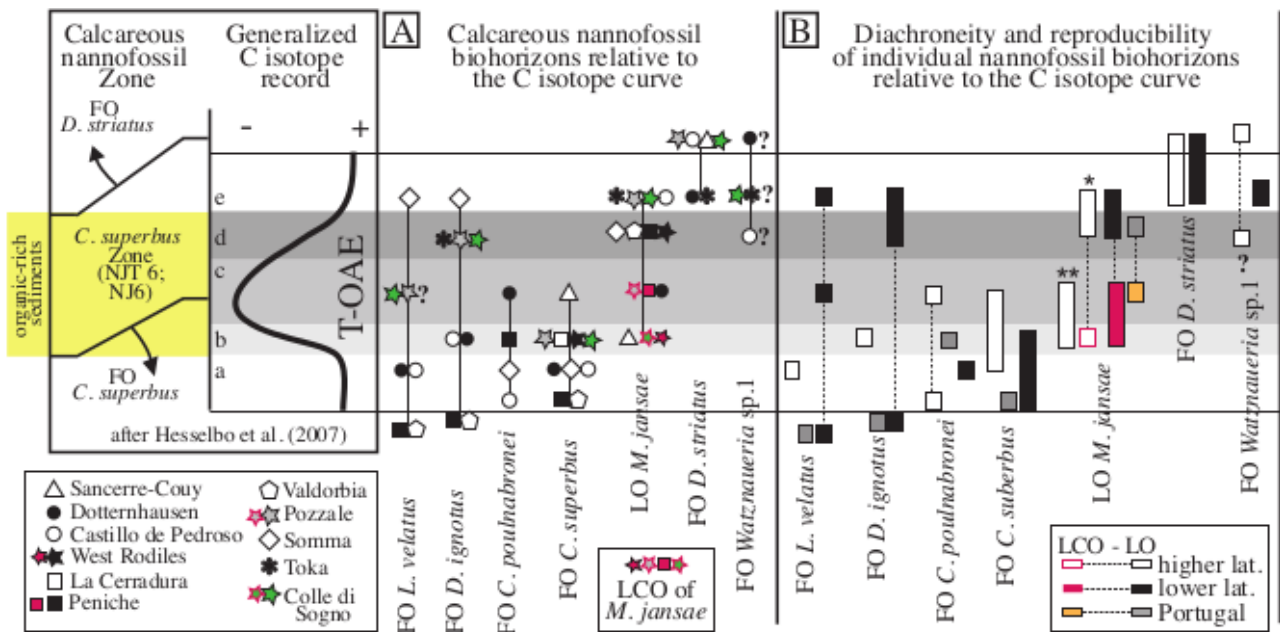


Fig. 3.7 – A) Calcareous nannofossil biohorizons plotted against the C isotope generalized curve, divided into five intervals as follows: a) pre-excursion, white band; b) rapid decrease, light grey band; c) interval with minimum values, medium grey band; d) recovery, dark grey band; e) values comparable to the pre-excursion ones, white band. Following Hesselbo et al., (2007), the yellow box indicates organic-rich sediments deposited during the T-OAE. B) Diachroneity and reproducibility of individual biohorizons relative to the C isotopic anomaly (after Casellato and Erba, 2015).

Unlike Casellato and Erba (2015) who separated the calibration into two distinct schemes (Figs. 3.6 and 3.7), here the Upper Pliensbachian and Lower Toarcian nannofossil events are simultaneously calibrated relative to the ammonite zonations and the C isotopic anomaly (Fig. 3.8). The latter was divided into eight sub-intervals:

- A - Late Pliensbachian pre-anomaly
- B - Uppermost Pliensbachian rapid decrease
- C - Lowermost Toarcian recovery
- D - pre-excursion of the T-OAE
- E - rapid decrease (light grey)
- F – minimum values (medium grey)
- G – recovery (dark grey)
- H - post T-OAE recovery.

The same ammonite zones adopted in Casellato and Erba (2015) are here used. Individual calcareous nannofossil events are discussed below in stratigraphic order following Mattioli and Erba (1999) from the FO of *Calyculus* to the FO of genus *Watznaueria*. Discussions for higher latitudes (Northern Spain,

Germany, Northern France, England) are separated from those for lower latitudes (Italy, Southern and Eastern Spain, Southern France, Greece, Hungary) and from those for Portugal.

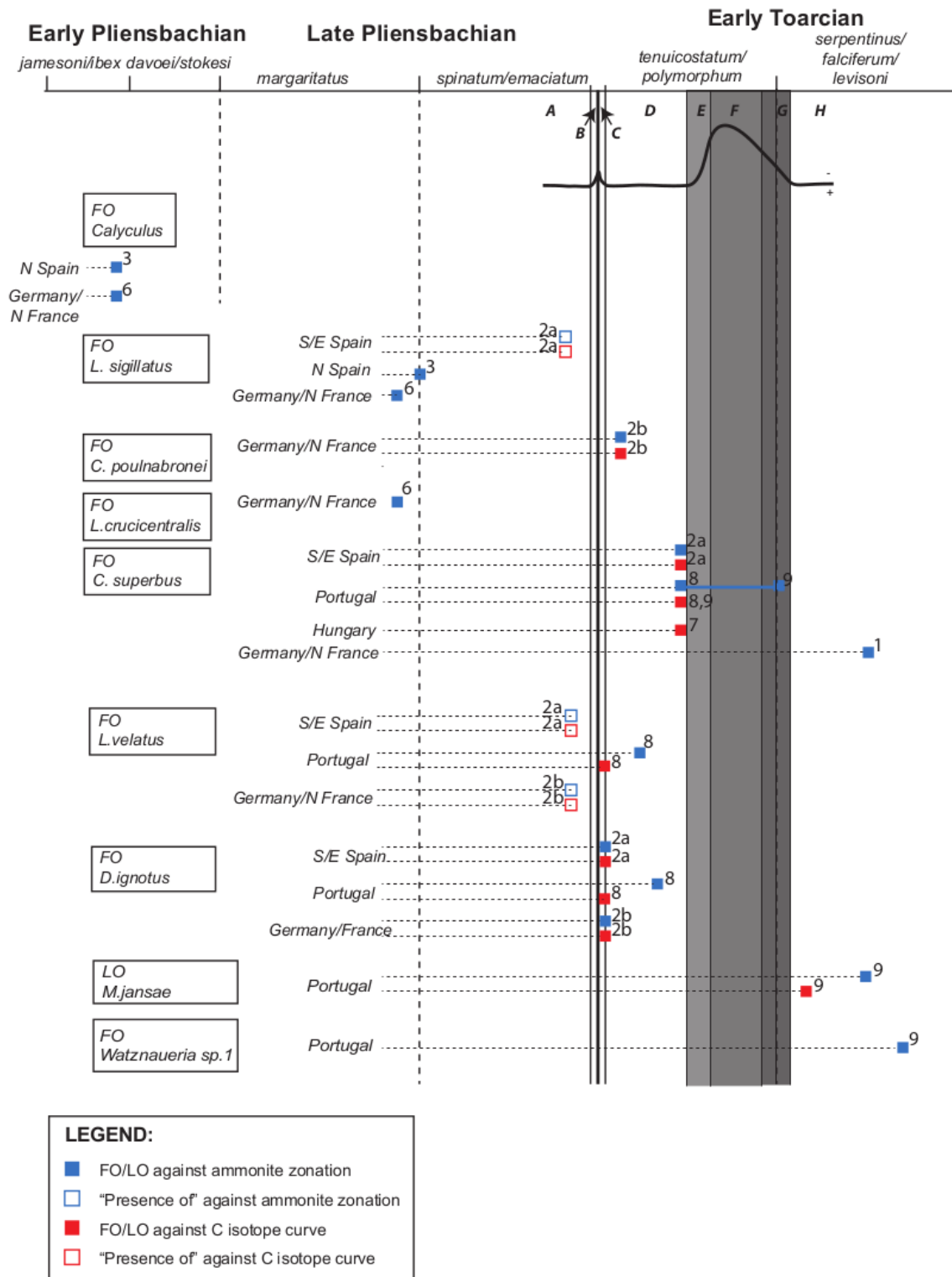


Fig. 3.8 – Calcareous nannofossil biohorizons plotted relative to the ammonite zonation and the C isotopic anomaly for papers published later than Casellato and Erba (2015). Numbers refer to the papers reported in appendix B and highlighted in red. Where papers deal with more than one section letters are used to distinguish different sections.

- **FO of *Calyculus***

Higher latitudes. Recently this event was correlated to the uppermost *ibex* AZ in East Rodiles (i.e. Fraguas et al. 2018) and Sancerre-Couy (i.e. Peti and Thibault, 2017) sections.

- **FO of *L. sigillatus***

Lower latitudes. The presence of this taxon was documented from the upper *spinatum* AZ and within sub-interval A in La Almunia section (i.e. Menini et al. 2018).

Higher latitudes. Recently this event was calibrated to the base of the *spinatum* AZ in East Rodiles (i.e. Fraguas et al. 2018) and in the uppermost *margaritatus* AZ in Sancerre-Couy (i.e. Peti and Thibault, 2017) section.

- **FO of *C. poulabronei***

Higher latitudes. This event was correlated to the lower *tenuicostatum* AZ and within sub interval D in Anse St. Nicolas (i.e. Menini et al. 2018) section.

- **FO of *L. crucicentralis***

Higher latitudes. Recently this event was calibrated to the uppermost *margaritatus* AZ in Sancerre-Couy (i.e. Peti and Thibault, 2017) section.

- **FO of *C. superbus***

Lower latitudes. This event was correlated to the middle *tenuicostatum* AZ and within the uppermost sub interval D in La Almunia (i.e. Menini et al. 2018) section. The latter position is consistent with the datum recorded in Reka (i.e. Müller et al. 2017).

Higher latitudes. Recently this event was calibrated to the middle *serpentinus* AZ in Schandelah (i.e. Van de Schootbrugge et al. 2018).

Portugal. This event was correlated to the middle *tenuicostatum* AZ and within the uppermost sub interval D in Peniche (i.e. Da Rocha et al. 2016) section. The latter position is consistent with the datum recorded in Rabaçal (i.e. Ferreira et al. 2015) although ammonite calibration reveals a younger age, at the base of the *levisoni* AZ.

- **FO of *L. velatus***

Lower latitudes. The presence of this taxon was documented from the upper *spinatum* AZ and within sub-interval A in La Almunia (i.e. Menini et al. 2018) section.

Higher latitudes. The presence of this taxon (both with ammonite and C isotope anomaly calibrations) was documented from the upper *spinatum* AZ and within sub-interval A in Anse St. Nicolas (i.e. Menini et al. 2018) section.

Portugal. Recently, this event was calibrated to the lower *polymorphum* AZ and within the uppermost sub-interval C in Peniche (i.e. Da Rocha et al. 2016) section.

- **FO of *D. ignotus***

Lower latitudes. This event was correlated to the lowermost *tenuicostatum* AZ and within the uppermost sub-interval C in La Almunia (i.e. Menini et al. 2018) section.

Higher latitudes. This event was correlated to the lowermost *tenuicostatum* AZ and within the uppermost sub-interval C in Anse St. Nicolas (i.e. Menini et al. 2018) section.

Portugal. Recently, this event was calibrated to the middle *polymorphum* AZ in Peniche (i.e. Da Rocha et al. 2016) section, although C isotope anomaly calibration reveals an older age, within the uppermost sub-interval C.

- **LO of *M. jansae***

Portugal. Recently, this event was calibrated to the middle *levisoni* AZ in Rabaçal (i.e. Ferreira et al. 2015) section, although C isotope anomaly calibration reveals an older age, within the lowermost sub-interval H.

- **FO of *Watznaueria* sp.1**

Portugal. Recently, this event was calibrated to the upper *levisoni* AZ in Rabaçal (i.e. Ferreira et al. 2015) section.

In order to evaluate diachroneity and reproducibility of individual calcareous nannofossil events, the data base studied by Casellato and Erba (2015) (Figs. 3.7 and 3.8) is integrated here with recent data and presented in Fig. 3.9. The new implemented data base reveals a major diachroneity for some events as discussed below.

Calibration to AZ. The FOs of *L. sigillatus* and *L. crucicentralis* reveal a major diachroneity at higher latitudes, whereas the FO of *C. superbus* both at higher latitudes and in Portugal. The FO of *L. velatus* displays a major diachroneity both at higher and low latitudes, whereas the FO of *D. ignotus* is a diachronous event at higher latitudes, low latitudes and in Portugal. As far as the FO of *Watznaueria* sp. 1 is concerned, the data base post Casellato and Erba (2015) offers the opportunity to evaluate the reproducibility of this event for the first time in Portugal, revealing that it is slightly younger compared to the database at low latitudes.

Calibration to the C isotope anomaly. The FO of *C. superbus* and the LO of *M. jansae* show a major diachroneity in Portugal, whereas the FO of *L. velatus* display it both at higher and low latitudes. The FO of *D. ignotus* reveals a major diachroneity both at higher and low latitudes and in Portugal.

In addition to the events of the Tethys biozonation scheme, the biohorizons reported in the Boreal zonal scheme of Bown and Cooper (1998) between the FO of *C. imponentus* and the LO of *O. hamiltoniae* (i.e. FO of *C. imponentus*, LO of *C. primulus*, LO of *B. finchii* and LO of *O. hamiltoniae*) are here discussed to assess diachronety and reproducibility at higher latitudes (Boreal Realm) (Fig. 3.10). For this aim, only papers published later than Bown and Cooper (1998) are considered. Individual calcareous nannofossil events are discussed below in stratigraphic order.

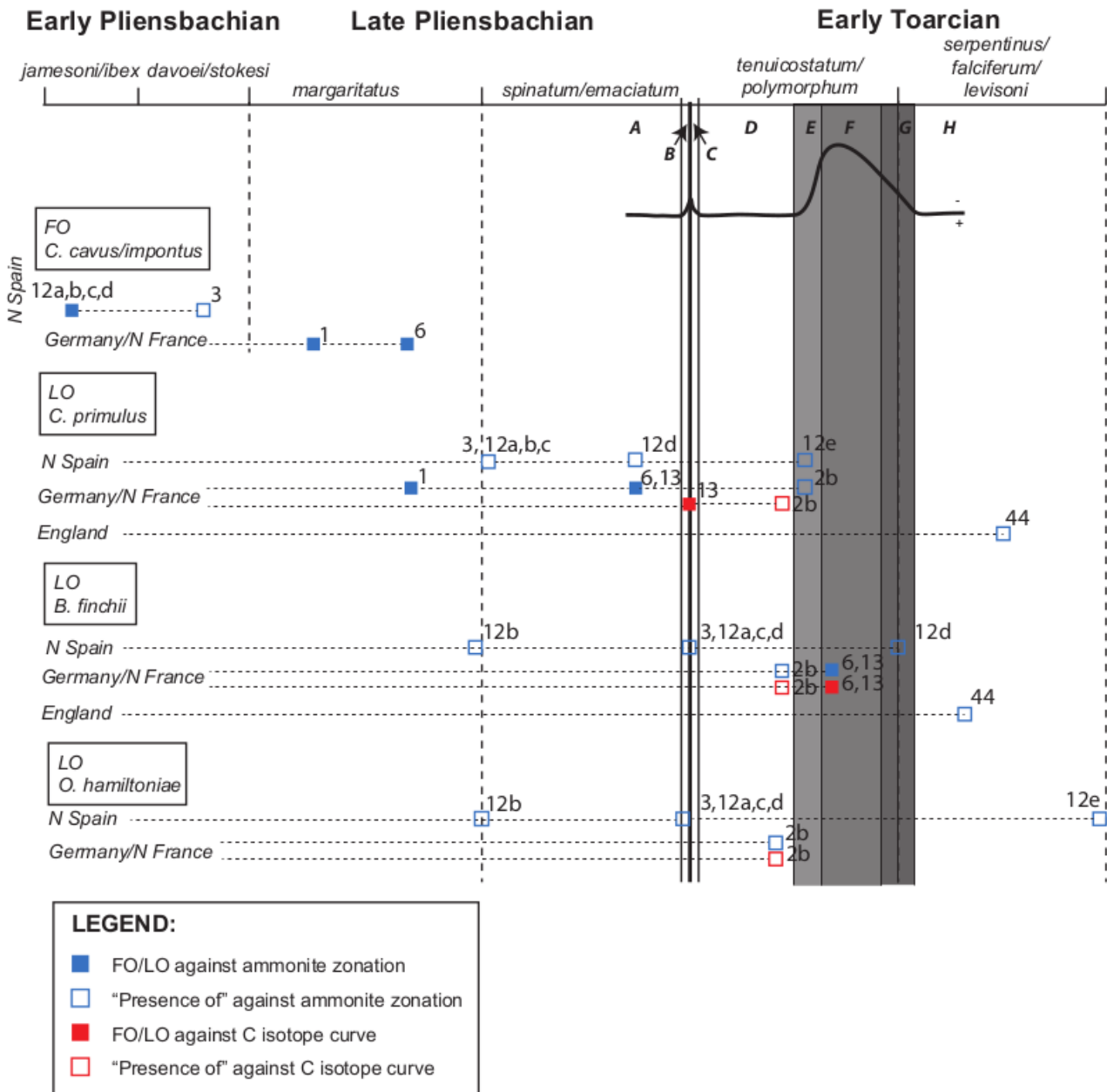


Fig. 3.10 – Calcareous nannofossil biohorizons of the Boreal zonal scheme simultaneously plotted relative to the ammonite zonation and the C isotopic anomaly. The data base is a synthesis of papers published post Bown and Cooper (1998). Numbers refer to the manuscripts reported in appendix B and highlighted in yellow and red. Where papers deal with more than one section letters are used to distinguish different sections.

- **FO of *C. impontus***

This event was correlated to the lower *jamesoni* AZ in Santotis, Tudanca, Camino and San Andrés (Fraguas et al. 2015) sections. The presence of this taxon is documented from the lower *stokesi* AZ in East Rodiles (i.e. Fraguas et al. 2018). The same event was reported in the lower *margaritatus* AZ in Schandelah (i.e. Van de Schootbrugge et al. 2018) section and in the upper *margaritatus* AZ in Sancerre-Couy (i.e. Peti and Thibault, 2017) section.

- **LO of *C. primulus***

The presence of this taxon was documented up to the lowermost *spinatum* AZ in East Rodiles (i.e. Fraguas et al. 2018), Santotis, Tudanca and Camino sections; up to the upper *spinatum* AZ in San Andrés section and up to the middle *tenuicostatum* AZ in West Rodiles (i.e. Fraguas et al. 2015). This event was correlated to the upper *margaritatus* AZ in Schandelah (i.e. Van de Schootbrugge et al. 2018) and to the upper *spinatum* AZ in Sancerre-Couy (i.e. Peti and Thibault, 2017) although chemostratigraphy reveals a younger age included between sub-intervals B and C. The presence of this taxon is documented up to the middle *tenuicostatum* AZ and upper sub-interval D in Anse St. Nicolas (i.e. Menini et al. 2018) section. In Brown Moor (i.e. Bucefalo Palliani et al. 2002) section, the presence of this taxon was attested up to the middle *falciferum* AZ.

- **LO of *B. finchii***

The presence of this taxon was reported up to the uppermost *margaritatus* AZ in Tudanca (i.e. Fraguas et al. 2015) section; up to the *emaciatum/polymorphum* boundary in East Rodiles, Santotis, Camino and San Andrés (i.e. Fraguas et al. 2015; 2018) sections; up to the uppermost *levisoni* AZ in West Rodiles (i.e. Fraguas et al. 2015). In Anse St. Nicolas section, the presence is attested up to the middle *tenuicostatum* AZ and the upper sub-interval D (i.e. Menini et al. 2018). This event was correlated to the upper *tenuicostatum* AZ and within sub-interval F in Sancerre-Couy (i.e. Peti and Thibault, 2017) section. In Brown Moor (i.e. Bucefalo Palliani et al. 2002) section, the presence of this taxon was attested up to the lower *falciferum* AZ.

- **LO of *O. hamiltoniae***

No manuscript published post Bown and Cooper (1998) reported this event in the Late Pliensbachian to Early Toarcian time interval. The presence of this taxon was documented up to the uppermost *margaritatus* AZ in Tudanca (i.e. Fraguas et al. 2015) section; up to the uppermost *emaciatum* in East

Rodiles, Santotis, Camino and San Andrés (i.e. Fraguas et al. 2015; 2018) sections; up to the the uppermost *serpentinus* AZ in West Rodiles (i.e. Fraguas et al. 2015). In Anse St. Nicolas (i.e. Menini et al. 2018) section, the presence of this taxon was reported up to middle *tenuicostatum* AZ and within the sub-interval D.

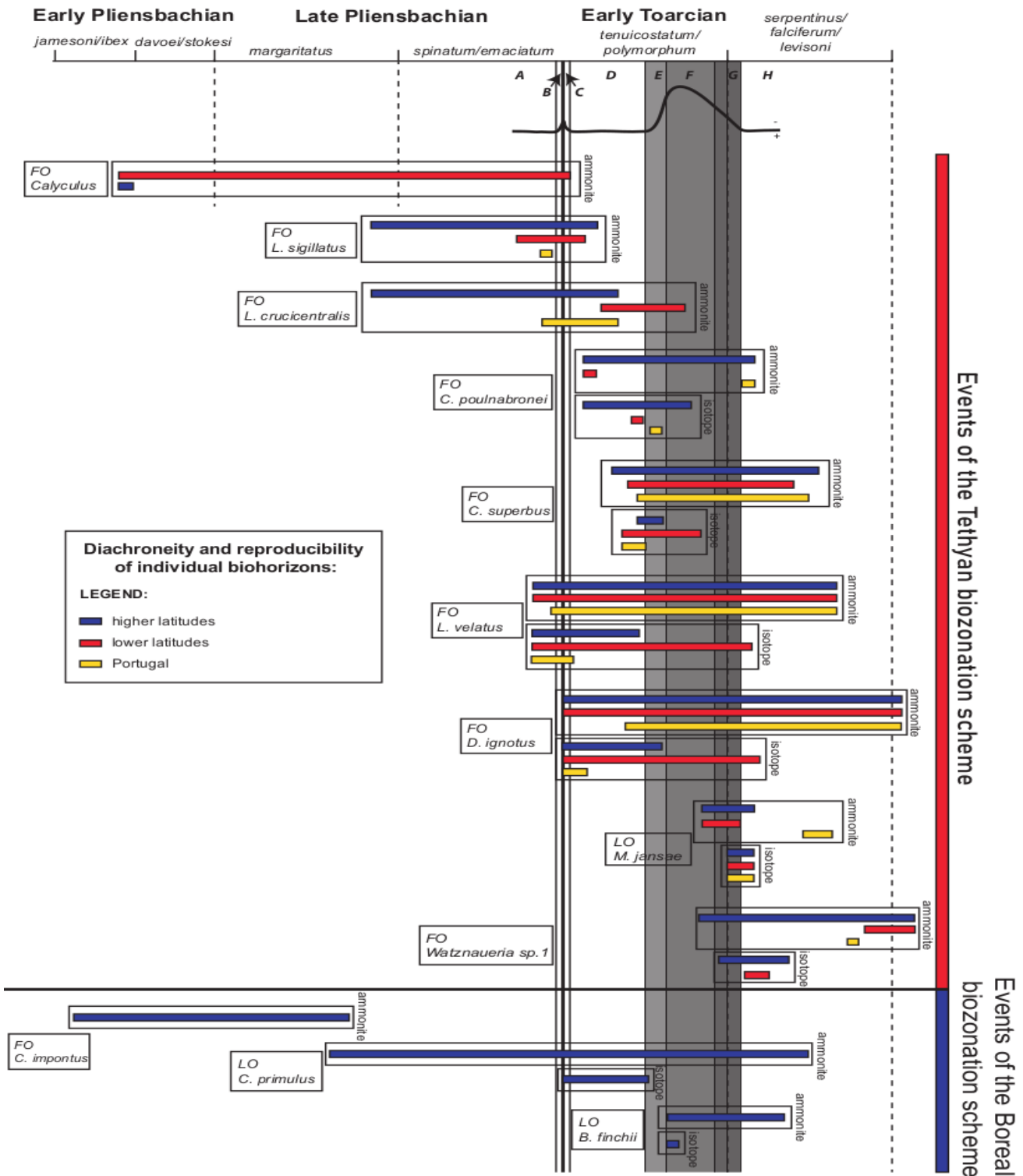


Fig. 3.11 - Reliability of individual calcareous nannofossil biohorizons plotted relative to the ammonite zonations and the C isotopic anomaly. For the events of the Tethyan biozonation the data base of Casellato and Erba (2015) is implemented with recent papers. For the events of the Boreal biozonation only papers published later than Bown and Cooper (1998) are considered.

Based on the database implemented for the events of the Tethyan biozonation scheme and the analyses conducted on the events of the Boreal biozonation scheme, a detailed scheme illustrating diachroneity and reproducibility of individual biohorizons across the T-OAE is reported in Fig. 3.11. Critical comments are reported below.

The critical evaluation of calcareous nannofossil events of the Tethyan biozonation reveals that the succession of biohorizons is not always consistent with the original scheme of Mattioli and Erba (1999). Older ages recently detected for the FOs of *L. velatus* and *D. ignotus* at lower latitudes (both with AZ and C isotope anomaly calibrations) suggest a revision of the Tethyan biozonation. As far as the events of the Boreal biozonation scheme are concerned, their succession results consistent with the scheme of Bown and Cooper (1998).

All the events display diachroneity of variable time extension. Some events appear severely diachronous (e.g. FO of *Calyculus*) but others show a limited diachroneity (e.g. LO of *M. jansae*). In some circumstances diachroneity seems justifiable by the rareness of taxa, especially in their initial ranges, and in part with very poor preservation of nannofossil assemblages. Moreover, the delicate structures of some species and taxonomic uncertainties discussed by some authors may have contributed to the diachroneity. These mainly regard the confusion between *Watznaueria* sp. 1 with *W. fossacincta* (discussed by Casellato and Erba, 2015) and *L. velatus* with *L. aff. L. velatus* (discussed by Mattioli et al. 2013; Da Rocha et al. 2016). Nevertheless, when the C isotope curve is taken as reference for calibration, calcareous nannofossil events display much reduced diachroneity relative to the calibration against ammonite zones. This fact further reinforces the problematic use of ammonite zonation as stratigraphic reference framework (Jenkyns et al. 2002; Mattioli et al. 2004; Hesselbo et al. 2007; Casellato and Erba, 2015).

As already pointed out by Casellato and Erba (2015) latitudinal time differences of some biohorizons are evident: this is the case of *L. sigillatus* and *L. crucicentralis* which appear earlier at higher latitudes. Casellato and Erba (2015) observed that *C. poulabronei* also appears earlier at higher latitudes, whereas *C. superbus* appears earlier at lower latitudes. Both observations were confirmed by recent papers (when data are calibrated to the C isotope anomaly). Moreover, our results reveal that the FO *C. superbus* at lower latitudes appears to be synchronous to that in Portugal.

The compiled data - set reveals that a few events are useful to constrain the Pliensbachian/Toarcian boundary and the T-OAE. Although the lack of a chemostratigraphic calibration, the FO of *L. sigillatus* appears a good marker to approximate the Pliensbachian/Toarcian boundary at least at lower latitudes. As already pointed out by Casellato and Erba (2015) when the C isotope curve is taken as reference, the FO of *C. superbis* correlates with the onset of the T-OAE anomaly at higher and lower latitudes as well as in Portugal. The LO of *M. jansae* is an excellent event to constrain the termination of the T-OAE at lower latitudes and in Portugal. The database available for higher latitudes is still limited to assess the reliability of this event as stratigraphic tool constraining the end of the T-OAE in the Boreal Realm. The FO of *Watznaueria* sp. 1 appears to be a potential event post-dating the T-OAE. As far as the events of the boreal biozonation are concerned, when the C isotope curve is taken as reference, the LO of *C. primulus* approximates the Pliensbachian/Toarcian boundary. Although the available database for *B. finchii* is limited, its LO appears as an excellent event within the T-OAE.

Chapter 4

Studied sections

In surface outcrops, often sedimentary rocks and particularly black shales are badly degraded and, consequently, drilling is crucial to ensure the recovery of high-quality fresh cored material. For this reason, investigations were carried out on three cores, namely the Sogno Core from the Southern Alps and the L1 and Schandelah Cores from the Lower Saxony Basin.

In the following chapters the location of the individual drillsite and the core lithostratigraphes are described.

4.1. The Sogno Core

The following description is taken from the manuscript by Erba et al.(2019b) reported in Appendix G.

Jurassic pelagic successions in the Southern Alps have been extensively investigated for stratigraphy, sedimentology, palaeontology and geochemistry (Bernoulli and Jenkyns 2009; Erba et al. 2019a). In particular, multi- and interdisciplinary studies have demonstrated that the Jurassic pelagic successions of the Lombardy Basin represent 'type-sections' of the Tethyan southern margin. Indeed, the Lombardy Basin is part of the relatively undeformed portion of Adria interpreted as an African "promontory" or as a microplate (Fig. 4.1). In the latest Triassic-earliest Jurassic a rifting phase caused the breakup of carbonate platforms into a series of "horst and graben" that exerted a physiographic control on sediment type and distribution for most of the Jurassic (Bernoulli and Jenkyns, 1974; 2009; Bosence et al. 2009; Santantonio and Carminati 2011).

As a consequence, sedimentation was differentiated with the deposition of thick complete pelagic successions in the deeper zones, while sedimentation was typically condensed and incomplete in correspondence of the structural highs. During the Jurassic, the Lombardy Basin was globally a deep area between the Lugano High to the West and the Trento Plateau to the East (Fig. 4.1). However, the latest Triassic-earliest Jurassic rifting disentangled a number of troughs and paleohighs that are, from west to east: Monte Nudo Trough, Lugano High, Generoso Trough, Corni di Canzo High, Albenza Plateau, Monte Cavallo High, Sebino Trough, Botticino High (Gaetani, 1975; 2010). In the troughs, Lower Jurassic marlstone-limestone partially resedimented sequences may reach a non-decompacted thickness of 3000 m (e.g. in the Generoso Trough), but condensation and hiatuses characterize the paleohigh sections with reddish nodular facies. Along slopes connecting structural highs to the troughs, sedimentation was marked by slumps, resedimented bodies and locally megabreccias within

condensed and occasionally incomplete facies (Gaetani and Erba, 1990; Gaetani, 2010) (Fig. 4.1). In addition to regional tectonics, the Lombardy Basin successions record global climatic and oceanographic changes including the T-OAE (Erba et al. 2019a).

The T-OAE in the Lombardy Basin is represented by the Livello a Pesci (Tintori, 1977; Gaetani and Poliani, 1978; Erba and Casellato, 2010; Erba et al. 2019a), with an average thickness of 0.5 to 5 m, but reaching few tens of meters in the most expanded sections. Black shales are rarely recorded on paleo-highs, whereas, they are ubiquitous in deeper basins. As the T-OAE occurred at a global scale, the local lack of black shales is usually the result of condensation and/or stratigraphic gaps.

The Lower Jurassic section at Colle di Sogno was selected for continuous coring through the Toarcian organic-rich black shale interval (Fig. 4.1). The relatively expanded sedimentary succession deposited on a pelagic structural high, namely the Albenza Plateau (Gaetani and Erba, 1990; Gaetani, 2010). The Colle di Sogno site (Fig. 4.1) was selected because the Jurassic sequence exposed is pelagic, stratigraphically continuous and relatively expanded (Gaetani and Erba, 1990; Muttoni et al. 2005; Channell et al. 2010; Casellato and Erba 2015). It consists of limestone and marlstone, with chert and marly claystone as minor lithologies. The T-OAE is here represented by ~5 meters of dark grey to black marly claystones of the Livello a Pesci. At Colle di Sogno, the type-section of the Sogno Fm. (Gaetani and Poliani, 1978), located along the road SP 179 on the northern slope of Mt. Brughetto, was proved to be suitable for high-resolution multidisciplinary studies of litho-, bio-, chemo-, magneto-, and cyclo-stratigraphy (Gaetani and Poliani, 1978; Jenkyns and Clayton, 1986; Gaetani and Erba, 1990; Hinnov et al. 2000; Channell et al. 2010; Casellato and Erba, 2015).

The Sogno coring took place in June 2013 and drilling operations were performed with the DELTABASE 520 Modular Hydraulic Rotary Drill. The Sogno coring was accomplished with a T2 double corer, using narrow-kerf, sawtoothed drill bits that cut a 101 mm-diameter borehole and 84 mm-diameter cores.

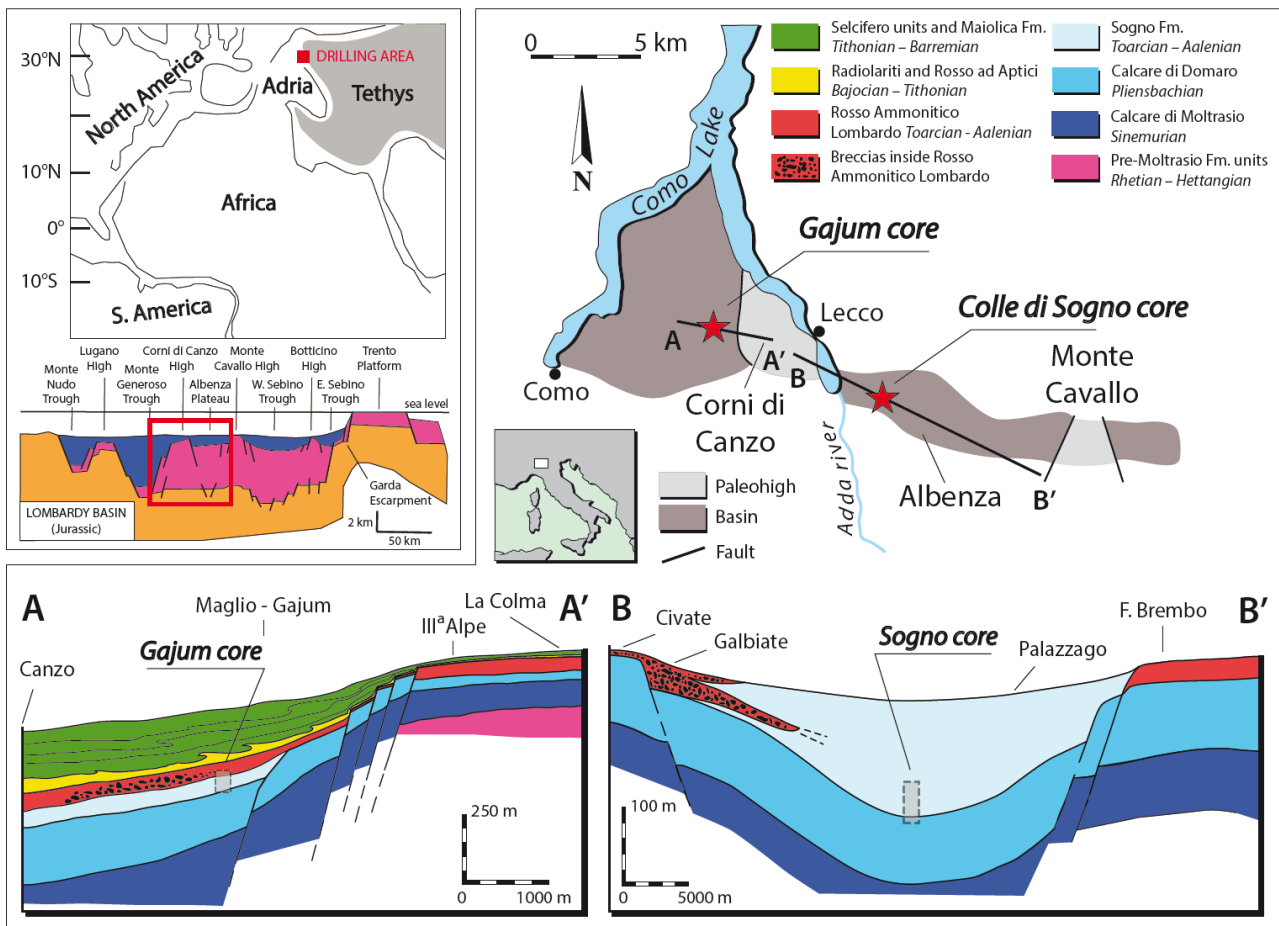


Fig. 4.1 - Location of the Sogno and Gajum drilling sites relative to paleo- and current geography. The drilling area was part of the Lombardy Basin (Southern Alps). The Sogno Core was drilled on the Albenza Plateau while the Gajum Core in an inner basin along the western slope of the Corni di Canzo High as detailed in the geological sections in the lower part of the figure (Erba et al. 2019b).

All cores were initially described on site and a preliminary log was produced. Then, cores were packed, labeled, and put in PVC plastic boxes to prevent contamination and transported to the Department of Earth Sciences in Milan where they are archived. Here, during lab preparation, all cores were longitudinally split along dip and divided into an archive and a sampling half, both marked at cm-scale. The archive half was photographed in high resolution and a composite photologs were produced for each site.

Four distinct boreholes (S1, S2, S3, and S4) were drilled at Colle di Sogno along the SP 179 road (45°47'20.5''N, 9°28'30.0''E). The outcropping beds show a strike of 150° and a dip of 68° to the southwest (240°).

Initially, a single borehole was planned to penetrate the lower Toarcian-uppermost Pliensbachian interval and reach the base of the Sogno Fm at ~35 m penetration depth. However, at ~25 m penetration depth (core S1-27) a sharp dip increase to 88° revealed the occurrence of a fold, partially

faulted and reversed, persisting for ~ 4 meters (cores S1-27, S1-28 and S1-29). Indeed, core S1-30 perfectly correlates with the lower part of core S1-26 and two black shales were used as lithostratigraphic markers. Coring was extended for ~2 meters (cores S1-31 and S1-32) penetrating the top of the black shale interval and then operations were interrupted to shift drilling to borehole S2 (Fig. 4.2). Due to steep dip, it was decided to perform a 10°-inclined coring to decrease the total penetration depth down into the Domaro Limestone Fm. Borehole S2 started just above the top of the black shale interval of the Livello a Pesci, perfectly duplicating core S1-32. However, technical problems prevented coring below a few meters and operations stopped after recovery of core S2-3. The third borehole (S3) was moved of 0.5 meter relative to S2 and was cored vertically. Again, the recovered succession started from just above the top of the black shale interval with core S3-1 triplicating cores S1-32 and S2-1. Coring was protracted to 40 m penetration depth, reaching the uppermost part of the Domaro Limestone Fm. (Fig. 4.2). A fourth borehole (S4) was performed to duplicate the middle and lower portion of the black shale interval to ensure material for multidisciplinary investigations. The recovery percentage for the four boreholes is 99.9%.

Lithostratigraphic units were defined on the basis of lithological features (i.e. lithology and colors determined with the Munsell Rock Color Chart) and sedimentary structures (i.e. presence/lack of bioturbation and/or lamination). For each core at least four dip measurements were taken during lab preparation to calculate the stratigraphic thickness of the drilled section that results to be of 25.33 m after 1.5 m of rubbles at the top. A complete composite section, representing the upper Pliensbachian–lower Toarcian interval, was created combining the data obtained from the S1 and S3 boreholes (Fig. 4). The following key observations were derived:

1. The first 1.5 meters of the S1 borehole are represented by soil cover and rubble.
2. The S1 Core, despite the occurrence of a faulted fold disturbing the succession, recovered a complete section above the Livello a Pesci. The bottommost part of the well reached the uppermost part of the black shale interval. This correlates with the top black shale interval recovered in the upper part of the S3 Core.
3. The upper limit of the black shale interval was cored both at S1 and S3 sites.
4. The S3 Core recovered few meters of succession above the black shale interval, the entire Livello a Pesci, and the lower portion of the Sogno Fm., in addition to the topmost part of the Domaro Lmst. In particular, at 25.47 meters, the lithostratigraphic boundary between the Sogno Fm. and Domaro Limestone Fm. was recovered.

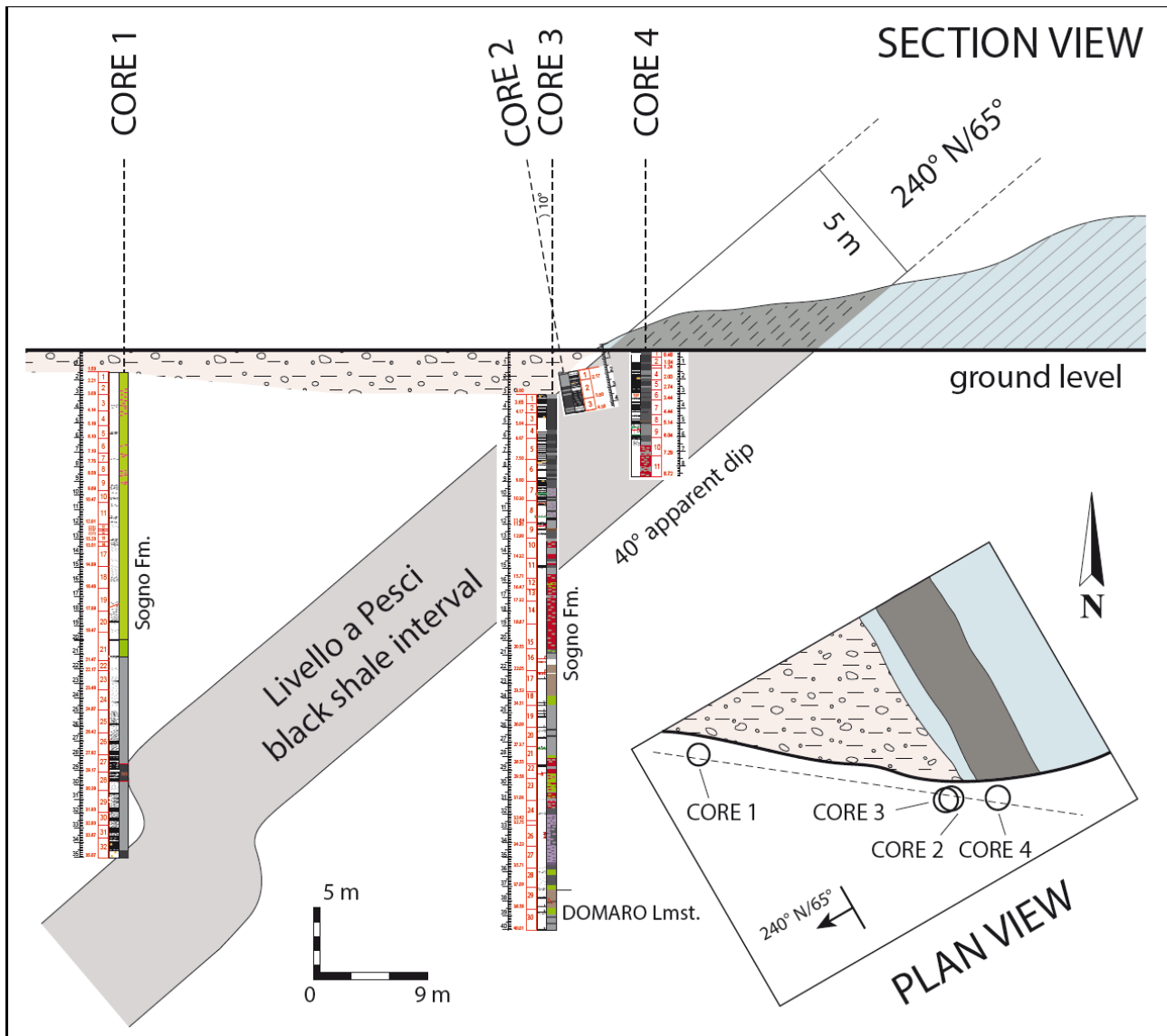


Fig. 4.2 - Scheme reporting in section and in plan view the relative position of the four boreholes drilled at Colle di Sogno. A pronounced fold was encountered at ~ 25 m penetration depth in Sogno borehole 1 that was abandoned after reaching the topmost part of the black shale interval. Three additional boreholes were cored as explained in the text Erba et al., 2019b).

Combining the above information and considering the dip measured in individual cores (variable in the range of 60° to 87°), the “stratigraphic thickness” of each lithostratigraphic unit was calculated. The overlapping intervals (i.e. U1-5 and U3-1) were matched and duplications were eliminated. The lithologic log of the composite S1-S3 Sogno Core, in stratigraphic depths (from 1.5 to 26.83 meters), is illustrated in Figure 5. The composite S1-S3 Sogno Core section recovered a complete upper Pliensbachian–lower Toarcian interval, with the S1 Core representing its upper portion, and the S3 Core the lower part.

The following lithostratigraphic units (U1-1 to U1-5, and U3-2 to U3-11, of the S1 and S3 Cores, respectively) are described, from the topmost to the bottommost:

- Unit 1* (1.50 to 4.82 meters): marly limestones, olive-grey in colour. In the upper and lowermost parts of the unit, high concentrations of reddish mottles and sporadic bioturbation are documented.
- Unit 2* (4.82 to 9.54 meters): marly limestones, olive-grey in colour, characterised by intense bioturbation; in particular, the uppermost part of the unit documents the presence of frequent *Planolites*.
- Unit 3* (9.54 to 10.52 meters): marly limestones, grey in colour, are characterised by intense bioturbation. Locally, faintly laminated intervals are observed.
- Unit 4* (10.52 to 11.87 meter): marly limestones with evident and widespread bioturbations; locally, cm-thick black shales and laminated intervals are present.
- Unit 5* (11.87 to 14.55 meters): black shales characterised by evident lamination, especially in the uppermost part, in addition to pyrite nodules. In the lower portion, very little bioturbation is documented.
- Unit 6* (14.55 to 15.93 meters): marly limestones, grey to very dark-grey in colour, with reddish to greyish spots. Bioturbations dimensions increase within this unit and thin esmerald-green laminae are documented.
- Unit 7* (15.93 to 16.86 meters): marly limestones, with variations in colour from grey, to very dark-grey and dark-red. In the lowermost portion, bioturbations and laminations are observed.
- Unit 8* (16.86 to 19.10 meters): marly limestones, dark-red in colour, with sporadic greyish spots.
- Unit 9* (19.10 to 19.45 meters): marly limestones, grey in colour.
- Unit 10* (19.45 to 21.35 meters): marly limestones, grey-brown in colour. This is a disturbed interval comprising a level of pebbly marlstones (between 19.45 and 20.03 m), with partially sliding structures. Sporadic stylolites are present.
- Unit 11* (21.35 to 22.92 meters): marly limestones, grey in colour, characterised by frequent stylolite structures. In addition, two cm-thick black shale intervals are documented at ~ 21.8 and 22 meters, respectively.
- Unit 12* (22.92 to 24.35 meters): marly limestones, alternating in colour from reddish to olive-grey. Sporadic bioturbations and laminations.
- Unit 13* (24.35 to 24.99 metres): marly limestones, reddish-greyish in colour.
- Unit 14* (24.99 to 25.47 meters): marly limestones, light-brown to grey-brown in colour. Small and large (cm-thick) bioturbations are documented. The base of this unit corresponds to the base of the Sogno Fm.
- Unit 15* (25.47 to 26.83 meters): marly limestones, olive-grey to dark-grey in colour. Little bioturbations and frequent stylolite structures are observed. This unit corresponds to the uppermost part of the Domaro Limestone Fm.

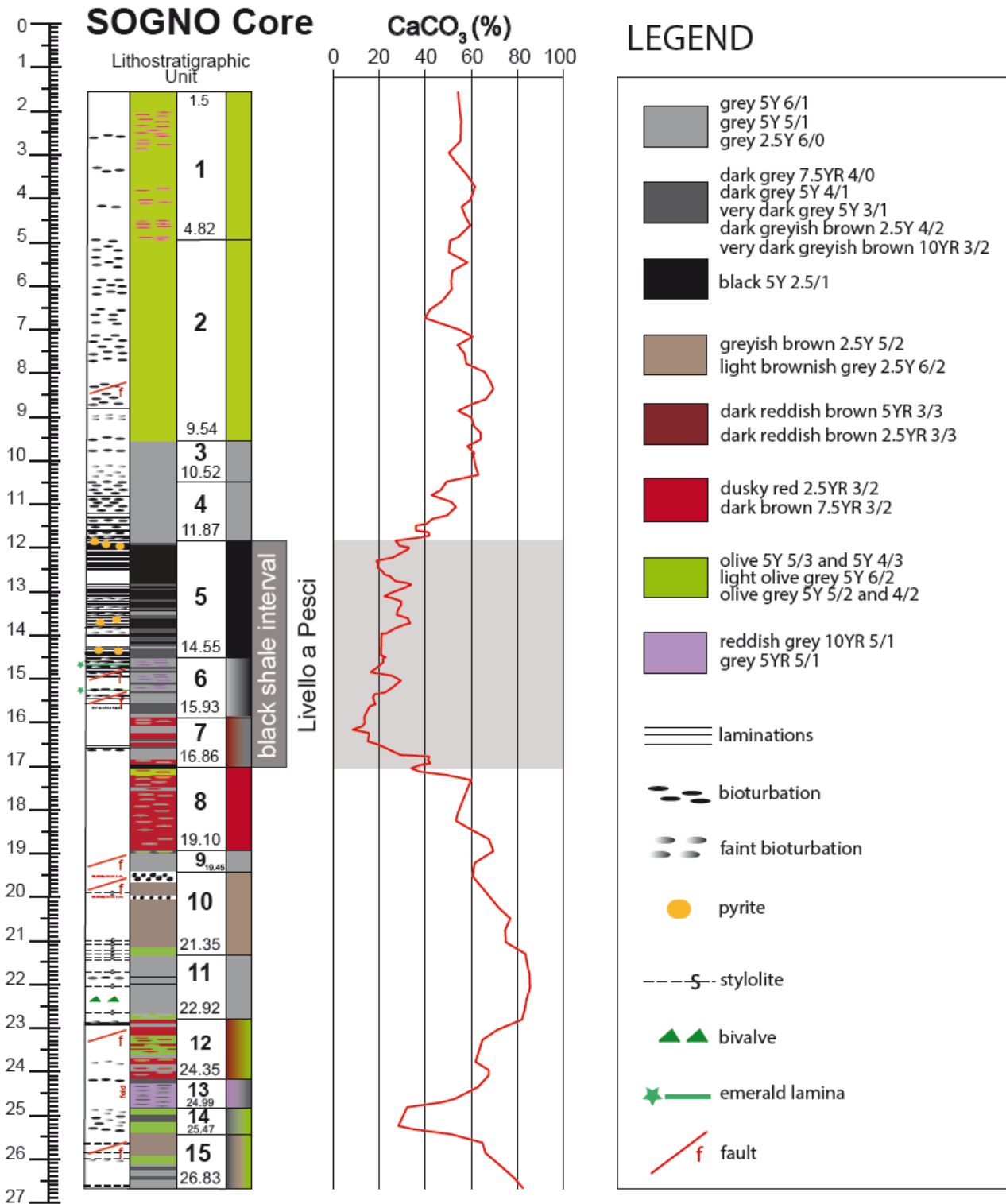


Fig. 4.3 - Lithostratigraphy and calcium carbonate content of the Sogno Core. The grey pattern highlights the Livello a Pesci black shale interval that is the lithostratigraphic record of the T-OAE in the Lombardy Basin (Erba et al., 2019b).

4.2. The L1 and Schandelah Cores.

The Lower Saxony Basin is a highly differentiated sedimentary basin filled with marine, lacustrine, and hypersaline sedimentary rocks of Late Jurassic and Early Cretaceous age (Kockel et al. 1994). It is located at the southern margin of the Central European Basin System and flanks to the north the London-Brabant, Rhenish and Bohemian Massifs. It is superimposed on the Late Carboniferous Variscan foredeep basin and the frontal structures of the Variscan fold belt. The Lower Saxony Basin represents an E-W-striking, highly differentiated Meso-Cenozoic basin (Betz et al. 1987; Baldschuhn et al. 1991; Kockel et al. 1994) and was initiated by rifting and/or thermal subsidence of the lithosphere during the Permian (Senglaub et al. 2006). Continental siliciclastic sediments of the Rotliegendes as well as evaporites and limestones of the Zechstein were deposited (Kästner et al. 2008). During the Late Permian and Early Triassic, the break-up of Pangea (Ziegler, 1990) led to the formation of intracratonic basins in Central Europe. Siliciclastic sediments were deposited during the Early and Late Triassic. Multi- and interdisciplinary studies have demonstrated that the Jurassic successions of the Lower Saxony Basin represent ‘type-sections’ of the Boreal province.

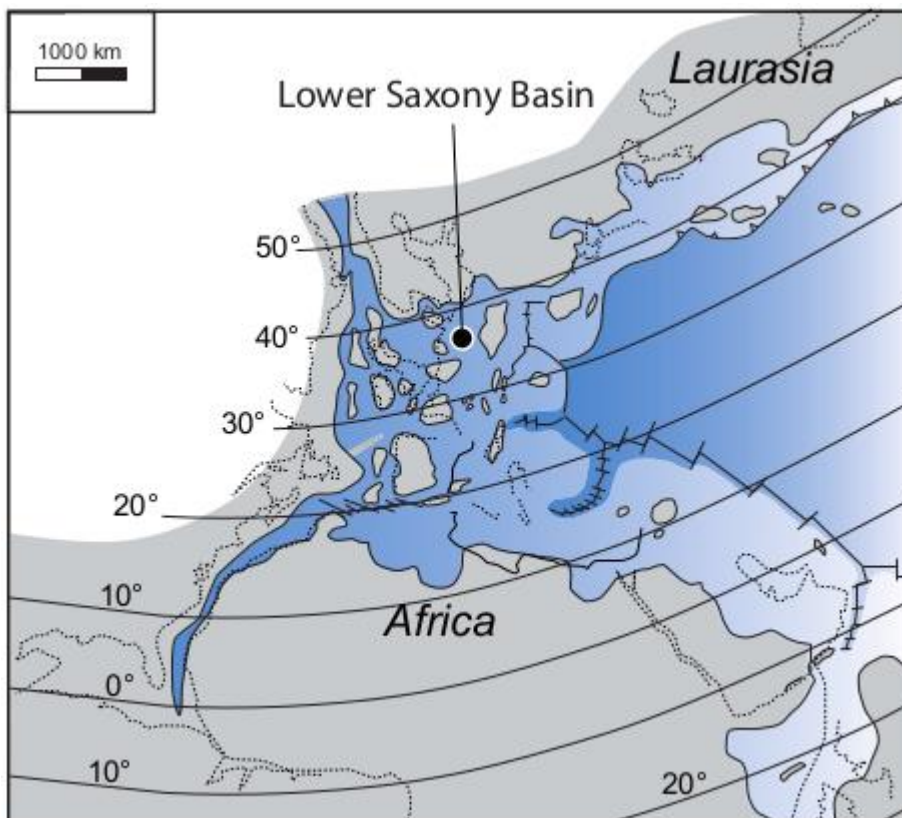


Fig. 4.4 – Paleogeographic reconstruction of western Tethys during the early Toarcian (after Bassoullet et al. 1993) showing the position of the Lower Saxony Basin.

During the Early Jurassic, present-day Europe was located on the broad and extensive Laurussian continental shelf that opened towards the southeast into the deep Tethyan Ocean (Ziegler, 1982). This shallow shelf area contained numerous deeper sub-basins separated by various submarine sills and islands of variable size. All these structural features contributed to episodic restrictions of water circulation across the shallow shelf, especially during periods of sea level lowstand (Frimmel et al., 2004). The Early Toarcian is characterized by an extensive transgressive phase, associated with the breakup of Pangea (Haq et al. 1988; Hallam, 2001) which led to the deposition of organic-rich mudrocks (black shales) across Europe. The lithological expression of black shales in the Lower Saxony Basin is the Posidonia Shale (“Posidonienschiefer” in German) which is present throughout the entire Lower Saxony Basin except for the westernmost part (Kockel et al. 1994).

Two cores were drilled in the Hildesheim-Braunschweig area, close to the villages of Laatzen (L1 Core) and Schandelah (Schandelah Core) in northern Germany (Fig 4.4). Samples from the L1 Core were collected in the core shed of Wintershall-Dea oil company in Wietze (Germany). Samples from the Schandelah Core were collected in the core depository of the Geological Survey of Germany in Berlin Spandau (German Mineral Resources Agency – DERA).

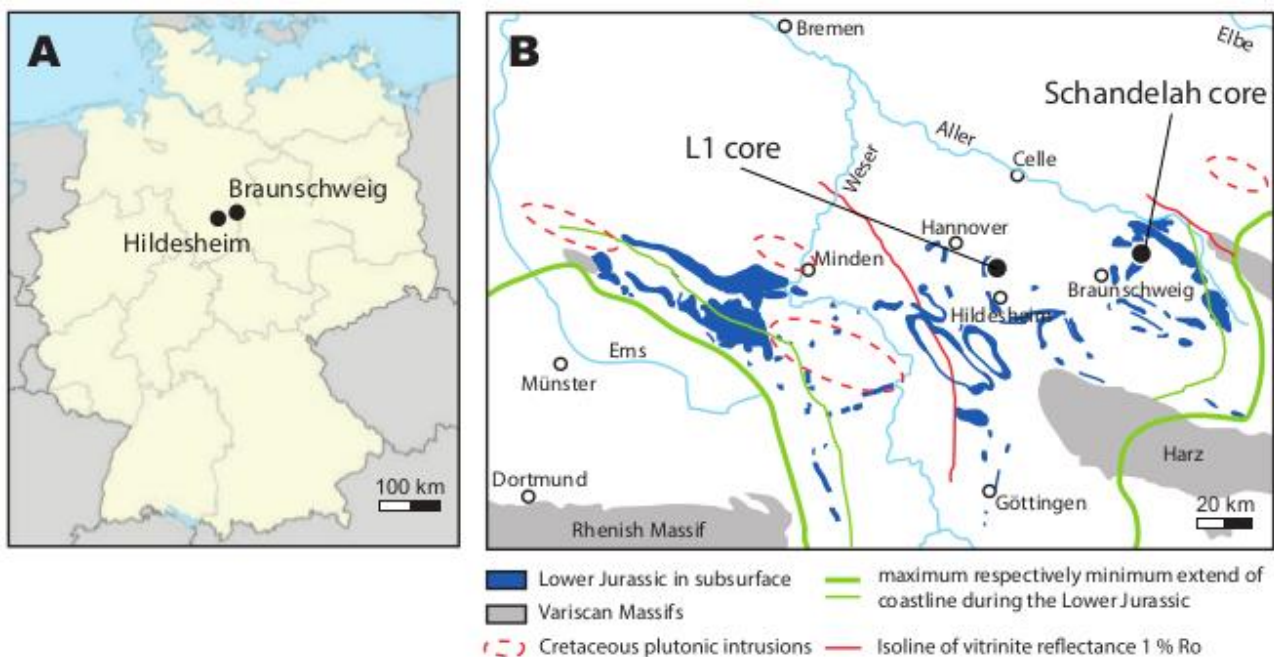


Fig. 4.5 – Location map of the investigated cores (A) Map of Germany with Hildesheim and Braunschweig, the largest towns in the vicinity of L1 and Schandelah. (B) Map of the Lower Saxony with the occurrences of Lower Jurassic sediments showing the position of four Late Cretaceous magmatic intrusions. Locations of the drilled area are provided for the L1 and Schandelah cores. The isoline of vitrinite reflectance for 1% Ro was drawn after Koch and Arnemann (1975) and Teichmüller et al. (1984). (Modified from van de Shootbrugge et al. 2018)

The lithostratigraphy of the L1 and Schandelah Cores are reported in Figs. 4.5 and 4.6, respectively. The studied 16 m of the L1 Core span the interval of the upper Amaltheenton Formation and the lower Posidonienschiefer Formation. The 46.5 m of the Schandelah Core include the upper Amaltheenton Formation, and the lower, middle and upper Posidonienschiefer Formation. A total of eight lithostratigraphic stratigraphic units were recognized, described from bottom to top. Unit 8 (Amaaltheenton Fm.) is represented by dark greenish grey claystone with silty to sandy light brownish grey lenses. Isolated carbonate concretions are detected. Unit 7, corresponding to the lowermost part of the Posidonienschiefer, is constituted by dark brown to black marly claystones and fissile black shales with some isolated carbonate concretions. According to several studies, this portion represents the lithological expression of the T-OAE in the studied cores. The transition between the Amaaltheenton / Posidonienschiefer Formations appears sharp in the L1 core and more gradual in the Schandelah core. Most of the previous authors reported a number of concretionary levels (named after their corresponding ammonite species, e.g. *Siemensi* concretions, *Elegantulum* concretions, *Boreale* concretions) from the base of the Toarcian. Some concretionary levels were found within units 7 and 8 in both cores (Figs. 4.5, 4.6). Nevertheless, it is hardly possible to combine each concretion to the ammonite zone for the lack of a reliable ammonite zonation for our material. Units 6 and 4 yield light grey limestone intervals. Units 5 and 3 represent medium brown bituminous clay marlstones and Unit 2 consists of light grey limestones including the “Monotis Bank” (or Monotis - *Dactylioceras* Bed). This regional marker bed (Schmitz, 1980) displays a peculiar wavy lamination. It shows a conspicuous shell accumulation mainly from left valves of the bivalve *Meleagrinnella substriata* and local accumulations of the ammonite *Dactylioceras athleticum* (Arp and Gropengießer, 2016). Unit 1, recovered exclusively in the Schandelah core, represents an undisturbed sequence of medium brown bituminous organic-rich marly claystones (“Posidonienschiefer”-style facies, i.e. paper shales). Several macrofossils were found within this unit. (e.g. fish remains, bivalves, ammonites, belemnites).

Core L1

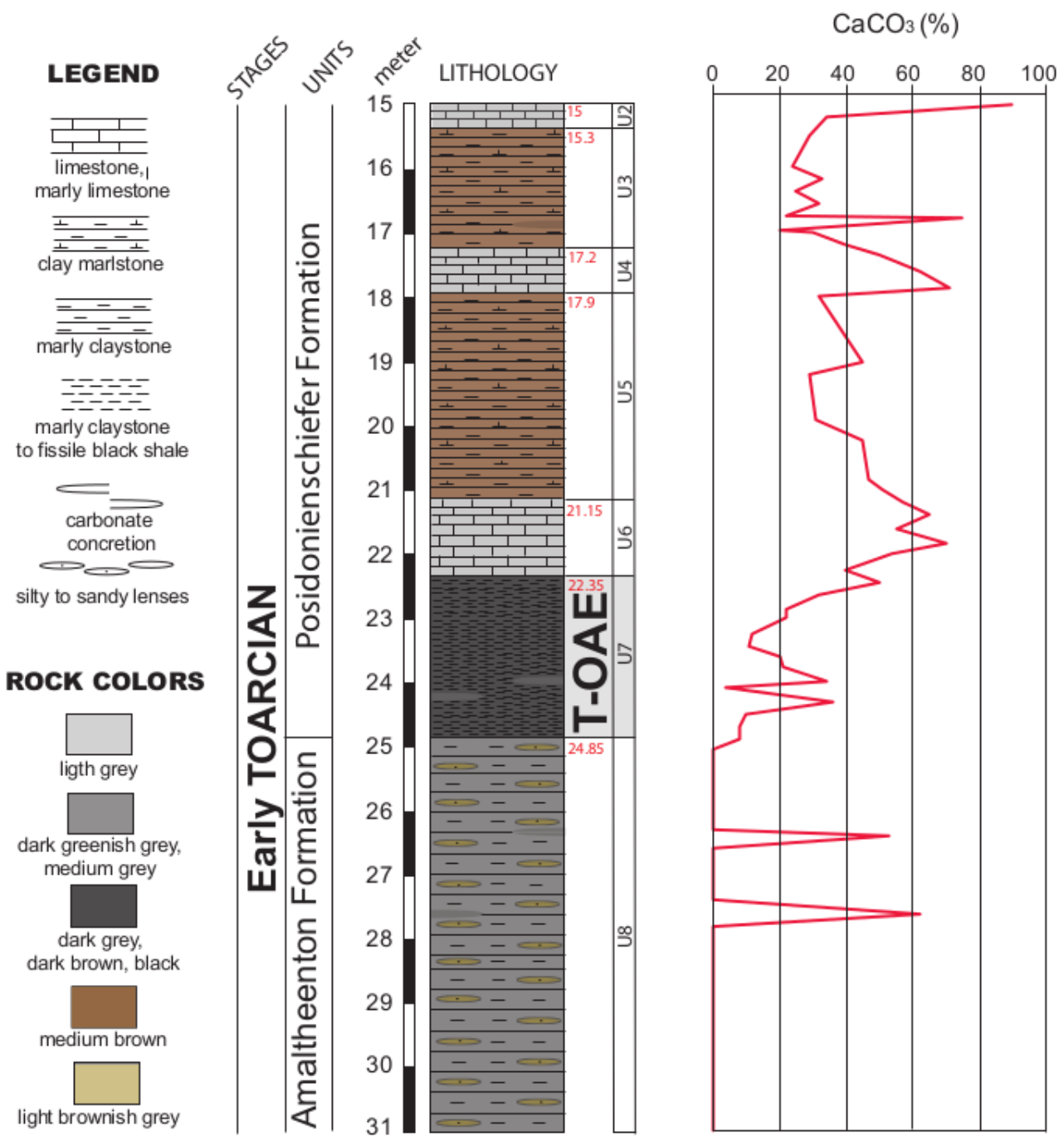


Fig. 4.6 –

Lithostratigraphy and calcium carbonate content of the L1 Core.

Core Schandelah

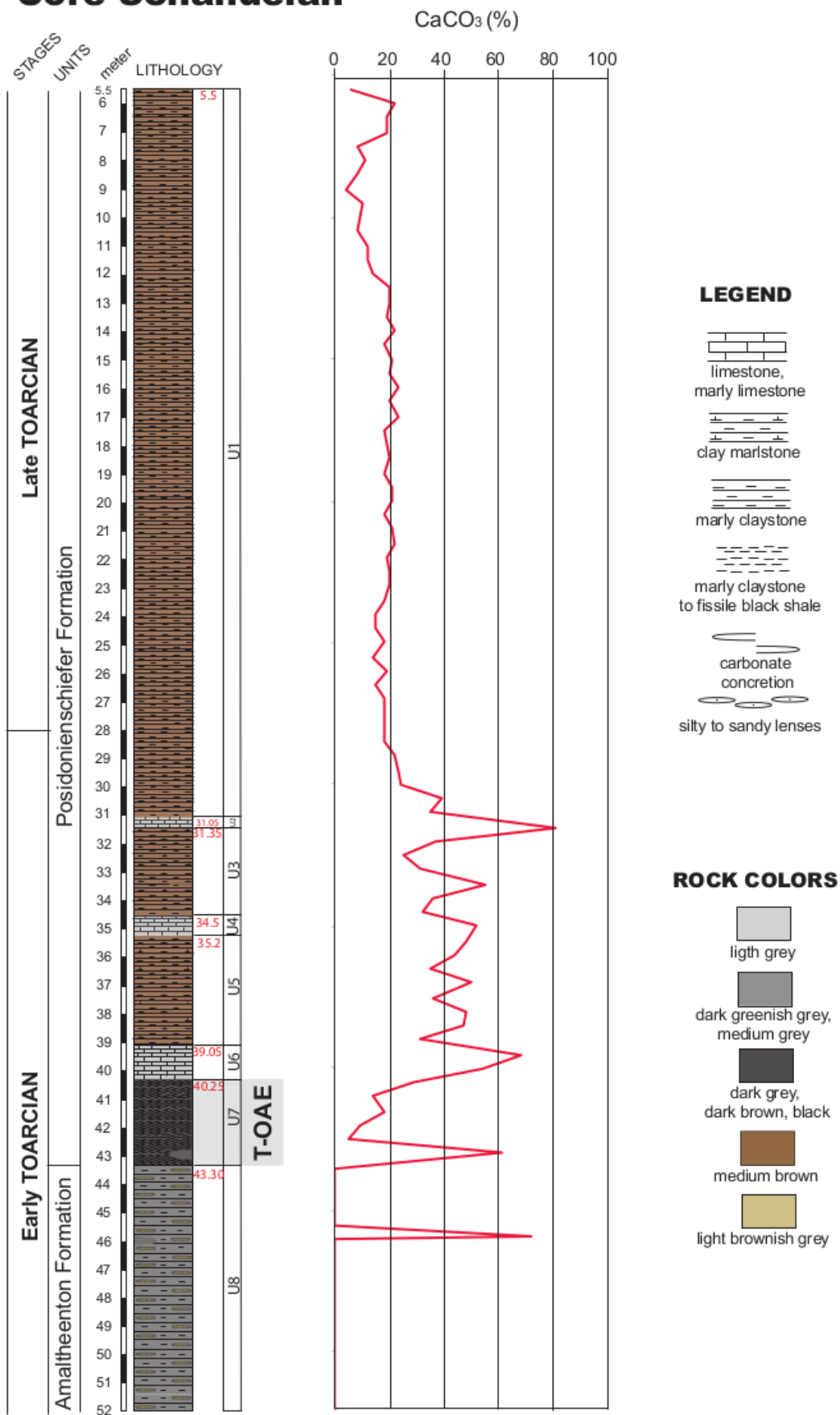


Fig. 4.6 – Lithostratigraphy and calcium carbonate content of the Schandelah Core.

Chapter 5

Materials and Methods

Sample preparations for biostratigraphy were performed both at the Earth Sciences Department Labs of the University of Milan and at the Geologie, Mineralogie & Geophysik Department Labs of Ruhr-Universität Bochum. Carbon isotope analyses of organic carbon (exclusively for the L1 and Schandelah Cores) were performed at the GeoZentrum Nordbayern, Friedrich-Alexander Universität Erlangen-Nürnberg.

5.1. Sample preparations techniques

Sogno Core

A total of 154 samples were selected for calcareous nannofossil biostratigraphy. The average sampling rate adopted is 12 cm: the lowermost 9 m and the uppermost 10 m are characterized by a less resolutive sampling rate, whereas the Fish Level was sampled every 6 cm. Collected samples were prepared from marly limestones and limestones of the Domaro Lmst. and marlstones, limy marlstones, marly claystones and black shales of the Sogno Fm. Smear slides preparation consists of the following steps: a) a small amount of sediment is chopped off and dried in an oven for 24 hours at 50 °C; b) 10-50 mg of sediment is selected and weighted using a microbalance (Mettler AE 260 with a precision of 10^{-6} g); c) after adding a small amount of water, the sample is ultrasonicated until all particles are in suspension. Generally, normal tap water buffered with NH_3 (pH 8.5) to prevent etching with a small amount of Triton X100 detergent are added to remove surface tension; d) the suspended sample is transferred to a volumetric flask and diluted to 1000cm^3 . Afterwards the suspension is homogenized by a magnetic stirrer for several minutes followed by 4 inversions of the flask; e) the suspension is poured into the settling device and left to settle for 24 hours; f) the water is drained carefully, once the remaining water on the cover slide has air dried the slides are mounted; g) the device is cleaned thoroughly after each usage in order to avoid contamination.

L1 and Schandelah Cores

Calcareous nannofossil biostratigraphy was performed on a total of 168 samples: 73 samples were collected from the upper Amaltheenton Fm. / lower Posidonienschiefer Fm. of the L1 Core and 95 samples were selected from the upper Amaltheenton Fm. / lower-middle Posidonienschiefer Fm. of the Schandelah Core. The sampling resolution varies between 1 sample/20 cm for the L1 Core (Units 1, 2, 3, 4, 6, 7 and 8) to 1 sample/50 cm (Unit 5) and 1 sample/50 cm for the Schandelah Core. Simple smear slides were prepared following the method of Bown and Young (1998): a small amount of rock material was powdered adding few drops of bi-distillate water, without centrifuging, ultrasonic cleaning or settling the sediment in order to retain the original composition. The obtained suspension was mounted onto a slide, covered with a cover slide and fixed with Norland Optical Adhesive.

Carbon isotope analyses of organic carbon were performed on the same samples selected for biostratigraphy with a Flash EA 2000 elemental analyser connected online to ThermoFinnigan Delta V Plus mass spectrometer. All carbon isotope values were calibrated to the V-PDB (Vienna-PDB) standard. Accuracy and reproducibility of the analyses were checked by replicate analyses of laboratory standards calibrated to international standards USGS 40 and 41. A schematic synthesis of investigated cores with related number of samples and applied technique and investigation is provided in Tab. 5.1. Different techniques were applied according to trivial investigations performed in the Lombardy Basin (e.g. Casellato and Erba, 2015) and in the Lower Saxony Basin (e.g. Van de Schootbrugge et al. 2018).

CORE	SAMPLES	TECHNIQUE	INVESTIGATION
SOGNO	154	Settling slides	Semiquantitative (6 cross sections)
L1	73	Standard smear slides	300-specimen counting + Semiquantitative (8 cross sections)
SCHANDELAH	95	Standard smear slides	300-specimen counting + Semiquantitative (8 cross sections)

Tab. 5.1 – Schematic synthesis of investigated cores, number of samples, applied technique and investigation.

5.2. Nannofossil preservation and abundance analysis

Sogno Core

Settling smear slides were investigated using a light polarizing microscope, Leica DM 2700 P, at 1250X magnification. The preservation of calcareous nannofossils was evaluated using the visual criteria of Roth and Thierstein (1972) and Roth (1983). These criteria include etching (E) and overgrowth (O) with E1-O1 standing for minor, E2-O2 for moderate and E3-O3 for major etching-overgrowth. See Fig. 5.1 for further details. Calcareous nannofossil abundances were evaluated by examining at least 6 longitudinal cross-sections, corresponding to 750 fields of view, in each smear slide. Calcareous nannofossil taxa recognized are listed in Appendix A. The range chart is reported in Appendix D.

L1 and Schandelah Cores

Smear slide were examined using a Leica DM 2700 P light polarizing microscope with a magnification of 1250X. The preservation of calcareous nannofossils was evaluated using the visual criteria of Roth and Thierstein (1972) and Roth (1983) (Fig. 5.1.). At least 300 determinable nannofossil specimens were counted in each slide. Additional 8 cross-sections, corresponding to 1000 fields of view, were investigated for rare species. Several samples belonging to the Amaltheenton Fm. are barren, others contain extremely rare abundances of specimens (less than 10 specimens in 1000 fields of view). In these, the 300-specimen counting was not possible. Vertical distribution of taxa is reported in Appendix E.

ETCHING	DESCRIPTION
E1	<u>slight etching</u> : many coccolith show serrate outlines; delicate structures have been somewhat affected by dissolution but are generally preserved.
E2	<u>moderate etching</u> : the more delicate species have been preferentially dissolved; delicate central structures have been destroyed in many specimens; irregular outlines of shields are common.
E3	<u>strong dissolution</u> : salmpe contains mainly dissolution-resistant species, more delicate forms are very rare; nannofossil fragments are abundant.
OVERGROWTH	DESCRIPTION
O1	<u>slight overgrowth</u> : irregular secondary growth of crystallites and slight thickening of central area structures.
O2	<u>moderate overgrowth</u> : delicate central structures are frequently overgrown to a degree that makes them difficult to be recognized; irregular growth of crystallites in common.
O3	<u>strong overgrowth</u> : delicate species are often so much covered with secondary calcite that identification is nearly impossible.
notes	frequently slight to moderate etching and slight to moderate overgrowth has been observed in the same sample, which might be indicative of secondary overgrowth on larger forms at the expense of the delicate/tiny ones.

Fig. 5.1 – Calcareous nannofossil preservation scheme adopted in this thesis (after Roth, 1983).

Chapter 6

Taxonomic notes

6.1. General taxonomic observations

In the present thesis all the taxonomic notes pointed out by Casellato and Erba (2015) have been confirmed and all the morphotypes described have been detected except for *Rucinolithus* sp. ind.

Specifically, regarding the species *Crepidolithus crassus*, the specimens characterized by a length $< 5 \mu\text{m}$ and width $< 3.5 \mu\text{m}$ were grouped as “small *C. crassus*”. As far as *M. jansae* is concerned, specimens with thickness of outer elements $< 1 \mu\text{m}$ displaying bright white to yellow colours were attributed to “thin *M. jansae*”.

Within the species *Schizosphaerella punctulata* three morphotypes were separated: *S. punctulata*, “small *S. punctulata*” and “encrusted *S. punctulata*”. Taxonomic distinction between *S. punctulata* and “small *S. punctulata*” is based on the diameter, namely $> 7 \mu\text{m}$ for the former whereas $< 7 \mu\text{m}$ for the latter. “Encrusted *S. punctulata*” is distinguished for the presence of a fringing crust of radiating prismatic crystals surrounding the specimens. A diagenetic origin of such crusts is not questioned (Kälin, 1980; Kälin and Bernoulli, 1984). Nevertheless, as already stated by Casellato and Erba (2015) our observations further confirm that diagenetic processes affect exclusively specimens with diameter $> 7 \mu\text{m}$ (*S. punctulata*).

In the Sogno Core all these morphotypes were recognized. In the L1 and Schandelah Cores “small *C. crassus*”, both morphotypes of *M. jansae* and “encrusted *S. punctulata*” were not observed.

Additional remarks concerning morphometric variations of a few taxa are discussed as observed under the light polarizing microscope.

Genus *Biscutum* Black in Black and Barnes, 1959

Biscutum finchii (Crux, 1984) Bown, 1987b

Remarks. This species was introduced by Crux (1984) and subsequently emended by Bown (1987b). De Kaenel and Bergen (1993) and Mattioli (2004b) proposed the inclusion of *B. finchii* within the genus *Similiscutum* because of the unicyclic distal shield structure. Cobianchi (1990; 1992) and Picotti and Cobianchi (1996) distinguished specimens characterized by a distal shield length $< 6 \mu\text{m}$ as *B. aff.*

B. finchii and “small *B. finchii*”, respectively. Later, Casellato and Erba (2015) detected specimens smaller than the holotype (5.6 µm length – 4.7 µm width) with a subcircular outline and a prominent distal shield. These were grouped by the authors as “small *B. finchii*” similarly to previous authors. The “small *B. finchii*”, as defined by Casellato and Erba (2015) were detected also in the Sogno Core. During my investigations, specimens bigger than the maximum range reported for *B. finchii* (7.0 µm length) were observed in the L1 and Schandelah Cores and were separated as “large *B. finchii*”. This morphotype possibly corresponds to *S. giganteum* observed by Maillot et al. (2006), Ferreira et al. (2015) and da Rocha et al. (2016; fig.7.9) for the Peniche and Rabaçal sections and to *S. aff. S. finchii* “large” reported by Kafousia et al. (2014) and Menini et al. (2018; pl. 2) for the Toka, La Almunia and St. Nicolas sections.

Stratigraphic observations. Specimens of “small” *B. finchii* and *B. finchii* co-occur, although sporadically, throughout the Sogno Core. Specimens of *B. finchii* are generally more abundant than the smaller ones. In the L1 and Schandelah Cores, the smaller morphotype was not detected. In these cores, *B. finchii* and “large” *B. finchii* appear consistently from the base of the Posidonienschiefer Fm. and both disappear soon after, within the NJ6 Zone. In both L1 and Schandelah Cores the larger morphotype disappears slightly before than the standard one.

6.2. Taxonomic revision of genus *Carinolithus*

The genus *Carinolithus*, which originated in the earliest Toarcian, is represented by four species, namely *C. superbus* (Bown, 1987), *C. magharensis* (Bown, 1987), *C. cantaluppii* (Cobianchi, 1990) and *C. poul nabronei* (Mattioli, 1996). The first occurrence (FO) of *C. superbus* marks the inception of the NJT6 and NJ6 zones in the standard biozonation schemes proposed for the Tethyan (Mattioli and Erba, 1999) and Boreal (Bown, 1987; Bown et al. 1988; Bown and Copper, 1998) realms, respectively. Furthermore, this biohorizon is calibrated with the onset of the T-OAE at a supraregional scale (Mattioli et al. 2004; Casellato and Erba, 2015). The FOs of *C. magharensis*, *C. cantaluppii* and *C. poul nabronei* are not used as zonal/subzonal markers in the zonal schemes but rather as additional events.

The genus *Carinolithus*, was initially established as *Rhabdolithus* by Deflandre in Deflandre and Fert (1954). In the same work, the author introduced the species *R. sceptrum*, *R. superbus* and *R. clavatus* (Fig. 6.1.). Later, Prins in Grün et al. (1974) established the genus *Carinolithus* and revised the previous species as *C. sceptrum*, *C. superbus* and *C. clavatus*. Bown (1987) interpreted *C. clavatus* and *C. sceptrum* as variants of *C. superbus*, in the same way *C. clavatus* was considered an incomplete *C. superbus* without the distal shield whereas *C. sceptrum* is thought to be the consequence of a dimorph

or intraspecific variation. Consequently, the species *C. clavatus* and *C. sceptrum* were rejected. Species *C. magharensis* was initially included in genus *Hexalithus*, established by Gardet (1955). Moshkovitz and Ehrlich (1976) established the species *H. magharensis* that Bown (1987) emended as *C. magharensis* (fig. 6.1). *C. cantaluppii* and *C. poul nabronei*, were established by Cobianchi (1990) and Mattioli (1996), respectively (Fig. 6.1).

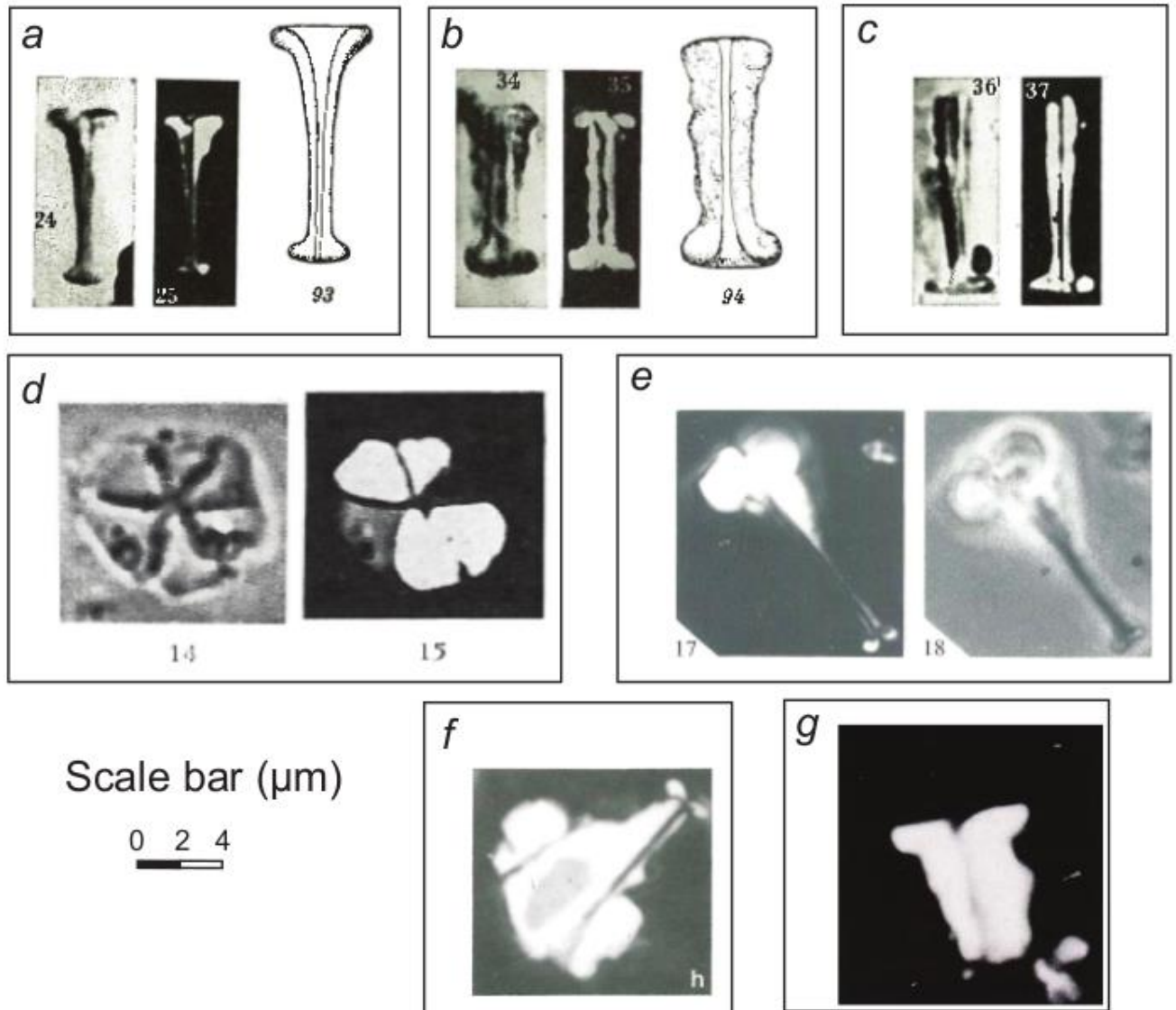


Fig. 6.1 – Holotypes of *R. sceptrum* (a), *R. superbus* (b), *R. clavatus* (c), *H. magharensis* (d), *C. cantaluppii* (f) and *C. poul nabronei* (g). A specimen of *C. magharensis* as emended by Bown (1987) is also reported (e).

Both species are characterized by diagnostic characters that cannot be confused with other species whereas the taxonomy of *C. superbus* and *C. magharensis* can be revised. According to Bown, (1987) the two taxa are well discriminated if detected in distal view (DV) as the number of wedge-shaped

elements forming their distal shield is ten to twelve in *C. superbus* and six in *C. magharensis*. Taxonomic incongruity emerges when the nannoliths are detected in side view (SV). Bown (1987) observed that the distal shield of *C. magharensis* flares sharply (roughly at right angles) from the stem and has a rectangular shape whereas that of *C. superbus* flares more gradually.

In this thesis morphometric analyses were applied to *C. superbus* and *C. magharensis* specimens in order to clarify their taxonomy. Moreover, a detailed study of diagenetic modifications was conducted to ascertain morphological variations derived from overgrowth/etching. In particular, 50 specimens of *C. cantaluppii* were qualitatively investigated to assess the potential role of diagenesis on its morphology. Four pictures were taken for each specimen, both with and without quartz lamina, both at 0° and 45° to the polarizers.

A total of 100 specimens belonging to the *C. superbus* and *C. magharensis* groups were investigated for morphometric analyses. A total of 63 images were selected from published works (Appendix C) complemented with 37 additional specimens that were digitally photographed from new sampling of sections in the Tethys Ocean: the Sogno Core (Lombardy Basin, Northern Italy) and the Breggia section (Lombardy Basin, Southern Switzerland). Smear slides were prepared with the random settling technique (Giesen et al. 1999) for the Sogno Core and standard technique (Bown and Young, 1998) for the Breggia section. Photographs were acquired using a Leitz Laborlux optical polarizing light microscope at 1250X magnification and a digital camera. Images were then analysed using a PC with Q-capture Pro suite software adapted for nannofossil analyses. Measurements were taken using ImageJ software, with an error of measurements of $\pm 0.08 \mu\text{m}$. Six parameters were measured for each taxon: the Total Height (TH); the Height without proximal and distal shields (H); the Stem Width (SW); the Proximal Shield diameter (PS); the Distal Shield diameter (DS) and the Thickness of the Distal Shield (TDS) as reported in Fig. 6.2. In certain specimens some parameters were excluded from measurement because they were not in top view or were broken or heavily overgrown. A total of 341 measurements were obtained: 29 for the TH, 29 for the H, 75 for the SW, 29 for the PS, 100 for the DS, 79 for the TDS.

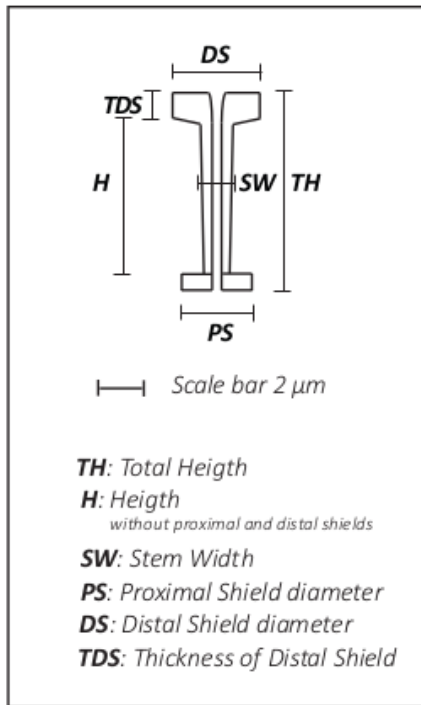


Fig. 6.2 – Schematic illustration of a *Carinolithus* specimen in side view.

Statistical parameters like mean, mode, median, standard deviation and 95% confidence level were calculated using the Matlab and PAST softwares. Moreover, a mixture analysis was run, using PAST software (Hammer et al. 2001), in order to find the overall mixing proportions of specimens belonging to different taxa. This statistical analysis is a maximum-likelihood method for estimating the parameters (mean, standard deviation and proportion) of two or more univariate normal distributions, based on a pooled univariate sample (Hammer and Harper, 2006).

Results - morphometry

In fig. 6.3, the results for each investigated parameter (TH, H, SW, PS, DS and TDS) are illustrated: blue dots refer to specimens belonging to the *C. superbis* group whereas red dots refer to those included in the *C. magharensis* group. Based on the DS and TDS two different-sized groups of nannoliths are distinguished. As far as the DS is concerned, one group of specimens ranges from 2.8 to 6.8 μm whereas the latter from 7.8 to 10.9 μm . The bigger-sized group is totally represented by specimens of the *C. magharensis* group whereas the smaller-sized from nannoliths of both groups. Regarding the TDS, the first group varies from 0.4 to 1.5 μm whereas the second one from 7.8 to 10.9 μm . This latter bigger-sized group entirely consists of specimens belonging to the *C. magharensis* group while the former smaller-sized comprises specimens of the *C. superbis* group.

Parameters like TH, H and PS display a more homogeneous trend and no different-sized groups are detected. Nevertheless, diagrams show *C. magharensis* group mainly occupies higher values of TH and H and lower of PS. Mode, median, mean and standard deviation are provided in tab. 6.1 for each parameter by considering a) all the investigated specimens; b) specimens of the *C. magharensis* group; c) specimens of the *C. superbis* group.

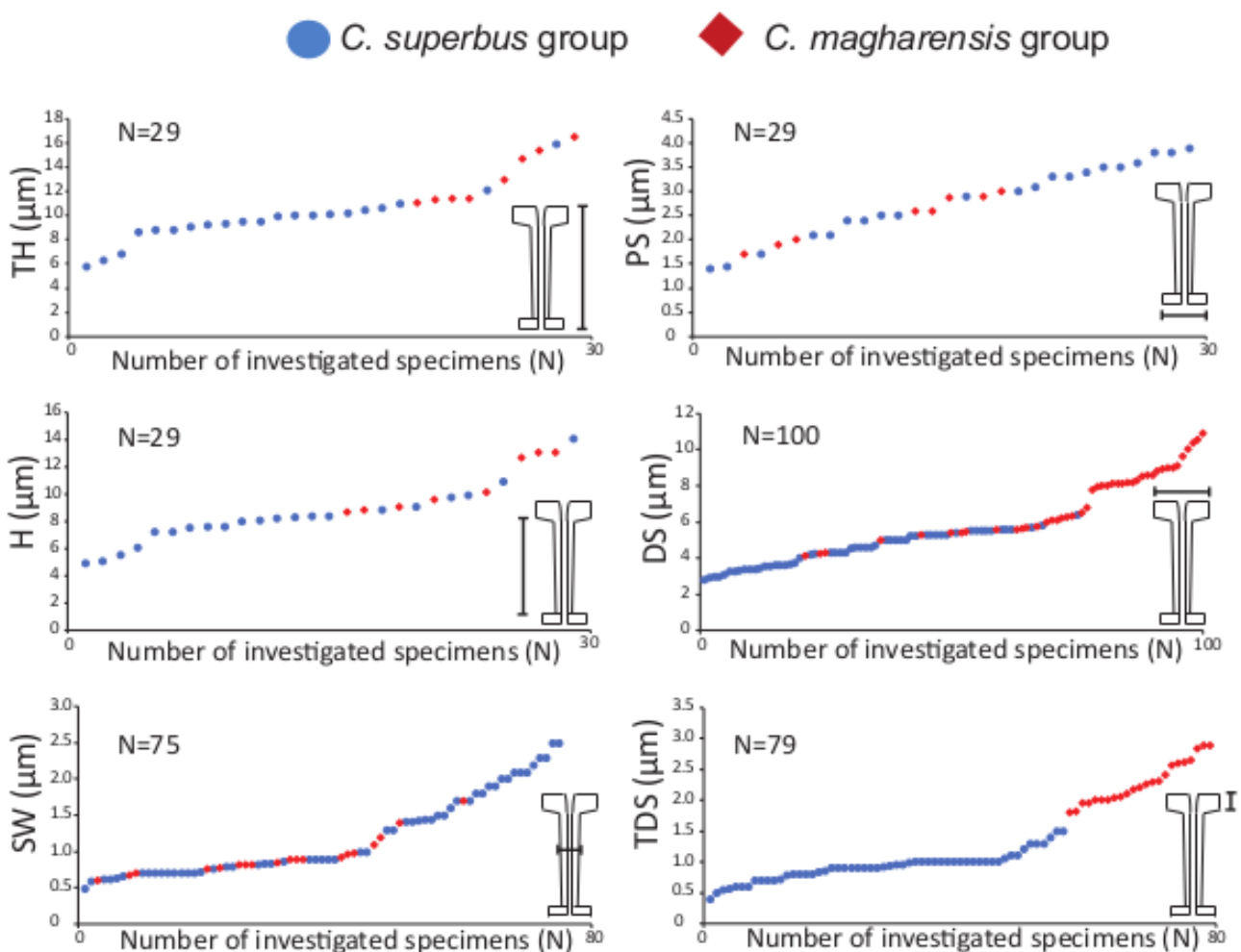


Fig. 6.3 – Size values of each measured specimens for every parameter: TH, H, SW, PS, DS, TDS. Blue dots indicate specimens of the *Carinolithus superbus* group whereas red diamonds represent specimens of the *Carinolithus magharensis* group. The number of specimens measured (N) for each taxonomic character is indicated.

	TH	H	SW	PS	DS	TDS
a						
	Total specimens					
Number of specimens	29	29	75	29	100	79
Mode (µm)	8.80	8.40	0.70	1.70	5.00	1.00
Median (µm)	10.10	8.40	0.90	2.87	5.40	1.00
Mean (µm)	10.58	8.83	1.17	2.73	5.71	1.32
Standard deviation	2.61	2.30	0.55	0.73	1.97	0.67
b						
	<i>Carinolithus magharensis</i> group					
Number of specimens	8.00	8.00	19	8	44	23
Mode (µm)	11.40	/	0.90	/	8.10	2.00
Median (µm)	12.19	9.89	0.90	2.59	7.88	2.20
Mean (µm)	11.65	10.66	0.94	2.44	7.28	2.28
Standard deviation	2.17	1.97	0.26	0.51	1.81	0.34
c						
	<i>Carinolithus superbus</i> group					
Number of specimens	21	21	56	21	56	56
Mode (µm)	8.80	8.40	0.70	2.40	5.00	1.00
Median (µm)	9.50	8.10	0.95	3.00	4.60	0.93
Mean (µm)	9.62	8.13	1.25	2.84	4.47	0.92
Standard deviation	2.08	2.05	0.59	0.78	0.95	0.23

Tab. 6.1. – Number of specimens, mean, median, mode and standard deviation of measured taxonomic characters (TH, H, SW, PS, DS, TDS): a) all specimens; b) *C. magharensis* group (red); c) *C. superbus* group (blue).

The Pearson's correlation coefficient was calculated for each pair of parameters and illustrated in Fig. 6.4. A positive Pearson's correlation coefficient ($r > 0$) was obtained for TH/H, TH/DS, TH/TDS, H/PS, H/DS, H/TDS, SW/PS, SW/DS, PS/DS, DS/TDS. A negative Pearson's correlation coefficient ($r < 0$) characterize TH/SW, TH/PS, H/SW, SW/TDS, PS/TDS. These results suggest a strong and positive correlation existing for TH/H ($r = 0.97$), DS/TH ($r = 0.69$), TDS/TH ($r = 0.66$), DS/H ($r = 0.61$), TDS/H ($r = 0.5$), TDS/DS ($r = 0.64$).

The Pearson's correlation coefficient was also calculated separately for the *C. magharensis* and *C. superbus* groups in each diagram. Regarding the former, significant values are obtained for TH/H ($r = 0.97$), TH/TDS ($r = 0.64$), SW/PS ($r = 0.93$), SW/DS ($r = 0.87$), PS/DS ($r = 0.8$). As far as the latter group is concerned, a strong correlation is obtained for TH/H ($r = 0.97$), TH/DS ($r = 0.62$), H/DS ($r = 0.51$). A clear distinction between the two groups is evidenced only for the TH/TDS, H/TDS, SW/TDS, PS/TDS, and DS/TDS ratio, as illustrated by the red and blue clouds.

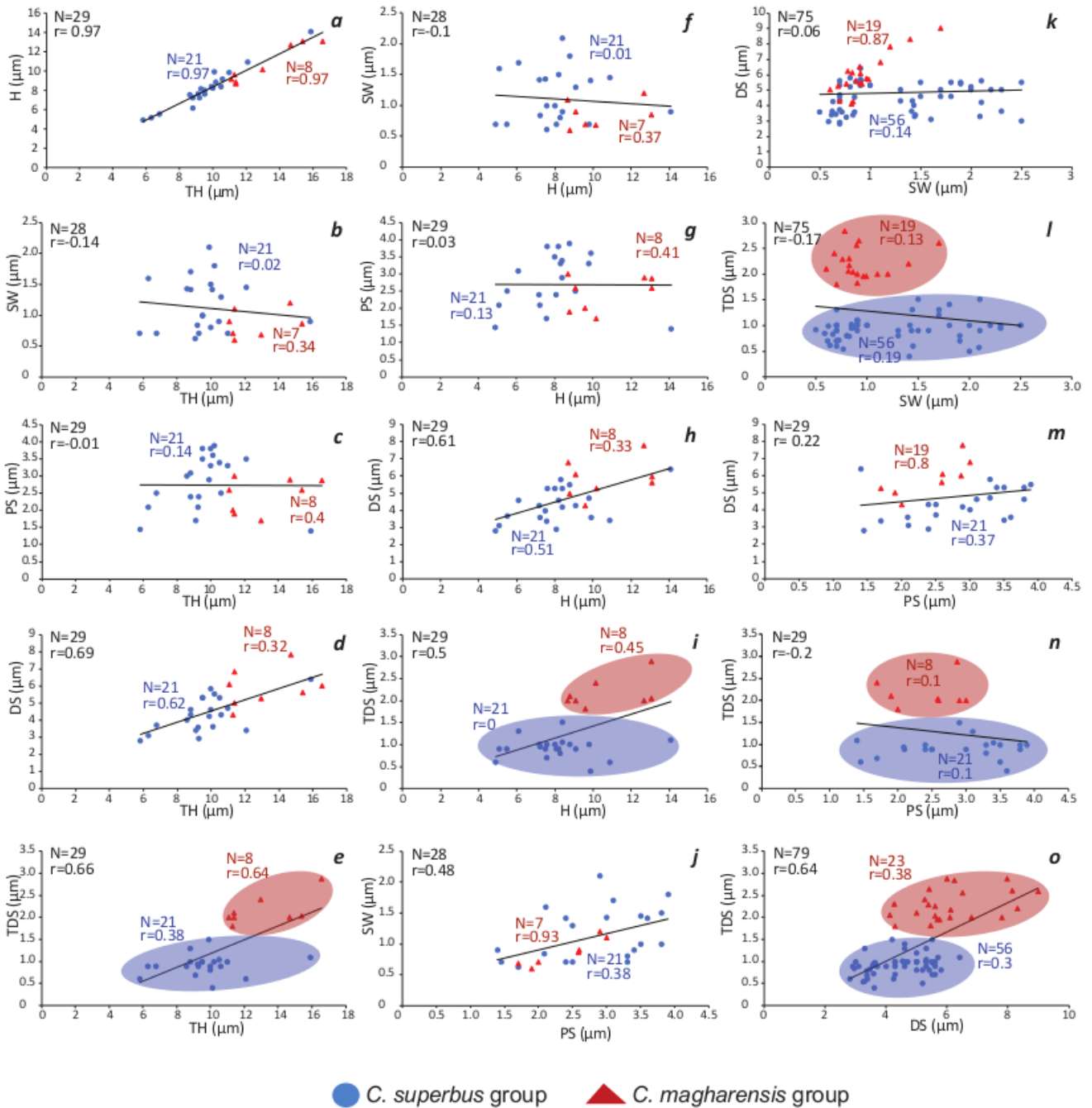


Fig. 6.4. – Scatter plots of the measured parameters: a) plots between TH and H; b) TH and SW; c) TH and PS; d) TH and DS; e) TH and TDS; f) H and SW; g) H and PS; h) H and DS; i) H and TDS; j) SW and PS; k) SW and DS; l) SW and TDS; m) PS and DS; n) PS and TDS; o) DS and TDS for all measured specimens. The Pearson's correlation coefficients (r), the linear regression line, the number of measured specimens (N) are shown for the total measured specimens (black), for *C. magharensis* (red) specimens and for *C. superbus* (blue) specimens.

Morphometric analyses turned out to be an excellent tool to discriminate between the *C. magharensis* and *C. superbus* groups. In particular, TDS clearly separates specimens of the two groups.

Further subdivisions within the two groups are based on the DS and SW, as shown by histograms reported in Fig. 6.5. In fact, the DS (Fig. 6.5a) discriminates 23 nannoliths with a DS varying from 7.8 to 10.9 μm from a group of 77 specimens with a DS spanning from 2.8 to 6.8 μm . The group of specimens with a DS of 7.8 to 10.9 μm corresponds large *C. magharensis* (= *H. magharensis*).

Within the group of specimens with DS of 2.8 - 6.8 μm , the TDS separates two clusters (Fig. 6.5b). One cluster includes 56 specimens characterized by a TDS ranging from 0.4 to 1.5 μm and a second one grouping 18 specimens with a TDS varying from 1.8 to 2.9 μm . The TDS is therefore diagnostic to separate *C. magharensis* (sensu Bown, 1987) with a thicker distal shield relative to *C. superbus* with a thinner distal shield.

A further subdivision was obtained using the SW to specimens with DS of 2.8 - 6.8 μm (Fig. 6.5a) and TDS of 0.4 - 1.5 (Fig. 6.5b): a group includes 30 specimens characterized by a SW spanning from 0.5 to 1.0 μm and another cluster contains 26 nannoliths with a SW varying from 1.3 to 2.5 μm . Therefore, within *C. superbus*, the SW separates thin and thick morphotypes.

In conclusion, morphometric analyses allowed the identification of *C. magharensis sensu strictu*, small *C. magharensis*, thin *C. superbus* and thick *C. superbus*.

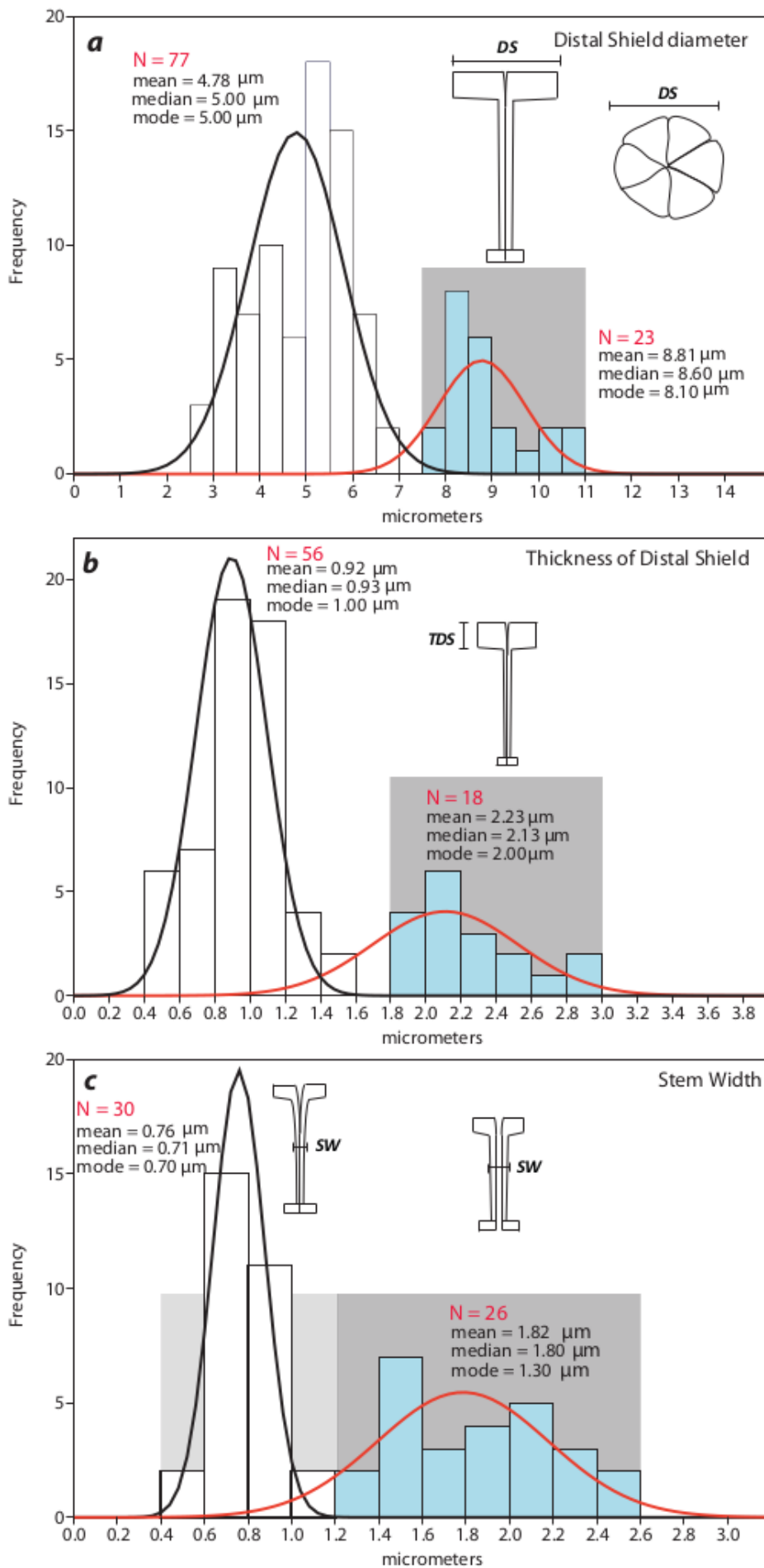


Fig. 6.5. – Results of mixture analysis of samples containing in a) *C. magharensis sensu strictu*; b) small *C. magharensis*; c) thin *C. superbus* and thick *superbus* with estimated means, median and mode and number of analysed specimens (N). See text for further details.

The holotype of *H. magharensis* established by Moshkovitz and Ehrlich (1976) has a DS of 8 μm and the group with the DS of 7.8-10.8 μm is fully consistent with the original definition of the species. Since Wiegand (1984) and Bown (1987) documented that hexaliths of genus *Hexalithus* and detached distal shields of *Carinolithus* specimens, we maintain the name *C. magharensis* for these large morphotypes being the holotype of Moshkovitz and Ehrlich (1976; pl. 8; figs 14-15) the distal shield in distal view.

The group of specimens possessing a DS smaller than 6.8 μm and a TDS of 1.8-2.9 μm is attributed to *C. magharensis* sensu Bown (1987) who described a DS varying from 4.5 to 5.9. We, therefore, propose to separate the new species *C. premagharensis* maintaining the holotype of Bown (1987; pl. 14; Fig. 17, 18).

Within the *C. superbus* group, having the smaller TDS and DS, two clusters are clearly distinguishable based on the SW. Specifically, specimens with SW < 1.0 μm are consistent with the original description of *R. superbus*, whereas specimens with SW > 1.3 μm are consistent with the original description of *R. sceptrum*. In fact, the holotype of *R. superbus* (Deflandre in Deflandre & Fert, 1954; figs 24, 25) has a SW of 0.7 μm and the holotype of *R. sceptrum* (Deflandre in Deflandre & Fert, 1954; figs 34, 35) has a SW of 1.4 μm . We agree with Bown (1987) in considering *C. superbus* and *C. sceptrum* as species included in the genus *Carinolithus* and separates here the subspecies *C. superbus superbus* and *C. superbus sceptrum*.

Recently, Ferreira et al. (2019) documented specimens of *C. superbus* characterized by a thinner and longer stem named as “*C. superbus* thin and long”. In the same work the authors made a distinction between *C. magharensis* and “large *C. magharensis*”. The qualitative taxonomic subdivision adopted by Ferreira et al., (2019) is consistent with our results: their *C. superbus* corresponds to *C. superbus sceptrum*, *C. superbus* “thin and long” corresponds to *C. superbus superbus*, their *C. magharensis* is consistent with *C. premagharensis* whereas their *C. magharensis* “large” is analogous to the species here emended as *C. magharensis*.

Fig. 6.6 summarizes the morphometric data of the holotype and specimens analysed in this thesis for *C. superbus sceptrum*, *C. superbus superbus*, *C. premagharensis* and *C. magharensis*. Light polarizing microscope photos are presented in pl. 6.1 for taxa here emended.




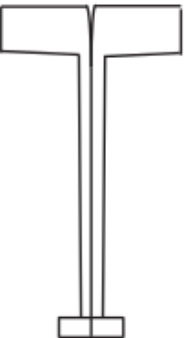
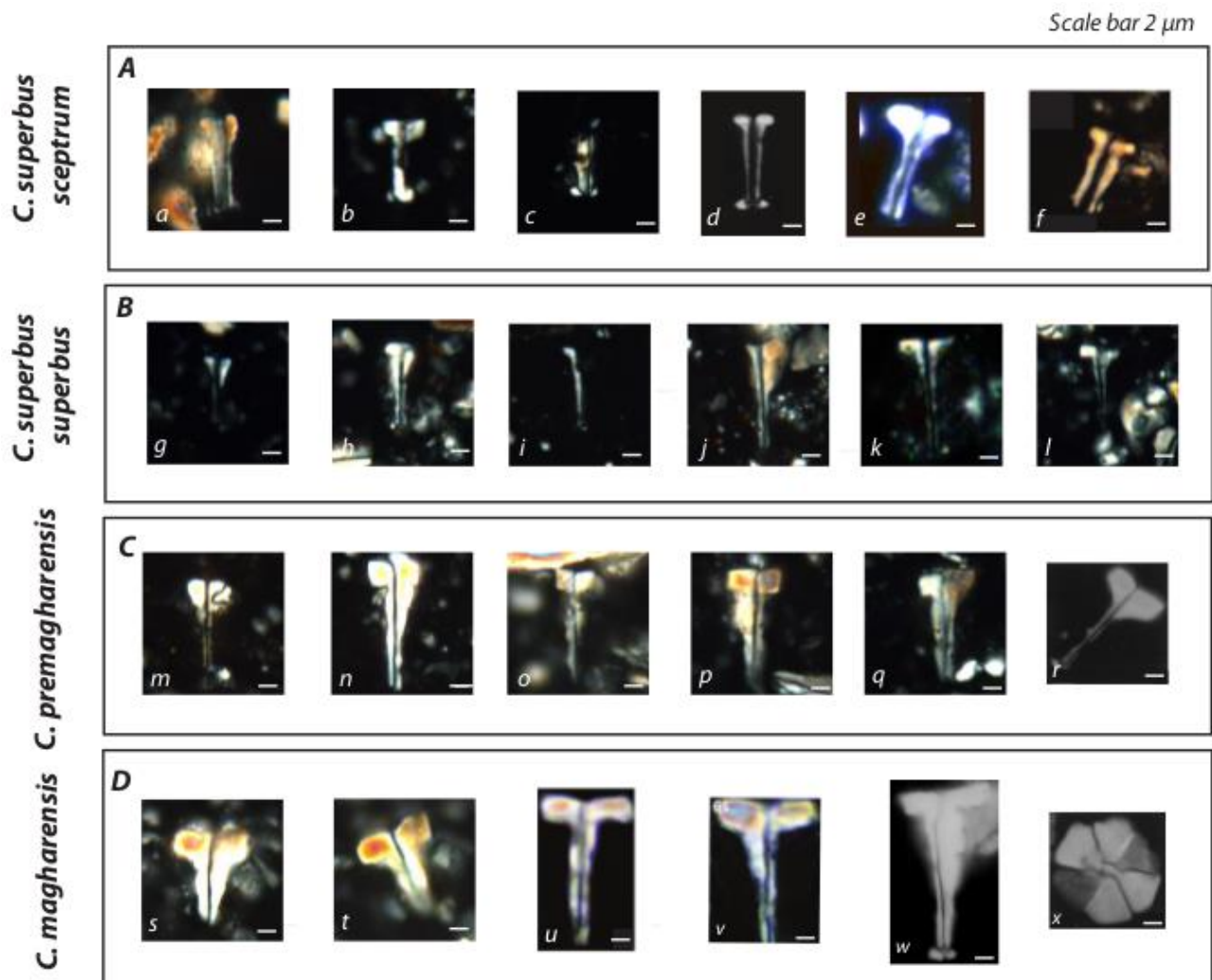
HOLOTYPE		TH	H	SW	PS	DS	TDS
 <i>C. superbus sceptrum</i>	<i>Holotype</i>						
	9.3	7.3	1.4	3.3	4.1	1.2	
	<i>Variability among investigated specimens</i>						
	<i>N=10</i>	<i>N=10</i>	<i>N=26</i>	<i>N=10</i>	<i>N=26</i>	<i>N=26</i>	
	6.3 - 12.1	5.1 - 10.9	1.3 - 2.5	2.1 - 3.9	3.0 - 5.6	0.4 - 1.5	
 <i>C. superbus superbus</i>	<i>Holotype</i>						
	10.3	8.5	0.7	2.7	4.3	1.0	
	<i>Variability among investigated specimens</i>						
	<i>N=11</i>	<i>N=11</i>	<i>N=30</i>	<i>N=11</i>	<i>N=30</i>	<i>N=30</i>	
	5.8 - 15.9	4.9 - 14.1	0.5 - 1.0	1.4 - 3.9	2.8 - 5.8	0.5 - 1.3	
 <i>C. premagharensis</i>	<i>Holotype</i>						
	11.7	8.9	0.6	1.7	4.8	2.2	
	<i>Variability among investigated specimens</i>						
	<i>N=7</i>	<i>N=7</i>	<i>N=16</i>	<i>N=7</i>	<i>N=21</i>	<i>N=18</i>	
	11.1 - 16.6	8.7 - 13.1	0.6 - 1.1	1.7 - 3.0	4.1 - 6.8	1.8 - 2.9	
 <i>C. magharensis</i>	<i>Holotype</i>						
	/	/	/	/	8	/	
	<i>Variability among investigated specimens</i>						
	<i>N=1</i>	<i>N=1</i>	<i>N=3</i>	<i>N=1</i>	<i>N=23</i>	<i>N=5</i>	
	/	/	1.2 - 1.7	/	7.8 - 10.9	2.0 - 2.9	

Fig. 6.6. – Holotype and variability of taxonomic characters resulting from morphometric analyses. Number of specimens measured (N) are provided for each parameter.



Pl. 6.1. – Plate illustrating the new taxonomic scheme adopted. A = *C. superbus sceptrum* (a-f), B = *C. superbus superbus* (g-l), C = *C. premagharensis* (m-r), D = *C. magharensis* (s-x). Specimens d, e, f, r, u, v, w, x are from: (d) Bown (1987 pl. 14, fig. 15); (e) Menini et al. (2018, pl. 1, fig. 33); (f) van de Schootbrugge et al. (2018, pl. 6, fig. 11); (r) Bown and Cooper (1998, pl. 4.13, fig. 8); (u) Aguado et al. (2017, fig. 8,y); (v) Aguado et al. (2008, fig. 5, 19); (w) Bown and Cooper (1998, pl. 4.13, fig. 6); (x) Bown and Cooper (1998, pl. 4.13, fig. 7). Scale bar 2 μ m.

Results - diagenesis

The species *C. cantaluppii* was established by Cobianchi (1990; fig. 4h) as follows:

A species of *Carinolithus* with a small proximal shield and a large distal spine. This spine typically broadens at about $\frac{1}{4}$ (from the base) maintaining the size (width) up to the distal shield. Under crossed nicols this species shows high birefringence colours (from white to orange) and a clear extinction line in the middle of the spine. Proximal shield = 2.3-2.8 μm ; Distal shield = 3.0-4.0 μm ; Height = 8.0-10 μm .

Cobianchi (1990) introduced the term “spine” which is the equivalent of “stem” and, therefore, the “broadening of the spine” corresponds to the “broadening of the stem”. Based on the original description, *C. cantaluppii*, similarly to other *Carinolithus* species, should have a symmetric shape possessing an equal size “broadening of the stem” extending further downstem in both sides. However, the only specimen (presumably the holotype) illustrated by Cobianchi (1990) is clearly asymmetric as the two sides of the stem broaden at different points and with different widths. The right side of the stem broadens at about $\frac{1}{4}$ from the base (as provided by the author’s description) whereas the left side of the stem slightly broadens (less wide and with a different shape) at about $\frac{1}{2}$ from the base. Several photos of *C. cantaluppii* show an extremely asymmetric shape of this species (e.g. Cobianchi 1990, fig. 4h; Perilli and Duarte, 2006, pl. 1, fig. 5; Ferreira et al. 2015, pl. 1, fig. 12) whereas other specimens appear broadly symmetric (e.g. Gardin and Manivit, 1994, pl. 3, fig. 11; Perilli and Duarte, 2006, pl. 1, fig. 9; Sandoval et al. 2012, figs. 10, 8,9,10). In both cases, the stem broadens at different points. The drawing of this taxon provided by Mattioli (1996; fig. 3) shows a perfectly symmetric stem broadening at about $\frac{3}{4}$ from the base.

To investigate the diagnostic “broadening of the stem” in *C. cantaluppii* a detailed characterization was conducted on specimens arranged in four different configurations under the light polarizing microscope: with and without quartz lamina, both at 0° and 45° to the polarizers (Fig. 6.7). Pictures at 0° to the polarizers show that specimens are never symmetric. Moreover, specimens have an extremely different broadening of the stem. Pictures at 45° to the polarizers best document the overgrowth of the stem while showing the original distal shield and stem.

The extremely high birefringence colours of the broadening of the stem together with different heights of broadening and stem width suggest variable degrees of diagenetic overgrowth. The species *C. cantaluppii* established by Cobianchi (1990) is, therefore, considered an artifact due to diagenesis and not a taxonomic pristine character. The use of the lamina at 45° to the polarizers turned out to be an excellent tool to recognize the species which underwent the diagenetic modification. In all cases, in fact, the original taxon could be identified.

Fig. 6.7. – Holotype of *C. cantaluppii* (Cobianchi (1990; fig. 4h). Specimens of *C. cantaluppii* from samples of the Sogno Core and Breggia section photographed in four different combinations: both with and without quartz lamina, both at 0° and 45° to the polarizers.

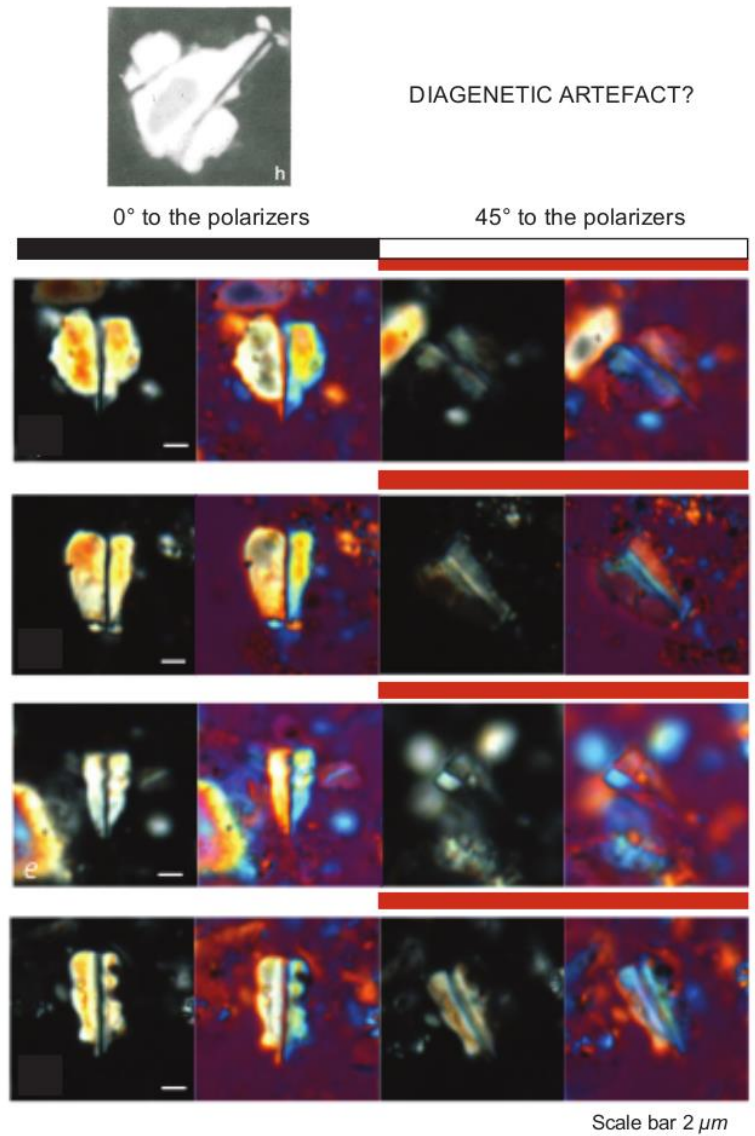
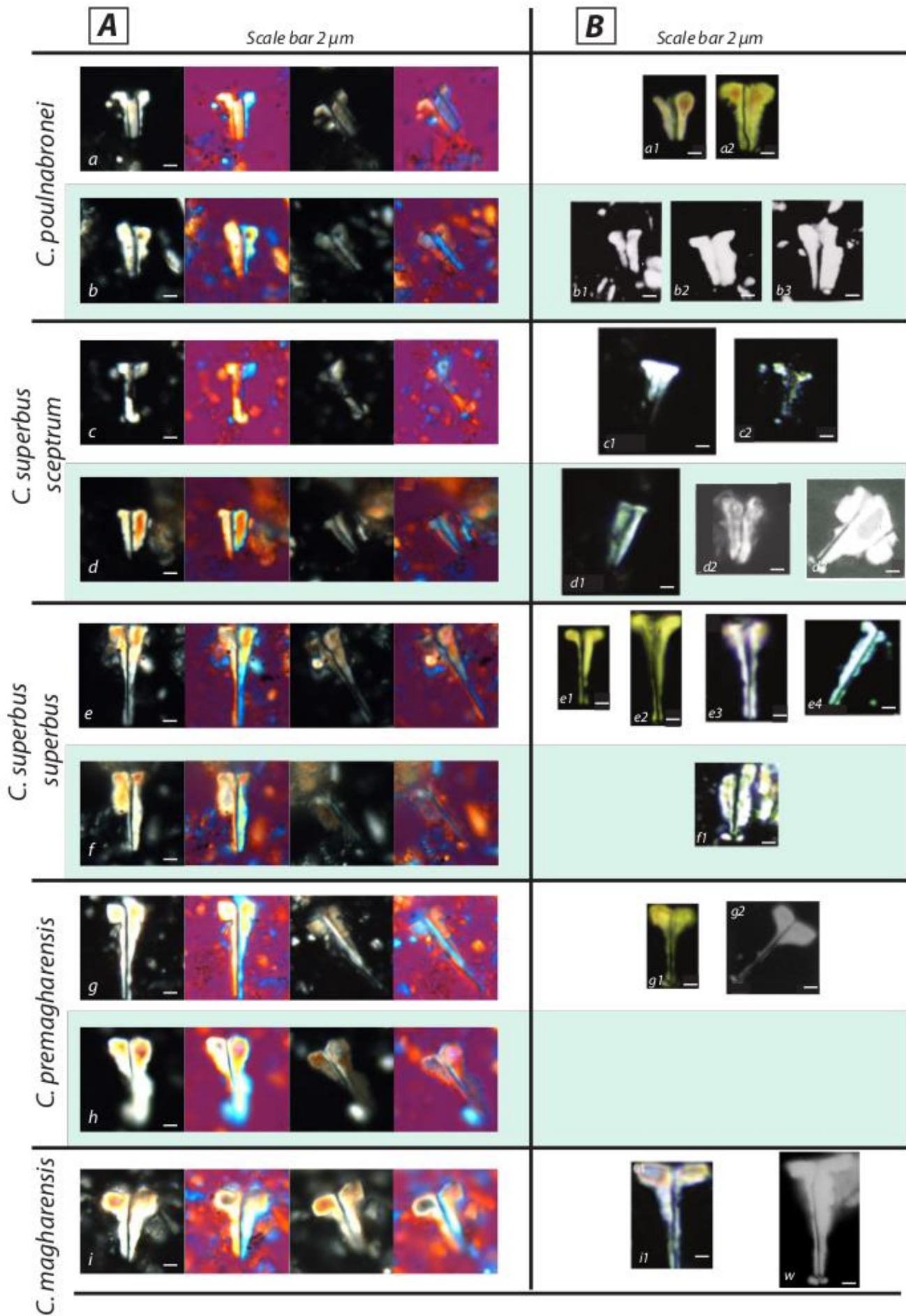


Plate 6.2 includes pictures of moderately preserved and overgrown specimens of *C. poulabronei*, *C. superbus sceptrum*, *C. superbus superbus*, *C. premagharensis* and *C. magharensis*. The light blue rectangle (Pl. 2, figs. b, d, f, h) evidence overgrown specimens similar to *C. cantaluppii* of Cobianchi (1990). Specimens characterized by moderate preservation show an intermediate diagenetic phase (Pl. 2, figs. a, c, e, g, i). The use of the quartz lamina at 45° to the polarizer appears most useful to recognize the taxon which underwent the diagenetic modification, as in the case of photos 6.2a and b = *C. poulabronei*; 6.2 c and d = *C. superbus sceptrum*; 6.2 e and f = *C. superbus superbus*; 6.2 g and h = *C. premagharensis*; 6.2 I = *C. magharensis*.



Pl. 6.2 - Specimens of *Carinolithus* belonging to the investigated samples of the Sogno Core and the Breggia section (A) and published works (B). In A, specimens are illustrated with four different pictures: with and without quartz lamina; at 0° and 45° in respect to the polarizers. Based on the description proposed by Cobianchi, 1990 specimens in b, d, f and h (light blue rectangles) should be grouped as *C. cantaluppii*. Intermediate diagenetic phase for every taxon is presented in white rectangles. See text for further details. New taxonomic identification of *Carinolithus* species based on this work: (a,b) *C. poulhabronei*; (c,d) *C. superbus sceptrum*; (e,f) *C. superbus superbus*; (g,h) *C. premagharensis*; (i) *C. magharensis*. (a1, a2) Sandoval et al. (2012, fig. 10; 16, 17). (b1, b2, b3) Mattioli (1996, pl. 2; 9,11,12). (c1) Reolid et al. (2014, fig. 6; CE30). (c2) Casellato and Erba (2015, pl. 1; 16). (d1) Reolid et al. (2014, fig. 6; CE30). (d2) Bodin et al. (2010, fig. 5; i). (d3) Cobianchi (1992, fig. 20; g). (e1) Sandoval et al. (2012, fig.10; 12). (e2) Aguado et al. (2008, fig. 5; 18). (e3) Sandoval et al. (2012, fig. 10; 20). (e4) Molina et al. (2018, fig. 8; LL6). (f1) Ferreira et al. (2015, pl. 1; 12). (g1) Sandoval et al. (2012, fig. 10; 19). (g2) Bown and Cooper (1998, fig. 4.13; 8). (i1) Aguado et al. (2008, fig. 5; 19). (i2) Bown and Cooper, (1998, pl. 4.13; fig. 6).

Based on these observations, three diagenetic phases have been recognized and illustrated in Fig. 6.7. Phase 1 characterizes specimens with no or negligible diagenetic modification ($O = 0$). In phase 2 diagenesis affects the uppermost part of the stem without reaching the middle point of the stem ($0 < O < H/2$) (Pl. 6.2 specimens a, c, e, g, i). In phase 3 overgrowth becomes more pervasive and exceeds the middle point of the stem ($O > H/2$) (Pl. 2 specimens b, d, f, h). Based on all investigated specimens, overgrowth generally starts at the base of the distal shield downwards, proceeding further downstem and eventually reaching the proximal shield. Furthermore, diagenetic modifications are generally prevalent on one sides and often shows differentiate degrees: that's why the common appearance of *C. cantaluppii* is asymmetric as in the case of the holotype of Cobianchi (1990; fig. 4h). The recognition of the diagenetic phase in *Carinolithus* specimens can be used as a tool to assess the impact of overgrowth and therefore the diagenetic degree in the studied material. In Appendix C we present the characterization of the diagenetic phase for all the investigated specimens from the literature.

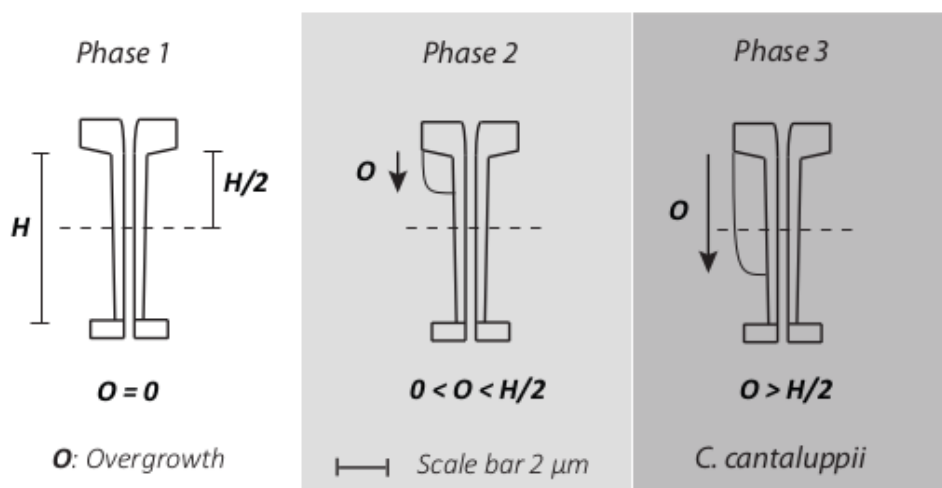


Fig. 6.8. – Schematic representation of the diagenetic phases of *Carinolithus* specimens: H = nannolith Height; H/2 = half the height; O = overgrowth. **Phase 1**: no or negligible diagenetic overprint (O=0); **Phase 2**: diagenesis affects the uppermost part of the stem without reaching its middle point ($0 < O < H/2$); **Phase 3**: diagenesis becomes more pervasive and exceeds the middle point of the stem ($O > H/2$). Overgrowth may affect one or both sides of the stem and with different degrees.

Implications for biostratigraphy

The taxonomic revision of the genus *Carinolithus* has implications for the biostratigraphic characterization of the Toarcian-Aalenian interval. First occurrences (FOs) of *C. superbus sceptrum*, *C. superbus superbus*, *C. premagharensis* and *C. magharensis* may be used as additional events to increase biostratigraphic resolution. In Fig. 6.8, the FOs of *C. poul nabronei*, *C. superbus sceptrum* and *C. superbus superbus* are reported as deduced from literature (Appendix C) and my investigations.

Several authors illustrate *C. poul nabronei* in their works (e.g. Mattioli, 1996; Bucefalo Palliani and Mattioli, 1998; Parisi et al. 1998; Perilli and Duarte, 2006; Mattioli et al. 2006; Sandoval et al. 2012; Reolid et al. 2014; Casellato and Erba, 2015; Ferreira et al. 2015; da Rocha et al. 2016; Molina et al. 2018; Menini et al. 2018). The oldest age proposed for the FO of *C. poul nabronei* is that of Sandoval et al. (2012; fig. 10; 11) and Perilli and Duarte (2006; fig. 1; 9 and fig. 2; 6,10) in the Lower Toarcian NJT5b. This datum is very consistent with that proposed by the Standard Biozonation Scheme of Mattioli and Erba (1999).

As far as *C. superbus sceptrum* is concerned (e.g. Bown, 1987; Baldanza and Mattioli, 1992; Cobianchi, 1992; Reale et al. 1992; Gardin and Manivit, 1994; Bown and Cooper, 1998; Parisi et al. 1998; Bodin et al., 2010; Casellato and Erba, 2015; da Rocha et al. 2016; Menini et al. 2018; van de Schootbrugge et al. 2018) the oldest FO proposed is that of da Rocha et al. (2016, figs. 7; 3,4), Casellato and Erba (2015, fig. 1; 16,17) and Reolid et al. (2014, fig. 6; CE30) dated as Lower Toarcian.

Specimens of *C. superbus superbus* (e.g. Crux, 1987; Bown et al. 1988; Erba, 1990; Baldanza and Mattioli, 1992; Gardin and Manivit, 1994; Parisi et al. 1998; Mattioli et al. 1999; Perilli and Duarte, 2006; Aguado et al. 2008; Maillot et al. 2006; Sandoval et al. 2012; Ferreira et al. 2015; Aguado et al. 2017; Molina et al. 2018) show an oldest age in the *Harpoceras Serpentinus* AZ, roughly corresponding to the Lower/Middle Toarcian boundary (Baldanza and Mattioli, 1992; fig. 1; 5). The

biostratigraphy performed in this thesis on the Schandelah Core confirms the FO of *C. superbus superbus* in the Middle Toarcian, specifically, in the lowermost part of the NJ7 zone.

The FO of *C. superbus sceptrum* is older than that of *C. superbus superbus* and the former corresponds to the FO of *C. superbus* proposed in the Standard Biozonation Schemes of Mattioli & Erba (1999) and Bown & Cooper (1998) marking the base of the NJT6 and NJ6 Zones, respectively. Based on the current taxonomic revision, we therefore propose here to consider the FO of *C. superbus sceptrum* as the zonal marker for the base of these zones. Further investigations are currently going on in order to discriminate reliable FOs of *C. premagharensis* and *C. magharensis*.

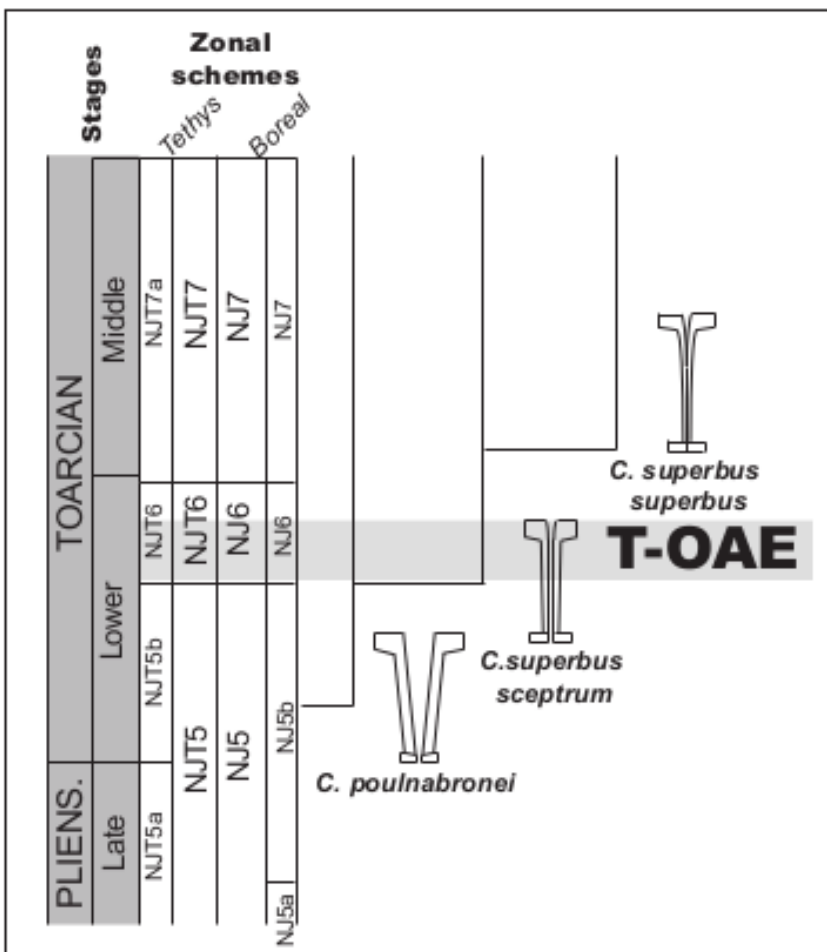


Fig. 6.9. – Stratigraphic distribution of *C. poul nabronei*, *C. superbus sceptrum* and *C. superbus superbus*.

Implications for evolutionary trends

During the Upper Pliensbachian – Lower Toarcian time interval, calcareous nannoplankton underwent an intense phase of diversification evidenced by the appearance of several species and genera (Mattioli and Erba 1999; Erba, 2004). The hypothesis, already discussed by Crux (1987); Bown (1987) and Mattioli (1996), that the genus *Carinolithus* derives from the genus *Calyculus* is widely accepted by the scientific community. The evolutive lineage between the two genera is well documented in Mattioli (1996; fig. 3): the transition between *Calyculus* spp. and *C. poulabronei* passes through a gradual vertical development of the stem and the thickening of the distal shield with the contemporary closing of the axial channel and thinning of the stem. The hypothesis that *C. cantaluppii* was descended from *C. poulabronei* is here rejected since the former species, as aforementioned, represents a diagenetic artefact due to overgrowth. *C. poulabronei* passes to *C. superbus sceptrum* through a further gradual decrease of both shield widths and distal shield thickness with the contemporary thinning of the stem (Mattioli, 1996). The V- shape of both the stem and the axial channel of *C. poulabronei* is replaced by the typical T-shape of *C. superbus sceptrum*. A further decrease of the stem width characterizes *C. superbus superbus*. The transition between the *C. superbus* group and the *C. magharensis* group seems due to a variation in both size and shape of the distal shield. As already stated by Bown (1987), we observed that specimens included in the *C. magharensis* group have distal shield sharply flaring from the stem and a more rectangular shape compared to that of *C. superbus* group. Morphometry also displays a progressive thickening of the distal shield: the TDS is strongly correlated to TH and DS ($r = 0.66$ and 0.64 respectively) suggesting a progressive increase of both TH and DS passing from *C. superbus superbus* to *C. premagharensis*. Morphometric analyses evidence a further increase of the DS diameter passing from *C. premagharensis* to *C. magharensis*. Within the *C. magharensis* group the increase of DS diameter is strongly connected to an increase of PS and SW ($r = 0.8$ and 0.87 respectively), suggesting bigger values of these taxonomic parameters in *C. magharensis* compared to *C. premagharensis*.

Chapter 7

Results

7.1. Sogno Core

Preservation and abundance

Calcareous nannofossil preservation and abundance vary through the studied section, generally increasing from the Domaro Lmst. to the Sogno Fm. The preservation is generally classified as moderate/good varying from moderate/poor in some samples of the Domaro Lmst. and the Fish Level to moderate/good - good. In the Sogno Core the degree of etching varies from E1 to E2, stronger dissolution is noted within the Fish Level (units U3-4 to U3-2) whereas the degree of overgrowth fluctuates between O0 and O2 and is slightly higher in the Domaro Lmst. (unit U3-11). As far as the abundance is concerned, it is somehow lithology dependent. Nannofossils are rare to rare/frequent in the Domaro Lmst. whereas in the Sogno Fm. they are generally frequent, although calcareous nannofloras are rather rare in the uppermost part of the studied interval. A drastic decrease in abundance is observed within the Fish Level, varying between virtually barren to rare. The range chart is reported in appendix D. Pictures under light polarizing microscope of selected taxa are reported in plates 1 and 2. Scanning Electron Microscope (SEM) pictures are not provided in this thesis as taxonomic differences are easily distinguished by optical microscope.

Biostratigraphy

The biostratigraphic scheme valid for the Tethyan Realm and here adopted is that of Mattioli and Erba (1999). A total of ten calcareous nannofossil events were recognized in the Sogno Core (Fig. 7.1.) and the following zones were identified:

- *Lotharingius hauffii* (NJT5) Zone, divided into the *Biscutum finchii* (NJT 5a) and *Lotharingius sigillatus* (NJT 5b) Subzones;
- *Carinolithus superbus* (NJT 6) Zone.

According to the zonation of Mattioli & Erba (1999), the lowermost studied sample S3 C30 476 (26.83 m) is attributed to the *Lotharingius hauffii* (NJT 5) Zone, and specifically, to the *Biscutum finchii* (NJT 5a) Subzone based on the presence of *L. hauffii* and absence of *L. sigillatus*. The FO of *L. sigillatus* in sample S3 C30 473 (26.69 m) marks the boundary between the NJT5a and the NJT5b Subzones.

Within the NJT 5b Subzone additional biohorizons are recognized, namely: the FOs of *C. poulabronei* (24.27 m), *L. crucicentralis* (23.65 m), *L. velatus* (21.46 m), *D. ignotus* (20.21 m) and *D. constans* (17.16 m). The FO of *C. superbus sceptrum* (17.39 m) (*C. superbus* in Mattioli and Erba, 1999) defines the base of the NJT6 Zone. Within the *Carinolithus superbus* NJT6 Zone the LOs of *M. jansae* (11.45 m), “thin *M. jansae*” (11.26 m) and the FO of *Watznaueria* sp.1 (9.06 m) are detected. The NJT6/NJT7 zonal boundary was not identified due to the absence of *D. striatus* in the studied core.

Drastic variations in abundance of certain taxa were also recorded. Specifically, the *Schizosphaerella* decline (sensu Casellato and Erba, 2015) at the Domaro Lmst. / Sogno Fm. boundary (25.69 m); the *Schizosphaerella* and *M. jansae* (sensu Casellato and Erba, 2015) crises at the base of the Fish Level (onset of the T-OAE) (16.79 m) and the *Schizosphaerella* recovery (sensu Casellato & Erba, 2015) after the Fish Level deposition (termination of the T-OAE) (11.86 m).

The calcareous nannofossil assemblage of the NJT5b Subzone is dominated by *S. punctulata* and *M. jansae*. Among schizosphaerellids, *S. punctulata* is the more abundant morphotype (rare to common) whereas “small *S. punctulata*” and “encrusted *S. punctulata*” are subordinated (extremely rare to few/common and extremely rare to rare/few, respectively). Within the genus *Mitrolithus*, *M. jansae* is slightly more abundant (extremely rare to few/common) than “thin *M. jansae*” (extremely rare to rare/few). Within genus *Lotharingius* a slight increase in abundance in the upper part of the subzone is observed in *L. hauffii*, *L. frodoi* and *L. sigillatus*.

Nannofossil assemblages characterizing the lower part of NJT 6 Zone corresponding to the Fish Level shows a drastic reduction in abundance of both *Schizosphaerella* and *Mitrolithus* (*Schizosphaerella* and *M. jansae* crises). In particular, both *S. punctulata* and “small *S. punctulata*” become extremely rare, and “encrusted *S. punctulata*” appears only sporadically. As far as *M. jansae* is concerned, the thin morphotype becomes dominant showing abundances generally varying between rare to rare/few whereas the standard morphotype shows a bigger drop in abundance.

In the lower part of the NJT 6 Zone *Lotharingius* becomes the dominant genus: *L. hauffii*, *L. frodoi* and *L. sigillatus* are the most abundant species. In this interval, an increase in abundance in the genera *Calyculus* and *Carinolithus* is also recorded.

Calcareous nannofossil assemblages of the uppermost part of the NJT 6 Zone (above the Fish Level) are characterized by a general recovery in abundance of schizosphaerellids (*Schizosphaerella* recovery): however, extremely rare to few *S. punctulata* and extremely rare to rare/few “small *S. punctulata*” are observed, whereas “encrusted *S. punctulata*” remains sporadic.

Through the studied section, genera *Biscutum*, *Calyculus* and *Crepidolithus* are characterized by a general rare abundance, whereas *Bussonius*, *Diductius*, *Similiscutum* and *Tubirhabdus* are extremely rare.

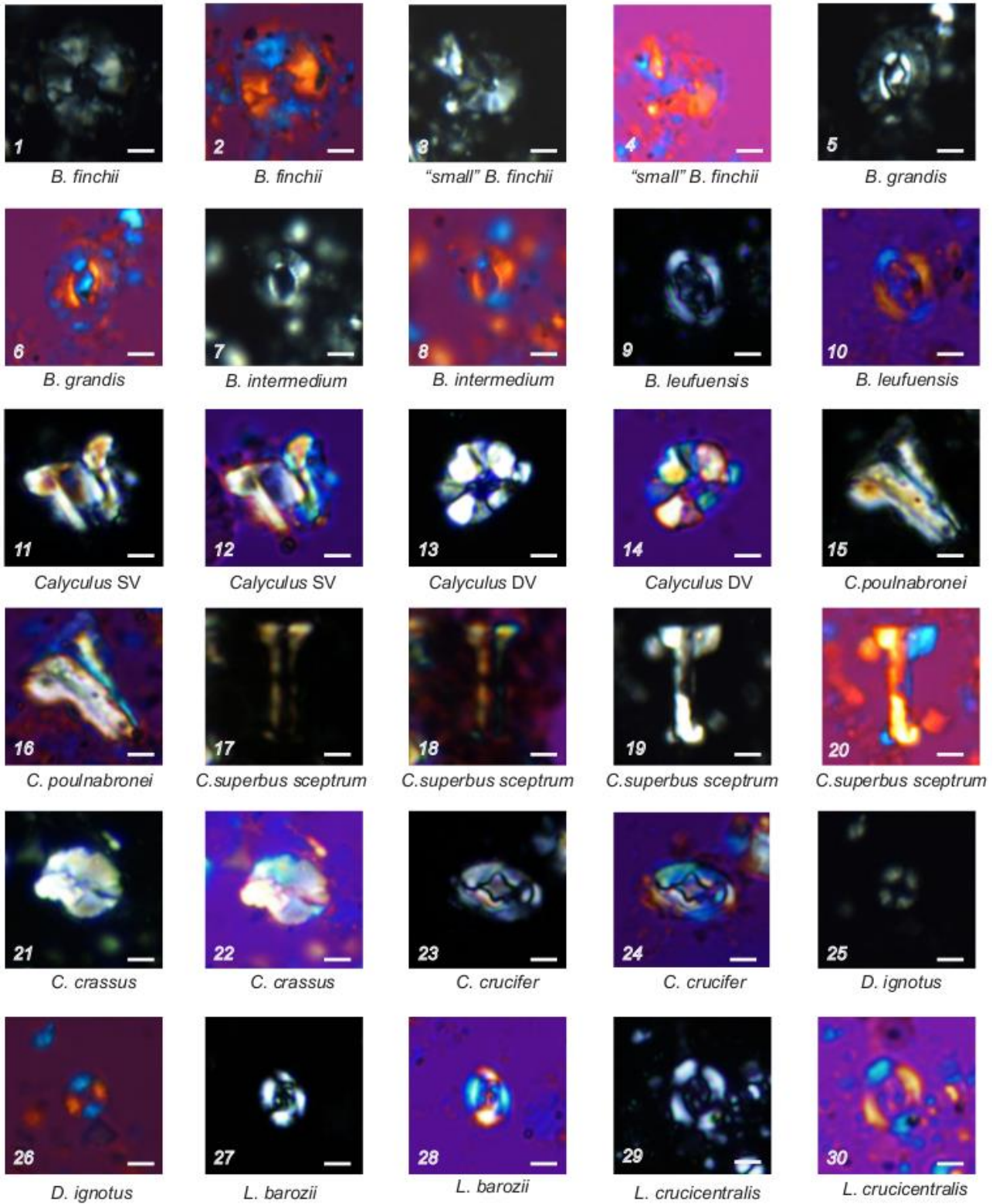


PLATE 1

Scale bars represent 2 μm

Figs. 1-2 - *B. finchii*, 1) cross-polarized light, 2) quartz lamina, sample S3 C12 330 (17.16 m)

Figs. 3-4 - "*small B. finchii*", 3) cross-polarized light, 4) quartz lamina, sample S3 C12 330 (17.16 m)

Figs. 5-6 - *B. grandis*, 5) cross-polarized light, 6) quartz lamina, sample S3 C12 330 (17.16 m)

Figs. 7-8 - *B. intermedium*, 7) cross-polarized light, 8) quartz lamina, sample S3 C12 330 (17.16 m)

Figs. 9-10 - *B. leufuensis*, 9) cross-polarized light, 10) quartz lamina, sample S3 C12 327 (17.01 m)

Figs. 11-12 - *Calyculus SV*, 11) cross-polarized light, 12) quartz lamina, sample S3 C29 456 (25.5 m)

Figs. 13-14 - *Calyculus DV*, 13) cross-polarized light, 14) quartz lamina, sample S3 C21 416 (22.95 m)

Figs. 15-16 - *C. poulabronei*, 17) cross-polarized light, 18) quartz lamina, sample S3 C22 423 (23.42 m)

Figs. 17-18 - *C. superbus sceptrum*, 19) cross-polarized light, 20) quartz lamina, sample S3 C6 317b (14.04 m)

Figs. 19-20 - *C. superbus sceptrum*, 15) cross-polarized light, 16) quartz lamina, sample S3 C5 313 (13.42 m)

Figs. 21-22 - *C. crassus*, 21) cross-polarized light, 22) quartz lamina, sample S1 C7 35 (4.24 m)

Figs. 23-24 - *C. crucifer*, 23) cross-polarized light, 24) quartz lamina, sample S3 C19 389 (21.23 m)

Figs. 25-26 - *D. ignotus*, 25) cross-polarized light, 26) quartz lamina, sample S3 C12 330 (17.16 m)

Figs. 27-28 - *L. barozii*, 27) cross-polarized light, 28) quartz lamina, sample S3 C6 315a (13.7 m)

Figs. 29-30 - *L. crucicentralis*, 29) cross-polarized light, 30) quartz lamina, sample S1 C7 35 (4.24 m)

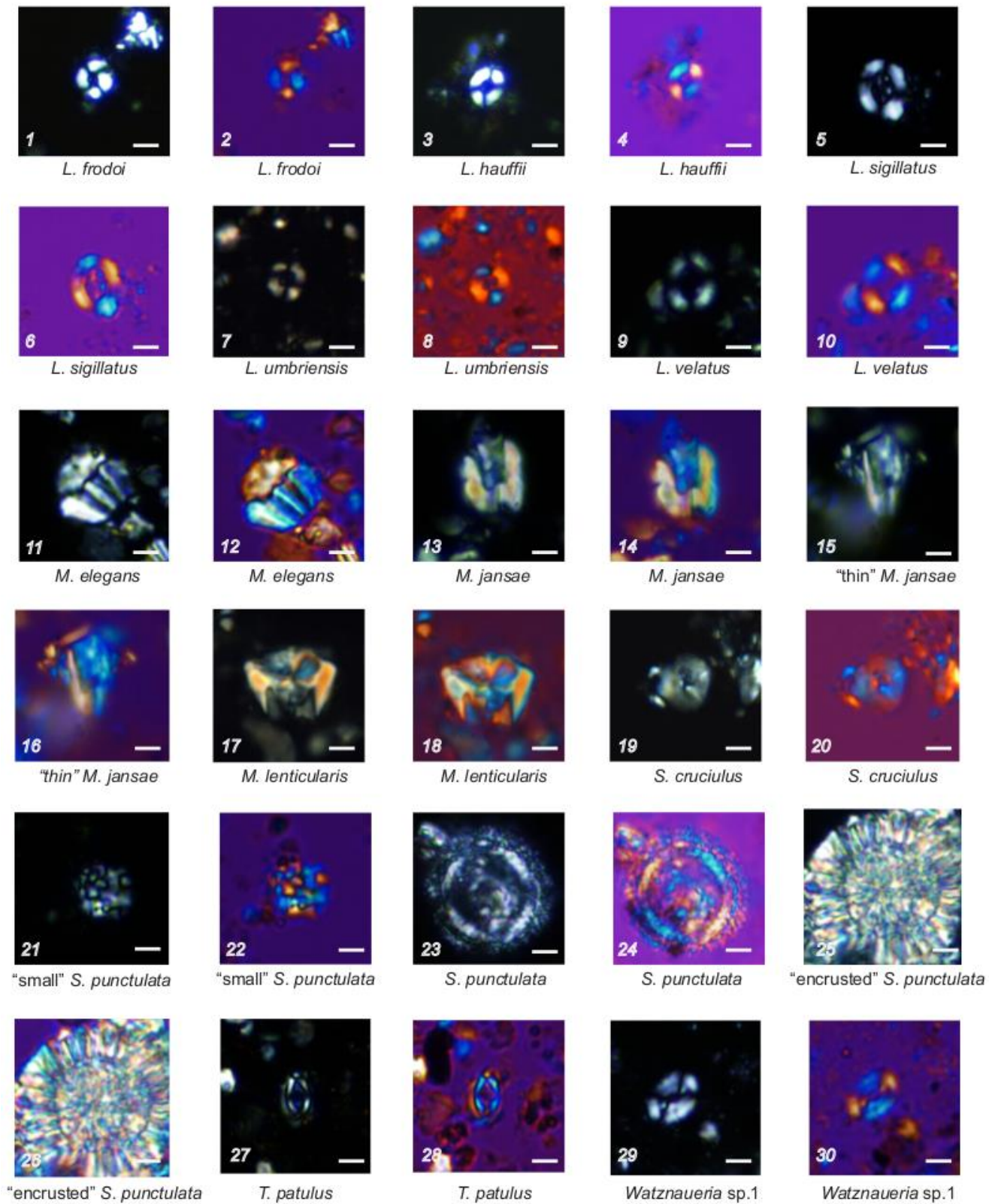


PLATE 2

Scale bars represent 2 μm

- Figs. 1-2 - *L. frodoi*, 1) cross-polarized light, 2) quartz lamina, sample S1 C21 138 (9.13 m)
- Figs. 3-4 - *L. hauffii*, 3) cross-polarized light, 4) quartz lamina, sample S3 C3 307 (12.76 m)
- Figs. 5-6 - *L. sigillatus*, 5) cross-polarized light, 6) quartz lamina, sample S3 C30 466 (26.2 m)
- Figs. 7-8 - *L. umbriensis*, 7) cross-polarized light, 8) quartz lamina, sample S3 C5 314 (13.5 m)
- Figs. 9-10 - *L. velatus*, 9) cross-polarized light, 10) quartz lamina, sample S1 C21 130 (9.2 m)
- Figs. 11-12 - *M. elegans*, 11) cross-polarized light, 12) quartz lamina, sample S3 C30 466 (26.2 m)
- Figs. 13-14 - *M. jansae*, 13) cross-polarized light, 14) quartz lamina, sample S3 C24 441 (24.38 m)
- Figs. 15-16 - “*thin M. jansae*”, 15) cross-polarized light, 16) quartz lamina, sample S3 C24 441 (24.38 m)
- Figs. 17-18 - *M. lenticularis*, 17) cross-polarized light, 16) quartz lamina, sample S3 C12 330 (17.16 m)
- Figs. 19-20 - *S. cruciulus*, 19) cross-polarized light, 20) quartz lamina, sample S3 C12 330 (17.16 m)
- Figs. 21-22 - “*small S. punctulata*”, 21) cross-polarized light, 22) quartz lamina, sample S3 C24 439 (24.22 m)
- Figs. 23-24 - *S. punctulata*, 23) cross-polarized light, 24) quartz lamina, sample S3 C20 409 (22.5 m)
- Figs. 25-26 - “*encrusted S. punctulata*”, 25) cross-polarized light, 26) quartz lamina, sample S3 C20 401 (22 m)
- Figs. 27-28 - *T. patulus*, 27) cross-polarized light, 28) quartz lamina, sample S3 C13 335 (17.45 m)
- Figs. 29-30 - *Watznaueria sp.1*, 29) cross-polarized light, 30) quartz lamina, sample S1 C24 164 (10.47 m)

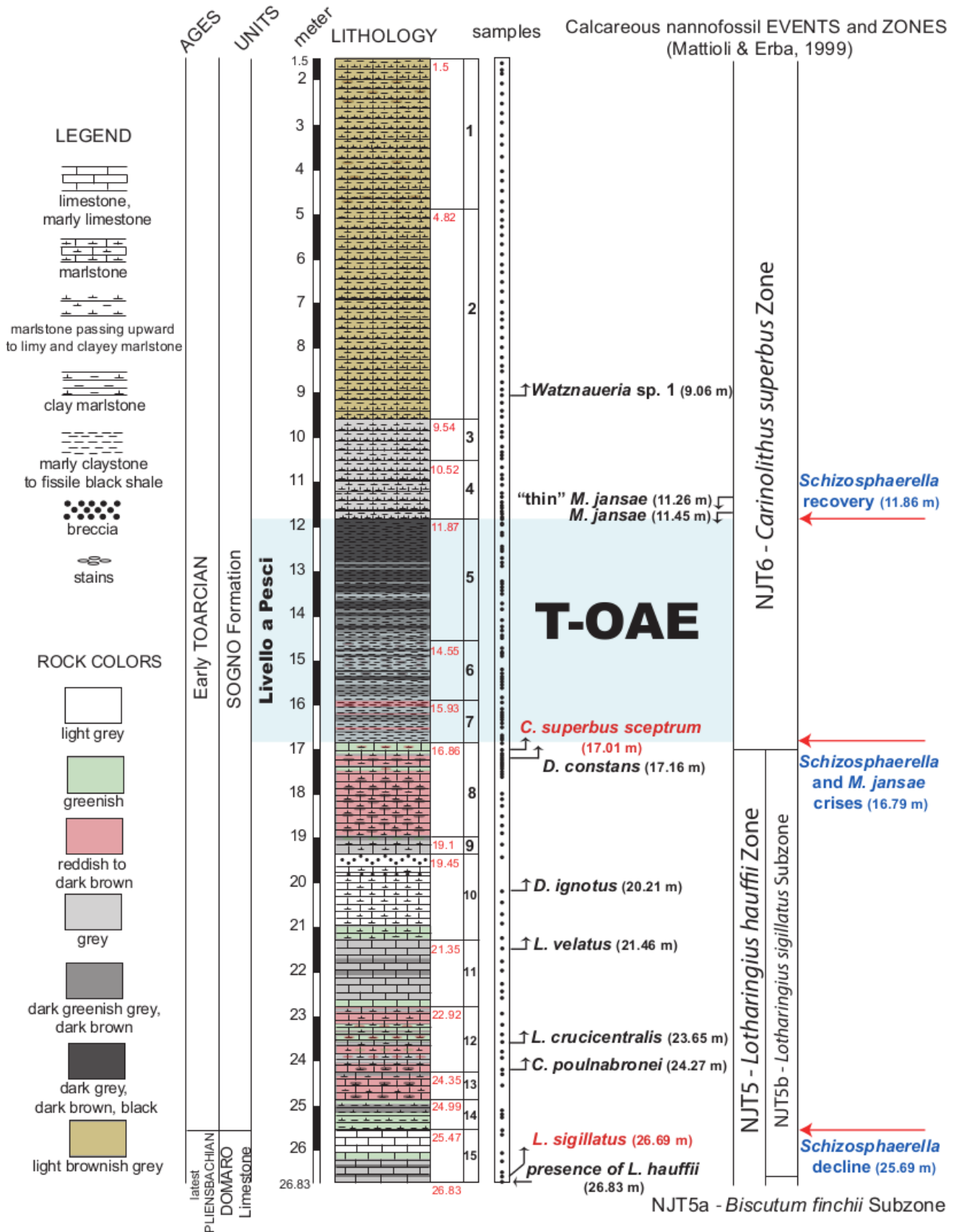


Fig. 7.1 – Lithostratigraphy and biostratigraphy of the Sogno Core. Calcareous nannofossil events in red are the primary events (used as zonal and subzonal boundaries) of the zonal scheme of Mattioli and Erba (1999). *Schizosphaerella* decline, crisis, recovery and *M. jansae* crisis (sensu Casellato and Erba 2015) are reported in blue.

7.2. L1 and Schandelah Cores

Preservation

Calcareous nannofossil preservation observed from the U1 to U6 interval varies between moderate to good, with generally minor to moderate etching (E1 to E2) and minor overgrowth (O1). Samples characterized by a moderate/poor preservation with moderate etching (E2) and moderate overgrowth (O2) are restricted to the “Monotis Bank” (15 m of the L1 Core) and the lower part of U1 (from sample 26.50 to sample 26.00 m of the Schandelah Core). Samples included in the uppermost U1 (13.5 to 5.5 m of the Schandelah Core) show poor to moderate preservation with moderate to major etching (E2 to E3) and minor overgrowth (O1). In the U7 unit calcareous nannofossils display minor/moderate to moderate/major etching (E1/2 to E2/3) and negligible to moderate overgrowth (O0 to O2) with a general moderate/poor to moderate preservation. Most samples belonging to the Amaltheenthon Fm. are barren of nannofossils. For the few nannofossil-bearing samples, a moderate to moderate/good preservation is observed with minor/moderate etching (E1/2) and negligible to minor overgrowth (O0 to O1). In a few intervals calcareous nannofossils are poorly preserved and replaced by siderite showing yellowish colours, moderate etching and major overgrowth (sample 30.40 m of L1 Core and 51 and sample 50 m of Schandelah Core). Pictures of selected taxa under light polarizing microscope are reported in plates 3 and 4. The stratigraphic range charts of calcareous nannofossils in the L1 and Schandelah Cores are reported in Appendix E. Scanning Electron Microscope (SEM) pictures are not provided in this thesis as taxonomic differences are easily distinguished by optical microscope.

Biostratigraphy of the L1 Core

The biozonation scheme adopted is that of Bown (1987b) revised in Bown et al. (1988) and Bown and Cooper (1998) valid for the Boreal Realm. A total of seven calcareous nannofossil events were detected (Fig. 7.2.) allowing the recognition of the:

- *Lotharingius hauffii* Zone (NJ5), divided into the *Biscutum finchii* Subzone (NJ5a) and *Crepidolithus impontus* Subzone (NJ5b);
- *Carinolithus superbus* Zone (NJ6);
- *Discorhabdus striatus* Zone (NJ7).

The lowermost investigated sample (31 m) is assigned to the earliest Toarcian NJ5b Subzone for the presence of *C. impontus* (*C. cavus*). The FO of *C. superbus sceptrum* (24.9 m) (*C. superbus* in Bown and Cooper, 1998) defines the NJ5/NJ6 zonal boundary. In the same sample the FO of *D. constans* was recognized. In the NJ6 Zone several biohorizons were detected within the T-OAE: the LOs of *C.*

granulatus (24.7 m), *P. liasicus* (24.5 m), “large” *B. finchii* (24.3 m), *B. finchii* (24.1 m) and *B. grandis* (23.45 m). The uppermost investigated sample (15 m) is still assigned to the Early Toarcian NJ6 Zone due to the absence of *D. striatus*.

Calcareous nannofossil assemblage characterizing the upper part of the NJ5b Subzone is extremely poor and several samples are barren. The genera *Bussonius*, *Lotharingius*, *Crepidolithus* and *Schizosphaerella* are detected sporadically. An important drop in abundance is recorded in *Schizosphaerella* at the Amaaltheenton Fm. / Posidonienschiefer Fm. boundary. This is assigned to the so called “*Schizosphaerella* crisis” (24.9 m), affecting both *S. punctulata* and “small *S. punctulata*”. Calcareous nannofossil assemblages characterizing the lower part of the NJ6 Zone (both across and above the T-OAE interval) is dominated by genus *Crepidolithus* (*C. crassus* and *C. cavus* are the most abundant species) and *Lotharingius* (*L. hauffii*, *L. frodoi*, *L. barozii* and *L. sigillatus* are the most abundant species). A slight decrease in abundance of genera *Biscutum*, *Bussonius*, *Calyculus*, *Carinolithus* and *Ortigonoides* is observed after the termination of the T-OAE. In the studied core, genera *Biscutum*, *Bussonius*, *Calyculus*, *Carinolithus*, *Mitrolithus*, *Schizosphaerella* and *Ortigonoides* are subordinated whereas genera *Axopodorhabdus*, *Discorhabdus*, *Diductius*, *Parhabdolithus* and *Tubirhabdus* are sporadic.

Biostratigraphy of the Schandelah Core

A total of fifteen calcareous nannofossil events were detected (Fig. 7.3) and three biozones were identified, namely the:

- *Lotharingius hauffii* Zone (NJ5);
- *Carinolithus superbis* Zone (NJ6);
- *Discorhabdus striatus* Zone (NJ7).

The lowermost investigated sample (52 m) was assigned to the earliest Toarcian NJ5 *Lotharingius hauffii* Zone, and specifically to the NJ5b *Crepidolithus imponentus* Subzone for the presence of *C. imponentus* (*C. cavus*). The FO of *C. superbis sceptrum* (43.5 m) defines the NJ5/NJ6 zonal boundary. In the same sample, the FO of *D. constans* was recognized. In the lower part of the NJ6 Zone (within the T-OAE) several biohorizons were detected: the LOs of *C. granulatus*, *P. liasicus* and “large *B. finchii*” (42.5 m), *B. finchii* (41.5 m) and *B. grandis* (40.5 m). In the upper part of the NJ6 Zone an important drop in abundance of *L. hauffii* was observed, and here reported as LO of *L. hauffii* acme 1 (31.5 m) (*L. hauffii* acme in Bown and Cooper, 1998). The FO of *W. colacicchi* (30 m) was also detected. The FO of *D. striatus* (28 m) defines the NJ6/NJ7 zonal boundary. In the same sample the

FO of *Watznaueria* sp. 1 was recognized. Within the Late Toarcian NJ7 Zone four events were found: FO of *C. superbus superbus* (26 m), LO of *O. hamiltoniae* (21.5 m), FO of *D. criotus* (19 m) and a further drop in abundance of *L. hauffii* named LO of *L. hauffii* acme 2 (18.5 m). The uppermost investigated sample (5.5 m) is still included in the Late Toarcian NJ7 Zone due to the absence of *R. incompta*.

Calcareous nannofossil assemblage characterizing the upper NJ5b is extremely poor and several samples are barren. The genera *Bussonius*, *Lotharingius*, *Crepidolithus* and *Schizosphaerella* are sporadic. The “*Schizosphaerella* crisis” is not recognized in the Schandelah Core in absence of a drop in its abundance. The NJ6 (both across and above the T-OAE) calcareous nannofossil assemblages are dominated by the genera *Crepidolithus* (*C. crassus* and *C. cavus* are the most abundant species) and *Lotharingius* (*L. hauffii*, *L. frodoi*, *L. barozii* and *L. sigillatus* are the most abundant species). A slight decrease in abundance of the genera *Biscutum*, *Bussonius*, *Calyculus*, *Carinolithus* and *Ortgonoides* is observed after the termination of the T-OAE. An increase in abundance of *Schizosphaerella*, the so called “*Schizosphaerella* recovery” (29.5 m) affecting both *S. punctulata* and “small” *S. punctulata*, is recorded close to the NJ6/NJ7 zonal boundary. Calcareous nannofossils characterizing the NJ7 Zone are still dominated by genera *Crepidolithus* and *Lotharingius*. The decrease in abundance of *L. hauffii* is balanced by an increase of larger *Lotharingius*, such as *L. crucicentralis* and *L. velatus*. An increase of *Bussonius* and *Discorhabdus* is also observed. In the Schandelah Core, genera *Biscutum*, *Bussonius*, *Calyculus*, *Carinolithus*, *Mitrolithus*, *Schizosphaerella* and *Orthogonoides* are subordinated, whereas genera *Axopodorhabdus*, *Discorhabdus*, *Diductius*, *Parhabdolithus*, *Tubirhabdus* and *Watznaueria* are sporadic.

Geochemistry

For the L1 Core, $\delta^{13}\text{C}_{\text{org}}$ values range from $-25.18 \pm 0.08 \text{ ‰}$ at 27.4 m to $-33.13 \pm 0.08 \text{ ‰}$ at 23.75 m. The most negative values are restricted to the Carbon Isotope Excursion (CIE) documented in the lower part of the Posidonienschiefer (sample from 24.1 m to 23.45 m). As far as the Schandelah Core is concerned, $\delta^{13}\text{C}_{\text{org}}$ values range from $-25.71 \pm 0.08 \text{ ‰}$ at 49 m to $-32.78 \pm 0.08 \text{ ‰}$ at 41.5 m. As for the former core, the lower part of the Posidonienschiefer displays the most negative values (sample from 42 m to 40.5 m).

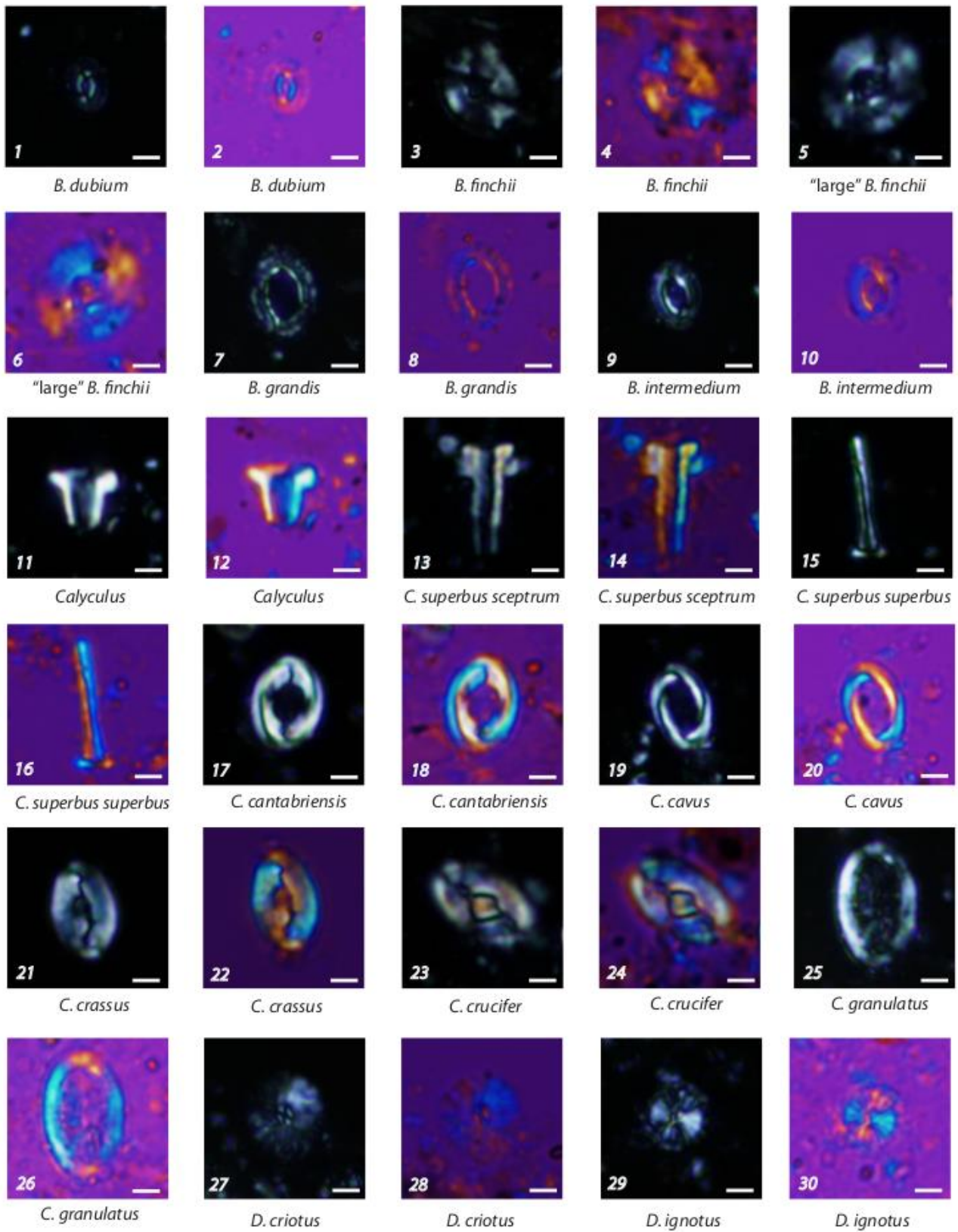


PLATE 3

Scale bars represent 2 μm .

Figs. 1-2 - *B. dubium*, 1) cross - polarized light, 2) quartz lamina, Schandelah Core 22.5 mbsf.

Figs. 3-4 - *B. finchii*, 3) cross - polarized light, 4) quartz lamina, L1 Core 24.5 mbsf.

Figs. 5-6 - “large” *B. finchii*, 5) cross - polarized light, 6) quartz lamina, L1 Core 24.9 mbsf.

Figs. 7-8 - *B. grandis*, 7) cross - polarized light, 8) quartz lamina, L1 Core 24.1 mbsf.

Figs. 9-10 - *B. intermedium*, 9) cross - polarized light, 10) quartz lamina, L1 Core 22.85 mbsf.

Figs. 11-12 - *Calyculus spp.*, 11) cross - polarized light, 12) quartz lamina, L1 Core 23.75 mbsf.

Figs. 13-14 - *C. superbus sceptrum*, 13) cross - polarized light, 14) quartz lamina, L1 Core 19.2 mbsf.

Figs. 15-16 - *C. superbus superbus*, 15) cross-polarized light, 16) quartz lamina, Schandelah Core 26 mbsf.

Figs. 17-18 - *C. cantabriensis*, 17) cross-polarized light, 18) quartz lamina, L1 Core 24.5 mbsf.

Figs. 19-20 - *C. cavus*, 19) cross-polarized light, 20) quartz lamina, L1 Core 21.2 mbsf.

Figs. 21-22 - *C. crassus*, 21) cross-polarized light, 22) quartz lamina, L1 Core 21.0 mbsf.

Figs. 23-24 - *C. crucifer*, 23) cross-polarized light, 24) quartz lamina, Schandelah Core 39 mbsf.

Figs. 25-26 - *C. granulatus*, 25) cross-polarized light, 26) quartz lamina, L1 Core 24.9 mbsf.

Figs. 27-28 - *D. criotus*, 27) cross-polarized light, 28) quartz lamina, Schandelah Core 19.5 mbsf.

Figs. 29-30 - *D. ignotus*, 29) cross-polarized light, 30) quartz lamina, Schandelah Core 22.5 mbsf.

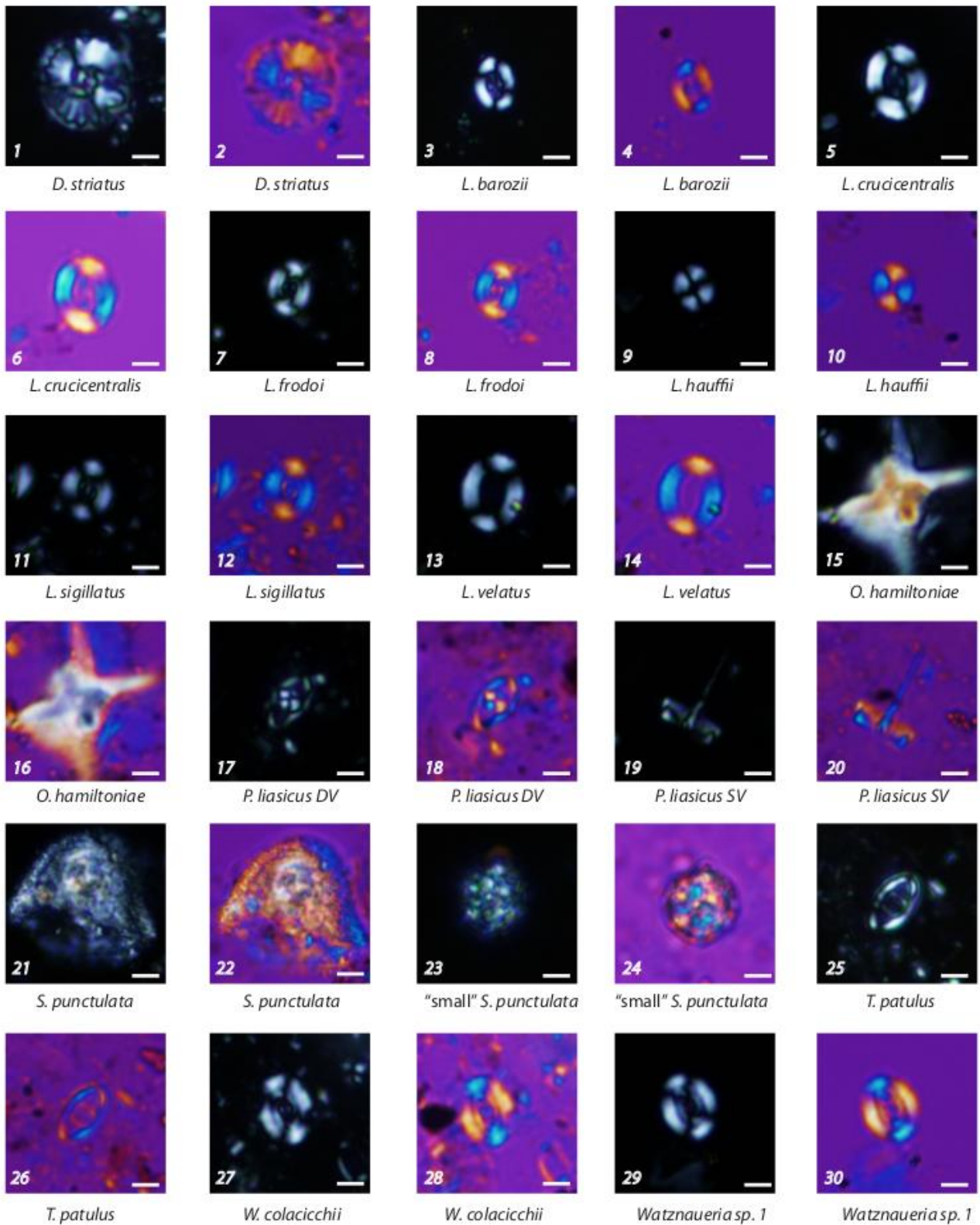


PLATE 4

Scale bars represent 2 μm .

Figs. 1-2 - *D. striatus*, 1) cross-polarized light, 2) quartz lamina, Schandelah Core 27.5 mbsf.

Figs. 3-4 - *L. barozii*, 3) cross-polarized light, 4) quartz lamina, Schandelah Core 22.5 mbsf.

Figs. 5-6 - *L. crucicentralis*, 5) cross-polarized light, 6) quartz lamina, L1 Core 19.9 mbsf.

Figs. 7-8 - *L. frodoi*, 7) cross-polarized light, 8) quartz lamina, L1 Core 22.65 mbsf.

Figs. 9-10 - *L. hauffii*, 9) cross-polarized light, 10) quartz lamina, Schandelah Core 25.0 mbsf.

Figs. 11-12 - *L. sigillatus*, 11) cross-polarized light, 12) quartz lamina, L1 Core 21.85 mbsf.

Figs. 13-14 - *L. velatus*, 13) cross-polarized light, 14) quartz lamina, L1 Core 27.5 mbsf.

Figs. 15-16 - *O. hamiltoniae*, 15) cross-polarized light, 16) quartz lamina, L1 Core 24.9 mbsf.

Figs. 17-18 - *P. liasicus* distal view, 17) cross-polarized light, 18) quartz lamina, L1 Core 24.7 mbsf.

Figs. 19-20 - *P. liasicus* side view, 19) cross-polarized light, 20) quartz lamina, L1 Core 24.7 mbsf.

Figs. 21-22 - *S. punctulata*, 21) cross-polarized light, 22) quartz lamina, Schandelah Core 30.0 mbsf.

Figs. 23-24 - "small" *S. punctulata*, 23) cross-polarized light, 24) quartz lamina, Schandelah Core 30.5 mbsf.

Figs. 25-26 - *T. patulus*, 25) cross-polarized light, 26) quartz lamina, Schandelah Core 24.5 mbsf.

Figs. 27-28 - *W. colacicchii*, 27) cross-polarized light, 28) quartz lamina, Schandelah Core 19.5 mbsf.

Figs. 29-30 - *Watznaueria* sp.1, 29) cross-polarized light, 30) quartz lamina, Schandelah Core 21.0 mbsf.

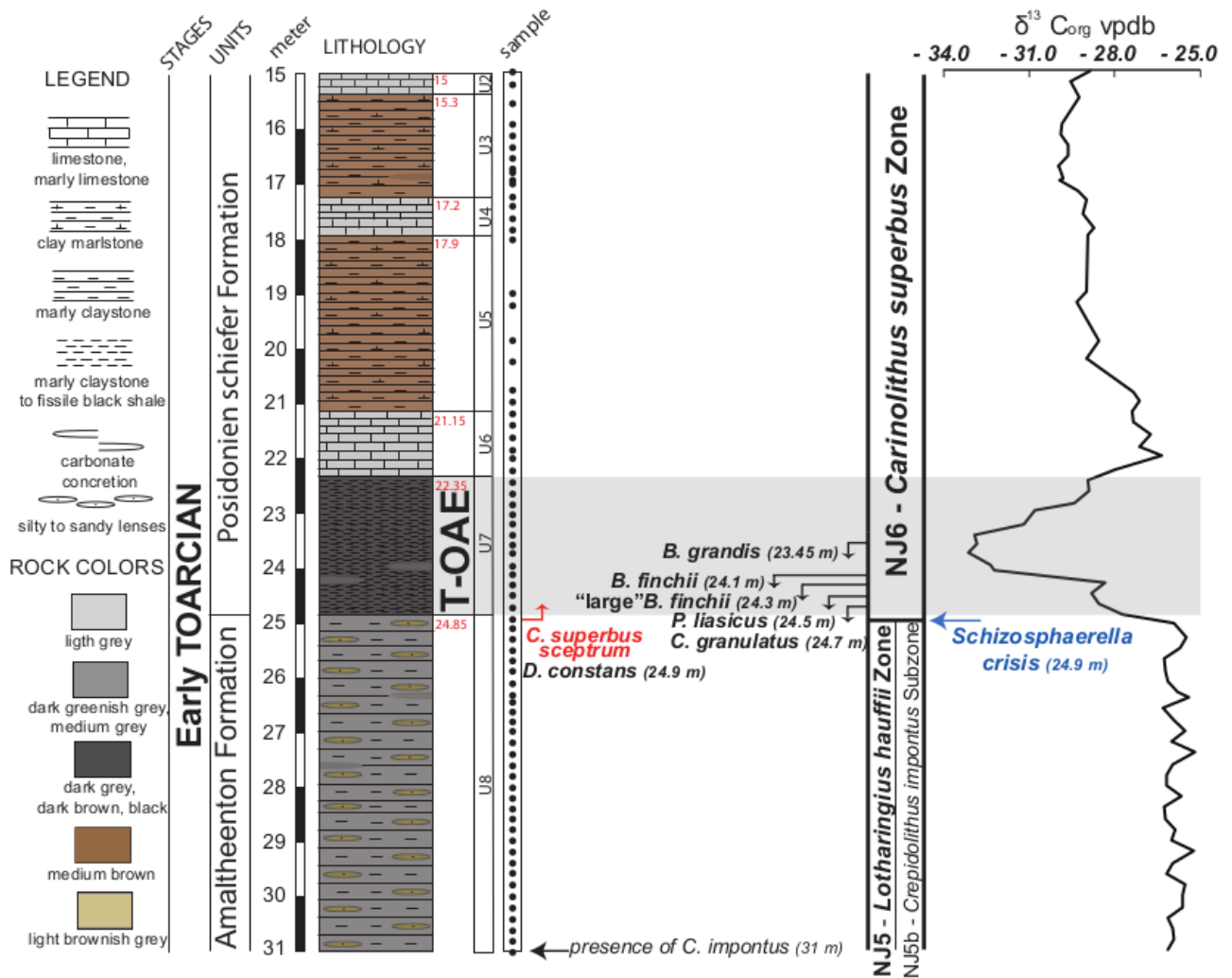


Fig. 7.2. – Litostratigraphy, calcareous nannofossil biostratigraphy and organic C isotope curve of the L1 Core. The zonal event of Bown and Cooper (1998) is reported in red. The “*Schizosphaerella crisis*” (sensu Casellato and Erba 2015) is reported in blue.

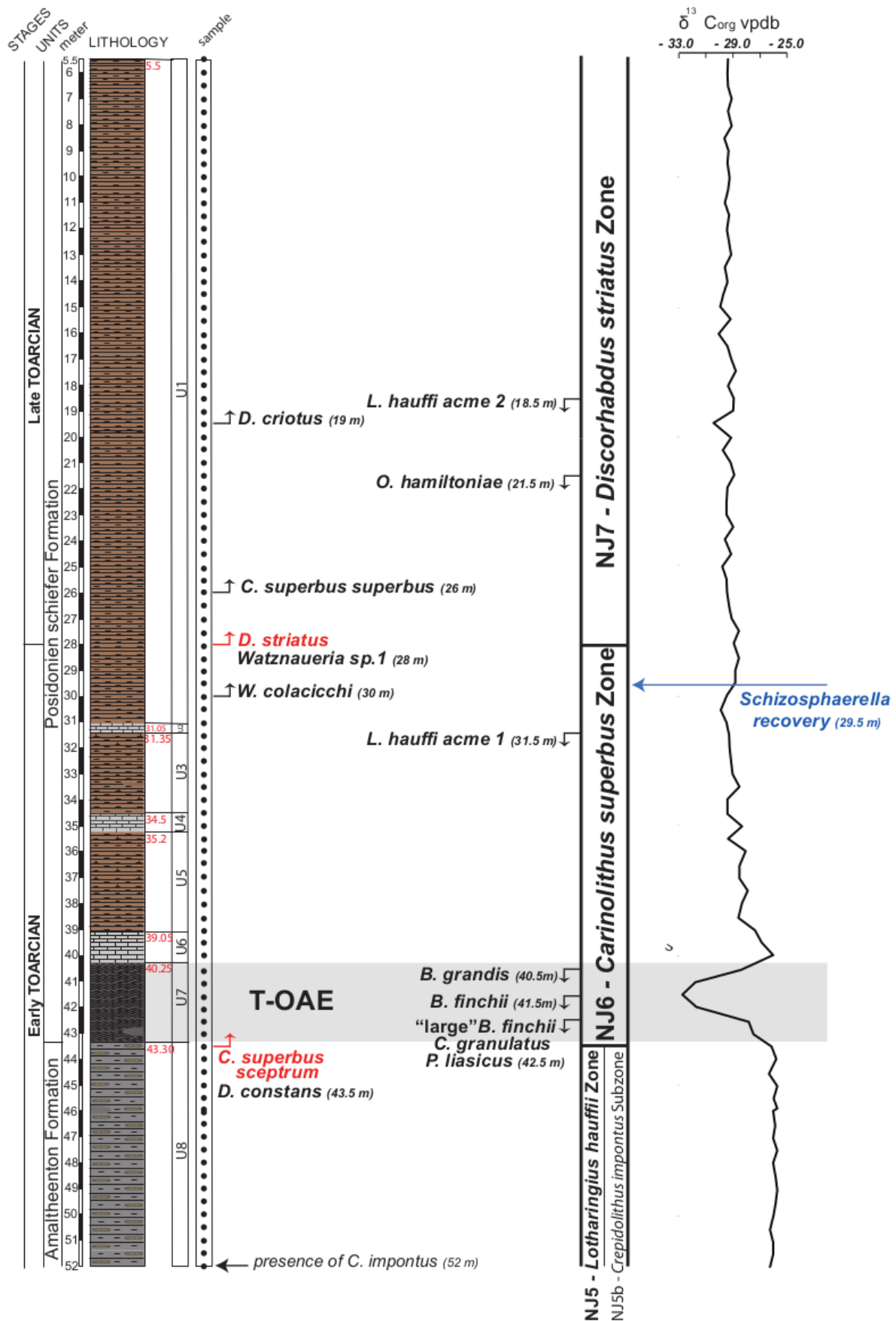


Fig. 7.3. – Litostratigraphy, calcareous nannofossil biostratigraphy and organic C isotope curve of the Schandelah Core. The zonal events of Bown and Cooper (1998) are reported in red. The “*Schizosphaerella* recovery” (sensu Casellato and Erba 2015) is reported in blue.

Chapter 8

Discussion

8.1. Sogno Core

Comparison with the Tethyan biozonation scheme (Mattioli and Erba, 1999)

Calcareous nannofossil events recognized in the Sogno Core (Fig. 8.1B) are compared to those identified by Mattioli and Erba (1999) for the standard Tethyan biozonation (Fig. 8.1C) to discuss analogies and differences.

The highly resolute biostratigraphy performed in the Sogno Core allows to detect all the main events included between the FOs of *L. sigillatus* and the genus *Watznaueria* except for the FO of *W. colacicchii*. The absence of *W. colacicchii* may be imputed to an extreme rareness of this taxon, and perhaps some taxonomic problems. The FO of *L. sigillatus* was detected in the uppermost Pliensbachian in the Sogno Core whereas this event is reported in the lowermost Toarcian in the zonal scheme. A major difference regards the FOs of *L. velatus* and *D. ignotus*. In the Sogno Core the two events were detected between the FOs of *L. crucicentralis* and *C. superbus sceptrum*, definitively before the onset of the T-OAE, whereas in Mattioli and Erba (1999) they are reported between the FOs of *C. superbus* and *W. colacicchii*. The FOs of *L. crucicentralis*, *C. poulabronei*, *C. superbus sceptrum* (*C. superbus* in Mattioli and Erba, 1999), *Watznaueria* sp. 1 (*W. fossacincta* in Mattioli and Erba, 1999) are very consistent with the data of the standard Tethyan biozonation.

The FO of *B. leufuensis* is the only “rare event” reported in the zonal scheme for the studied interval. This event was not recognized because only sporadic specimens of *B. leufuensis* were detected in the studied interval, hampering its use.

The FO of *D. constans* is not proposed as an event in the zonal scheme of Mattioli and Erba (1999), but it has been identified in the Sogno Core below the FO of *C. superbus sceptrum* and here considered a “secondary event”.

Regarding “events subject to further investigations” in the Mattioli and Erba (1999) zonation, namely the FO of *S. lowei* and the LO of *M. jansae*, only the latter event was detected in the Sogno Core. In fact, *S. lowei* is extremely rare in the Sogno Core. Furthermore, my investigation confirms the LO of *M. jansae* just above the top of the Fish Level (after the T-OAE) and below the FO of *Watznaueria* sp.1.

Comparison with the stratotype at the Peniche section (da Rocha et al. 2016)

This paragraph is intended to compare events detected in the lower part of the Sogno Core (Fig. 8.1.B) with the calcareous nannofossil succession recorded in the Peniche section (Lusitanian Basin, Portugal), recently approved as Global Stratotype Section and Point (GSSP) for the Pliensbachian / Toarcian boundary and published by da Rocha et al. (2016) (Fig. 8.1.D). The Peniche section spans from the uppermost Pliensbachian to the lowermost Toarcian and a total of six events are recorded, namely: the FOs of *L. aff. L. velatus*, *B. intermedium*, *L. velatus*, *D. ignotus*, *C. superbus* and *D. constans*. In the Sogno Core most events were detected with the exception of the FOs of *L. aff. L. velatus* and *B. intermedium*. The former taxon, described by Mattioli et al. (2013) and Menini et al. (2018) as a slightly smaller and thinner *L. velatus*, was not observed in the Sogno Core. The species *B. intermedium* displays an extremely discontinuous range in the Sogno Core and, therefore, its FO cannot be identified reliably. On the contrary, our data show that the FOs of *L. velatus*, *D. ignotus*, *C. superbus sceptrum* and *D. constans* are consistent with the GSSP record. No specimens of *C. poulabronei* were reported at Peniche.

Differences in calcareous nannofossil abundances and consequently FOs and LOs position between the Sogno Core and the Peniche section may be imputed to different paleogeographic position of the Lombardy Basin of the Southern Alps (Sogno Core) and Portugal during the Early Toarcian. As pointed out by Reggiani et al. (2010b), the Lusitanian Basin represents a North-South seaway where exchanges occurred between the North-West Europe basins and Tethyan areas. This may have led to slightly different calcareous nannofossil assemblages characterising the NJT5 and NJT6 zones as also recently pointed out by Ferreira et al. (2019).

Comparison with the Colle di Sogno section (Casellato and Erba, 2015)

Calcareous nannofossil events detected in the Sogno Core (Fig. 8.1.B) are compared to those reported in the Colle di Sogno section (Casellato and Erba, 2015) (Fig. 8.1.A). The geological interval studied in the outcrop spans from the Upper Pliensbachian (Domaro Lmst.) to the Lower Toarcian (Sogno Fm.) (Casellato and Erba, 2015; fig. 3) and is longer than the cored succession. In particular, the bottom part of the Sogno Core is younger and the FOs of *Calyculus* spp., *B. grandis*, *B. prinsii*, *L. frodoii* and *B. leufuensis* were not detected.

As far as the “main events” are concerned, all FOs and LOs reported in Casellato and Erba (2015) were detected also in the Sogno Core and, as expected, consistent results were obtained for the FOs of *C. poulabronei*, *L. crucicentralis*, *Watznaueria* sp. 1 and LO of *M. jansae*. In Casellato and Erba, (2015; fig. 8), the LO of “thin *M. jansae*” was distinguished from that of *M. jansae*. Based on absolute

abundances obtained in thin sections, Casellato & Erba (2015) placed the LO of *M. jansae* at the base of the Fish Level (onset of the T-OAE). Nevertheless, looking at the biostratigraphic range chart (Casellato and Erba, 2015; appendix 2) sporadic specimens of *M. jansae* are still present in the Fish Level. This datum is consistent with our investigation of the Sogno Core: the two morphotypes co-occur in the Fish Level, although sporadically, and both last occur after the T-OAE termination.

The FOs of *L. sigillatus* and *C. superbus sceptrum* (*C. superbus* in Casellato and Erba, 2015) were detected slightly before in the Sogno Core (i.e. *L. sigillatus* in the uppermost Pliensbachian Domaro Lmst. and *C. superbus sceptrum* just below the Fish Level). These differences are due to the higher sampling resolution and a general better nannofossil preservation in the Sogno Core that recovered unweathered material. Presumably for the same reasons, differences emerged with the FOs of *L. velatus* and *D. ignotus*: in the Sogno Core these events were detected below the Fish Level whereas in the outcrop were reported within it. In addition, the difference may be due to an extremely discontinuous occurrence of these taxa in their initial ranges (see range chart in Appendix D). As far as the FOs of *L. velatus* and *D. ignotus* are concerned, some authors already detected these events in the Lower Toarcian before the T-OAE (see fig. 3.6). Moreover, according to Mattioli et al. (2013), *D. ignotus* behaves as a “Lazarus species”, being absent during the T-OAE in different sections (e.g. Valdorbis, Peniche and Amellago). Consequently, it is difficult to assess the real FOs of these events for their extreme rareness.

Regarding the FO of *D. constans*, my datum is consistent with the outcrop, although a slightly older occurrence in the Sogno Core is attributable to higher resolution and better nannofossil preservation.

The LO of *S. cruciulus* was indicated by Casellato and Erba (2015) as a potential “rare event”. However, the sporadic occurrence of this taxon in the Sogno Core prevented the use of this biohorizon. Moreover, in the zonal scheme of Mattioli and Erba (1999) the LO of *S. cruciulus* is reported in the uppermost Aalenian

“Additional events” such as the “*Schizosphaerella* crisis”, “*M. jansae* crisis” and “*Schizosphaerella* recovery” were also detected in the Sogno Core consistently with results of Casellato and Erba (2015).

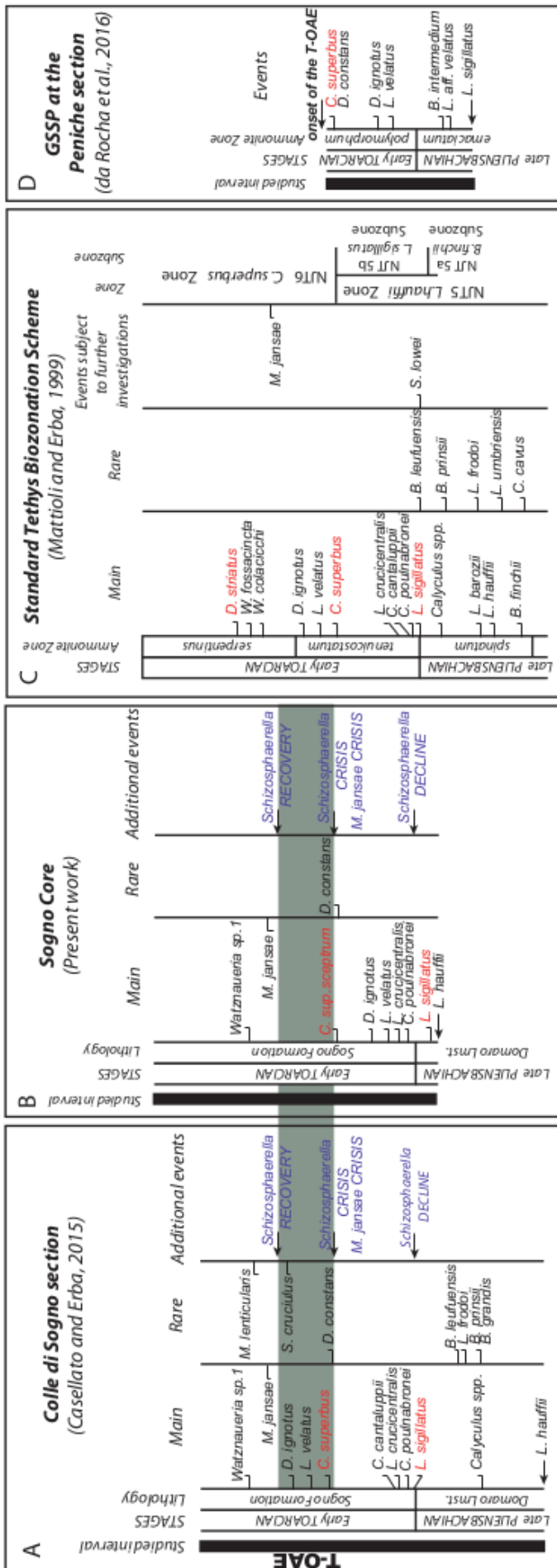


Fig. 8.1 – Comparison between calcareous nannofossil events detected in the Sogno Core (B) with those reported in the standard Tethyan biozonation scheme (C), in the Peniche section (D) and the events recognized in the outcrop of Colle di Sogno (A).

Comparison with the biostratigraphic database of literature survey

This paragraph is intended to compare the results obtained for the Sogno Core with the biostratigraphic database of literature survey discussed in chapter 3 (Fig. 8.2). Calcareous nannofossil events detected in the Sogno Core are compared to those documented for Tethyan and low-latitude sections. In chapter 3 events were calibrated simultaneously against ammonite zones and C isotope anomaly. As no ammonite zonation is available for the Sogno Core, only calibrations against the carbon isotope excursion are considered for all the events except the FOs of *Calyculus*, *L. sigillatus* and *L. crucicentralis*. For these events, we used the published calibration against ammonite zones.

- The **FO of *C. poulabronei*** detected in the Sogno Core fits well with the biostratigraphic database for lower and higher latitudes. It is older than that reported for Portugal.
- The **FO of *C. superbus sceptrum*** recognized in the Sogno Core is consistent with the biostratigraphic database at lower latitudes, higher latitudes and Portugal. Our result further confirms that this event is an excellent stratigraphic marker constraining the onset of the T-OAE at a supraregional scale.
- The **FOs of *L. velatus* and *D. ignotus*** detected in the studied core are younger than data at lower and higher latitudes as well as in Portugal.
- The **LO of *M. jansae*** in the Sogno Core is consistent with the database of literature survey at lower latitudes, at higher latitudes and Portugal and suggests that this event may be used to constrain the termination of the T-OAE.
- The **FO of *Watznaueria* sp. 1** detected in the Sogno Core fits well with the biostratigraphic database at lower latitudes and is slightly younger than that at higher latitudes.
- As previously discussed, the **FO of *Calyculus*** is not present in the investigated interval.
- The **FO of *L. sigillatus*** detected in the studied core is relatively consistent with the biostratigraphic database at lower latitudes and Portugal. An older age is reported in literature at higher latitudes.
- The **FO of *L. crucicentralis*** recognized in the Sogno Core is fully consistent with the datum at lower latitudes. This event has an older age at higher latitudes and Portugal.

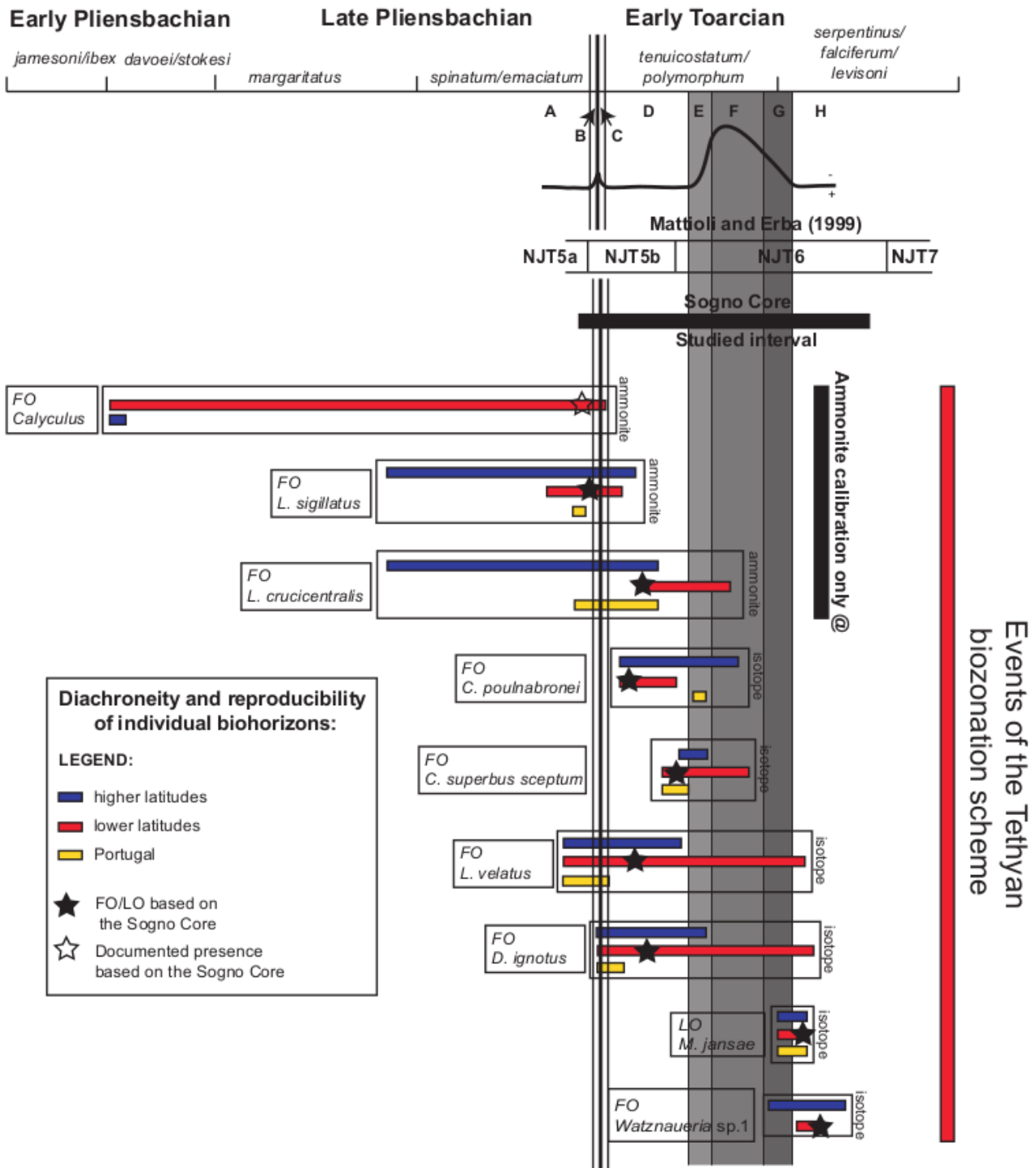


Fig. 8.2 – Reproducibility of individual biohorizons of the Tethyan biozonation scheme. The results obtained for the Sogno Core are reported.

8.2. L1 and Schandelah Cores

Comparison of the L1 and Schandelah Cores

Calcareous nannofossil preservation, biostratigraphy, abundance and organic carbon isotope data display very consistent results between the two investigated cores. Variations in calcareous nannofossils and the preservation observed across stratigraphic units is very similar in the two cores although a general slightly higher degree of overgrowth is noted in the Schandelah Core. The FOs of *C. superbis sceptrum*, *D. constans* and the LOs of *P. liasicus*, *C. granulatus*, “large” *B. finchii*, *B. finchii* and *B. grandis* appear very consistent in the two cores. Little differences regarding the event position depend on the different sampling densities adopted (higher in the L1 Core). Consequently, in the Schandelah Core, some events are detected within the same sample (i.e. LOs of *P. liasicus*, *C. granulatus*, “large” *B. finchii* in sample 42.5 m). Calcareous nannofossil variations in abundance are also very consistent.

The only remarkable difference observed regards the genus *Schizosphaerella*. A meaningful drop in abundance at the base of the Posidonienschiefer is noted exclusively in the L1 Core (Fig. 8.3). No variation in abundance is observed in Schandelah making a recognition of the “*Schizosphaerella* crisis” in this core impossible. Recently, van de Schootbrugge et al. (2018) observed the “*Schizosphaerella* crisis” also in the Schandelah Core slightly above the Pliensbachian-Toarcian boundary. This datum is not confirmed by our investigation. The sporadic presence of nannofossils, including *Schizosphaerella*, in the Aamalthenton Fm. prevents the exact recognition of this event. The “*Schizosphaerella* crisis”, marked by an average decrease of both abundance and size, is an event documented by several authors in the Tethyan Realm (Picotti and Cobianchi, 2001; Mattioli and Pittet, 2002; Erba, 2004; Casellato and Erba, 2015), Portugal (Suan et al. 2008; 2010; Mattioli et al. 2009) and Boreal Realm (Mailliot, 2009; Clémence et al. 2015; Peti and Thibault, 2017) at the base of the T-OAE. In the Lower Saxony Basin, where the Aamalthenton Fm. underlies the Posidonienschiefer Fm. the recognition of the “*Schizosphaerella* crisis” is not always possible due to the sporadic presence of nannofossils in the Aamalthenton Fm.

Comparison with the Boreal biozonation scheme (Bown and Cooper, 1998)

Calcareous nannofossil events recognized in the L1 and Schandelah Cores (Fig. 8.4. B, C) are compared to the biohorizons of Bown and Cooper (1998) (Fig. 8.4. A). For the Early to Late Toarcian time interval (*Harpoceras Serpentinum* to *Haugia variabilis* AZs) the authors reported 6 calcareous

nannofossil events (LO of *C. superbus*, LO of *B. finchii*, LO of *O. hamiltoniae*, FO of *D. striatus*, FO of *D. criotus*, LO of *L. hauffii* acme) and defined three zones (NJ5, NJ6 and NJ7). In the studied cores all biohorizons of Bown and Cooper (1998) were recognized. The succession of the events displays minor differences with the standard biozonation scheme. The FOs of *C. superbus*, *D. striatus*, *D. criotus* and the LO of *B. finchii* are consistent with the datum reported by Bown and Cooper (1998). The LO of *O. hamiltoniae* is detected slightly before the FO of *D. criotus* in the studied material, whereas Bown and Cooper (1998) reported this event slightly before the FO of *D. striatus*. This major difference is most probably imputed to the rareness of *O. hamiltoniae* in its final range. This taxon seems to have a strong affinity with organic rich sediments in the studied cores, being a fundamental constituent of calcareous nannofossil assemblages during the T-OAE (unit 7) in both the L1 and the Schandelah Cores. After the organic carbon isotope anomaly its abundance decreases drastically and becomes sporadic. In order to discuss the *L. hauffii* acme reported by Bown and Cooper (1998) we compiled the abundances of this taxon across the studied cores (Fig. 8.3). Two drops in abundance are recorded in the Schandelah Core. The first, which is more drastic, is observed at 31.5 m (*L. hauffii* acme 1) whereas the second, minor one, at 19.5 m (*L. hauffii* acme 2). The event reported in the standard biozonation scheme better correlates to the *L. hauffii* acme 2, though it is a weaker signal. Apart from these six biohorizons, which are strictly reported in the zonal scheme of Bown and Cooper, (1998; fig. 4.1) the authors discussed in their synthesis additional events in the studied interval. Those are the LOs of *P. liasicus*, *M. elegans* and *C. granulatus* within the NJ5b subzone and the LO of *B. grandis* within the NJ6 zone without specifying the detailed position at which these events are exactly placed (Fig. 8.4.). Except for the LO of *M. elegans*, not detected in our study as this taxon is observed up to the top of both cores, the other events are recognized in our investigation. Unlike Bown and Cooper (1998) the LOs of *P. liasicus* and *C. granulatus* have been both observed in the lowermost NJ6 zone in our study. The LO of *B. grandis*, being recognized in the NJ6 in our investigation, shows consistent results with the zonal scheme. Specifically, our investigation reveals that all these LOs (*C. granulatus*, *P. liasicus*, *B. finchii*, *B. grandis*) are recognized within the $\delta^{13}\text{C}_{\text{org}}$ isotope excursion of the early Toarcian Oceanic Anoxic Event in our cores. Other calcareous nannofossil events in our investigations are not reported in the standard zonal scheme (i.e. FO of *D. constans*, FO of *Watznaueria* sp.1, FO of *W. colacicchi*).

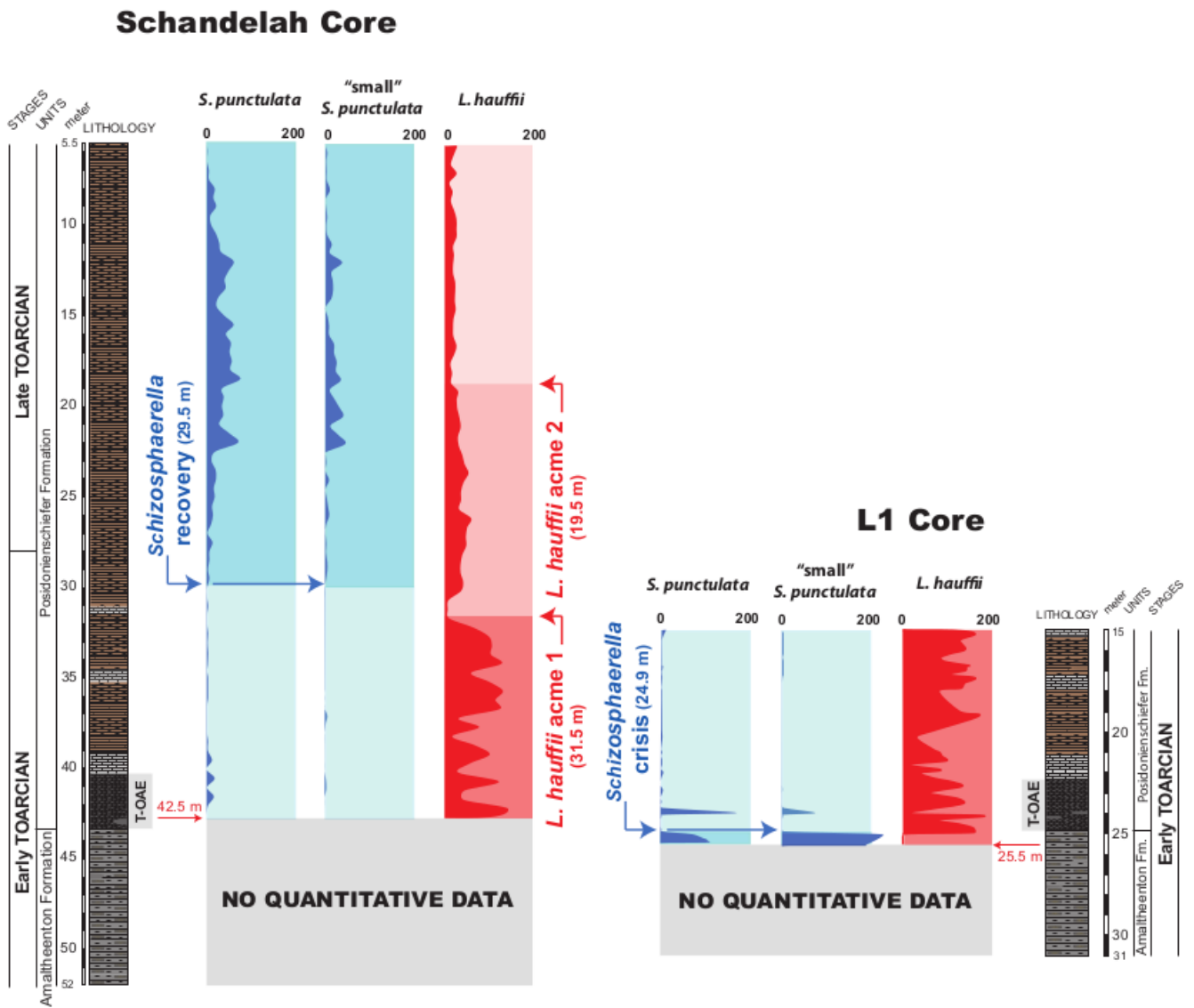


Fig. 8.3 – Abundances of *S. punctulata*, “small” *S. punctulata* and *L. hauffii* across the Schandelah and L1 Cores for the interval in which the 300-specimens counting was possible. *Schizosphaerella* crisis and recovery together with *L. hauffii* acme 1 and 2 are reported.

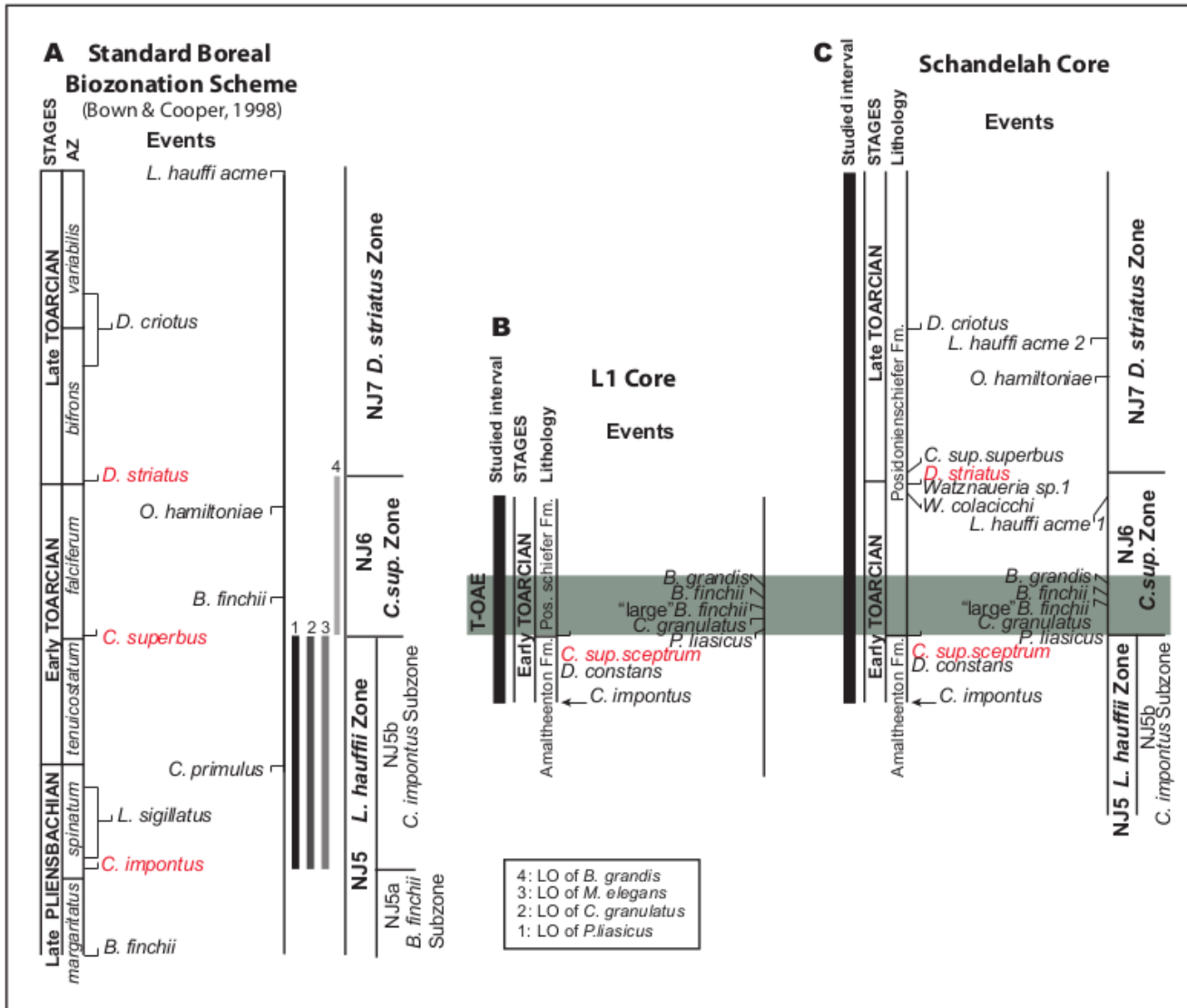


Fig. 8.4 - Comparison between calcareous nannofossil events reported by Bown and Cooper (1998) (A) and the biohorizons recognized in the L1 (B) and Schandelah (C) Cores.

Comparison with the biostratigraphic database of literature survey

This paragraph is intended to compare the results obtained in the L1 and Schandelah Cores with the biostratigraphic database of literature survey discussed in chapter 3 (Fig. 8.5). Calcareous nannofossil events detected in the L1 and Schandelah Cores are compared to those reported for Boreal and higher-latitude sections. As for Fig. 8.2, only calibrations against the carbon isotope excursion are considered for comparison because of the absence of an ammonite zonation for the L1 and Schandelah Cores. Calibrations against the C isotope curve are available for all the events except for the FOs of *C. imponentus* and *L. sigillatus*. For these events, we try to compare the results of the Sogno Core with the reproducibility obtained with the calibration against ammonite zones.

- As previously discussed, the **LO of *C. primulus*** is not present in the investigated interval.
- The **FO of *C. superbis sceptrum*** recognized in the studied cores is consistent with the biostratigraphic database of literature survey at higher latitudes, lower latitudes and Portugal. This datum is also very consistent with that of the Sogno Core further reinforcing the utility of this event as stratigraphic marker documenting the base of the T-OAE at a supraregional scale.
- The **LO of *B. finchii*** detected in the L1 and Schandelah Cores is very consistent with the biostratigraphic database of literature survey at higher latitudes. This event appears a potential stratigraphic tool to characterize the T-OAE at higher latitude.
- As previously discussed, the **presence of *C. imponentus* and *L. sigillatus*** is documented from the base of the studied cores.

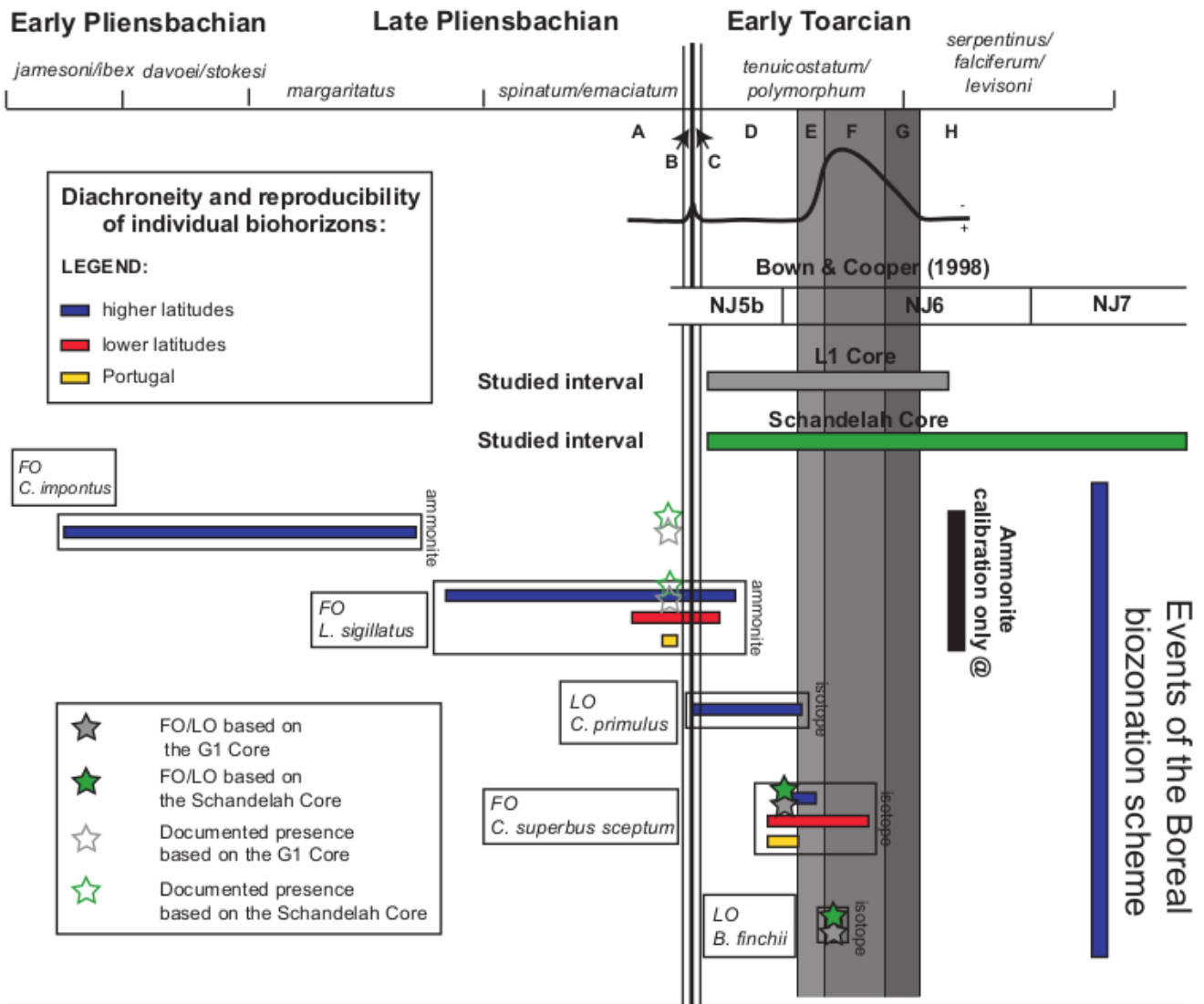


Fig. 8.5 – Reproducibility of individual biohorizons of the Boreal biozonation scheme. The results obtained for the L1 and Schandelah Cores are reported.

8.3. Synthesis of calcareous nannofossil events in the uppermost Pliensbachian-Lower Toarcian interval

Tethyan Realm

This chapter is aimed at presenting a synthesis of calcareous nannofossil events characterizing the uppermost Pliensbachian-Lower Toarcian interval from the Tethyan Realm based on literature survey and investigations performed on the Sogno Core (Fig. 8.6). Primary events are distinguished from secondary ones. The former category includes the “main events” of the zonal scheme of Mattioli and Erba (1999) and whose high reliability has been confirmed by literature survey. These are the FOs of *C. poulabronei*, *L. crucicentralis*, *C. superbus sceptrum*, *Watznaueria* sp. 1 and *D. striatus*. Within the primary events, also the FO of *L. sigillatus*, the *Schizosphaerella* crisis and the LO of *M. jansae* have been included although these events show some differences relative to the biozonation of Mattioli and Erba (1999). In fact, literature survey revealed an older age for the FO of *L. sigillatus* compared to the datum of the zonal scheme (latest Pliensbachian instead of earliest Toarcian). However, this event remains a highly reliable biohorizon.

The *Schizosphaerella* crisis was not included in the biozonation of Mattioli and Erba (1999), and, indeed, this biohorizon was coded by Erba (2004). Several works documented its reproducibility at the base of the NJT6 zone in the Tethyan Realm (e.g. Cobianchi and Picotti, 2001; Mattioli and Pittet, 2002; Erba, 2004; Reolid et al. 2014; Casellato and Erba, 2015) as well as in the Sogno Core, and thus should be considered an important stratigraphic marker.

The LO of *M. jansae* was considered an event “subject to further investigations” in the zonal scheme of Mattioli and Erba (1999); it is here introduced among the primary events for the high reproducibility and reliability documented in the literature.

The FO of *W. colacicchii*, instead, was considered a “main event” of the zonal scheme by Mattioli and Erba (1999) but is here considered unreliable and not reproducible as a result of my literature survey and investigations.

In Fig. 8.6 the “secondary events” are less reproducible. They are the FOs of *L. velatus* and *D. ignotus* that were included within the “main events” by Mattioli and Erba (1999). However, the literature survey revealed a low reliability and older ages for the FOs of *L. velatus* and *D. ignotus* in the Late Pliensbachian and across the Pliensbachian/Toarcian boundary, respectively. Similarly, the FO of *Calyculus* spp., has been re-assigned to the Early Pliensbachian.

In the synthesis scheme of the Tethys area, the *Schizosphaerella* decline, FO of *D. constans*, *M. jansae* crisis and *Schizosphaerella* recovery have been detected exclusively in the Sogno Core and Colle di Sogno outcrop and further investigations are needed to assess their reproducibility and reliability.

Based on my synthesis the Pliensbachian/Toarcian boundary appears to be constrained between the FOs of *L. sigillatus* and *C. poulabronei*. Due to its scarce reliability, the FO of *D. ignotus* should not be used as a marker for this boundary.

My synthesis shows that the FOs of *L. sigillatus*, *L. velatus*, *C. superbus sceptrum*, *Watznaueria* sp. 1, *D. striatus* and LO of *M. jansae* are reproducible in Portugal as documented by Ferreira et al. (2019) in the Lusitanian Basin zonal scheme. Specifically, the LO of *M. jansae* has been added within the zonal markers, defining the base of a new subzone, the NJT6b. As suggested by Ferreira et al. (2019), the FO of *D. ignotus* is earliest Toarcian in age, prior to the stratigraphic level indicated by Mattioli and Erba (1999) and my findings in the Sogno Core. On the contrary, the FO of *C. poulabronei* is reported at a higher stratigraphic level in the zonal scheme of Ferreira et al. (2019) compared to the biozonation of Mattioli and Erba (1999) and my findings as well as literature survey (Lower Toarcian NJT6a instead of lowermost Toarcian NJ5b).

The FO of *L. crucicentralis* is Late Pliensbachian in age in the zonal scheme of Ferreira et al. (2019) instead of earliest Toarcian in the Tethyan area (Mattioli and Erba, 1999; this work and literature survey). Moreover, Ferreira et al. (2019) upgrade this event as subzonal marker to define the base of the NJT5b subzone (Fig. 8.6)

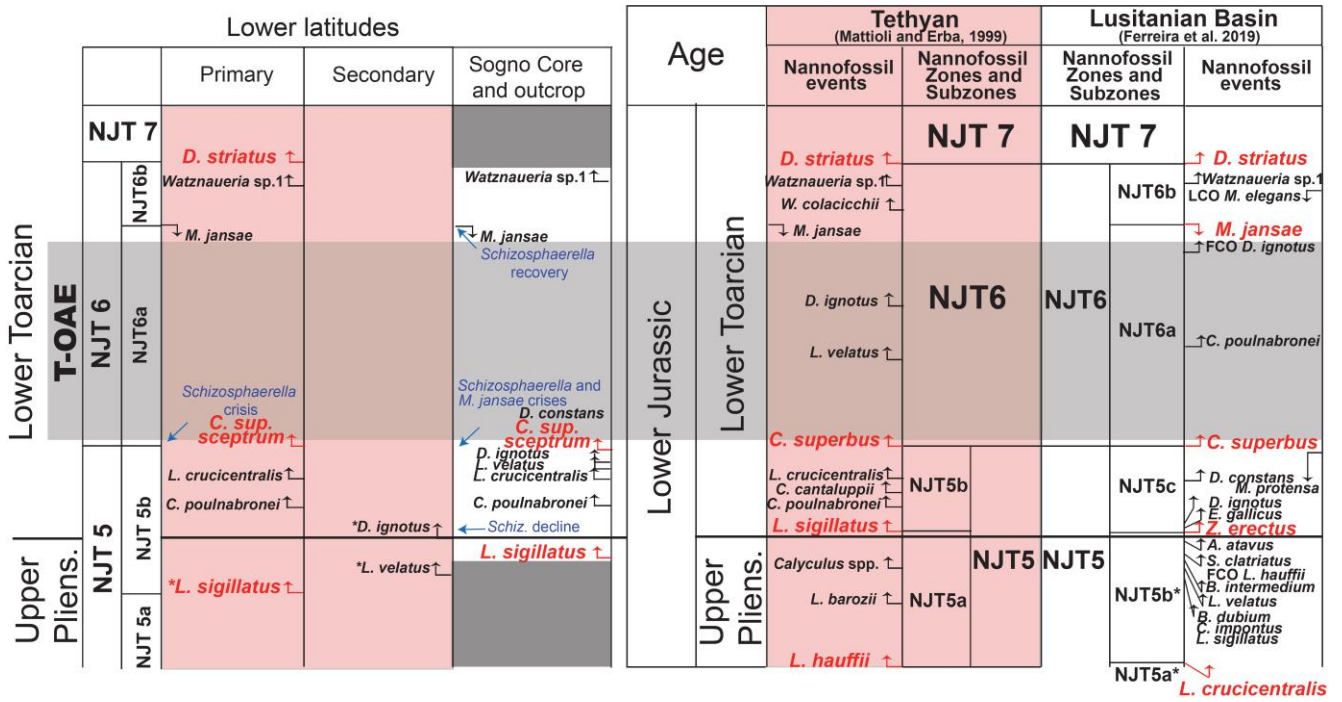


Fig. 8.6 – Primary and secondary events characterizing the Upper Pliensbachian-Lower Toarcian interval in the Tethyan Realm resulting from the literature survey (left side) compared to the zonal schemes of Mattioli and Erba (1999) and Ferreira et al. (2019) (right side). The events detected in the Sogno Core and outcrop are also provided.

Boreal Realm

Following the same criteria applied to the Tethyan area, primary events in the Boreal Realm include those of the zonal scheme of Bown and Cooper (1998) whose high reliability has been tested by literature survey and investigations of the L1 and Schandelah Cores. These are the FOs of *C. impontus*, *L. sigillatus*, *C. superbus sceptrum*, *D. striatus* and LOs of *C. primulus* and *B. finchii*.

Some of the secondary events include those discussed in the zonal scheme but without a precise age. This is the case of the LOs of *C. granulatus*, *P. liasicus* and *B. grandis* detected in the L1 and Schandelah Cores and assessed in other sections through literature survey. Other secondary events include “main events” of the Tethyan zonal scheme and reproduced in Boreal sections (FOs of *L. crucicentralis*, *L. velatus*, *D. ignotus*, *C. poul nabronei* and *Watznaueria* sp. 1). The Tethyan *Schizosphaerella* crisis has been also documented in various sections (Clémence et al. 2015; Peti and Thibault 2017; van de Schootbrugge et al. 2018) as well as in the L1 Core.

The FO of *D. constans* has been detected exclusively in the L1, Schandelah Cores and in Anse st. Nicolas section (Menini et al. 2018), thus displaying a spotty reproducibility. The LOs of *O. hamiltoniae* and *M. elegans*, two events of the zonal scheme, have not been considered in my synthesis as these events have not been documented after the zonation of Bown and Cooper (1998).

My synthesis confirms that the Pliensbachian/Toarcian boundary correlates with the LO of *C. primulus*. Due to its limited reliability, the FOs of *D. ignotus* should not be considered as a marker for this boundary.

The FOs of *L. sigillatus* and *C. superbus sceptrum* are reproducible also in Northern Spain (Fraguas et al., 2015). Other events are not reported in the zonal scheme of Fraguas et al. (2015); however, in the range charts *C. granulatus*, *B. finchii*, *P. liasicus* (both *P. liasicus liasicus* and *distinctus*) and *B. grandis* are detected up to the top of the investigated sections suggesting younger LOs of these taxa in Northern Spain compared to the Boreal Realm. Similarly, the FO of *C. impontus* is present from the base of the zonal scheme, thus implying an older age for this event in Northern Spain. The range charts do not document the presence of *L. velatus*, *L. crucicentralis* and *D. ignotus* in the investigated sections. The FO of *C. poul nabronei* and LO of *C. primulus* are not provided by the authors probably for the extremely discontinuous range of these taxa, thus preventing the identification of their FOs.

Among the primary events, my analysis revealed that the FO of *C. superbus sceptrum* is the only biohorizon reproducible in all the zonal schemes. The FO of *Watznaueria* sp. 1 and *D. striatus* are reproducible in the Tethyan and Boreal Realms, as well as in Portugal. Further analyses are required to verify whether these events are consistent also in Northern Spain since the zonal scheme of Fraguas et al. (2015) applies to an older time interval.

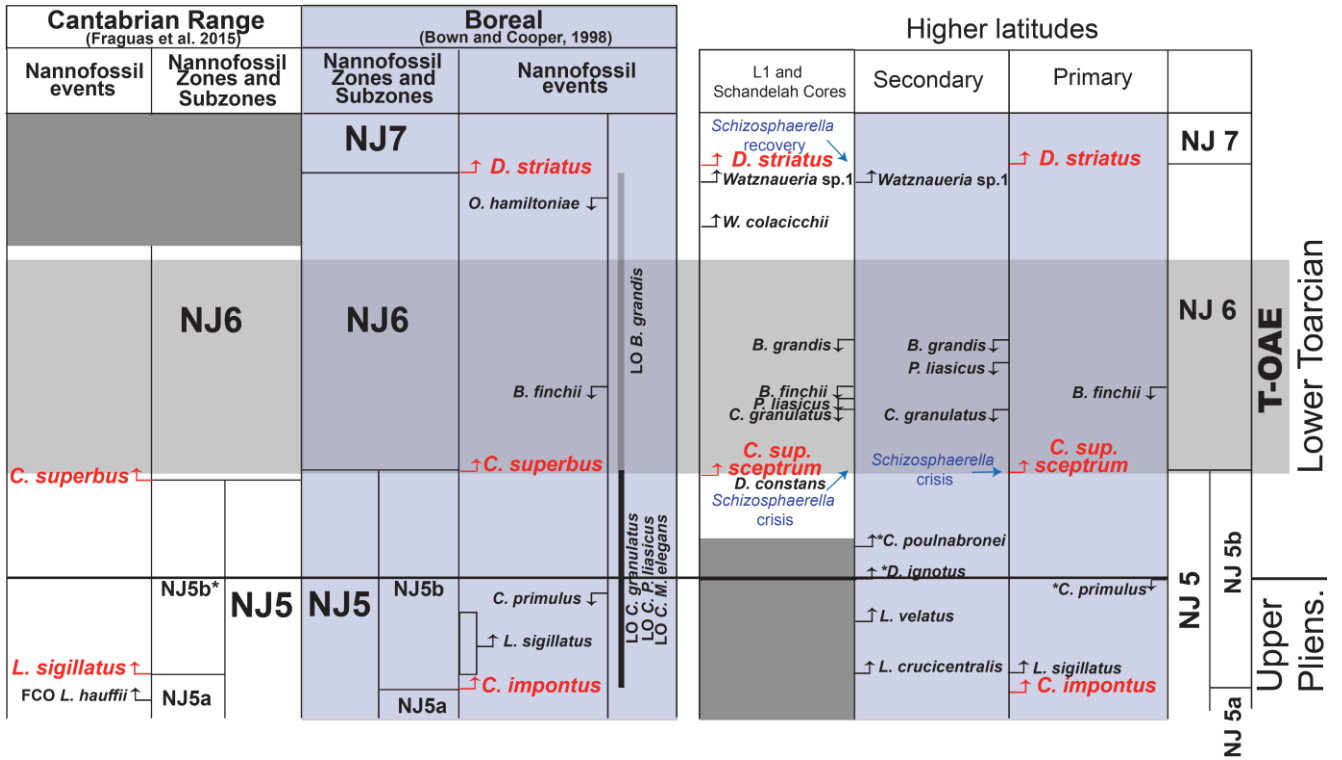


Fig. 8.7 – Primary and secondary events characterizing the Upper Pliensbachian-Lower Toarcian interval of the Boreal Realm resulting from the literature survey (right side) compared to the zonal scheme of Bown and Cooper (1998) and Fraguas et al. (2015) (left side). The events detected in the L1 and Schandelah Cores are also provided.

8.4. Biostratigraphic constraints of the T-OAE

Sogno, L1 and Schandelah Cores

Highly resolutive calcareous nannofossil investigations revealed that few events consistently constrain the T-OAE in the Sogno Core and in the L1 and Schandelah Cores, showing that calcareous nannoplankton displays a partial differentiation in the two paleogeographic realms (Bown, 1987b; Bown, 1992; Bown and Cooper, 1998; Baldanza et al. 1995; Mattioli and Erba, 1999). In the Sogno Core, the T-OAE is constrained by the FOs of *C. superbus sceptrum*, *D. constans*, “*Schizosphaerella* and *M. jansae* crises” at the onset and by the LO of *M. jansae* and the “*Schizosphaerella* recovery” at its termination. As far as the L1 and Schandelah Cores are concerned, the T-OAE is analogously constrained by the FOs of *C. superbus sceptrum*, *D. constans* and “*Schizosphaerella* crisis” at the onset. The “*Schizosphaerella* recovery” was identified only in the Schandelah Core at a younger stratigraphic level compared to that recognized in the Sogno Core, close to the NJ6/NJ7 zonal boundary. The “*M. jansae* crisis” and the LO of *M. jansae* were not recognized in the L1 and Schandelah Cores due the absence of this taxon in the studied interval.

Additional events, such as the LOs of *C. granulatus*, *P. liasicus*, *B. finchii* and *B. grandis* are recognized within the isotopic anomaly exclusively in the L1 and Schandelah Cores (Fig. 8.6).

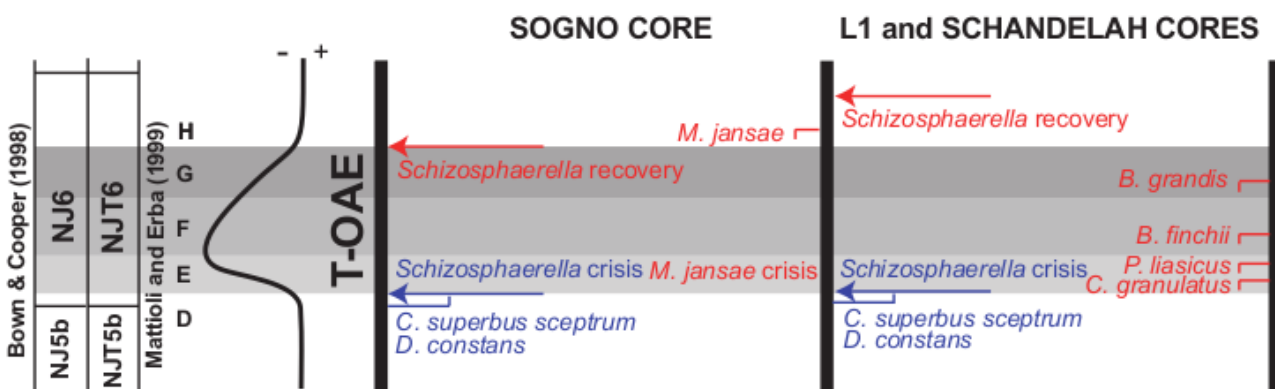


Fig. 8.8 – Calcareous nannofossil events constraining the T-OAE in the Sogno Core and L1 and Schandelah Cores. Analogies are reported in blue whereas differences in red.

Lower latitudes, higher latitudes and Portugal

This paragraph is intended to verify which events consistently constrain the T-OAE at a supraregional scale.

As previously discussed, the data recorded for **the FO of *C. superbus sceptrum*** in the Sogno, L1 and Schandelah Cores together with the exhaustive literature survey (Figs. 8.2; 8.5; 8.6; 8.7) confirm that this event is an excellent marker for the onset of the T-OAE at a supraregional level.

On the contrary, as previously pointed out by Casellato and Erba (2015), the **LO of *M. jansae*** represents a good event constraining the termination of the T-OAE exclusively at lower latitudes and in Portugal. At higher latitudes, however, the last occurrence of this taxon is attested in Northern Spain, Central-North France and South Germany but less documented. Moreover, in North Germany no specimen of this species is observed confirming that this taxon is better adapted to lower latitudes (Bucefalo Palliani et al. 2002; Mattioli et al. 2008; Reggiani et al. 2010b). As a result, we confirm that the LO of *M. jansae* is a consistent event documenting the end of the T-OAE exclusively at lower latitudes and in Portugal.

The “***Schizosphaerella crisis***” represents an additional event marking the onset of the T-OAE at a supraregional scale. As already discussed, Cobianchi and Picotti (2001), Mattioli and Pittet (2002), Erba (2004), Reolid et al. (2014), Casellato and Erba (2015), documented this event for the Brasa, Somma, Colle di Sogno and La Cerradura sections (lower latitudes); Suan et al. (2008; 2010); Mattioli et al. (2009) for the Peniche section (Portugal); Clémence et al. (2015); Peti and Thibault (2017); van de Schootbrugge et al. (2018) recorded this abundance drop in the Sancerre-Couy section and Schandelah Core. Consistent results were reported also by Tremolada et al. (2005) for Castillo de Pedroso (higher latitudes). This event is also documented in the Sogno and L1 Cores. Unlike van de Schootbrugge et al. (2018), we do not recognize this event in the Schandelah Core for the general rareness of nannofossils, including schizosphaerellids, below the Posidonienschiefer (Aamaltheenton Fm.).

An increase in abundance of *Schizosphaerella* (“***Schizosphaerella recovery***” sensu Casellato and Erba, 2015) is documented after the T-OAE exclusively for the Colle di Sogno section at lower latitudes. Clémence et al. (2015) and Tremolada et al. (2005) documented the recovery in abundance of this taxon after the T-OAE for the Sancerre-Couy and Castillo de Pedroso sections (higher latitudes). This datum was observed also in the Sogno and the Schandelah Cores, although for the latter succession an increase in abundance of *Schizosphaerella* was detected at a younger stratigraphic level, close to the NJ6/NJ7 zonal boundary. No quantitative data to assess the “*Schizosphaerella*

recovery” sensu Casellato and Erba, (2015) are available for Portugal. The limited data record of this event requires further investigations.

The “*M. jansae* crisis” represents an event still poorly documented and exclusively at lower latitudes: Casellato and Erba (2015) reported this event for the Colle di Sogno section. It is confirmed in the Sogno Core. Nevertheless, the identification of this event exclusively in one location of the Lombardy Basin is not enough to guarantee a biostratigraphic constrain at lower latitudes. No quantitative data regarding *M. jansae* are available to assess its fluctuations in abundance in other sections.

In the L1 and Schandelah Cores few additional events were recognized across the T-OAE, namely the LOs of *C. granulatus*, *P. liasicus*, *B. finchii* and *B. grandis*. As previously discussed, all these events, except for the LO of *B. finchii*, were not formally used in the Boreal zonation of Bown and Cooper (1998). Our findings indicate that all these events are within the C isotope anomaly of the T-OAE (Fig. 8.6), at younger stratigraphic levels relative to the Bown and Cooper (1998) zonation. In order to evaluate their reproducibility at higher (France, North Spain, England, South and North Germany) and lower latitudes (Italy, South-East Spain, Hungary and Greece) and in Portugal, and their use as additional stratigraphic markers at supraregional or regional scale these events are evaluated against the C isotope curve (Fig. 8.7) (see appendix B for references). The FO of *D. constans* is also included in this analysis, being recognized at the base of the T-OAE in the studied cores. Moreover, no reproducibility investigations have been published yet for this event.

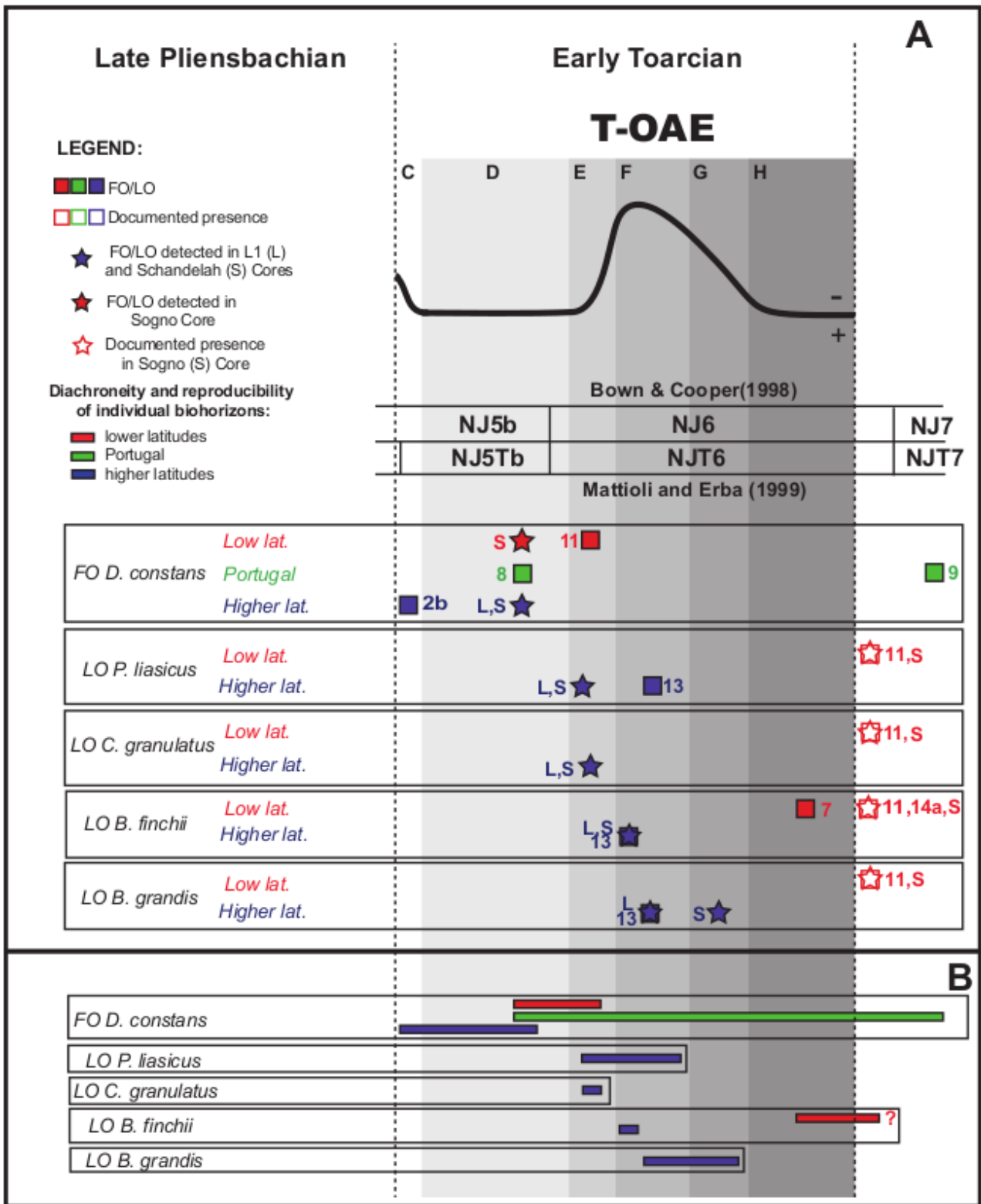


Fig. 8.9 - A) Calcareous nannofossil events detected in the L1 and Schandelah Cores prior and during the T-OAE, plotted against the C isotope generalized curve, divided into 6 intervals as follow: C = lowermost Toarcian recovery; D = pre-excursion; E = rapid decrease; F = interval with minimum values; G = recovery; H = values comparable to pre-excursion ones. Numbers refer to investigated sections reported in appendix X. B) Diachroneity of individual biohorizons relative to the C isotopic excursion.

Each calcareous nannofossil event is discussed below in stratigraphic order:

- The **FO of *D. constans*** is found within sub-interval D in both L1 and Schandelah Cores. Our result displays a strong consistency with the datum recognized in the Sogno Core and the Peniche section. This event was correlated to sub-interval E in the Colle di Sogno section whereas in Rabaçal section was detected at a younger level within the NJT7b (Middle Toarcian). Moreover, in the Anse St. Nicolas section this event was detected in the sub-interval C.
- The **LO of *P. liasicus*** is detected within sub-interval E in both L1 and Schandelah Cores. This event was detected within the sub-interval C in the Sancerre-Couy section. The presence of this taxon was documented in the Sogno Core and in the Colle di Sogno section after the T-OAE.
- The **LO of *C. granulatus*** is recognized within sub-interval E in both L1 and Schandelah Cores. The presence of this taxon was documented in the Sogno Core and in the Colle di Sogno section after the T-OAE.
- The **LO of *B. finchii*** is detected within the lowermost sub-interval F in both L1 and Schandelah Cores. An analogous result was documented in the Sancerre-Couy section. This event was calibrated to the sub-interval H in the Reka section. The presence of this taxon was documented in the Sogno Core and the Colle di Sogno and Toka after the T-OAE.
- The **LO of *B. grandis*** is found within sub-interval F in L1 Core and within sub-interval G in Schandelah Core. The datum reported for the former succession is analogous to that proposed for the Sancerre-Couy section. The presence of this taxon was documented in the Sogno Core and Colle di Sogno section after the T-OAE.

Our analysis reveals that all the calcareous nannofossil events detected across the T-OAE in the L1 and Schandelah Cores show consistency with at least one section, except for the LO of *C. granulatus* which is recognized exclusively in the investigated German cores.

Based on my findings and literature survey, the **FO of *D. constans*** is an additional events for the onset of the T-OAE exclusively in the Colle di Sogno section and Sogno Core at lower latitudes. The datum proposed for the Rabaçal section (Portugal) is much younger compared to that of Peniche (Portugal), probably for the sporadic presence of this taxon. On the contrary, the datum recognized in Anse St. Nicolas (higher latitudes) is slightly older than that recorded in the L1 and Schandelah Cores, revealing a possible older age of this event at higher latitudes. The FO *D. constans* documented at Anse St. Nicolas is more reliable than that recorded in the L1 and Schandelah as the lower parts of the

investigated cores are mainly barren of nannofossils, preventing the recognition of the real FO of this taxon. Although a potential utility as biostratigraphic marker for the onset of the T-OAE is not excluded, further investigations are recommended in order to verify the reliability and reproducibility of this event.

The **LO of *C. granulatus*** is recognized exclusively in the investigated German cores. In the Tethys Realm, this event is younger (earliest Bajocian) as reported by Mattioli and Erba (1999).

The levels of the **LOs of *P. liasicus*, *B. finchii*, *B. grandis*** detected in the L1 and Schandelah Cores are relatively consistent with the Sancerre Couy section (higher latitudes), within the C isotope anomaly of the T-OAE in the Boreal Realm. However, in the Sancerre-Couy section the LO of *P. liasicus* is detected at a younger stratigraphic level compared to the LO of *B. finchii*. We, therefore, confirm that these events are potentially useful in the Boreal Realm, except for Northern Spain as discussed in the previous chapter. At lower latitudes these events are younger as documented in the Sogno Core, the Colle di Sogno and Toka sections as well as the zonal scheme of Mattioli and Erba (1999) who placed these events in the Lower (LO of *P. liasicus*) and Upper Aalenian (LOs of *B. grandis* and *B. finchii*). The same events are younger also in Portugal as pointed out by the recently published biozonation scheme of Ferreira et al. (2019) based upon sections belonging to the Lusitanian Basin where these taxa are present up to the lowermost Bajocian.

In the Lusitanian Basin zonal scheme, Ferreira et al. (2019) introduced the LO of *C. poulabronei* and the FCO of *D. ignotus* within the NJT6a (Fig. 8.6) without discussing whether these events can be used to discriminate the T-OAE or not in Portugal. The authors explain that two reference sections are used for the NJT6a, namely, Peniche and Rabaçal. The LO of *C. poulabronei* is reported exclusively in the Peniche section. Conversely, The FCO of *D. ignotus* is documented in both the Rabaçal and Peniche sections, suggesting a more reliable datum. This latter biohorizon may be considered a secondary event constraining T-OAE in Portugal. Specifically, being recognized in both sections in the upper part of the NJT6a and making a comparison with the C isotope anomaly provided in fig. 4 of Ferreira et al. (2019), it is observed that the FCO of *D. ignotus* could be a useful additional event to constraint the termination of the T-OAE.

In the Lusitanian Basin zonal scheme, Ferreira et al. (2019) introduced the LO of *C. poulabronei* and the FCO of *D. ignotus* within the NJT6a (Fig. 8.6) without discussing whether these events can be used to discriminate the T-OAE or not in Portugal. The authors explain that two reference sections are used for the NJT6a, namely, Peniche and Rabaçal. The LO of *C. poulabronei* is reported exclusively in the Peniche section. Conversely, The FCO of *D. ignotus* is documented in both the Rabaçal and

Peniche sections, suggesting a more reliable datum. This latter biohorizon may be considered a secondary event constraining T-OAE in Portugal. Specifically, being recognized in both sections in the upper part of the NJT6a and making a comparison with the C isotope anomaly provided in fig. 4 of Ferreira et al. (2019), it is observed that the FCO of *D. ignotus* could be a useful additional event to constraint the termination of the T-OAE.

The available biostratigraphic database (literature survey) together with the highly resolutive calcareous nannofossil investigations of the Sogno, L1 and Schandelah Cores allow to derive a synthesis of calcareous nannofossil events across the T-OAE (Fig. 8.10).

- At lower latitudes (sections in Italy, South-East Spain, South France, Greece and Hungary), our study confirms that the T-OAE is well constrained by three main events: the FOs of *C. superbus sceptrum*, the *Schizosphaerella* crisis at the onset and the LO of *M. jansae* at its termination. These events are reproducible in Portugal with the addition of the FCO of *D. ignotus* marking the termination of the event.
- At higher latitudes (sections in Central-North France, North Spain, England and Germany) our study confirms that the T-OAE is constrained by the FOs of *C. superbus sceptrum* and the “*Schizosphaerella* crisis” at the onset of the T-OAE. Additional stratigraphic events, not reproducible in North Spain, are the LOs of *C. granulatus*, *B. finchii*, *P. liasicus* and *B. grandis* within the T-OAE.

Specifically, the FO of *C. superbus sceptrum* is included in the “primary events” whereas the “*Schizosphaerella* crisis” and the LOs of *C. granulatus*, *B. finchii*, *P. liasicus* and *B. grandis* in the “secondary events”.

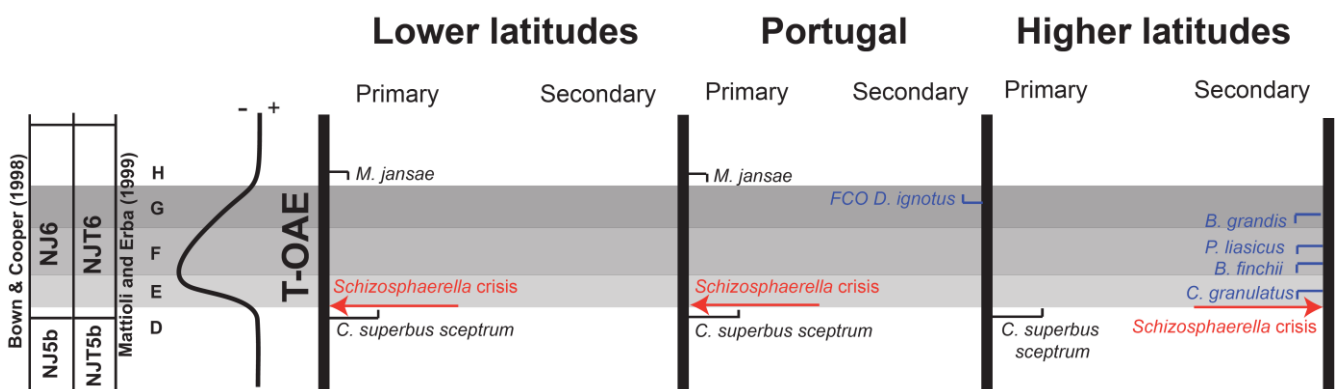


Fig. 8.10 - Calcareous nannofossil events constraining the T-OAE at lower latitudes, in Portugal and at higher latitudes. Events are divided into primary (left side) and secondary (right side). Events in blue are introduced in this thesis as new stratigraphic markers.

Chapter 9

Conclusions

Calcareous nannofossil investigations conducted in this PhD thesis resulted in major taxonomic and biostratigraphic clues in the latest Pliensbachian and Toarcian time interval.

High-resolution calcareous nannofossil biostratigraphy of the Sogno Core allowed the identification of ten events in the latest Pliensbachian to the Early Toarcian, including the T-OAE. The standard biozonation scheme of Mattioli and Erba (1999) valid for the Tethyan Realm was successfully applied and the NJT5a, NJT5b and NJT6 zones were identified. Calcareous nannofossil biostratigraphy of the L1 and Schandelah Cores allowed the identification of seven and fifteen calcareous nannofossil events in the Early Toarcian and Early to Late Toarcian time interval respectively. The zonation proposed for the Boreal Realm (Bown and Cooper, 1998) was successfully applied and the NJ5b and NJ6 zones were identified for the L1 Core and the NJ5b, NJ6, NJ7 zones for the Schandelah Core.

Calcareous nannofossil events detected in the Sogno, L1 and Schandelah Cores do not always display consistent results with the standard zonal schemes. The highly resolute calcareous nannofossil investigations of the Sogno, L1 and Schandelah Cores together with available biostratigraphic database allowed to achieve a revised and improved framework of events of the uppermost Pliensbachian-Lower Toarcian interval in the Tethyan and Boreal Realms. For the Tethyan sections, the primary events include the FOs of *L. sigillatus*, *C. poulabronei*, *L. crucicentralis*, *C. superbus sceptrum*, *Watznaueria* sp. 1, *D. striatus*, *Schizosphaerella* crisis and LO of *M. jansae* while the FOs of *L. velatus* and *D. ignotus* are considered here secondary events. Likewise, for the Boreal Realm, my synthesis resulted in the separation of primary events including the FOs of *C. impontus*, *L. sigillatus*, *C. superbus sceptrum*, *D. striatus* and LOs of *C. primulus* and *B. finchii* from the secondary events comprising the FOs of *L. crucicentralis*, *L. velatus*, *D. ignotus*, *C. poulabronei*, *Watznaueria* sp. 1, *Schizosphaerella* crisis and LOs of *C. granulatus*, *P. liasicus* and *B. grandis*.

The comparison of my literature survey with the four zonal schemes available revealed that the FO of *C. superbus sceptrum* is the only event reproducible at a supraregional level. My study confirmed that the Pliensbachian/Toarcian boundary is approximated by the FOs of *L. sigillatus* (slightly below) and *C. poulabronei* (slightly above) in the Tethyan Realm and by the LO of *C. primulus* in the Boreal.

At lower latitudes (sections in Italy, South-East Spain, South France, Greece and Hungary), my study revealed that the T-OAE is well constrained by the FOs of *C. superbus sceptrum* and the “*Schizosphaerella* crisis” at the onset and by the LO of *M. jansae* at its termination. These events are

reproducible in Portugal, with the addition of the FCO of *D. ignotus* marking the termination of the event.

At higher latitudes (sections in Central-North France, North Spain, England and Germany) my study confirms that the onset of the T-OAE is constrained by the FO of *C. superbus sceptrum* and the *Schizosphaerella* crisis. Secondary events, not reproducible in North Spain, are the the LOs of *C. granulatus*, *B. finchii*, *P. liasicus* and *B. grandis* within the event.

These results can be used as a reference for future biostratigraphic characterization of the Upper Pliensabchian-Lower Toarcian interval and could be of great help in detecting the onset and termination of the T-OAE with calcareous nannofossils.

Morphometric investigations applied on *Carinolithus superbus* and *C. magharensis* groups turned out to be extremely useful to clarify taxonomy and establish a new taxonomic scheme for the genus *Carinolithus* with further implications for biostratigraphic events. Specifically, based on biometry of selected parameters (distal shield diameter, distal shield thickness and stem width), two new subspecies of *C. superbus* (*C. superbus sceptrum* and *C. superbus superbus*) and a new species (*C. premagharensis*) were established and one species (*C. magharensis*) was emended. Qualitative investigations of *C. cantaluppii* specimens indicate that this taxon should be rejected as it is a diagenetic artefact of *Carinolithus* specimens. The revised taxonomy indicates that the FO of *C. superbus sceptrum* should be considered the marker for the base of the NJT6 and NJ6 zones and that the FO of *C. superbus superbus* is an additional event approximating the Early/Middle Toarcian boundary. Moreover, the recognition of diagenetic phases in *Carinolithus* specimens is a potential proxy to assess the impact of overgrowth and the diagenetic degree and thus can be applied in future investigations to better evaluate the state of preservation of the studied material. Future perspectives will be mainly devoted at dating the FOs of *C. premagharensis* and *C. magharensis* for a higher resolute biostratigraphy and a comprehensive understanding of the evolutive lineage of the genus *Carinolithus*.

References

- Aguado R., O'Dogherty L., Sandoval J., (2008)** - Fertility changes in surface waters during the Aalenian (mid-Jurassic) of the Western Tethys as revealed by calcareous nannofossils and carbon-cycle perturbations. *Marine Micropaleontology*: 68, 268-285.
- Aguado R., O'Dogherty L., Sandoval J., (2017)** - Calcareous nannofossil assemblage turnover in response to the Early Bajocian (Middle Jurassic) palaeoenvironmental changes in the Subbetic Basin. *Palaeogeography, Palaeoclimatology, Palaeoecology*: 472, 128-145.
- Al-Suwaidi A. H., Angelozzi G. N., Baudin F., Damborenea S. E., Hesselbo S. P., Jenkyns H. C., Manceñido M.O., Riccardi, A. C. (2010)** - First record of the Early Toarcian oceanic anoxic event from the Southern Hemisphere, Neuquén Basin, Argentina. *Journal of the Geological Society*: 167 (4), 633-636.
- Arkell W. J. (1956)** - *Jurassic geology of the world*. Oliver and Boyd Ltd. *Edinburgh, London*.
- Arp G. Gropengießer S., (2016)** – The Monotis-Dactyloceras Bed in the Posidonienschiefer Formation (Toarcian Southern Germany): condensed section, tempestite, or tsunami generated deposit? *Palaontologische Zeitschrift*; 90 (2), 271-286.
- Arthur M. A., Jenkyns H. C., Brumsack H.-J., Schlanger S. O. (1990)** - Stratigraphy, geochemistry, and paleoceanography of organic-carbon-rich Cretaceous sequences, in *Cretaceous Resources, Events and Rhythms*, NATO ASI Series, 304, (ed.) by R. N. Ginsburg and B. Beaudoin, 75-119, Kluwer Academia, Dordrecht, Netherlands.
- Asgar-Deen M., Hall R., Craig J., Riediger C., (2003)** – New biostratigraphic data from the Lower Jurassic Fernie Formation in the subsurface of west-central Alberta and their stratigraphic implications. *Canadian Journal of Earth Sciences*: 40, 45-63.
- Baldanza A., Mattioli E. (1992)** - Biostratigraphical synthesis of nannofossils in the Early Middle Jurassic of Southern Tethys. *Knihovnicka ZPN*: 14a, (1), 111-141.
- Baldanza A., Bucefalo Palliani, R., & Mattioli, E. (1995)** - Calcareous nannofossils and dinoflagellate cysts from the Late Liassic of Hungary and comparison with Central Italy assemblages. *Paleopelagos*: 5, 161-174.
- Baldschuhn R., Best G., Kockel F. (1991)** – Inversion tectonics in the north-west German basin. In: Spencer A.M, ed., *Generation, accumulation, and production of Europe's hydrocarbons. European Association of Petroleum Geoscientists Special Publication: 1, 149-159.*
- Barnard T, Hay W.W. (1974)** – On Jurassic coccoliths: A tentative zonation of the Jurassic of the Southern England and North France. *Eclogae Geologicae Helvetiae*: 67 (3) 563 – 586.
- Bassoulet J.P., Elmi S., Poisson A., Cecca F., Bellion Y., Guiraud R., Baudin F. (1993)** – Mid Toarcian. In Dercourt J., Ricou L.E., Vrielynck B., ed., *Atlas Tethys Palaeoenvironmental Maps. Beicip Franlab*: 63 -84.
- Baumann K. H., Andruleit, H., Böckel B., Geisen M., Kinkel H. (2005)** - The significance of extant coccolithophores as indicators of ocean water masses, surface water temperature, and palaeoproductivity: a review. *Paläontologische Zeitschrift*: 79, 93-112.
- Beerling D. J., Royer D. L. (2002)** - Reading a CO₂ signal from fossil stomata. *New Phytologist*: 153(3), 387-397.

- Beerling D. J., Brentnall S. J. (2007)** - Numerical evaluation of mechanisms driving Early Jurassic changes in global carbon cycling. *Geology*, 35(3), 247-250.
- Bernoulli D., Jenkyns H. C. (1974)** - Alpine, Mediterranean, and Central Atlantic Mesozoic facies in relation to the early evolution of the Tethys, in: Modern and Ancient Geosynclinal Sedimentation, edited by: Dott, R.H., and Shaver R.H., *Society of Economic Paleontologists and Mineralogists, Special Publications*, 19, 129–160.
- Bernoulli D., Jenkyns H. C., (2009)** - Ancient oceans and continental margins of the Alpine-Mediterranean Tethys: Deciphering clues from Mesozoic pelagic sediments and ophiolites, *Sedimentology*: 56(1), 149–190.
- Betz D., Führer F., Greiner G., Plein E., (1987)** – Evolution of the Lower Saxony basin. *Tectonophysics*: 137, 127-170.
- Bodin S., Mattioli E., Fröhlich S., Marshall J.D., Boutib L., Lahsini S., Redfern J., (2010)** – Toarcian carbonate isotope shifts and nutrient changes from the Northern margin of Gondwana (High Atlas, Morocco, Jurassic): Palaeoenvironmental implications. *Palaeogeography, Palaeoclimatology, Palaeoecology*: 297, 377-390.
- Bosence D., Procter E., Aurell M., Kahla A. B., Boudagher-Fadel M., Casaglia F., Cirilli S., Mehdie M., Nieto L., Rey J., Scherreiks R., Soussi M., Waltham, D. (2009)** - A Dominant Tectonic Signal in High-Frequency, Peritidal Carbonate Cycles? A Regional Analysis of Liassic Platforms from Western Tethys. *Journal of Sedimentary Research*: 79, 389 – 415.
- Boulila S., Galbrun B., Huret E., Hinnov L.A., Rouget I., Gardin S., Bartolini A., (2014)** - Astronomical calibration of the Toarcian Stage: Implications for sequence stratigraphy and duration of the early Toarcian OAE. *Earth and Planetary Science Letters*: 386, 98-111.
- Bour I., Mattioli E., Pittet B. (2007)** – Nannofacies analysis as a tool to reconstruct paleoenvironmental changes during the Early Toarcian anoxic event. *Palaeogeography, Palaeoclimatology, Palaeoecology*: 249, 58-79.
- Bown P. R. (1987)** - Taxonomy, evolution, and biostratigraphy of Late Triassic-Early Jurassic calcareous nannofossils. *Palaeontological Association, Special papers on Palaeontology*: 32, 1-118
- Bown P.R., Cooper M.K.E., Lord A.R. (1988)** - A Calcareous Nannofossil Biozonation Scheme for the early to mid-Mesozoic. *Newsletter on Stratigraphy*: 20, 91-114.
- Bown P.R., Young J., (1998)** – Techniques. In: Bown P.R. (ed.) - Calcareous nannofossil biostratigraphy. *British Micropaleontological Society Published Series*: 16-27.
- Bown P.R., Copper M.K.E. (1998)** - Jurassic. In: Bown P.R. (ed.) - Calcareous nannofossil biostratigraphy. *British Micropaleontological Society Published Series*: 34-85.
- Bown P.R., Lees J.A., Young J.R. (2004)** – Calcareous nannoplankton evolution and diversity through time. In: Thierstein H.R., Young J.R. (eds) – Coccolithophores: from molecular processes to global impact: 481-508.
- Brazier, J. M., Suan G., Tacail T., Simon L., Martin J.E., Mattioli E., Balter V. (2015)** - Calcium isotope evidence for dramatic increase of continental weathering during the Toarcian oceanic anoxic event (Early Jurassic). *Earth and Planetary Sciences Letters*: 411, 164–176.
- Bucefalo Palliani R., Mattioli E. (1998)** - High resolution integrated microbiostratigraphy of the Lower Jurassic (late Pliensbachian- early Toarcian) of central Italy. *Journal of Micropaleontology*: 17, 153-172.

- Bucefalo Palliani R., Cirilli S., Mattioli E., (1998)** - Phytoplankton response and geochemical evidence of the lower Toarcian relative sea level rise in the Umbria-Marche basin (Central Italy) *Palaeogeography, Palaeoclimatology, Palaeoecology*, 142: 33-50.
- Bucefalo Palliani R., Mattioli M., Riding J. B., (2002)** - The response of marine phytoplankton and sedimentary organic matter to the early Toarcian (lower Jurassic) oceanic anoxic event in northern England. *Marine Micropalaeontology*: 46, 223-245.
- Caruthers A. H., Gröcke D. R., Smith P. L. (2011)** - The significance of an Early Jurassic (Toarcian) carbon-isotope excursion in Haida Gwaii (Queen Charlotte Islands), British Columbia, Canada. *Earth and Planetary Science Letters*: 307(1-2), 19-26.
- Casellato C.E., Erba E. (2015)** - Calcareous nannofossil biostratigraphy and paleoceanography of the Toarcian Oceanic Anoxic event at Colle di Sogno (southern Alps, northern Italy). *Rivista Italiana di Paleontologia e Stratigrafia*: 121 (3), 297-327.
- Channell J.E.T., Erba E., Lini A. (1993)** - Magnetostratigraphic calibration of the Late Valanginian carbon isotope event in pelagic limestones from Northern Italy and Switzerland. *Earth Planetary Science Letters*: 118, 145-166.
- Channell, J. E. T., Casellato, C. E., Muttoni, G., Erba, E. (2010)** - Magnetostratigraphy, nannofossil stratigraphy and apparent polar wander for Adria-Africa in the Jurassic–Cretaceous boundary interval, *Palaeogeography, Palaeoclimatology, Palaeoecology*, 293 (1-2), 51–75.
- Claps M., Erba E., Masetti D., Melchiorri F. (1995)** – Milankovitch-type cycles recorded in Toarcian black shales from Belluno Through (Southern Alps, Italy). *Memorie della società Geologica*, 47: 179-188.
- Clémence M.E., Gardin S., Bartolini A., (2015)** – New insights in the pattern and timing of the Early Jurassic calcareous nannofossil crisis. *Palaeogeography, palaeoclimatology, palaeoecology*: 427, 100-108.
- Cobianchi M. (1990)** - Calcareous nannofossil biostratigraphy of the Domerian-Toarcian Boundary in the Navezze Valley (Brescia) *Atti Ticinensi di Scienze della Terra*: 33, 127-142.
- Cobianchi M. (1992)** - Sinemurian - Early Bajocian calcareous nannofossil biostratigraphy of the Lombardian Basin (Southern calcareous Alps; Northern Italy). *Atti Ticinensi di Scienze della Terra*, 35: 61-106.
- Cobianchi M., Vincenzo P., (2000)** - Sedimentary and biological response to sea-level and palaeoceanographic changes of a Lower-Middle Jurassic Tethyan platform margin (Southern Alps, Italy) *Palaeogeography, Palaeoclimatology, Palaeoecology*: 169, 219-244.
- Cohen A. S., Coe A. L., Harding S. M., Schwark L. (2004)** - Osmium isotope evidence for the regulation of atmospheric CO₂ by continental weathering. *Geology*: 32 (2), 157-160.
- Crux J. L. (1987)** - Early Jurassic calcareous nannofossil biostratigraphic events. *Newsletter on Stratigraphy*, 17: 79-100.
- Dal Piaz, G. (1907)**. *Le Alpi Feltrine*. C. Ferrari.
- Da Rocha R.B., Mattioli E., Duarte L., Pittet B., Elmi S., Mouterde R., Cabral M.C., Comas-Rengifo M., Gomez J., Goy A., et al., (2016)** – Base of the Toarcian Stage of the Lower Jurassic defined by the Global Boundary Stratotype Section 83 and Point (GSSP) at the Peniche section (Portugal) *Episodes: Journal of International Geoscience*: 39 (3), 460-481.
- Deflandre, G., Fert, C., (1954)** - Observations sur les coccolithophoridés actuels et fossiles en microscopie ordinaire et électronique. *Annales de Paléontologie*: 40, 115-176.

- Dera, G., Brigaud B., Monna F., Laffont R., Pucéat E., Deconinck J.F., Pellenard P., Joachimiski M.M., Durlet C., (2011)** - Climatic ups and downs in a disturbed Jurassic world. *Geology*: 39, 215–218.
- De Kaenel E., Bergen J.A., (1993)** – New early and Middle Jurassic coccolith taxa and biostratigraphy from the eastern proto-Atlantic (Morocco, Portugal and DSDP Site 547 B). *Eclogae Geologicae Helvetiae*: 86, 861-908.
- Demaison G.J., Moore G.T. (1980)** – Anoxic environments and oil source bed genesis. *Organic Geochemistry*: 2 (1), 9-31.
- Duarte L.V., Perilli N., Dino R., Rodrigues R., Paredes R. (2003)** - Lower to Middle Toarcian from the Coimbra region (Lusitanian Basin, Portugal): Sequence stratigraphy, calcareous nannofossils and stable isotope evolution. *Rivista Italiana di Paleontologia e Stratigrafia*: 110 (1), 115-127.
- Duarte L. V., Mattioli E., da Rocha R. B., Silva R. L. (2017)** - The Lower Jurassic at Peniche (Lusitanian Basin): recent advances in Stratigraphy and Sedimentary Geology. *Ciências da Terra/Earth Sciences Journal*, 19 (1), 35-51.
- Duncan R. A., Hooper P. R., Rehacek J., Marsh J. S., Duncan A. R. (1997)** - The timing and duration of the Karoo igneous event, southern Gondwana. *Journal of Geophysical Research*: 102, 18127–18138.
- Erba E. (1990)** - Calcareous nannofossils biostratigraphy of some Bajocian sections from the Digne area (SE France). *Memorie Descrittive della Carta Geologica d'Italia*: XL: 237-256.
- Erba E. (2004)** - Calcareous nannofossils and Mesozoic oceanic anoxic events. *Marine Micropaleontology*: 52, 85 -106.
- Erba E. (2006)** – The first 150 million years history of calcareous nanoplankton: Biosphere – Geosphere interaction. *Palaeogeography, palaeoclimatology, palaeoecology*: 232, 237-250.
- Erba E., Casellato C. E. (2010)** - Paleoceanografia del Giurassico nella Tetide occidentale: l'archivio geologico del Bacino Lombardo, *Rendiconti dell'Istituto Lombardo, Accademia di Scienze e Lettere, Special Publication on "Una nuova Geologia per la Lombardia"*, 447, 115–140.
- Erba E., Bottini C., Faucher G., Gambacorta G., Visentin S. (2019a)** – The response of calcareous nanoplankton to Oceanic Anoxic Events: the Italian pelagic record. *Bollettino della Società Paleontologica Italiana*, 58 (1), 51-71.
- Erba E., Gambacorta G., Visentin S., Chavalheiro L., Reolon D., Faucher G., Pegoraro M. (2019b)** – Coring the sedimentary expression of the Early Toarcian Oceanic Anoxic Event: new stratigraphic records from the Tethys Ocean. *Scientific Drilling*, 7, 1-12.
- Ferreira J., Mattioli E., Pittet B., Cachao M., Spangerberg J.E. (2015)** - Palaeocological insights on Toarcian and Lower Aalenian calcareous nannofossils from the Lusitanian Basin (Portugal). *Palaeogeography, palaeoclimatology, palaeoecology*: 436, 245-262.
- Ferreira J., Mattioli E., van de Schootbrugge B. (2017)** - Palaeoenvironmental vs. evolutionary control on size variation of coccoliths across the Lower-Middle Jurassic. *Palaeogeography, Palaeoclimatology, Palaeoecology*: 465, 177-192.
- Ferreira J., Mattioli E., Sucheràs-Marx B., Giraud F., Duarte V. L., Pittet B., Suan G., Hassler A., Spangenberg J.E. (2019)** – Western Tethys Early and Middle Jurassic calcareous nannofossil biostratigraphy. *Earth-Science Reviews*: DOI 10.1016.
- Fraguas Á., Erba E. (2010)** - Biometric analyses as a tool for the differentiation of two coccolith species of the genus *Crepidolithus* (Pliensbachian, Lower Jurassic) in the Basque-Cantabrian Basin (Northern Spain). *Marine Micropaleontology*: 77(3-4), 125-136.

- Fraguas, Á., Young, J. R. (2011)** - Evolution of the coccolith genus *Lotharingius* during the Late Pliensbachian-Early Toarcian interval in Asturias (N Spain). Consequences of the Early Toarcian environmental perturbations. *Geobios*, 44(4), 361-375.
- Fraguas A., Comas-Rengifo M.J., Gomez J.J., Goy A. (2012)** - The calcareous nannofossil crisis in Northern Spain (Asturias province) linked to the Early Toarcian warming-driven mass extinction. *Marine Micropaleontology*: 94-95, 58-71.
- Fraguas A., Comas-Rengifo M.J., Perilli N. (2015)** - Calcareous nannofossil biostratigraphy of the Lower Jurassic in the Cantabrian Range (Northern Spain) *Newsletter on Stratigraphy*: 48 (2), 179-199.
- Fraguas A., Comas-Rengifo M.J., Goy A., Gomez J.J. (2018)** - Upper Sinemurian-Pliensbachian calcareous nannofossil biostratigraphy of the E Rodiles section (Asturias, N Spain): a reference section for the connection between the Boreal and Tethys Realms. *Newsletter on Stratigraphy*: 51(2), 227-244.
- French K. L. Sepúlveda J., Trabucho-Alexandre J., Gröck, D. R., Summons, R. E. (2014)** - Organic geochemistry of the early Toarcian oceanic anoxic event in Hawsker Bottoms, Yorkshire, England. *Earth and Planetary Sciences Letters*: 390, 116–127.
- Frimmel A., Oschmann W., Schwark L. (2004)** – Chemostratigraphy of the Posidonia Black Shale, SW Germany. I. Influence of sea-level variation on organic facies evolution. *Chemical Geology*: (206) 199 – 230.
- Gaetani, M. (1975)** - Jurassic stratigraphy of the Southern Alps: a review, *Geology of Italy*, 1, 377–402
- Gaetani M., Erba E. (1990)**: Il bacino Lombardo: un sistema paleoalto/fossa in un margine continentale passivo durante il Giurassico, 75° Congresso Società Geologica Italiana, Guida all'escursione A3.
- Gaetani M. (2010)** - From Permian to Cretaceous: Adria as pivotal between extensions and rotations of Tethys and Atlantic Oceans, in: *The Geology of Italy*, (ed) by: Beltrando, M. , Peccerillo, A., Mattei, M., Conticelli, S. and Doglioni, C., *Journal of the Virtual Explorer*: 36, 5.a.
- Gaetani M., Poliani G. (1978)** – Il Toarciano e il Giurassico medio in Albenza (Bergamo). *Rivista Italiana di Paleontologia e Stratigrafia*: 84 (2), 349 – 382.
- Gardet M., (1955)** – Contribution à l'étude des cocclithes des terrains néogènes de l'Algérie. *Publications du Service de la Carte Géologique de l'Algérie (Nouvelle Série)*: 5, 477-550.
- Gardin S., Manivit H. (1994)** - Biostratigraphie des nannofossiles calcaires du Toarcien du Quercy (Sud-Ouest de la France). Comparisone avec la coupe stratotypique de la cimenterie d'Airvault (Deux Sevrès, France) *Geobios*: 17, 229-244.
- Geisen M., Bollmann J., Herrle J.O., Mutterlose J., Youg J. R. (1999)** – Calibration of the random settling technique for calculation of absolute abundances of calcareous nannoplankton. *Micropaleontology*: 45, 437-442.
- Grün W., Prins P., Zweili F., (1974)** - Coccolithophoriden aus dem Lias epsilon von Holzmaden (Deutschland). *Neues Jahrbuch für Geologie und Paläontologie Abhandlungen*: 147, 294-328.
- Hallam A., (2001)** – A review of the broad pattern of Jurassic sea-level changes and their possible causes in the light of current knowledge. *Palaeogeography, palaeoclimatology, palaeoecology*: 167, 23-37.
- Hammer Ø., Harper D.A.T. (2006)** - Paleontological Data Analysis. *Blackwell, London*: 351.

- Hammer Ø., Harper D.A.T., Ryan P.D., (2001)** - PAST: palaeontological statistics software package for education and data analysis. *Palaeontologia Electronica*: 4-9.
- Haq B.U., Hardenbol J., Vail P.R., (1988)** – Mesozoic and Cenozoic chronostratigraphy and cycles of sea-level change in Sea-Level Changes: An Integrated Approach, (ed.) C. K. Wil-gus et al., *Special Publication Society of Economic Paleontologist and Mineralogist*: 42, 71–108, 198.
- Haq B. U., Hardenbol J., Vai, P. R. (1988)** - Mesozoic and Cenozoic chronostratigraphy and cycles of sea-level change. *SEPM Special Publication 42*.
- Hardenbol J. A. N., Thierry J., Farley M. B., Jacquin T., De Graciansky P. C., Vail P. R. (1998)** - Mesozoic and Cenozoic sequence chronostratigraphic framework of European basins. *SEPM Special Publication 60*.
- Hermoso M., Le Callonnec L., Minoletti F., Renard M., Hesselbo, S. P (2009)** - Expression of the early Toarcian negative carbon-isotope excursion in separated carbonate microfactions (Jurassic, Paris Basin). *Earth and Planetary Sciences Letters*: 277, 194–203.
- Hesselbo S.H., Gröcke D.R., Jenkins H.C., Bjerrun C.J., Farrimond P., Morgans Bell H.S., Green O.R. (2000)** – Massive dissociation of gas hydrate during a Jurassic oceanic anoxic event. *Nature*: 406, 392-395.
- Hesselbo S.H., Jenkyns H.C., Duarte L.V. & Oliveira L.C.V. (2007)** - Carbon-isotope record of the Early Jurassic (Toarcian) Oceanic Anoxic Event from fossil wood and marine carbonate (Lusitanian Basin, Portugal). *Earth and Planetary Sciences Letters*, 253: 455-470.
- Hinnov L.A., Park, J., Erba E. (2000)** - Lower-Middle Jurassic rhythmites from the Lombard Basin, Italy: a record of orbitally forced carbonate cycles modulated by secular environmental changes in West Tethys, in: *Advances in Jurassic Research*,(ed): Hall R. L., and Smith P. L., *Trans Tech Publications*, 437–454.
- Izumi K., Miyaji, T., Tanabe K. (2012)** - Early Toarcian (Early Jurassic) oceanic anoxic event recorded in the shelf deposits in the northwestern Panthalassa: Evidence from the Nishinakayama Formation in the Toyora area, west Japan. *Palaeogeography, Palaeoclimatology, Palaeoecology*: 315, 100-108.
- Jenkyns H.C. (1980)** - Cretaceous anoxic events: From continents to oceans. *Journal of the Geological Society of London* - 137, 171-188.
- Jenkyns H. C. (1985)** - The Early Toarcian and Cenomanian-Turonian anoxic events in Europe: comparisons and contrasts, *Geologische Rundschau*: 74(3), 505–518, 1985.
- Jenkyns H.C. (1988)** – The Early Toarcian (Jurassic) anoxic event: stratigraphic, sedimentary, and geochemical evidence. *American Journal of Science*, 288: 101-151.
- Jenkyns H.C. (2003)** – Evidence for rapid climate change in the Mesozoic – Paleogene greenhouse world. *Philosophical Transaction Royal Society London Academy*: 361, 1885 – 1916
- Jenkyns H.C. (2010)** - Geochemistry of ocean anoxic events. *Geochemistry, Geophysics, Geosystems*: 11(3), DOI:10.1029/2009GC002788.
- Jenkyns H.C., Clayton C.J. (1986)** – Black shales and carbon isotopes in pelagic sediments from the Tethyan Lower Jurassic. *Sedimentology*: 33, 87-106.
- Jenkyns H.C., Jones C.E., Gröcke D.R., Hesselbo S.P., Parkinson D.N., (2002)**. chronostratigraphy of the Jurassic System: applications, limitations and implications for palaeoceanography. *Journal of the Geological Society, London*: 159, 351–378.

- Jourdan F., Féraud G., Bertrand H., Watkeys M. K., Renne P. R. (2007)** - Distinct brief major events in the Karoo large igneous province clarified by new $^{40}\text{Ar}/^{39}\text{Ar}$ ages on the Lesotho basalts. *Lithos*: 98(1-4), 195-209.
- Kafousia N., Karakitsios V., Mattioli E., Kenjo S., Jenkyns H.C., (2014)** - The Toarcian Oceanic Anoxic Event in the Ionian Zone, Greece. *Palaeogeography, Palaeoclimatology, Palaeoecology*: 393, 135-145.
- Kälin O. (1980)** – *Schizosphaerella punctulata* Deflandre & Dangeard: wall ultrastructure and preservation in deep-water carbonate sediments of the Tethyan Jurassic. *Eclogae Geologicae Helvetiae*: 73(3), 983-1008.
- Kälin O. Bernoulli D. (1984)** - *Schizosphaerella* Deflandre & Dangeard in Jurassic deeper-water carbonate sediments, Mazagan Continental Margin (Hole 547B) and Mesozoic Tethys. *Initial Reports DSDP*: 79, 411-429.
- Kästner M., Schülke I., Winsemann J., (2008)** – Facies architecture of a Late Jurassic carbonate ramp: the Korallenoolith of the Lower Saxony Basin. *International Journal of Earth Sciences*: 97, 991-1021.
- Kemp D.B., Coe A.L., Cohen A.S., Schwark L., (2005)** - Astronomical pacing of methane release in the Early Jurassic period. *Nature*: 437, 396–399.
- Kockel F., Wehner H., Gerling P. (1994)** – Petroleum system of the Lower Saxony Basin, Germany: Chapter 34: Part VI. Case Studies – Eastern Hemisphere. *AAPG Special volumes*, 573-586.
- Korte C., Hesselbo S. P. (2011)** - Shallow marine carbon and oxygen isotope and elemental records indicate icehouse-greenhouse cycles during the Early Jurassic. *Paleoceanography*: 26(4).
- Küspert W. (1982)** - Environmental changes during oil-shale deposition as deduced from stable isotope ratios. In: Einsele, G., Seilacher, A. (eds.), *Cyclic and Event Stratification*. Springer, Berlin: 482–501.
- Lin S. C., van Keken P. E. (2005)** - Multiple volcanic episodes of flood basalts caused by thermochemical mantle plumes. *Nature*, 436(7048), 250.
- Lini A., Weissert H., Erba E. (1992)** - The Valanginian carbon isotope event: a first episode of greenhouse climate conditions during the Cretaceous. *Global Change Special Issue, Terra Nova*: 4, 374-384.
- Lohmann H. (1909)**. Die gehäuse und gallertblasen der appendicularien und ihre bedeutung für die erforschung des lebens im meer. *Verhandlungen Deutsche Zoologische Gesellschaft*: 19, 200-239.
- López-Otálvaro G.E., Henriches M.H. (2018)** – High resolution calcareous nannofossil biostratigraphy from the Bathonian ASSP of the Cabo Mondego Section (Lusitanian Basin, Portugal). *Newsletter on Stratigraphy*, 51: 477-492.
- Lord A.L., Cooper M.K.E., Corbett P.W.M., Fuller N.G., Rawson P.F., Rees A.J.J. (1987)** – Microbiostratigraphy of the Volgian Stage (Upper Jurassic), Volga River, USSR. *Neues Jahrbuch für Geologie und Paläontologie Mh.*: 10, 577-605.
- Mailliot S., Mattioli E., Guex J., Pittet B., (2006)** - The Early Toarcian anoxia, a synchronous event in the Western Tethys? An approach by quantitative biochronology (Unitary Associations), applied on calcareous nannofossils. *Palaeogeography, Palaeoclimatology, Palaeoecology*: 240, 562-586.

- Mailliot, S., Elmi, S., Mattioli, E., & Pittet, B. (2009)** - Calcareous nannofossil assemblages across the Pliensbachian/Toarcian boundary at the Peniche section (Ponta do Trovão, Lusitanian Basin). *Ciências da Terra/Earth Sciences Journal*: 16, 51-62.
- Mailliot, S., Mattioli E., Bartolini A., Baudin F., Pittet B., Guex J., (2009)** - Late Pliensbachian–Early Toarcian (Early Jurassic) environmental changes in an epicontinental basin of NW Europe (Causses area, central France): A micropaleontological and geochemical approach. *Palaeogeography, Palaeoclimatology, Palaeoecology*: 273, 346-364.
- Mattioli E. (1993)** - Quantitative analysis of calcareous nannofossils in the Liassic portion of Pozzale section (Martani Mts., Central Italy): preliminary report. *Paleopelagos*, 3, 261-279.
- Mattioli E. (1996)** – New calcareous nannofossil species from the Early Jurassic of Tethys. *Rivista Italiana di Paleontologia e Stratigrafia*: 102, 397-412.
- Mattioli E. (1997)** - Nannoplankton productivity and diagenesis in the rhythmically bedded Toarcian-Aalenian Fiuminata section (Umbria-Marche Apennine, central Italy). *Palaeogeography, Palaeoclimatology, Palaeoecology*: 130 (1-4), 113-133.
- Mattioli E., Erba E. (1999)** - Synthesis of calcareous nannofossil events in Tethyan Lower and Middle Jurassic successions. *Rivista Italiana di Paleontologia e Stratigrafia*, 105 (3): 343-376.
- Mattioli E., Pittet B. (2002)** - Contribution of calcareous nannoplankton to carbonate deposition: a new approach applied to the Lower Jurassic of Central Italy. *Marine Micropaleontology*: 45, 175-190.
- Mattioli E., Pittet B. (2004)** - Spatial and temporal distribution of calcareous nannofossil along a proximal-distal transect in the Lower Jurassic of the Umbria-Marche Basin (Central Italy). *Palaeogeography, Palaeoclimatology, Palaeoecology*: 205, 295-316.
- Mattioli E., Pittet B., Bucefalo Palliani R., Rohl H.J., Schmid-Rohl A., Morettini E. (2004a)** - Phytoplankton evidence for the timing and correlation of paleoceanographical changes during the early Toarcian oceanic anoxic event (Early Jurassic). *Journal of Geological Society of London*: 161, 685-693.
- Mattioli E., Pittet B., Young J.R., Bown P.R., (2004b)** – Biometric analysis of Pliensbachian-Toarcian (Lower Jurassic) coccoliths of the family Biscutaceae: intra and interspecific variability versus palaeoenvironmental influence. *Marine Micropaleontology*: 52, 5-27.
- Mattioli E., Pittet B., Suan G., Mailliot S., (2008)** - Calcareous nannoplankton changes across the early Toarcian oceanic anoxic event in the western Tethys. *Paleoceanography*: 23, 1-17.
- Mattioli E., Pittet B., Petipierre L., Mailliot S. (2009)** – Dramatic decrease of pelagic carbonate production by nannoplankton across the Early Toarcian anoxic event (T-OAE). *Global Planetary Change*: 65, 134 - 145.
- Mattioli E., Planq J., Boussaha M., Duarte L.V., Pittet B. (2013)** - Calcareous nannofossil biostratigraphy: new data from the Lower Jurassic of the Lusitanian Basin. *Comunicações Geológicas*: 100 (Especial I), 69-76.
- McElwain J.C., Wade-Murphy J., Hesselbo S.P., (2005)** - Changes in carbon dioxide during an oceanic anoxic event linked to intrusion into Gondwana coals. *Nature*: 435, 479–482.
- Medd A. W. (1982)** - Nannofossil zonation of the English middle and upper Jurassic. *Marine Micropaleontology*: 7(1), 73-95.
- Menini A., Mattioli E., Spangenberg, J. E., Pettit B., Guillaume S., (2018)** – New calcareous nannofossil and carbon isotope data for the Pliensbachian/Toarcian boundary (Early Jurassic) in

- the western Tethys and their paleoenvironmental implications. *Newsletter on Stratigraphy*, DOI 10.1127/nos/2018/0476.
- Molina J. M., Reolid M., Mattioli E., (2018)** - Thin shelled bivalve buildup of the lower Bajocian, South Iberian paleomargin: development of opportunists after oceanic perturbations. *Facies*: 64, 19.
- Moshkovitz S., Ehrlich A. (1976)** – Distribution of Middle and Upper Jurassic calcareous nannofossils in the northeastern Negev, Israel and in Gebel Maghara, northern Sinai. *Bulletin of the Geological Survey of Israel*: 69, 1-47.
- Muller T., Price G.D, Bajnai D., Nyerges A., Kesjar D., Raucsik B., Varga A., Judik. K., Fekete J., May Z., Palfy J. (2017)** - New multiproxy record of the Jenkyns Event (also known as the Toarcian Oceanic Anoxic Event) from the Mecsek Mountains (Hungary): Differences, duration and drivers. *Sedimentology*: 64, 66-86.
- Mutterlose J., Bornemann A., Herrle J. O. (2005)**. Mesozoic calcareous nannofossils—state of the art. *Paläontologische Zeitschrift*, 79(1), 113-133.
- Muttoni G., Erba E., Kent D.V., Bachtadse V. (2005)**: Mesozoic Alpine facies deposition as a result of past latitudinal plate motion. *Nature*, 434, 59–63.
- Pálfy J., & Smith, P. L. (2000)** - Synchrony between Early Jurassic extinction, oceanic anoxic event, and the Karoo-Ferrar flood basalt volcanism. *Geology*, 28(8), 747-750.
- Parisi G., Baldanza A., Benedetti L., Mattioli E., Venturi F., Cresta S., (1998)** – Toarcian stratigraphy of the Colle d’Orlando section (Umbria, Central Italy, northern Apennine). *Bollettino Società Paleontologica Italiana*: 37, 3-39.
- Perilli N. (1999)** - Calibration of Early-Middle Toarcian Nannofossil events in two expanded and continuous sections from the Basque-Cantabrian Area (Northern Spain). *Revista Española de Micropaleontología*: 31(3), 393-401.
- Perilli N., (2000)** - Calibration of Early-Middle Toarcian nannofossil events based on high-resolution ammonite biostratigraphy in two expanded sections from the Iberian Range (East Spain). *Marine Micropaleontology*, 39 293-308.
- Perilli N., Comas-Rengifo M.J. (2002)** - Calibration of Pliensbachian calcareous nannofossil events in two ammonite-controlled sections from northern Spain (Basque-Cantabrian Area). *Rivista italiana di Paleontologia e Stratigrafia*: 108 (1) (1), 133-152.
- Perilli N., Comas-Rengifo M.J. Goy A., (2004)** - Calibrations of the Pliensbachia-Toarcian calcareous nannofossil zone boundaries based on ammonites. (Basque Cantabrian Area, Spain). *Rivista Italiana di Paleontologia e Stratigrafia*, 110 (1), 97-107.
- Perilli N., Duarte L.V. (2006)** - Toarcian nannobiohorizons from the Lusitanian Basin (Portugal) and their calibration against ammonite Zones. *Rivista Italiana di Paleontologia e Stratigrafia*: 112 (3) (2). 417-434.
- Perilli N., Fraguas A., Comas-Rengifo M.J. (2010)** - Reproducibility and reliability of the Pliensbachian calcareous nannofossil biohorizons from the Basque- Cantabrian Basin (Northern Spain). *Geobios*: 43 (1), 77-85.
- Peti L., Thibault, N. (2017)** - Abundance and size changes in the calcareous nannofossil *Schizosphaerella*—Relation to sea-level, the carbonate factory and palaeoenvironmental change from the Sinemurian to earliest Toarcian of the Paris Basin. *Palaeogeography, palaeoclimatology, palaeoecology*, 485, 271-282.

- Peti L., Thibault N., Clémence M.E., Korte C., Dommergues J.L., Bougealt C., Pellenard P., Jelby M E., Ulmann C.V. (2017)** - Sinemurian–Pliensbachian calcareous nannofossil biostratigraphy and organic carbon isotope. *Palaeogeography, Palaeoclimatology, Palaeoecology*, 468: 142-161.
- Picotti V., Cobianchi M. (1996)** – Jurassic periplatform sequences of the eastern Lombardian Basin (Southern Alps): the deep-sea record of the tectonic evolution, growth and demise history of a carbonate platform. *Memorie Scienze Geologiche Padova*: 48, 171-219, Padova.
- Posenato R., Bassi D., Trecalli A., Parente M. (2018)** - Taphonomy and evolution of Lower Jurassic lithotid bivalve accumulations in the Apennine Carbonate Platform (southern Italy). *Palaeogeography, palaeoclimatology, palaeoecology*: 489, 261-271.
- Prins B. (1969)** – Evolution and stratigraphy of Coccolithinids from the Lower and Middle Lias. *Proceeding I International Conference Planktonic Microfossils, Geneva*: 2, 547-558.
- Reale V., Baldanza A., Monechi S., Mattioli E. (1992)** - Calcareous nannofossil biostratigraphic events from the Early-Middle Jurassic sequences of the Umbria-Marche area (Central Italy). *Memorie di Scienze Geologiche*: 43 (allegato): 41-75.
- Reggiani L., Mattioli E., Pittet B., Duarte L.V., Veiga de Oliveira L.C., Comas-Rengifo M.J. (2010a)** - Pliensbachian (Early Jurassic) calcareous nannofossils from the Peniche section (Lusitanian Basin, Portugal): a clue for paleoenvironmental reconstructions. *Marine Micropaleontology*: 75, 1-16.
- Reggiani L., Mattioli E., Pittet B. (2010b)** - Spatial distribution of Late Pliensbachian (Early Jurassic) calcareous nannofossils within the Lusitanian basin (Portugal). *Geobios*: 43(1), 87-97.
- Riegel W., Loh H., Maul B., Prauss M., (1986)** – Effects and causes in a black shale event – The Toarcian Posidonia Shale of North West Germany. *A contribution to Project Global bio-events*. 267-276.
- Reolid M., Mattioli E., Nieto L.M., Rodriguez-Tovar F.J. (2014)** - The Early Toarcian Oceanic Anoxic Event in the External Subbetic (Southiberian Paleomargin, Westernmost Tethys): geochemistry, nannofossils and ichnology. *Palaeogeography, Palaeoclimatology, Palaeoecology*: 411, 79-94.
- Röhl H.-J., Schmid-Röhl A., Oschmann W., Frimmel A., Schwark L., (2001)**. The Posidonia Shale (Lower Toarcian) of SW-Germany: an oxygen-depleted ecosystem controlled by sea level and palaeoclimate. *Palaeogeography, Palaeoclimatology, Palaeoecology*: 165, 27–52.
- Robinson S.A., Heimhofer U., Hesselbo S.P., Petrizzo M.R. (2017)** - Mesozoic climates and oceans – a tribute to Hugh Jenkyns and Helmut Weissert. *Sedimentology*: 64, 1-15.
- Rood A.P., Barnard T., (1972)** – On Jurassic coccoliths: *Stephanolithion*, *Diadozygus* and related genera. *Eclogae Geologicae Helveticae*: 65, 327 – 342.
- Rood A.P., Hay, W.W., Barnard T., (1973)** – Electron microscope studies of lower and middle Jurassic coccoliths. *Eclogae Geologicae Helveticae*: 66 (2), 365 – 382.
- Rost B., Riebesell, U. (2004)**. Coccolithophores and the biological pump: responses to environmental changes. In *Coccolithophores*: 99-125. Springer, Berlin, Heidelberg.
- Roth P.H. (1983)** – Jurassic and Lower Cretaceous calcareous nannofossil in the Western North Atlantic (Site 534): biostratigraphy, preservation and some observations on biogeography and paleoceanography. *Initial Report DSDP*: 76, 587 – 621.

- Roth P.H., Thierstein, H. (1972)** - Calcareous nannoplankton: leg 14 of the DeepSea Drilling Project. In: Hayes, D.E., Pimm, A.C., et al. (eds.), *Initial Reports of the Deep Sea Drilling Project*: 14, 421–485.
- Saelen G., Doyle P., Talbot M.R., (1996)** - Stable isotope analyses of belemnite rostra from the Whitby Mudstone Fm., England: surface water conditions during deposition of a marine black shale. *Palaios*: 11, 97–117.
- Saelen G., Tyson R. V., Telnæs N., Talbot M. R. (2000)** - Constraining watermass conditions during deposition of the Whitby Mudstone (Lower Jurassic) and Kimmeridge Clay (Upper Jurassic) formations, UK. *Palaeogeography, Palaeoclimatology, Palaeoecology*. **163**, 163–196.
- Sandoval J., Markus B., Aguado R., O' Dogherty L., Rivas P., Morard A., Guex J., (2012)** - The Toarcian in the Subbetic basin (southern Spain): Bio-events (ammonite and calcareous nanofossils) and carbonate-isotope stratigraphy. *Palaeogeography, Palaeoclimatology, Palaeoecology*: 342-343, 40-62.
- Santantonio, M., and Carminati E. (2011)**: The Jurassic rifting evolution of the Apennines and Southern Alps (Italy): Parallels and differences, *Bulletin of the Geological Society of America*, 124, 468–484.
- Schmid-Röhl A., Röhl J., Oschmann W., Frimmel A., Schwark L., (2002)** - Palaeoenvironmental reconstruction of Lower Toarcian epicontinental black shales (Posidonia Shale, SW-Germany): global versus regional control. *Geobios*: 35, 13–20.
- Schmitz H.H., (1980)** – Excursion guide B 5: Oil shale in Germany. International geochemical exploration symposium. 8/1980/Hannover; DEU; DA. 1980; 8-10.
- Senglaub Y., Littke R., Brix MR., (2006)** – Numerical modelling of burial and temperature history as an approach for an alternative interpretation of the Bramsche anomaly, Lower Saxony Basin. *International Journal of Earth Sciences*: 95, 204-224.
- Stradner, H. N. (1963)** - New contributions to Mesozoic stratigraphy by means of nanofossils. In *6th World Petroleum Congress*. World Petroleum Congress.
- Suan G., Pittet B., Bour I., Mattioli E., Duarte L.V., Maillot S., (2008)** – Duration of the Early Toarcian carbon isotope excursion deduced from spectral analysis: Consequence for its possible causes. *Earth and Planetary Science Letters*: 267, 666-679.
- Suan G., Mattioli E., Pittet B., Lécuyer C., Suchéras-Marx B., Duarte L.V., Philippe M., Reggiani L., Martineau F., (2010)** – Secular environmental precursors to Early Toarcian (Jurassic) extreme climate changes. *Earth and Planetary Science Letters*: 290, 448-458.
- Suan G., van de Schootbrugge B., Adatte T., Fiebig J., Oschmann W. (2015)** - Calibrating the magnitude of the Toarcian carbon cycle perturbation. *Paleoceanography* 30, 495–509.
- Schlanger S.O., Jenkyns H.C. (1976)** - Cretaceous oceanic anoxic events: Causes and consequences. *Geologie en Mijnbouw*: 55, 179-184.
- Schouten S., van Kaam-Peters H.M.E., Rijpstra W.I.C., Schoell A. Frimmel et al. (2004)** – Chemostratigraphy of the Posidonia Black Shale, S-W Germany II. Assessment of extent and persistence of photic-zone anoxia using aryl isoprenoid distribution. *Chemical Geology*: 206, 199–230 229.
- Svensen H., Planke S., Chevallier L., Malthe-Sørensen A., Corfu F., Jamtveit B. (2007)** - Hydrothermal venting of greenhouse gases triggering Early Jurassic global warming. *Earth and Planetary Science Letters*: 256, 554–566.

- Tintori A. (1977)** - Toarcian fishes from the Lombardy Basin *Bollettino della Società Paleontologica Italiana*: 16(2), 143–152.
- Trecalli A., Spangenberg J., Adatte T., Föllmi K. B., Parente M. (2012)** - Carbonate platform evidence of ocean acidification at the onset of the early Toarcian oceanic anoxic event. *Earth and Planetary Science Letters*, 357, 214-225.
- Tremolada F., de Schootbrugge B.V., Erba E. (2005)** - Early Jurassic schizosphaerellid crisis in Cantabria, Spain: implications for calcification rates and phytoplankton evolution across the Toarcian oceanic anoxic event. *Paleoceanography*, 20, 1-11.
- Tsikos H., Jenkyns H. C., Walsworth-Bell B., Petrizzo M. R., Forster A., Kolonic S., Erba E., Premoli Silva I., Baas M., Wagner T. & Sinninghe Damsté J.S. (2004)** - Carbon-isotope stratigraphy recorded by the Cenomanian–Turonian Oceanic Anoxic Event: correlation and implications based on three key localities. *Journal of the Geological Society*, London: 161, 711-719.
- Ullmann C. V., Thibault N., Ruhl M., Hesselbo S. P., Korte, C. (2014)** - Effect of a Jurassic oceanic anoxic event on belemnite ecology and evolution. *Proceedings of the National Academy of Sciences of the USA*: 111, 10073–10076.
- Van Breugel Y., Baas M., Schouten S., Mattioli E., Sinninghe Damsté, J. S. (2006)** - Isorenieratane record in black shales from the Paris Basin, France: Constraints on recycling of respired CO₂ as a mechanism for negative carbon isotope shifts during the Toarcian oceanic anoxic event. *Paleoceanography*: 21(4).
- Van de Schootbrugge, B., McArthur, J.M., Bailey, T.R., Rosenthal, Y., Wright, J.D., Miller, K.G., (2005)** - Toarcian oceanic anoxic event: an assessment of global causes using belemnite C isotope records. *Paleoceanography* 20, 1–10.
- Van de Schootbrugge B., Richoz S., Pross J., Luppold F.W., Hunze S., Wonik T., Blau J., Meister C., van de Meijst C. M. H., Suan G., Fraguas A., Fiebig J., Herrle J.O., Guex J., Little C.T.S., Wignall P.B., Püttmann W. and W. Oschmann (2018)** - The Schandelah Scientific Drilling Project: A 25-million year record of Early Jurassic palaeoenvironmental change from northern Germany. *Newsletter on Stratigraphy*: DOI: 10. 1127/nos/2018/0259.
- Veiga de Oliveira L.C.V, Duarte L.V., Perilli N., (2007)** - Calcareous nannofossils and palynomorphs from Pliensbachian-Toarcian boundary in Lusitanian Basin, Portugal. *Revista brasileira de paleontologia*: 10 (1), 5-16.
- Walsworth-Bell E. B. (2001)** - Jurassic calcareous nannofossils and environmental cycles. *Unpubl (Doctoral dissertation, Ph. D. thesis, University College London, 1)*.
- Weissert H. (1989)** - C-isotope stratigraphy, a monitor of paleoenvironmental change: a case study from the Early Cretaceous. *Surveys in Geophysics*: 10, 1-61.
- Weissert H., Erba E. (2004)** - Volcanism, CO₂ and palaeoclimate: a Late Jurassic – Early Cretaceous carbon and oxygen isotope record. *Journal of the Geological Society*: 161, 695-702.
- Wiegand G. E., (1984)** – Jurassic nannofossils from the northwest African margin, DSDP Leg 79. *Init. Reps. Deep Sea Drilling Project*, 79: 657 – 670.
- Xu M., Ruhl M., Jenkyns H.C., Hesselbo S.P., Riding J. B., Selby D., Naafs B.D.A., Weijer J.W.H., Pancost R.D., Tegelaar E.W., Idiz E.F. (2017)** – Carbon sequestration in an expanded lake system during the Toarcian oceanic anoxic event. *Nature Geoscience*: 10, 129 – 134.

- Young J. R., Davis, S. A., Bown, P. R., & Mann, S. (1999)** - Coccolith ultrastructure and biomineralisation. *Journal of structural biology*: 126 (3), 195-215.
- Ziegler P.A. (1982)** – Faulting and graben formation in western and central Europe. *Philosophical Transactions of the Royal Society*. 305, 1489.
- Ziegler P.A. (1990)** – Collision related intra-plate compression deformations in Western and Central Europe. *Journal of Geodynamics*. 11, 357-388.

Appendix list

Appendix A – Taxonomic list

Appendix B – Table of studied papers

Appendix C – Morphometry of genus Carinolithus

Appendix D – Range chart of the Sogno Core

Appendix E – Range chart of the L1 and Schandelah Cores

Appendix F – Erba et al. 2019a

Appendix G – Erba et al. 2019b

Appendix H – Abstracts presented at international congresses

Appendix A

Taxonomic list

Calcareous nannofossil taxa observed in this study are here reported alphabetically ordered per genus, species and subspecies. Authors, date of the original description and emendations are provided.

- Biscutum dubium* (Noël, 1965) Grün *in* Grün et al. (1974)
B. finchii (Crux, 1984) Bown, (1987)
B. grandis Bown, (1987)
B. intermedium Bown, (1987)
B. novum (Goy, 1979) Bown, (1987)
Bussonius leufuensis Bown and Kielbowicz, (1987)
B. prinsii (Noël, 1973) Goy, (1979)
Calyculus Noël, (1973)
Carinolithus cantaluppii (Cobianchi, 1990) Visentin et al. (in preparation)
C. magharensis (Moshkovitz and Ehrlich, 1976) Bown, (1987)
C. poul nabronei Mattioli, (1996)
C. premagharensis Visentin et al. (in preparation)
C. superbus sceptrum (Deflandre, 1954) Prins *in* Grün et al. (1974)
C. superbus superbus (Deflandre, 1954) Prins *in* Grün et al. (1974)
Crepidolithus cavus Rood, Hay and Barnard, (1973)
C. cantabriensis Fraguas, (2014)
C. crassus (Deflandre *in* Deflandre and Fert, 1954) Noël, (1965)
C. crucifer (Prins 1969) *ex* Rood et al. (1973) Fraguas and Erba (2010)
C. granulatus Bown, (1987)
Diductius constans Goy, (1979)
Discorhabdus criotus Bown, (1987)
D. ignotus (Gorka, 1957) Perch-Nielsen, (1968)
D. striatus Moshkovitz and Ehrlich, (1976)
Lotharingius barozii Noël, (1973)
L. crucicentralis (Medd, 1971) Grün and Zweili, (1980)
L. frodoi Mattioli, (1996)
L. hauffii Grün and Zweili *in* Grün et al., (1974)
L. sigillatus (Stradner, 1961) Prins *in* Grün et al., (1974)
L. umbriensis Mattioli, (1996)
L. velatus Bown and Cooper, (1989)
Mitrolithus elegans Deflandre, (1954)
M. jansae (Wiegand, 1984) Bown *in* Young et al. (1986)
M. lenticularis Bown, (1987)
Orthogonoides hamiltoniae Wiegand, (1984)
Parhabdolithus liasicus Deflandre, (1952)
Schizosphaerella punctulata Deflandre and Dangeard, (1938)
Similiscutum cruciulus De Kaenel and Bergen, (1993)
Tubirhabdus patulus Rood et al., (1973)
W. colacicchii Mattioli, (1996)
Watznaueria sp.1 Cobianchi, (1992)

Appendix B

Table of studied papers

Papers analyzed during my PhD are here reported. They are organized following the publication date and for each paper the following data are listed: a) regional setting; b) investigated basin/area; c) investigated section/s; d) time interval studied; e) methodology applied; f) taxonomy; g) biostratigraphy; h) plates; i) range chart; j) biozonation; k) ammonite stratigraphy; l) carbon and oxygen isotopic stratigraphy; m) magnetostratigraphy; n) ciclostratigraphy; o) paleoceanographic reconstructions; p) paleoecological investigations; q) morphometric investigations; r) principal component analyses investigations; s) cluster analyses.

Papers dealing with calcareous nannofossil biostratigraphy are highlighted in yellow and red. Those in red were published after Casellato and Erba (2015).

N°	PAPER	Realm	Basin	Section	Geological interval studied	Methodology	TAXONOMY	BIO STRATIGRAPHY	Plates	Range chart	New biozonation?	Ammonite stratigraphy	Chemo stratigraphy	Magneto stratigraphy	Ciclo stratigraphy	PALAEO OCEANOGRAPHY	PALAEO ECOLOGY	Morphometries	Principal component analyses	Cluster Analyses
1	Van de Schootbrugge et al. (2018)	Boreal	Lower Saxony Basin	Schandelah	Upper Rhaetian/Upper Toarcian	S	N	Y	Y	N	N	Y	Y	N	N	N	N	N	N	N
2	Menini et al. (2018)	Tethys / Boreal	Iberian Range/Paris Basin	La Almunia-Richa (a)/Anse St. Nicolas (b)	Upper Pliensbachian/Lower Toarcian	S	Y	Y	Y	Y	N	N	Y	N	N	N	N	N	N	N
3	Fraguas et al. (2018)	Boreal	Asturias	East Rodiles	Upper Sinemurian/Upper Pliensbachian	S	N	Y	N	Y	N	Y	N	N	N	N	N	N	N	N
4	Ferreira et al. (2017)	Portugal/Boreal	Lusitanian Basin/Causse Basin	Rabaçal /Brenha, Cabo Mondego, Truc de Balduc	Lower Toarcian/Lower Aalenian		N	N	Y	N	N	Y	N	N	N	Y	Y	Y	N	N
5	Peti & Thibault (2017)	Boreal	Paris Basin	Sancerre-Couy	Lower Toarcian		N	N	Y	N	N	Y	Y	N	N	Y	Y	Y	N	N
6	Peti et al. (2017)	Boreal	Paris Basin	Sancerre-Couy	Upper Hettangian/ Lower Toarcian	S	N	Y	Y	N	N	Y	Y	N	N	N	N	N	N	N
7	Muller et al. (2017)	Tethys/Boreal	Pannonian Basin	Reka	Lower Toarcian	S	N	Y	N	N	N	Y	Y	N	Y	N	N	N	N	N
8	da Rocha et al. (2016)	Portugal	Lusitanian Basin	Peniche	Upper Pliensbachian/Lower Toarcian	S	N	Y	Y	N	N	Y	Y	Y	Y	N	N	N	N	N
9	Ferreira et al. (2015)	Portugal	Lusitanian Basin	Rabacal (a)/Brenha (b)/Cabo Mondego (c)	Upper Pliensbachian/ Lower Aalenian	S	N	Y	Y	N	N	Y	Y	N	N	Y	Y	N	Y	N
10	Clémence et al. (2015)	Boreal	Paris Basin	Sancerre-Couy	Lower Toarcian		N	N	N	N	N	Y	Y	N	N	Y	N	Y	Y	Y
11	Casellato & Erba (2015)	Tethys	Lombardy Basin	Colle di Sogno	Upper Pliensbachian/ Lower Toarcian	S/QA	Y	Y	Y	Y	N	Y	Y	N	N	Y	Y	N	Y	N
12	Fraguas et al. (2015)	Boreal	Cantabrian Basin/ Asturias	Tudanca (a)/Santotis (b)/Camino (c)/San Andrés (d)/West Rodiles (e)	Upper Sinemurian/Lower Toarcian	S	N	Y	Y	Y	Y	Y	N	N	N	N	N	N	N	N
13	Bouilla et al. (2014)	Boreal	Paris Basin	Sancerre-Couy	Upper Pliensbachian/ Upper Toarcian	S	N	Y	N	N	N	Y	Y	N	Y	N	N	N	N	N
14	Kafousia et al. (2014)	Tethys	Ioanian Basin	Toka (a)/ Petousi (b) / Chionistra (c)	Upper Pliensbachian/ Lower Toarcian	S	N	Y	N	Y	N	N	Y	N	N	N	N	N	N	N
15	Reolid et al. (2014)	Tethys	Subbetic Basin	La Cerradura	Upper Pliensbachian /Lower Toarcian	S	N	Y	Y	N	N	Y	Y	N	N	Y	Y	Y	N	N
16	Mattioli et al. (2013)	Portugal	Lusitanian Basin/ Umbria-Marche Basin/ Morocco	San Pedro de Moel/Peniche/ Valdorbia/ Amellago	Upper Pliensbachian/ Lower Toarcian	S	N	Y	Y	N	N	Y	N	N	N	N	N	N	N	N
17	López-Otálvaro et al. (2012)	Portugal	Lusitanian Basin	Cabo Mondego	Upper Aalenian/Early Bajocian		Y	N	N	N	N	Y	Y	N	N	N	N	Y	N	N
18	Fraguas et al. (2012)	Tethys/Boreal	Cantabrian Basin/Asturias	Camino/ San Andrés/ Tudanca/ Santotis/West Rodiles	Upper Pliensbachian /Lower Toarcian	S	N	Y	N	N	N	Y	Y	N	N	Y	Y	N	Y	N
19	Sandoval et al. (2012)	Tethys	Subbetic Basin	La Cerradura/ Colomera/ Cerro Mendez/ Cerro Mendez 1/ Cerro Mendez J/ Fuente de la Vidriera/ Cerro de Mahoma	Upper Pliensbachian/ Lower Aalenian	S	N	Y	Y	Y	N	Y	Y	N	N	Y	Y	N	N	N
20	Fraguas & Young (2011)	Boreal	Asturias	West Rodiles	Upper Pliensbachian/ Lower Toarcian	S	N	N	N	N	N	N	N	N	N	N	N	Y	N	N
21	Reggiani et al. (2010b)	Portugal	Lusitanian Basin	Peniche	Upper Pliensbachian	S	N	Y	Y	N	N	Y	N	N	N	Y	Y	N	Y	N
22	Reggiani et al. (2010a)	Portugal	Lusitanian Basin	Peniche	Upper Pliensbachian	S	N	Y	Y	N	N	Y	N	N	N	Y	Y	N	Y	N
23	Fraguas & Erba (2010)	Tethys	Basque-Cantabrian Basin	Santotis	Lower Pliensbachian/ Upper Pliensbachian		N	N	N	N	N	N	N	N	N	Y	Y	Y	N	N
24	Perilli et al. (2010)	Tethys / Boreal	Basque-Cantabrian Basin	Camino/San Andrés/Santotis/Tudanca	Upper Pliensbachian	S	N	Y	N	N	N	Y	N	N	N	N	N	N	N	N
25	Mattioli et al. (2009)	Portugal	Lusitanian Basin	Peniche	Lower Toarcian		Y	N	N	N	N	Y	Y	N	N	Y	Y	Y	N	N
26	Maillo (2009)	Boreal	Causse Basin	St. Paul des Font/Tournadous	Upper Pliensbachian/ Lower Toarcian	S	N	Y	Y	N	N	Y	Y	N	N	Y	Y	N	N	N
27	Suan et al. (2008)	Portugal	Lusitanian Basin	Peniche	Upper Pliensbachian/ Lower Toarcian	S	N	N	N	N	N	Y	Y	N	N	Y	N	Y	N	N
28	Mattioli et al. (2008)	Portugal/ Boreal	Lusitanian Basin/ South Germany/ Paris Basin	Peniche/Dotterhausen/Andra	Upper Pliensbachian/ Lower Toarcian	S	N	Y	N	N	N	Y	Y	N	N	Y	Y	N	Y	N
29	Bour et al. (2007)	Portugal	Lusitanian Basin	Peniche	Lower Toarcian		N	N	N	N	N	Y	Y	N	N	Y	N	N	N	N
30	Maillo et al. (2007)	Portugal	Lusitanian Basin	Peniche	Upper Pliensbachian/ Lower Toarcian	S	N	Y	N	N	N	Y	N	N	N	N	N	Y	N	N

31	Veiga de Oliveira et al. (2007)	Portugal	Lusitanian Basin	Peniche	Upper Pliensbachian/ Lower Toarcian	S	N	Y	Y	Y	N	Y	N	N	N	Y	Y	N	N	N
32	Mailhot et al. (2006)	Tethys/Boreal/Portugal		18 sections of the western Tethys	Lower Toarcian		N	N	N	N	N	N	N	N	N	Y	Y	N	N	N
33	Perilli & Duarte (2006)	Portugal	Lusitanian Basin	Composite sections (Rabacal (2), Coimbra, Cantanhede, F.Foz, Peniche)	Lower Toarcian/ Lower Aalenian	S	N	Y	Y	Y	N	Y	N	N	N	N	N	N	N	N
34	Tremolada et al. (2005)	Tethys	Cantabrian Basin/ Asturias	Castillo de Pedroso	Upper Pliensbachian/ Lower Toarcian	S	N	Y	N	N	N	Y	Y	N	N	Y	Y	N	N	N
35	Perilli et al. (2004)	Tethys	Basque-Cantabrian Basin	Camino/ San Andrés	Lower Pliensbachian/ Upper Toarcian		N	N	N	Y	Y	Y	N	N	N	N	N	N	N	N
36	Mattioli et al. (2004)	Tethys / Boreal	Umbria-Marche Basin/South Germany/North Yorkshire	Pozzale/ Somma/ Dotterhausen/ Brown Moor	Upper Pliensbachian/ Lower Toarcian	S	N	Y	N	N	N	Y	Y	N	N	Y	Y	N	N	N
37	Mattioli & Pittet (2004)	Tethys	Umbria-Marche Basin	Fonte Cerro/Pozzale (2)/Colle d'Orlando	Upper Pliensbachian/ Lower Toarcian	S	N	Y	N	N	N	Y	N	N	Y	Y	Y	N	N	N
38	Erba (2004)	Tethys	Lombardy Basin	Breggia/Colle di Sogno	Upper Pliensbachian/ Lower Aalenian	S	N	Y	N	N	N	Y	Y	N	N	Y	N	N	N	N
39	Mattioli et al. (2004)	Tethys / Boreal	Umbria-Marche Basin/South Germany	Sicily/offshore Marocco / Somma / Dotterhausen	Upper Pliensbachian/ Lower Toarcian	S	Y	N	Y	N	N	N	N	N	N	Y	Y	Y	N	N
40	Frimmel et al. (2004)	Boreal	South Germany	Dotterhausen	Lower Toarcian		N	N	N	N	N	Y	Y	N	N	Y	N	N	N	N
41	Duarte et al. (2003)	Portugal	Lusitanian Basin	Coimbra	Lower Toarcian/ Middle Toarcian	S	N	Y	N	Y	N	N	Y	N	N	N	N	N	N	N
42	Perilli & Comas Rengifo (2002)	Tethys / Boreal	Basque-Cantabrian Basin	Camino/San Andrés	Upper Pliensbachian	S	N	Y	Y	Y	N	Y	N	N	N	N	N	N	N	N
43	Mattioli & Pittet (2002)	Tethys	Umbria/Marche Basin	Somma	Upper Pliensbachian/ Lower Toarcian	S	N	N	N	N	N	N	N	N	N	Y	Y	Y	N	N
44	Bucefalo Palliani et al. (2002)	Boreal	North Yorkshire	Brown Moor	Upper Pliensbachian/ Lower Toarcian	QR	N	Y	N	N	N	Y	N	N	N	N	Y	N	N	N
45	Rohi et al. (2002)	Boreal	Dotterhausen	South Germany	Lower Toarcian		N	N	N	N	N	Y	Y	N	N	Y	Y	N	N	N
46	Rohi et al. (2001)	Boreal	Dotterhausen	South Germany	Lower Toarcian		N	N	N	N	N	Y	Y	N	N	Y	Y	N	N	N
47	Perilli (2000)	Tethys	Iberian Range	La Almunia-Richa (1)/Rambal del Salto	Lower Toarcian/ Lower Aalenian	S	N	Y	N	Y	N	Y	N	N	N	N	N	N	N	N
48	Perilli (1999)	Tethys	Basque-Cantabrian Basin	Camino/San Andrés	Lower Toarcian	S	N	Y	N	Y	N	Y	N	N	N	N	N	N	N	N
49	Cobianchi & Picotti (2000)	Tethys	Lombardy Basin	Brasa	Upper Pliensbachian/ Lower Toarcian	S	N	Y	N	N	N	Y	N	N	N	Y	Y	N	N	N
50	Mattioli & Erba (1999)	Tethys	Sections coming from the Tethyan Realm	Sections coming from the Tethyan Realm	Lower Hettangian/Upper Callovian		N	N	Y	N	Y	Y	N	N	N	N	N	N	N	N
51	Bown & Cooper (1998)	Boreal	Sections coming from the Boreal Realm	Sections coming from the Boreal Realm	Late Carnian/Recent		Y	N	Y	N	Y	Y	N	Y	N	N	N	N	N	N
52	Bucefalo Palliani et al. (1998)	Tethys	Umbria-Marche Basin	Colle d'Orlando/ Pozzale/ Fonte Cerro	Upper Pliensbachian/ Lower Toarcian	QR	N	Y	N	N	N	Y	N	N	N	N	N	N	N	N
53	Picotti & Cobianchi (1996)	Tethys	Lombardy Basin	Bocca Magno/ Valle del Lupo 1-2/ Brasa-sx/ Punta Cortor/ Pieve di Tremosine/ Campione/ Pregasio-1/Piovere/Monte Castello/Vione Valley/ Costa del Vecchio/ Denervo/ M.Denervo/ Carpeneda/ Fostaga/ Monte Covolo	Lower Sinemurian/Lower Aptian	S	N	Y	N	Y	N	N	N	N	N	N	N	N	N	N
54	Mattioli (1996)	Tethys	Different basins	Sections coming from the Tethyan Realm	Upper Pliensbachian/ Lower Toarcian		Y	N	Y	N	N	N	N	N	N	N	N	N	N	N
55	Baldanza et al. (1995)	Tethys	Pannonian Basin	Lokut Hill/ Reka	Upper Pliensbachian/ Lower Toarcian	S	N	Y	N	Y	N	Y	N	N	N	N	N	N	N	N
56	Gardin & Manivit (1994)	Tethys	Aquitainian Basin	Penne/Cerède	Upper Pliensbachian/ Lower Toarcian	S	N	Y	Y	N	N	Y	N	N	N	N	N	N	N	N
57	de Kaenel & Bergen (1993)	Tethys/Boreal/Portugal	Different basins	Tunnel de la Legion/ End/ Ouchbis Jebel Bouhaga/ Tzi n'Zou/ Kerrando-Gourrama/ DSDP Site 547 B/ San Pedro de Mal/ Peniche/ Brehna Road/ Boa Viagem-Quiaios/Cabo Mondego	Sinemurian/Lower Bajocian	S	Y	Y	Y	N	N	Y	N	N	N	N	N	N	N	N
58	Baldanza & Mattioli (1992)	Tethys / Boreal	Pannonian Basin/Lusitanian Basin/ Ionian Basin	Peniche, Rabacal, Ponta do Trovao, Anabrisada, Kaballos, Kalamitsi, Kozoskut Ravine, Lokut Hill, Kalvaia Hill, Reka, Valley	Upper Sinemurian/Lower Bajocian	S	N	Y	Y	N	N	Y	N	N	N	Y	Y	N	N	N
59	Reale et al. (1992)	Tethys	Umbria-Marche Basin	Valdorbria/ Monte Serrone/ Monte Civitella/ Pale/ Fonte Avellana/ Pozzale (1)/ Presale/ Infernaccio	Upper Pliensbachian/ Lower Bajocian	S	N	Y	Y	Y	Y	Y	N	N	N	N	N	N	N	N
60	Cobianchi (1992)	Tethys	Lombardy Basin	Clivio/Arzo/Breggia/Alpe Turati/ Val Ceppelline/ Val Varea/ Monte Domaro/ Caricatore/Molvina	Sinemurian/Lower Bajocian	S	Y	Y	Y	Y	N	Y	N	Y	N	N	N	N	N	N
61	Cobianchi (1990)	Tethys	Lombardy Basin	Caricatore	Upper Pliensbachian/ Lower Toarcian	S	Y	Y	Y	Y	N	Y	N	N	N	N	N	N	N	N
62	Bown et al. (1988)	Boreal	Sections coming from the Boreal Realm	Sections coming from the Boreal Realm from published data	Lower Hettangian/Lower Tithonian		N	N	Y	N	Y	Y	N	N	N	N	N	N	N	N
63	Bown (1987b)	Boreal	Sections coming from the Boreal Realm	Sections coming from the Boreal Realm from published data	Upper Rhaetian/Upper Toarcian		Y	N	Y	N	Y	Y	N	N	N	N	N	N	N	N
64	Bown (1987a)	Boreal/Portugal	North Yorkshire/Lusitanian Basin	Mochras/Brenha	Upper Rhaetian/Upper Toarcian	S	Y	Y	Y	Y	N	Y	N	N	N	N	N	N	N	N
65	Riegel et al. (1983)	Boreal	North West Germany	Marienburg	Lower Toarcian		N	N	N	N	N	Y	N	N	N	Y	N	N	N	N

Appendix C

Morphometry of genus *Carinolithus*

Data - set of *Carinolithus* specimens from literature used for the morphometric analyses of the genus. They are organized following the publication date and for each specimen the following data are listed: investigated core/section; nomenclature adopted by the author(s); revised nomenclature; age; ammonite and calcareous nannofossil zones and subzones. Specimens selected for morphometric analyses are listed with an X. The other specimens were used to characterize the diagenetic overprint. *Carinolithus spp.** is reported for specimens not attributable to a species due to high overgrowth.

Paper	Investigated section	Plate/Figure	Nomenclature adopted by the author(s)	Revised nomenclature	Diagenetic phase	Age	Ammonite Zones and (Subzones)	Nannofossil Zone	Morphometrics
Van de Schootbrugge et al., (2018)	Schandelah (Germany)	6; 11	<i>C.superbus</i>	<i>C.superbus sceptrum</i>	1	Lower Toarcian	Uppermost Serpentinus	Lowermost NJT6	X
Menini et al., (2018)	La Almunia (Spain)	1; 31	<i>C.poulabronei</i>	<i>C.poulabronei</i>	3	Lower Toarcian		NJT5b	
		1; 32	<i>C.poulabronei</i>	<i>C.poulabronei</i>	3	Lower Toarcian		NJT5b	
		1; 33	<i>C.superbus</i>	<i>Carinolithus spp.*</i>	3	Lower Toarcian		NJT6	
		1; 34	<i>C.superbus</i>	<i>C.superbus sceptrum</i>	2	Lower Toarcian		NJT6	X
Molina et al., (2018)	La Losilla (Spain)	8; LL-2	<i>C.poulabronei</i>	<i>C.poulabronei</i>	3	Aalenian/Bajocian boundary interval		Lower NJT9	
		8; LL-2	<i>C.superbus</i>	<i>Carinolithus spp.*</i>	3	Aalenian/Bajocian boundary interval		Lower NJT9	
		8; LL6	<i>C.superbus</i>	<i>C.superbus superbus</i>	3	Aalenian/Bajocian boundary interval		NJT8/NJT9 boundary	X
		8; LL1	<i>C.magharensis</i>	<i>C.premagharensis</i>	1	Aalenian/Bajocian boundary interval		Lower NJT9	X
		8; LL-12	<i>C.magharensis</i>	<i>Carinolithus spp.*</i>	2	Aalenian/Bajocian boundary interval		Uppermost NJT8	
		8; LL7	<i>H.magharensis</i>	<i>C.premagharensis</i> (DV)		Upper Aalenian		Uppermost NJT8	X
López-Otávaro & Henriches, (2018)	Cabo Mondego (Portugal)	2; 02CM106	<i>C.magharensis</i>	<i>C.premagharensis</i> (DV)		Upper Bajocian	Upper Parkisoni (Bonfordi)	Uppermost NJT10b	X
Aguado et al., (2017)	Almendo Gordo (Spain)	8; t	<i>C.magharensis</i>	<i>C.magharensis</i> (DV)		Lower Bajocian	Lowermost Laeviuscula (Ovalis)	Lower NJT9	X
		8; y	<i>C.magharensis</i>	<i>C.magharensis</i>	1	Lower Bajocian	Lowermost Laeviuscula (Ovalis)	Lower NJT9	X
	Agua Larga (Spain)	8; u	<i>C.magharensis</i>	<i>C.magharensis</i> (DV)		Lower Bajocian	Lower Propinquans	Middle NJT10a	X
		8; z	<i>C. superbus</i>	<i>C.superbus superbus</i>	2	Lower Bajocian	Middle Propinquans	Middle NJT10a	X
Peti et al., (2017)	Sancerre-Couy (France)	5; w	<i>Carinolithus spp.</i>	<i>C. poulabronei</i>	3	Lower Toarcian	Uppermost Tenuicostatum	Uppermost NJT5b	
Rocha et al., (2016)	Peniche (Portugal)	7; 3	<i>C. superbus</i>	<i>C.superbus sceptrum</i>	1	Lower Toarcian	Polymorphum	Lowermost NJT6	X
		7; 4	<i>C. superbus</i>	<i>C.superbus sceptrum</i>	1	Lower Toarcian	Polymorphum	Lowermost NJT6	X
		7; 8	<i>C.poulabronei</i>	<i>C.poulabronei</i>	1	Lower Toarcian	Polymorphum	Lowermost NJT6	
Ferreira et al., (2015)	Brenha (Portugal)	1;11	<i>C.superbus</i>	<i>Carinolithus spp.*</i>	3	Middle Toarcian		Uppermost NJT7a	
		1; 12	<i>C.cantaluppii</i>	<i>C. superbus superbus</i>	3	Middle Toarcian		Lowermost NJT8a	X
	Rabacal (Portugal)	1; 13	<i>C.poulabronei</i>	<i>C.poulabronei</i>	2	Upper Toarcian	Upper Meneghini		
		2; 11	<i>H.magharensis</i>	<i>C. magharensis</i> (DV)		Uncorrected proof			X
Casellato & Erba, (2015)	Colle di Sogno (Italy)	1; 14	<i>C.poulabronei</i>	<i>C.poulabronei</i>	1	Lower Toarcian		Lower NJT6	
		1; 15	<i>C.poulabronei</i>	<i>C.poulabronei</i>	1	Lower Toarcian		Lower NJT6	
		1; 16,17	<i>C.superbus</i>	<i>C.superbus sceptrum</i>	2	Lower Toarcian		Lowermost NJT6	X
Fraguas et al., (2015)	Camino (Spain)	4; 9	<i>C.superbus</i>	<i>Carinolithus spp.*</i>	2	Lower Toarcian		NJT6	
Reolid et al., (2014)	La Cerradura (Spain)	6; CE28	<i>C.poulabronei</i>	<i>C.poulabronei</i>	3	Lower Toarcian	Lower Serpentinum	Lower NJT6	
		6; CE30	<i>C.poulabronei</i>	<i>C.poulabronei</i>	1	Lower Toarcian	Lower Serpentinum	Lower NJT6	
		6; CE30	<i>C.superbus</i>	<i>C.superbus sceptrum</i>	3	Lower Toarcian	Lower Serpentinum	Lower NJT6	X
		6; CE30	<i>C.superbus</i>	<i>C.superbus sceptrum</i>	2	Lower Toarcian	Lower Serpentinum	Lower NJT6	X
Sandoval et al., (2012)	Cerro de Mahoma (Spain)	10; 8	<i>C. cantaluppii</i>	<i>Carinolithus spp.*</i>	3	Middle Toarcian	Lower Bifrons (Sublevisoni)	NJT7a	

		10; 9	<i>C. cantaluppii</i>	<i>Carinolithus</i> spp.*	3	Middle Toarcian	Upper Bifrons (Bifrons)	Upper NJT7a	
		10;10	<i>C. cantaluppii</i>	<i>Carinolithus</i> spp.*	3	Middle Toarcian	Lower Bifrons (Sublevisoni)	NJT7a	
		10; 15	<i>C.poulabronei</i>	<i>C.poulabronei</i>	3	Middle Toarcian	Lower Bifrons (Sublevisoni)	NJT7a	
		10; 16	<i>C.poulabronei</i>	<i>C.poulabronei</i>	2	Middle Toarcian	Lower Bifrons (Sublevisoni)	NJT7a	
		10; 17	<i>C.poulabronei</i>	<i>C.poulabronei</i>	2	Middle Toarcian	Middle Bifrons (Sublevisoni)	NJT7a	
		10; 18	<i>C.superbus</i>	<i>C.superbus superbus</i>	2	Upper Toarcian	Middle Meneghini	Middle NJT8a	X
		10; 19	<i>C.superbus</i>	<i>C.premagnanensis/ C. superbus superbus</i>	2	Upper Toarcian	Middle Meneghini	Middle NJT8a	X
	La Cerradura (Spain)	10; 11	<i>C.poulabronei</i>	<i>C.poulabronei</i>	3	Lower Toarcian	Polymorphum	NJT5b	
	Cerro Méndez (Spain)	10; 12	<i>C.superbus</i>	<i>C.superbus superbus</i>	2	Upper Toarcian	Upper Aalenis	Middle NJT8b	X
		10; 13	<i>C.superbus</i>	<i>Carinolithus</i> spp.*	2	Upper Toarcian	Middle Meneghini	Middle NJT8a	
		10; 20	<i>C.superbus</i>	<i>C.superbus superbus</i>	3	Upper Toarcian	Middle Aalenis	Upper NJT8a	X
		10; 21	<i>C.superbus</i>	<i>C.superbus superbus</i>	1	Upper Toarcian	Upper Aalenis	Middle NJT8b	X
Bodin et al.,(2010)	Amellago (Marocco)	5; i	<i>C.superbus</i>	<i>C.superbus sceptrum</i>	3	Lower Toarcian	Middle Polymorphum		X
Aguado et al., (2008)	Agua Larga (Spain)	5; 17	<i>C.superbus</i>	<i>C.superbus superbus</i>	3	Uppermost Aalenian	Upper Concavum (Limitatum)	Uppermost NJT8b	X
		5; 18	<i>C.superbus</i>	<i>C.superbus superbus</i>	2	Uppermost Aalenian	Upper Concavum (Concavum)	Uppermost NJT8b	X
		5; 19	<i>C.magharensis</i>	<i>C.magharensis</i>	2	Uppermost Aalenian	Upper Concavum (Limitatum)	Uppermost NJT8b	X
		5; 20	<i>C.magharensis</i>	<i>C.magharensis</i> (DV)		Uppermost Aalenian	Upper Concavum (Limitatum)	Uppermost NJT8b	X
	Cerro de Mahoma (Spain)	5; 13	<i>C.magharensis</i>	<i>C.magharensis</i> (DV)		Upper Aalenian	Lowermost Concavum (Limitatum)	Upper NJT8b	X
Maillot et al., (2006)	Unknown	1; UAZII, UA3	<i>C.superbus</i>	<i>C.superbus superbus</i>	1	Unknown			X
		1; UAZIV, UA5	<i>C.poulabronei</i>	<i>C.poulabronei</i>	3	Unknown			
		1; UAZV, UA7	<i>C.magharensis</i>	<i>C.magharensis</i> (DV)		Unknown			X
Perilli & Duarte, (2006)	Peniche (Portugal)	1; 6	<i>C.superbus</i>	<i>C.superbus sceptrum</i>	3	Middle Toarcian	Lowermost Bifrons	Lowermost NJT7a	X
		1; 10	<i>C.superbus</i>	<i>C.superbus superbus</i>	3	Uncorrected proof			X
	Brenha (Portugal)	1; 5	<i>C.cantaluppii</i>	<i>Carinolithus</i> spp.*	3	Middle Toarcian	Lowermost Bifrons	Lowermost NJT7a	
	Fornos (Portugal)	1; 9	<i>C.cantaluppii</i>	<i>C. poulabronei</i>	3	Lower Toarcian	Lower Levisoni	NJT5b	
		2; 6	<i>C.poulabronei</i>	<i>C.poulabronei</i>	2	Lower Toarcian	Lower Levisoni	NJT5b	
		2; 10	<i>C.poulabronei</i>	<i>C.poulabronei</i>	1	Lower Toarcian	Lower Levisoni	NJT5b	
Asgar-Deen et al., (2003)	West-central Alberta (Canada)	1; 6	<i>C.superbus</i>	<i>Carinolithus</i> spp.*	1	Unknown			
		1; 7	<i>C.superbus</i>	<i>Carinolithus</i> spp.*	1	Unknown			
		1; 8	<i>C.superbus</i>	<i>Carinolithus</i> spp.*	1	Unknown			
		1; 9	<i>C.superbus</i>	<i>Carinolithus</i> spp.*	1	Unknown			
Mattioli & Erba, (1999)	Fiuminata (Italy)	2; 15	<i>C.superbus</i>	<i>C.superbus superbus</i>	3	Lower Aalenian			X
	Digne (France)	3; 19	<i>C.magharensis</i>	<i>C.magharensis</i> (DV)		Lower Bajocian			X
		3; 20	<i>C.magharensis</i>	<i>C.magharensis</i> (DV)		Lower Bajocian			X
Parisi et al., (1998)	Colle d'Orlando (Italy)	4; 10	<i>C.superbus</i>	<i>C.superbus superbus</i>	3	Middle Toarcian	Lower Bifrons		X
		4; 11	<i>C.superbus</i>	<i>C.superbus sceptrum</i>	3	Middle Toarcian	Lower Bifrons		X

		5; 3	<i>H.magharensis</i>	<i>C.magharensis</i> (DV)		Uppermost Aalenian			X
		5; 6	<i>C.poulabronei</i>	<i>C.poulabronei</i>	3	Lower Toarcian	Middle Polymorphism		
Bucefalo Palliani & Mattioli, (1998)	Monte Serrone	1; 8	<i>C.poulabronei</i>	<i>C.poulabronei</i>	3	Lower Toarcian	Tenuicostatum	NJT6	
		1; 13	<i>C.superbus</i>	<i>C.superbus sceptrum</i>	1	Lower Toarcian	Tenuicostatum	NJT6	X
Bown & Cooper, (1998)	Ilminster (United Kingdom)	4.13; 10	<i>C.superbus</i>	<i>C.superbus sceptrum</i>	1	Toarcian			X
		4.13; 11	<i>C.superbus</i>	<i>C.superbus sceptrum</i>	1	Toarcian			X
	Brenha (Portugal)	4.13; 6	<i>C.magharensis</i>	<i>C.magharensis</i>	3	Aalenian/Bajocian boundary interval			X
		4.13; 7	<i>C.magharensis</i>	<i>C.magharensis</i> (DV)		Aalenian/Bajocian boundary interval			X
		4.13; 8	<i>C.magharensis</i>	<i>C.premagharensis</i>	2	Aalenian/Bajocian boundary interval			X
		4.13; 8	<i>C.magharensis</i>	<i>C.magharensis</i> (DV)		Aalenian/Bajocian boundary interval			X
Mattioli, (1996)	Pozzale (Italy)	2; 9	<i>C.poulabronei</i>	<i>C.poulabronei</i>	3	Lower Toarcian	Tenuicostatum		
	Dotternhausen (Germany)	2; 10	<i>C.poulabronei</i>	<i>C.poulabronei</i>	3	Lower Toarcian	(Exaratum)		
	Fiuminata (Italy)	2; 11	<i>C.poulabronei</i>	<i>C.poulabronei</i>	3	Lower Aalenian			
		2; 12	<i>C.poulabronei</i>	<i>C.poulabronei</i>	3	Lower Aalenian			
Gardin & Manivit, (1994)	C�r�de (France)	3; 13,14	<i>C.superbus</i>	<i>C.superbus superbus</i>	2	Unknown			X
		3; 15	<i>C.superbus</i>	<i>C.superbus sceptrum</i>	2	Unknown			X
		3; 16	<i>C.superbus</i>	<i>Carinolithus spp.*</i>	1	Unknown			
		4; 1,2	<i>C.magharensis</i>	<i>C.magharensis</i> (DV)		Unknown			X
	Penne (France)	3; 11	<i>C.cantaluppii</i>	<i>Carinolithus spp.*</i>	3	Unknown			
Reale et al., (1992)	Monte Serrone (Italy)	2; 18,19	<i>C.superbus</i>	<i>C.superbus sceptrum</i>	3	Upper Toarcian	Erbaense		X
	Valdorbia (Italy)	2; 20,21	<i>C.superbus</i>	<i>C.superbus sceptrum</i>	2	Lower Toarcian	Serpentinus		X
Cobianchi, (1992)	Breggia (Switzerland)	20; i	<i>C.superbus</i>	<i>Carinolithus spp.*</i>	3	Upper Aalenian			
		20; l	<i>H.magharensis</i>	<i>C.magharensis</i> (DV)		Lower Bajocian			X
	Caricatore (Italy)	20; g	<i>C.cantaluppii</i>	<i>C.superbus sceptrum</i>	3	Lower Toarcian	Middle Tenuicostatum		X
Baldanza & Mattioli, (1992)	Kaballos (Greece)	1; 5	<i>C.superbus</i>	<i>C.superbus sceptrum</i>	2	Lower/Middle Toarcian boundary	Serpentinus		X
		1; 8	<i>C.superbus</i>	<i>C.superbus superbus</i>	1	Lower/Middle Toarcian boundary	Serpentinus		X
Erba (1990)	West Beaumont (France)	1; 2,3	<i>H.magharensis</i>	<i>C.magharensis</i> (DV)		Lower Bajocian	Discites		X
		1; 4	<i>H.magharensis</i>	<i>C.magharensis</i> (DV)		Lower Bajocian	Discites		X
		1; 16	<i>C.superbus</i>	<i>C.superbus superbus</i>	2	Lower Bajocian	Discites		X
Bown et al., (1988)	Ilminster, Dorset (United Kingdom)	1; 14	<i>C.superbus</i>	<i>C.superbus superbus</i>	2	Middle Toarcian	Bifrons		X
Bown, (1987)	Trimeusel (Germany)	14; 15,16	<i>C.superbus</i>	<i>C.superbus sceptrum</i>	1	Upper Toarcian	Levesquei		X
	Brenha (Portugal)	14; 17,18	<i>C.magharensis</i>	<i>C.premagharensis</i>	2	Bajocian			X
		14; 19,20	<i>C.magharensis</i>	<i>C.magharensis</i> (DV)		Bajocian			X
Crux, (1987)	Ilminster, Dorset (United Kingdom)	2; 11	<i>C.superbus</i>	<i>C.superbus superbus</i>	3	Upper Toarcian	Levesquei		X
	Southern North Sea	2; 17	<i>C.superbus</i>	<i>C.superbus superbus</i>	3	Toarcian			X

Appendix D

Range chart of the Sogno Core

Calcareous nannofossil range chart of the Sogno Core. Semi-quantitative abundance of all taxa detected are reported, as well as total abundance and preservation of calcareous nannofossils in each studied sample.

Total abundance:

CA (common to abundant): more than 10 specimens per field of view.

C (common): 6-10 specimens per field of view.

FC (few/common): 1-5 specimens per field of view.

F (few): 1 specimen in 1-5 fields of view.

RF (rare/few): 1 specimen in 6-10 fields of view.

R (rare): 1 specimen in 11-50 fields of view.

RR (very rare): 1 specimen in 51-100 fields of view.

VB (virtually barren): 1 specimen in more than 100 fields of view.

Abundance of individual taxa:

CA (common/abundant): >30 specimens in 50 fields of view.

C (common): >30 specimens in 100 fields of view.

FC (few/common): >30 specimens in 200 fields of view.

F (few): 11-30 specimens in 200 fields of view.

RF (rare/few): 6-10 specimens in 200 fields of view.

R (rare): 1-5 specimens in 200 fields of view.

RR (extremely rare): 1 specimen in 400 fields of view.

Preservation:

Preservation of calcareous nannofossils was characterized adopting the codes described by Roth & Thierstein (1972) and Roth (1983): E1 (slight etching); E2 (moderate etching); E3 (strong etching); O1 (slight overgrowth); O2 (moderate overgrowth); O3 (strong overgrowth). Furthermore, preservation was also coded as follows:

G (good): no evidence of etching and/or overgrowth; primary morphological characteristics are preserved.

M/G (moderate/good): very little evidence of etching and/or overgrowth; primary morphological characteristics are usually preserved.

M (moderate): little evidence of etching and/or overgrowth; primary morphological characteristics are often altered.

P/M (poor/moderate): evidence of etching and/or overgrowth; primary morphological characteristics are often altered.

P (poor): most specimens exhibit dissolution or overgrowth; primary morphological characteristics are often destroyed.

Appendix E

Range charts of the L1 and Schandelah Cores

Calcareous nannofossil range charts of the L1 and Schandelah Cores. Quantitative abundance of all taxa detected are reported, as well as preservation of each studied sample.

Abundance:

At least 300 determinable nannofossil specimens were counted in each slide. Additional 8 cross-sections, corresponding to 1000 fields of view, were investigated for rare species. Several samples belonging to the Amaltheenton Fm. are barren, others contain extremely rare abundances of specimens (less than 10 specimens in 1000 fields of view). In these, the 300-specimen counting was not possible.

Preservation:

Preservation of calcareous nannofossils was characterized adopting the codes described by Roth and Thierstein (1972) and Roth (1983): E1 (slight etching); E2 (moderate etching); E3 (strong etching); O1 (slight overgrowth); O2 (moderate overgrowth); O3 (strong overgrowth). Furthermore, preservation was also coded as follows:

G (good): no evidence of etching and/or overgrowth; primary morphological characteristics are preserved.

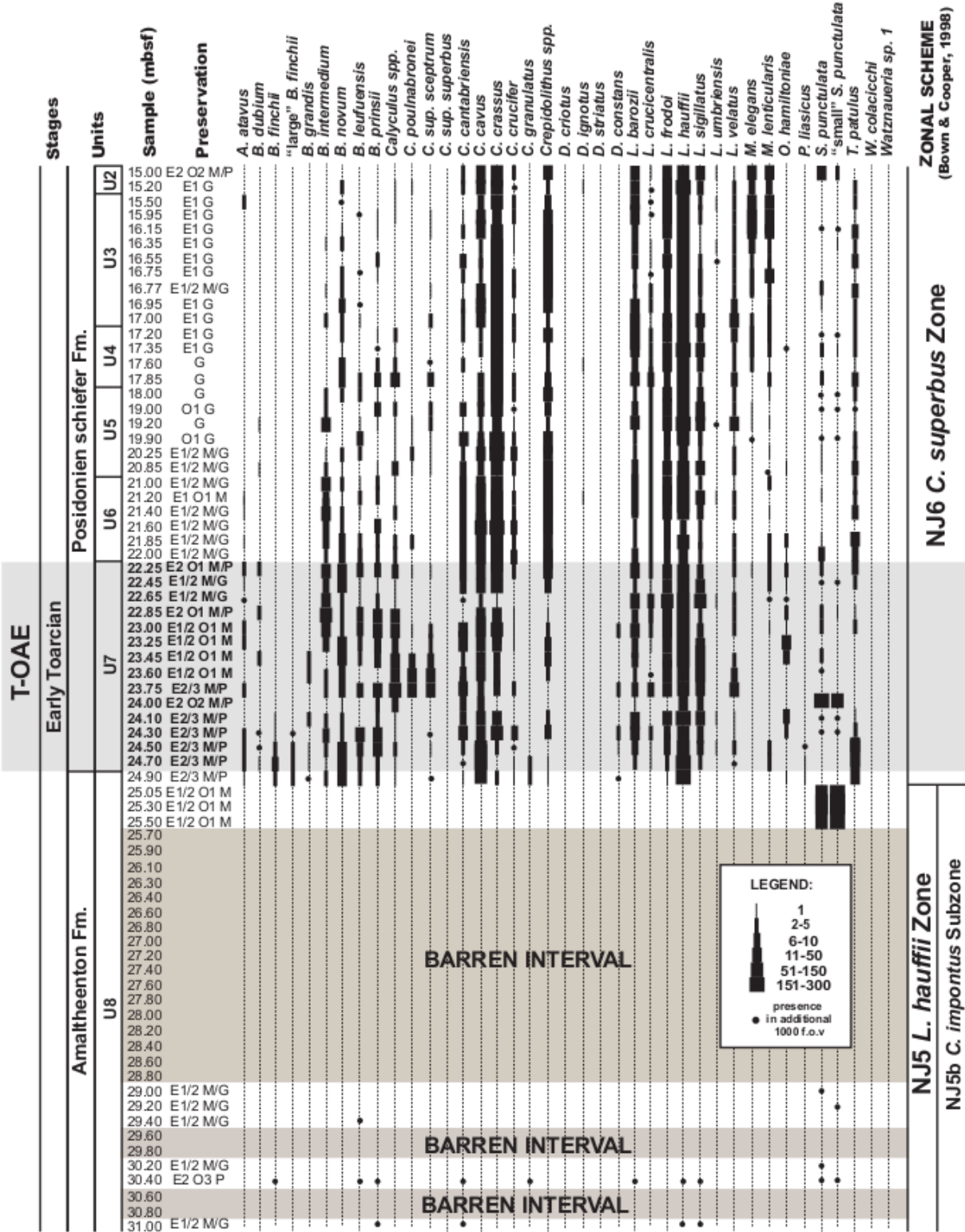
M/G (moderate/good): very little evidence of etching and/or overgrowth; primary morphological characteristics are usually preserved.

M (moderate): little evidence of etching and/or overgrowth; primary morphological characteristics are often altered.

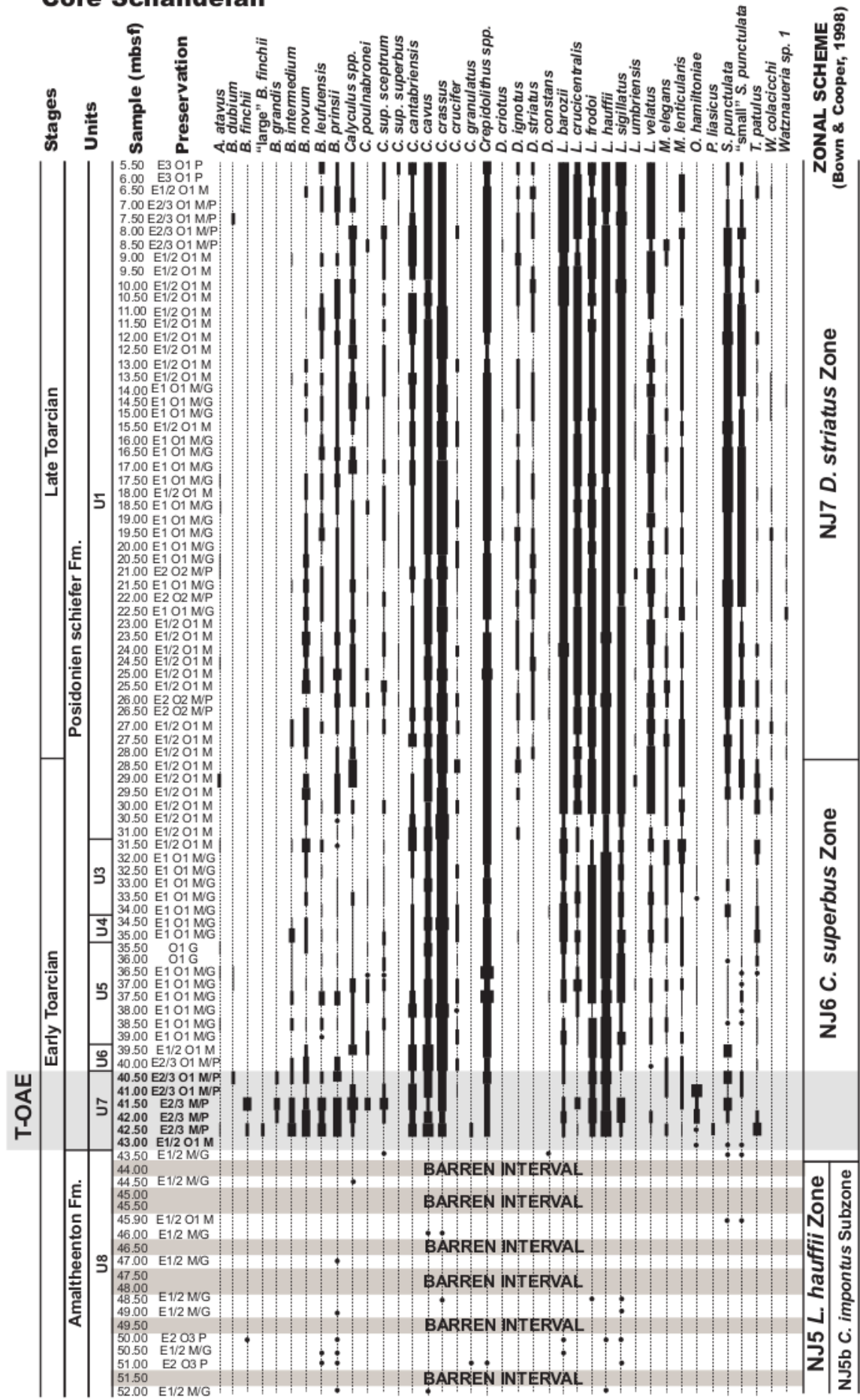
P/M (poor/moderate): evidence of etching and/or overgrowth; primary morphological characteristics are often altered.

P (poor): most specimens exhibit dissolution or overgrowth; primary morphological characteristics are often destroyed.

Core L1



Core Schandelah



Methodology

300 specimen counting + 1000 fields of view

1000 fields of view

Appendix F

Erba et al. 2019a

**The response of calcareous nannoplankton to Oceanic Anoxic Events:
The Italian pelagic record**

Elisabetta ERBA, Cinzia BOTTINI, Giulia FAUCHER,
Gabriele GAMBACORTA & **Stefano VISENTIN**

The response of calcareous nanoplankton to Oceanic Anoxic Events: The Italian pelagic record

Elisabetta ERBA, Cinzia BOTTINI, Giulia FAUCHER, Gabriele GAMBACORTA & Stefano VISENTIN

- E. Erba, Università degli Studi di Milano, Dipartimento di Scienze della Terra “Ardito Desio”, Via Mangiagalli 34, I-20133 Milano, Italy; elisabetta.erba@unimi.it
C. Bottini, Università degli Studi di Milano, Dipartimento di Scienze della Terra “Ardito Desio”, Via Mangiagalli 34, I-20133 Milano, Italy; cinzia.bottini@unimi.it
G. Faucher, Università degli Studi di Milano, Dipartimento di Scienze della Terra “Ardito Desio”, Via Mangiagalli 34, I-20133 Milano, Italy; giulia.faucher@unimi.it
G. Gambacorta, Università degli Studi di Milano, Dipartimento di Scienze della Terra “Ardito Desio”, Via Mangiagalli 34, I-20133 Milano, Italy; gabriele.gambacorta@guest.unimi.it
S. Visentin, Università degli Studi di Milano, Dipartimento di Scienze della Terra “Ardito Desio”, Via Mangiagalli 34, I-20133 Milano, Italy; stefano.visentin@unimi.it

KEYWORDS - Global anoxia, calcareous nannofossils, palaeoecology, Italian pelagic sections.

ABSTRACT - Earth history is punctuated by phases of extreme global stress of concurrent warming, ocean fertilisation and acidification that impacted biologic diversity and function. Under excess CO₂ and greenhouse conditions, the Mesozoic deep ocean became temporarily depleted of oxygen, promoting the accumulation of massive amounts of organic matter during Oceanic Anoxic Events (OAEs). Although global anoxia and enhanced organic matter burial are the most striking and intriguing palaeoceanographic phenomena, OAEs can be studied also to decipher the oceanic ecosystem response to CO₂ pulses. In Jurassic and Cretaceous oceans, calcareous nanoplankton were already common from coastal to open oceanic settings and of enough abundance and diversity to produce calcareous oozes. Indeed, Jurassic and Cretaceous pelagic micrites mainly consist of coccoliths and nannoliths, in addition to variable amounts of diagenetic carbonate. Therefore, pelagic limestones are ideal for epitomising variations in abundance and composition of calcareous phytoplankton at large scale to understand their response to global change.

Italian pelagic successions are a reference for the Tethys Ocean and, in general, for low to middle latitudes. We consider herein well-dated sections with quantitative nannofossil data across OAEs to synthesise changes in abundance of the dominant, micrite-forming, nannofossil taxa and species-specific variations in size to trace the response of calcareous nanoplankton as expressed by biocalcification across the early Toarcian T-OAE, late Valanginian Weissert-OAE, early Aptian OAE1a and latest Cenomanian OAE2. In general, a major decrease in nannofossil abundance is recorded for the highly calcified dominant forms, evidenced by the “Schizosphaerella crisis”, the “nannoconid decline” and the “nannoconid crisis” during the T-OAE, Weissert-OAE and OAE1a, respectively. An even more dramatic drop in coccolith/nannolith abundance characterises OAE2, with a nanoplankton biocalcification “blackout” through the Bonarelli Level in Italian sections. Despite these abundance crises, calcareous nannofloras recovered soon after the paleoenvironmental perturbation terminated, although the return to pre-OAE conditions occurred rather slowly and assemblage composition was renewed across the event. Species-specific changes in size were detected for Schizosphaerella across the T-OAE and for Biscutum constans (Górka, 1957) in the intervals of maximum perturbation within OAE1a and OAE2. Size of Nannoconus steimannii Kamptner, 1931, conversely, does not show variations across the Weissert-OAE and OAE1a. The T-OAE and OAE1a were preceded and accompanied by a few million-year-long origination phase, indicating the calcareous nanoplankton ability to positively respond to and overcome stressing oceanic conditions, as further evidenced by absence of extinctions. Calcareous nanoplankton reacted differently during the Weissert-OAE and OAE2 as the Valanginian “nannoconid decline” is gradual and followed by a symmetric increase in abundance, while the late Cenomanian nannofossil drop in abundance was as sudden as its recovery. In both cases, extinctions are paralleled by entry of new taxa, at a slower rate across the Weissert-OAE and at faster rates in the case of OAE2. The influence of palaeoenvironmental stress on calcareous nannofloral abundance and composition during the early Toarcian T-OAE, late Valanginian Weissert-OAE, early Aptian OAE1a and latest Cenomanian OAE2, are clearly recorded in Italian pelagic sections and at supra-regional to global scale. However, the effects on nanoplankton evolution, if any, was differentiated and resulted in overall originations. Calcareous nannofossil patterns underline the resilience of this phytoplankton group during OAE perturbations.

RIASSUNTO - [La risposta del nanoplancton calcareo agli Eventi Anossici Oceanici: il record pelagico in Italia] - La storia della Terra è punteggiata da eventi di stress globale estremo evidenziato da riscaldamento, fertilizzazione e acidificazione oceanica che hanno influito sulla diversità e sul funzionamento del biota marino. In condizioni di eccesso di CO₂ e di clima a effetto serra, durante il Mesozoico i fondali marini hanno sperimentato temporanea anossia e accumulo di materia organica durante eventi anossici oceanici (OAE). Sebbene l'anossia globale e il seppellimento di grandi quantità di carbonio organico siano i fenomeni paleoceanografici più intriganti, gli OAE possono essere studiati anche per decifrare la risposta dell'ecosistema oceanico a perturbazioni globali. Negli oceani del Giurassico e Cretacico, il nanoplancton calcareo era già diffuso dalle zone costiere all'oceano aperto, in sufficiente abbondanza e diversità per produrre sedimenti biogenici calcarei. Infatti, le micriti pelagiche del Giurassico e del Cretacico consistono principalmente di coccoliti e nannoliti, oltre a quantità variabili di carbonato diagenetico. Pertanto, i calcari pelagici sono ideali per quantificare le variazioni di abbondanza e composizione del fitoplancton calcareo e, di conseguenza, dei produttori primari per comprenderne la risposta ai cambiamenti globali.

Le successioni pelagiche italiane sono considerate di riferimento per l'Oceano della Tetide e, in generale, per le basse-medie latitudini. In questo lavoro, abbiamo considerato sezioni stratigrafiche ben datate e con dati quantitativi delle associazioni a nannofossili calcarei, per sintetizzare i cambiamenti in abbondanza dei taxa dominanti e le variazioni dimensionali di alcune specie al fine di tracciare la risposta del nanoplancton calcareo tramite la biocalcificazione durante il T-OAE del Toarciano inferiore, il Weissert-OAE del Valanginiano superiore, l'OAE1a dell'Aptiano inferiore e l'OAE2 del Cenomaniano sommitale. In generale, si registra una drastica diminuzione dell'abbondanza dei nannofossili, soprattutto per le forme dominanti altamente calcificate, come evidenziato dalla “crisi di Schizosphaerella”, dal “declino dei nannoconidi” e dalla “crisi dei nannoconidi” durante i T-OAE, Weissert-OAE e OAE1a, rispettivamente. Una riduzione ancora più drammatica dell'abbondanza di coccoliti/nannoliti caratterizza l'OAE2, con un “blackout” della biocalcificazione del nanoplancton durante

la deposizione del Livello Bonarelli nelle sezioni italiane. Nonostante queste crisi di abbondanza, le nannoflore calcaree si sono ristabilite subito dopo la fine della perturbazione paleoambientale, sebbene il ritorno a condizioni pre-OAE sia avvenuto piuttosto lentamente e le associazioni abbiano raggiunto una composizione diversa. Sono stati rilevati cambiamenti delle dimensioni di *Schizosphaerella* attraverso il T-OAE e di *Biscutum constans* (Górka, 1957) negli intervalli di massima perturbazione all'interno degli OAE1a e OAE2. Le dimensioni di *Nannoconus steimanni* Kamptner, 1931, al contrario, non mostrano variazioni durante il Weissert-OAE e l'OAE1a. Il T-OAE e l'OAE1a sono stati preceduti e accompagnati da una fase di speciazione del nannoplancton, durata alcuni milioni di anni, che indica la capacità del fitoplancton calcareo a rispondere positivamente superando condizioni oceaniche stressanti, come evidenziato anche dall'assenza di estinzioni. Il nannoplancton calcareo ha reagito in modo diverso durante il Weissert-OAE e l'OAE2 poiché il "declino dei nannoconidi" del Valanginiano è graduale e seguito da un altrettanto graduale aumento dell'abbondanza, mentre la riduzione dei nannofossili nel Cenomaniano sommitale è stata repentina come il suo recupero. In entrambi i casi, si sono verificate alcune estinzioni ma contemporaneamente anche la speciazione di nuovi taxa, a un ritmo più lento attraverso il Weissert-OAE e a tassi più rapidi nel caso dell'OAE2.

Mentre l'influenza dello stress paleoambientale sull'abbondanza e composizione delle nannoflore calcaree durante il T-OAE, il Weissert-OAE, l'OAE1a e l'OAE2 è chiaramente registrata nelle sezioni pelagiche italiane e spesso su scala sopra-regionale fino a globale, l'influenza degli OAE sull'evoluzione del nannoplancton, se causale, è stata differenziata e ha generalmente indotto delle speciazioni. Le variazioni riscontrate nelle associazioni a nannofossili calcarei sottolineano la resilienza di questo gruppo di fitoplancton durante le perturbazioni ambientali associate agli OAE.

INTRODUCTION

The early phase of the Deep Sea Drilling Project provided evidence of extensive occurrence of Cretaceous black shales from previously unsampled oceanic basins. As on-land, stratigraphies of pelagic successions showed that organic carbon-rich lithologies are confined to specific geologically short intervals (0.5 to 2 million years) suggesting a global rather than local to regional oxygen-depletion of bottom waters.

The term "Oceanic Anoxic Event" (OAE) was coined by Schlanger & Jenkyns (1976) after the recovery of mid-Cretaceous black shales at sites drilled in the Pacific Ocean. Such lithologic units were recognised as equivalent and coeval of well-known lithostratigraphic markers previously described in the Tethys and Atlantic Oceans. The term OAE was originally defined to signify time intervals during which black shale deposition was prevalent at a global scale. The original definition was, therefore, based on lithologic criteria and applied to two time intervals, namely the Aptian-Albian (OAE1) and the Cenomanian-Turonian (OAE2). Later investigations on land and in the oceans pointed out the occurrence of the Coniacian-Santonian OAE3 (Arthur & Schlanger, 1979; Jenkyns, 1980) and of the Toarcian OAE (Jenkyns, 1985, 1988). Based on integrated and higher resolution stratigraphy of the sedimentary record of organic-rich black shales, Arthur et al. (1990) subdivided OAE1 into discrete events OAE1a, OAE1b, OAE1c and OAE1d, still using the sedimentary record of organic C-rich black shales.

The most spectacular sedimentary expression of the early Aptian and latest Cenomanian events are the Livello Selli and Livello Bonarelli, respectively. For both the type area is the Umbria-Marche Basin (central Italy), where a continuous pelagic succession deposited in the Jurassic to

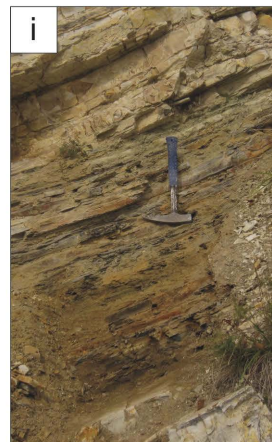
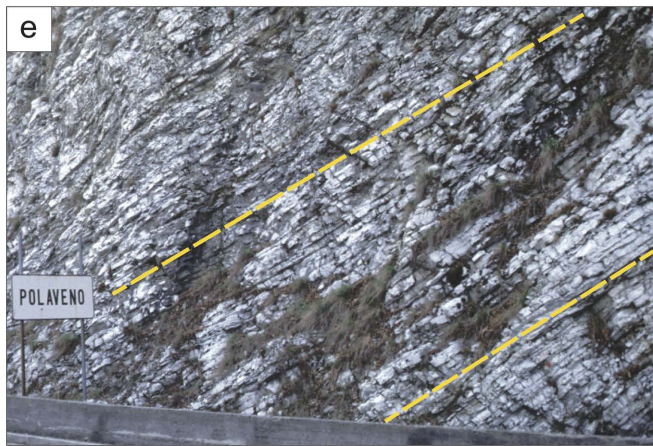
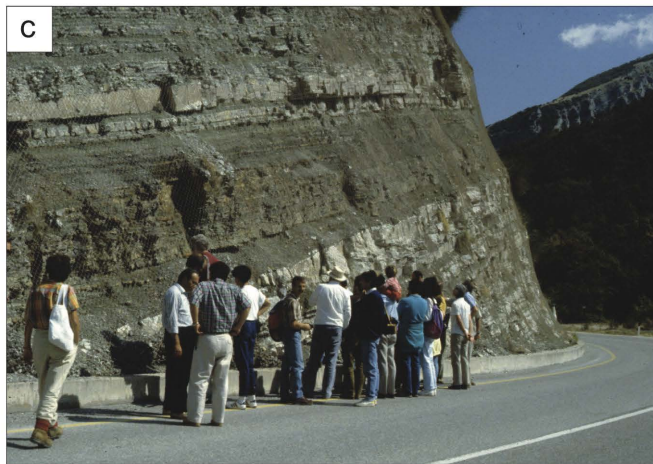
Paleogene interval. The first event that was recognised and the most studied one is the Bonarelli Level, named after its discoverer Guido Bonarelli. In fact, in 1891 Bonarelli described "uno strato di scisto nero bituminoso" (a level of black organic-rich shale), about 1 metre thick, in the uppermost part of the Scaglia Bianca in the region of Gubbio, close to the Cenomanian/Turonian boundary (Bonarelli, 1891) (Fig. 1).

At the beginning of the XX century, Dal Piaz (1907) described Toarcian organic-rich facies in pelagic Jurassic successions of the Alpi Feltrine in the Southern Alps, similarly to other occurrences in Germany and Switzerland (Posidonienschiefer), England (Jet Rock and Bituminous Shales) and France (Schistes Carton). Dal Piaz's perception of black shales as geological archives of major environmental changes was by far innovative and a precursor of modern palaeoceanography. A few decades later Gaetani & Poliani (1978) described a lower Toarcian black shale interval, named "Livello a Pesci" (Fish Level), in the pelagic succession of the Lombardy Basin (Fig. 1). In the 80s, Jenkyns (1985, 1988) labelled these black shale intervals as the Toarcian OAE (T-OAE).

The identification of the Livello Selli is much younger (Coccioni et al., 1987) and, again, was based on the occurrence of a 1-3 m thick marker bed described as a "livello radiolaritico-bituminoso-ittiolitico" (a black shale interval enriched in radiolarians, fish remains and organic matter) in the lowermost part of the Marne a Fucoidi Formation through the Umbria-Marche Basin (Fig. 1).

With the rapid development of chemostratigraphy, and specifically of C and O stable isotopic investigations, it became clear that the T-OAE, OAE1a and OAE2 are associated with negative and positive anomalies of carbon-isotope curves obtained from sedimentary carbonate and/or organic matter, which record major perturbations of

Fig. 1 - a) "Livello a Pesci", deposited during the T-OAE, at the Colle di Sogno section (n. 3 in Fig. 3 - Lombardy Basin, northwestern Italy). b) "Livello a Pesci" in the Sogno Core compared to the equivalent outcropping lithostratigraphic interval (n. 3 in Fig. 3 - Lombardy Basin, northwestern Italy). c) Selli Level, deposited during the OAE1a, at the Apecchiese section. The laterally equivalent interval was cored nearby in the Piobbico Core (n. 17 in Fig. 3 - Umbria-Marche Basin, central Italy). d) Selli Level equivalent recovered with the Cismon APTICORE placed next to the same outcropping lithostratigraphic interval (n. 11 and 12 in Fig. 3 - Belluno Basin, northeastern Italy). e) The Weissert-OAE interval (bounded by the two yellow dashed lines) at Polaveno (n. 6 in Fig. 3 - Lombardy Basin, northwestern Italy). f) The middle Cenomanian to lower Turonian succession at Furlo (n. 15 in Fig. 3 - Umbria-Marche Basin, central Italy) with the black shales of the Livello Bonarelli deposited during OAE2. g) Close up view of Livello Bonarelli in the Contessa outcrop (n. 24 in Fig. 3 - Umbria-Marche Basin, central Italy). h) Close up view of Livello Bonarelli in the Bottaccione Gorge section (n. 22 in Fig. 3 - Umbria-Marche Basin, central Italy). i) Close up view of Livello Bonarelli in the Monte Petrano section (n. 18 in Fig. 3 - Umbria-Marche Basin, central Italy).



the global carbon cycle (Jenkyns, 2010). The original definition of OAEs (Schlanger & Jenkyns, 1976) has become somehow misleading for various reasons: 1) anoxia is rarely reached; 2) black shale intervals were proved to be diachronous in many cases; 3) fully oxic continental and shallow marine successions also record the global C cycle anomalies; 4) anomalies are of long to short duration.

High-resolution integrated stratigraphy of marine and terrestrial records has produced a solid time framework for OAEs (Robinson et al., 2017), and $\delta^{13}\text{C}$ chemostratigraphy has grown as the prominent tool for identifying, characterising and correlating OAEs (e.g., Erba, 2004; Tsikos et al., 2004; Weissert & Erba, 2004; Jenkyns, 2010). A typical example is the discrete C isotope excursion of late Valanginian age identified in the Maiolica Formation of the Southern Alps (Weissert, 1989; Lini et al., 1992), which is not accompanied by a black marker bed (Fig. 1). Such an anomaly was constrained by bio-magnetostratigraphy (Channell et al., 1993) and used by Erba et al. (2004) to formalise the Valanginian event as the “Weissert OAE”. Global anoxia has not been documented, but discrete black shale levels enriched in organic matter are described from the Tethys and Pacific Oceans in the early phase of the Weissert-OAE (Erba et al., 2004).

In the past four decades OAEs have been recognised in oceanic and terrestrial sequences, highlighting local variations in depositional conditions, types and degrees of diagenesis, and preservation of organic matter. As summarised by Jenkyns (2010), equivalents of the Bonarelli, Selli, Weissert and Toarcian events have been recognised in a variety of sedimentary basins, and a number of geochemical anomalies have been detected in addition to C-isotope excursions. Yet, a lively debate about causes and consequences of OAEs and their influence on biota continues to involve experts from various disciplines within geosciences. The original hypotheses of Schlanger & Jenkyns (1976) are still discussed to discern and discriminate the role of productivity from that of organic matter preservation under anoxic conditions. Pelagic successions containing OAEs are crucial to understand the biotic variations in marine planktonic communities associated with such global perturbations of the ocean/atmosphere system. In marine ecosystems coccolithophores are part of phytoplankton responsible for primary productivity, energy transfer to higher trophic levels, export of biogenic particles to the seafloors and exchanges between the surface ocean and the atmosphere. The term calcareous nannoplankton was originally introduced by Lohman (1902) for planktonic organisms smaller than 63 μm and is now used for golden-brown algae coccolithophores (phylum Haptophyta) secreting tiny calcite crystals to build coccoliths and ultimately coccospheres. The global occurrence of calcareous nannoplankton and their biomineralisation make these phytoplanktonic algae a very effective producer of calcite on Earth. Calcareous nannofossils include the fossil remains of coccolithophores, namely coccoliths and coccospheres as well as associated nannoliths often of unknown biological affinity.

In Jurassic and Cretaceous oceans, calcareous nannoplankton were already the most efficient rock-forming group (e.g., Erba, 2006). Indeed, Jurassic and

Cretaceous pelagic micrites mainly consist of coccoliths and nannoliths, in addition to variable amounts of diagenetic calcite. Consequently, pelagic carbonates offer the opportunity of characterising variations in abundance and composition of calcareous nannofloras across OAEs to quantify their resilience to extreme conditions.

Italian pelagic successions represent excellent records of the Tethys Ocean (Figs 1-2) and, in fact, have been studied since a long time. The first documentations of nannofossil-rich limestones were based on scanning electron microscope investigations of Maiolica and Scaglia limestones (Farinacci, 1964). These pioneering studies unequivocally demonstrated the rock-forming role of calcareous nannoplankton as further discussed by Noël & Busson (1990) also for Jurassic pelagic successions of the Tethys. Indeed, it became clear that *Schizosphaerella* and *Nannoconus* can reach high abundances in pelagic and hemipelagic carbonates of Jurassic and Cretaceous age. The name “nannoconite” was proposed for *Nannoconus*-limestone (Bréhéret, 1983) and quantitative studies conclusively showed that Lower Cretaceous Maiolica limestones are nannoconites (Erba, 1994; Erba & Tremolada, 2004). Similarly, *Schizosphaerella* can be so abundant (e.g., Kälin & Bernoulli, 1984; Claps et al., 1995; Mattioli, 1997; Erba, 2004; Casellato & Erba, 2015; Peti & Tibault, 2017) as to produce a “schizosphaerellite”.

Quantitative studies of Cretaceous pelagic successions, comprising OAEs, reveal major shifts in the biogenic component: from carbonate-dominated to siliceous- and organic matter-dominated (Premoli Silva et al., 1999; Leckie et al., 2002; Erba, 2004). Usually, radiolarian and organic-walled micro-organisms become overwhelming in the black shales representing OAEs, while calcareous nannofossils are abundant below and above. The nannofossil record, in fact, traces major decreases in abundances across the perturbation, especially of the dominant forms that usually show incomplete recovery after termination of OAEs (Erba, 2004).

Erba (2004) reviewed changes in calcareous nannofossil assemblages across the T-OAE, OAE1a and OAE2 and proposed palaeoceanographic and palaeoecologic dynamics. In this work, we focus on calcareous nannofossil changes across OAEs recorded in pelagic Italian successions that are, still, reference records of global changes at low to middle latitudes. Our synthesis regards only well-dated sections with quantitative nannofossil data and $\delta^{13}\text{C}$ chemostratigraphy for the T-OAE, Weissert-OAE, OAE1a and OAE2. In particular, for each OAE we will highlight changes in abundance of the dominant (micrite-forming) nannofossil taxa and species-specific variations in size to trace the response of calcareous nannoplankton as expressed by their biocalcified remains.

MATERIAL AND METHODS

A geographical map showing the location of the sections considered for this work is given in Fig. 3, while Fig. 2 shows the palaeogeography of the Tethyan area during the Jurassic-Cretaceous interval. Considered sections mostly lie in the Southern Alps (sections 1 to 14) and the Umbria-Marche Basin (sections 15 to 27),

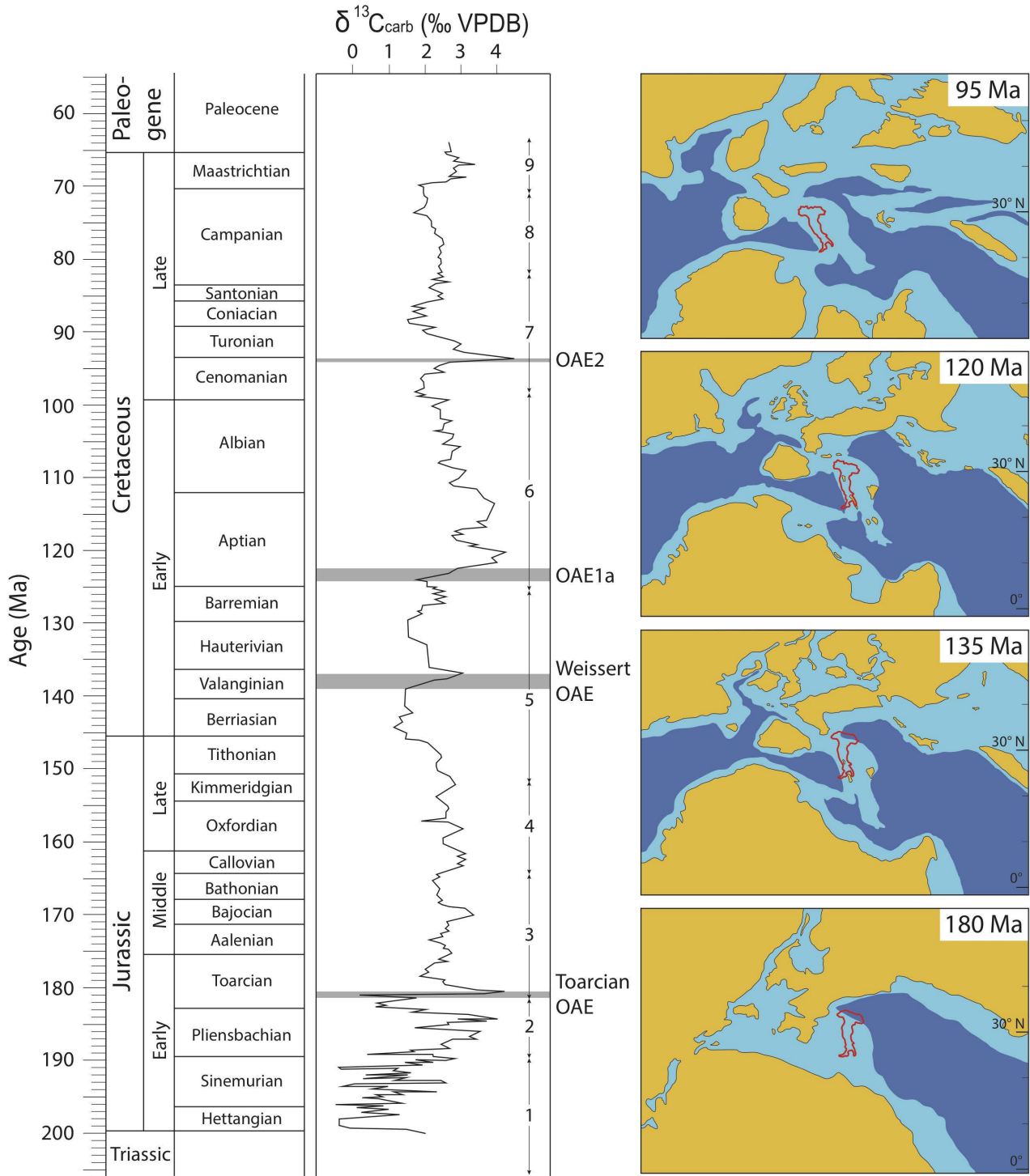


Fig. 2 - Bulk carbonate carbon isotope ($\delta^{13}\text{C}_{\text{carb}}$) stratigraphy of the Jurassic and Cretaceous (modified after Robinson et al., 2017). The stratigraphic position of T-OAE, Weissert-OAE, OAE1a and OAE2 are reported as grey bands. Carbon-isotope data from: (1) Van de Schootbrugge et al. (2005); (2) Hesselbo et al. (2000); (3) Morettini et al. (2002); (4) Dromart et al. (2003); (5) Weissert et al. (1998); (6) Erbacher et al. (1996); (7) Jenkyns et al. (1994); (8) Jarvis et al. (2002); and (9) Abramovich et al. (2003). On the right the relative position of Italy at 180 Ma, 135 Ma, 120 Ma and 95 Ma is reported as a red outline on palaeogeographic maps (modified after Scotese, 2014).

but a few key-successions were studied in the Gargano area (section 28), Sicily (sections 29 to 31) and Sardinia (section 32). The sedimentary expression of the T-OAE, Weissert-OAE, OAE1a and OAE2 in Italian key-sections is illustrated in Fig. 1. For this review we considered all the published papers documenting quantitative and

morphometric data for calcareous nannofossils across the T-OAE, Weissert-OAE, OAE1a and OAE2, within a well-defined framework of C-isotope stratigraphy (see Tabs 1-4). The data are summarised in a graphical form by reporting as bars the relative stratigraphic range of each section, separately for nannofossil and $\delta^{13}\text{C}$ data. In

case the same section was described in multiple papers, we synthesised in a single bar the cumulative extent of the data generated for the analysed stratigraphic interval (Tabs 1-4). The presence and extension of hiatuses are also reported. The resulting synthesis figures are intended to help the reader in rapidly identifying the relevant literature and have an overall framework of C-isotope chemostratigraphy applied to Jurassic and Cretaceous OAEs in Italian sections.

As previously discussed, the operational definition of OAEs has partially changed, and various authors based OAE boundaries (onset and termination) on lithostratigraphic or chemostratigraphic data. In most cases biostratigraphy was used to constrain age attribution and possibly identify/confirm hiatuses eliding part of the OAEs. It should also be stressed that in many cases black shales are diachronous, defying the original definition of Schlanger & Jenkyns (1976). The definitions adopted in this paper are as follows:

1. The T-OAE corresponds to the negative excursion in the carbonate and organic carbon isotope profile (Jenkyns, 2010).

2. The Weissert-OAE is based on the $\delta^{13}\text{C}$ curve: its beginning and end are placed at the base of the positive excursion and its climax, respectively (Erba et al., 2004).

3. The early Aptian OAE1a corresponds to the Selli Level. With reference to the $\delta^{13}\text{C}$ chemostratigraphy, it begins with the onset of the sharp negative shift named C3-Ap3, and terminates at the base of the extended positive excursion named C7-Ap7 (Menegatti et al., 1998; Bottini et al., 2015).

4. The definition of the latest Cenomanian OAE2 is based on the $\delta^{13}\text{C}$ curve: its beginning and end are placed at the base of the positive excursion and at its climax, respectively (Tsikos et al., 2004).

As discussed by Jenkyns (2010), the amplitude of the carbon isotope anomaly is usually greater in marine and terrestrial organic matter than in carbonate. However, when bulk $\delta^{13}\text{C}_{\text{carb}}$ chemostratigraphy is considered, absolute values and trends are very comparable in many marine sections, allowing the construction of reference synthesis curves (e.g., Erba, 2004; Weissert & Erba, 2004; Jarvis et al., 2006; Robinson et al., 2017; Bottini & Erba, 2018) (Fig. 3).

As far as Italian sections are concerned, quantitative analyses of nannofossil abundances of Lower Jurassic (T-OAE) and Lower Cretaceous intervals (Weissert-OAE and OAE1a) were performed on ultrathin sections by light polarising microscope at 1250 \times magnification. Thin sections were thinned to an average thickness of 7

ITALIAN PELAGIC SECTIONS WITH NANNOFOSSIL AND CARBON ISOTOPIC DATA FOR T-OAE

n.	Locality	Reference	Nannofossils	$\delta^{13}\text{C}$
1.	Val Ceppelline (Lombardy Basin, northwestern Italy)	Jenkyns & Clayton, 1986		•
3.	Colle di Sogno/Mt. Brughetto (Lombardy basin, northwestern Italy)	Jenkyns & Clayton, 1986 Casellato & Erba, 2015	•	•
8.	Brasa (Lombardy Basin, northwestern Italy)	Cobianchi & Picotti, 2001	•	
14.	Dogna (Belluno Basin, northeastern Italy)	Jenkyns et al., 2001		•
20.	Valdorbina (Umbria-Marche, central Italy)	Jenkyns & Clayton, 1986 Sabatino et al., 2009		• •
21.	Colle d'Orlando (Umbria-Marche, central Italy)	Bucefalo Palliani et al., 1998 Mattioli & Pittet, 2004	• •	
25.	Pozzale (Umbria-Marche, central Italy)	Bucefalo Palliani et al., 1998 Mattioli et al., 2004b Mattioli & Pittet, 2004	• • •	•
26.	Somma (Umbria-Marche, central Italy)	Mattioli & Pittet, 2002 Mattioli et al., 2004a Mattioli et al., 2004b Mattioli et al., 2009	• • • •	• •
27.	Fonte Cerro (Umbria-Marche, central Italy)	Bucefalo Palliani et al., 1998 Mattioli & Pittet, 2004	• •	

Tab. 1 - Compilation of papers documenting quantitative nannofossil and carbon isotope data for the T-OAE interval.



Fig. 3 - Geographic location of the Italian sections with available quantitative and morphometric nannofossil and/or carbon isotope data for the T-OAE, Weissert-OAE, OAE1a and OAE2.

mm in order to have an adequate view of nannofloras, and nannofossil absolute abundances were calculated counting all specimens in 1 mm² (Erba, 1994, 2004; Erba & Tremolada, 2004; Bottini et al., 2015; Casellato & Erba, 2015). For the OAE2 interval, total nannofossil abundances were obtained on simple smear slides: the nannofossil assemblages were quantified by counting at least 300 specimens in each sample using a light polarising microscope at 1250× magnification, and the total abundance was calculated as the average number of nannofossils per field of view (Erba, 2004).

In addition to trends of nannofossil abundances, we report here species-specific changes in size of selected taxa across the T-OAE, Weissert-OAE, OAE1a and OAE2. Particularly, morphometric investigations were applied to capture size fluctuations of: 1) *Schizosphaerella* across the T-OAE; 2) *Nannoconus steinmannii* Kamptner, 1931 across the Weissert-OAE; 3) *N. steinmannii* and *Biscutum constans* (Górka, 1957) across OAE1a; 4) *Biscutum constans* across OAE2. Size measurements were carried out on simple smear slides. Morphometry of *Schizosphaerella* and *B. constans* is based on digital photographs acquired with a camera mounted on a Leitz Laborlux light microscope and using the ImageJ64 software. Morphometric analyses of *N. steinmannii*, instead, were obtained with built-in camera Olympus

DP73 set on the light microscope Leica DM2700P and using the Fiji software (Schindelin et al., 2012).

Schizosphaerella specimens were measured taking into account the maximum diameter of the valve (Fig. 4), similarly to Mattioli & Pittet (2002). Nannoliths of *N. steinmannii* are shaped like an elongated frustum of cone, and measured parameters include the maximum width (base width), the minimum width (top width) and the height (Fig. 4). In addition, the volume of each specimen was calculated. Coccoliths of *B. constans* are elliptical in shape, consequently length and width were measured for individual specimens (Fig. 4).

NANNOFOSSIL ABUNDANCE AND SIZE CHANGES ACROSS OAES

Previous papers documented variations in calcareous nannofloral assemblage composition related to palaeotemperature and palaeofertility fluctuations and nannofossil indices were reconstructed for the intervals prior to, during and after OAES recorded in Italian sections (Erba, 2004; Bottini et al., 2015; Casellato & Erba, 2015; Bottini & Erba, 2018). In this chapter we synthesise and discuss the changes in calcareous nannofossil abundance and coccolith/nannolith size as potential proxies of bioalcalification adjustments under altered oceanic carbonate chemistry. Data are presented in stratigraphic order from the oldest to the youngest OAE.

The Toarcian T-OAE

A total of nine Italian pelagic sections cover the T-OAE (Fig. 5): the Val Ceppelline, Colle di Sogno and Brasa sections in the Lombardy Basin, the Dogna section in the Belluno Basin, the Valdorbia, Colle d'Orlando, Pozzale, Somma and Fonte Cerro sections in the Umbria-Marche Basin. Six out of the nine sections were investigated for carbon isotope chemostratigraphy, while for three sections the identification of the stratigraphic position of the T-OAE was based on biostratigraphy. As summarised in Tab. 1, a limited amount of papers documents the occurrence of the Toarcian C isotopic anomaly in Italian sections. In particular, it is important to stress that for the Val Ceppelline and Colle di Sogno sections nothing was published in recent years, as the only C isotopic data were presented by Jenkyns & Clayton (1986). The Dogna (Jenkyns et al., 2001) and Valdorbia (Sabatino et al., 2009) sections undoubtedly represent to date the best available Italian record, with a high-resolution comparable to

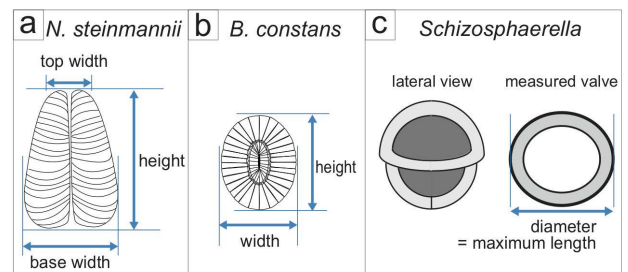


Fig. 4 - Measured parameters of selected nannofossil taxa: a) *Nannoconus steinmannii*; b) *Biscutum constans* and c) *Schizosphaerella*.

ITALIAN PELAGIC SECTIONS WITH NANNOFOSSIL AND CARBON ISOTOPIC DATA FOR WEISSERT-OAE

n.	Locality	Reference	Nannofossils	$\delta^{13}C$
2.	Pusiano (Lombardy Basin, northwestern Italy)	Channell et al., 1993	•	•
4.	Rio Corna (Lombardy Basin, northwestern Italy)	Lini et al., 1992		•
5.	Capriolo (Lombardy Basin, northwestern Italy)	Lini et al., 1992		•
6.	Polaveno (Lombardy Basin, northwestern Italy)	Lini et al., 1992		•
		Bersezio et al., 2002	•	
		Erba & Tremolada, 2004	•	
		This work	•	
9.	Valle Aviana (Trento Plateau, northeastern Italy)	Lini et al., 1992		•
13.	Val del Mis (Belluno Basin, northeastern Italy)	Channell et al., 1993		•
19.	Chiaserna Monte Acuto (Umbria-Marche, central Italy)	Sprovieri et al., 2006		•
32.	S'Ozzastru (Sardinia, Italy)	Bottini et al., 2018		•

Tab. 2 - Compilation of papers documenting quantitative nannofossil and carbon isotope data for the Weissert-OAE interval.

modern standards. We highlight that for the Brasa section in the Lombardy Basin and the Colle d'Orlando and Fonte Cerro sections in the Umbria-Marche Basin, no carbon isotopic data were published.

Quantitative and semiquantitative nannofossil data are available for the Colle di Sogno (Casellato & Erba, 2015), Brasa (Cobianchi & Picotti, 2001), Colle d'Orlando,

Pozzale, Somma and Fonte Cerro sections (Bucefalo Palliani et al., 1998; Mattioli & Pittet, 2004) (Fig. 5). Morphometric analyses of *Schizosphaerella* are available for the Somma section (Mattioli et al., 2004b, 2009) and were obtained for the Sogno Core (this study) drilled at Colle di Sogno. Quantitative analyses of *Schizosphaerella punctulata* Deflandre & Dangeard, 1938 and *Mitrolithus*

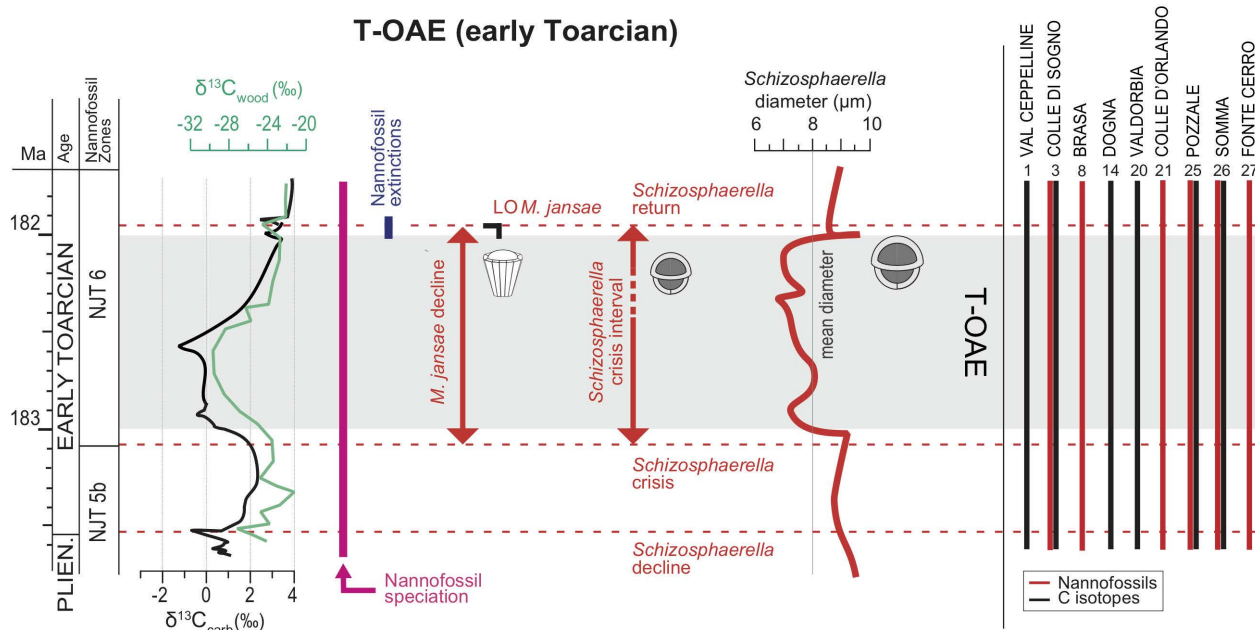


Fig. 5 - On the left: synthesis of calcareous nannofossil changes through the Toarcian-OAE (ca. 183 Ma). Nannofossil origination and extinction intervals are reported as pink and blue bars, respectively. The *Schizosphaerella* and *M. jansae* variations in abundance and the diameter of *Schizosphaerella* (three point moving average of the diameter) are reported (this study). On the right: the stratigraphic extent of published (semi)quantitative nannofossil data (red bar) and available inorganic and/or organic stable carbon isotope record (black bar) is reported for each section. Section numbering as in Fig. 3. The T-OAE is indicated with a grey band. The time scale is after Gradstein et al. (2012). Carbon isotope curve is modified after Hesselbo et al. (2007), Peniche section (Portugal).

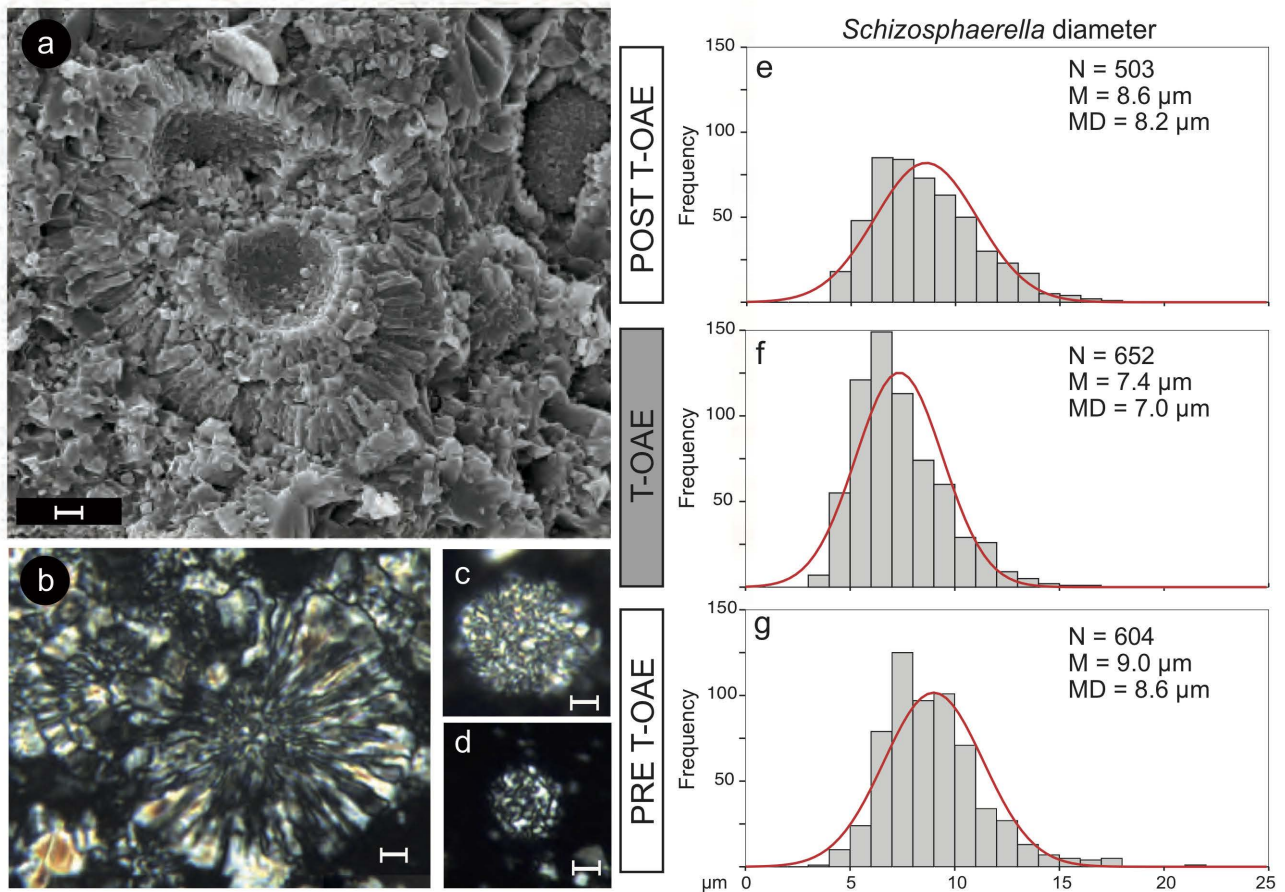


Fig. 6 - a-d) Images of *Schizosphaerella* from the Colle di Sogno section (after Casellato & Erba, 2015); scale bar = 2µm. a) Scanning electron microscope of a *Schizosphaerella*-micrite from the uppermost Domaro Limestone. b) Light polarising microscope image of a cluster of *Schizosphaerella* from the uppermost Domaro Limestone. c) Light polarising microscope image of *S. punctulata* from the topmost Domaro Limestone. d) Light polarising microscope image of "small *S. punctulata*" from the lowermost Sogno Formation. e-g) Results of mixture analysis of samples with estimated mean diameter (M), median diameter (MD) and number of specimens analysed (N) subdivided in three intervals: e) pre- T-OAE, f) T-OAE and g) post - T-OAE, analysed in the Colle di Sogno section and Sogno Core (this study).

jansae (Wiegand, 1984) identified changes in abundance of these taxa across the T-OAE (Casellato & Erba, 2015). After a period of stability and oligotrophy dominated by the rock-forming deep-dwellers (Fig. 5), enhanced nutrient availability under increased run-off, possibly induced the "*Schizosphaerella* decline" close to the Pliensbachian/Toarcian boundary, also accompanied by a marked decrease in abundance of *M. jansae* and an increase in abundance of *Biscutum* and *Lotharingius* (Casellato & Erba, 2015). Just before the onset of T-OAE, a further drop in abundance is shown by both *Schizosphaerella* and *M. jansae*, with the exclusion of "encrusted *S. punctulata*" and the survival of "thin *M. jansae*" (Casellato & Erba, 2015). In the Fish Level both *S. punctulata* and *M. jansae* drop in abundance while small coccoliths show an increase in abundance that, however, contributed very little to calcite production, justifying the low carbonate content of the T-OAE black shales at Colle di Sogno (Casellato & Erba, 2015). In the interval above the Fish Level, nannofossils are mostly represented by small taxa with some contribution by *S. punctulata*, while *M. jansae* barely survived the palaeoenvironmental stress and disappeared soon after the T-OAE termination (Fig. 5). Indeed, after the end of anoxia, palaeoceanographic conditions in the

photic zone resumed gradually to a pre-perturbation state, as suggested by calcareous nannofloral assemblages (Casellato & Erba, 2015).

The "*Schizosphaerella* crisis" is evidenced by its drastic reduction in abundance just prior to the T-OAE black shale interval and represents the temporary breakdown of such a rock-forming taxon (Erba, 2004; Tremolada et al., 2005). Similar and coeval decreases in abundance of *S. punctulata* - and in general in nannofossil total abundances - are reported from Portugal (Mattioli et al., 2008), Spain (Fraguas et al., 2012), and France (Hermoso et al., 2012), pointing to a major shift in nannofloral assemblages at supra-regional scale.

The T-OAE perturbation also affected the biomineralisation of *Schizosphaerella*, which shows reduced sizes as documented in the Somma section (Mattioli & Pittet, 2002; Mattioli et al., 2004b, 2009). Fig. 6 illustrates the size changes measured in the Sogno Core (this study) for the interval preceding the T-OAE, within the T-OAE and in samples from the overlying interval. Both the mean and median diameter values decrease in the black shale interval, further evidencing - contemporaneously to the abundance drop - reduced calcification of *Schizosphaerella*. Such decrease in size

was also documented in Italy for the Somma section (Mattioli et al., 2004b, 2009), in France (Clemence et al., 2015), Spain (Reolid et al., 2014), and Portugal (Suan et al., 2008, 2010).

The nannoplankton patterns described above for Italian pelagic sections confirm general trends documented elsewhere, indicating stepped palaeoenvironmental perturbations culminating into the T-OAE. The extreme conditions resulting from combined warming, ocean fertilisation and possibly acidification contributed to the establishment of very stressing surface waters with dominance of opportunistic taxa. Ocean acidification might have reached threshold values at the onset of the T-OAE inducing the “*Schizosphaerella* crisis”, the drop in abundance of *M. jansae* and the temporary size reduction in *Schizosphaerella*.

Environmental stress started to affect the ocean structure, fertility and chemistry at least one million years before the T-OAE, close to the Pliensbachian/Toarcian boundary, that was a time of accelerated nannoplankton speciation, a most spectacular case for calcareous nannoplankton evolution within the Mesozoic (Bown et al., 2004; Erba, 2006). Data from Italian pelagic sections support the interpretation of the T-OAE as a nutrification episode combined with some ocean acidification exerting a direct control on phytoplankton type and abundance, and influencing species-specific biocalcification.

The late Valanginian Weissert-OAE

Eight sections covering the Weissert-OAE were analysed for C isotopic chemostratigraphy (Fig. 7). In particular, five sections were studied in the Lombardy Basin (Pusiano, Rio Corna, Capriolo, Polaveno) and on the Trento Plateau (Valle Aviana section) while the Valle del Mis and Chiaserna sections are located in the Belluno and Umbria-Marche Basins, respectively. Finally, we also

considered here the S’Ozzastru section in Sardinia, which consists of relatively shallow-water sediments deposited during flooding of a carbonate ramp. Two major papers published in the nineties still represent the sole reference of the Weissert-OAE in Italy (Lini et al., 1992; Channell et al., 1993). However, recent works at the Chiaserna (Sprovieri et al., 2006) and S’Ozzastru sections (Bottini et al., 2018) document with new data the occurrence of the Weissert carbon isotopic anomaly. It should be noticed that not all of these outcrops cover the entire OAE: the Val del Mis section records just the descending trend of the event after the C-isotope anomaly, and the S’Ozzastru section covers the initial increase of the carbon isotopic excursion (Fig. 7).

Calcareous nannofossil absolute abundances were quantified only for the Polaveno section (Erba & Tremolada, 2004), but semiquantitative data are also available for the Pusiano section (Channell et al., 1993). The Weissert-OAE interval is marked by a decline in abundance of all nannoconids, called “nannoconid decline” (sensu Channell et al., 1993), whose onset correlates with magnetochron CM12 and predates the positive $\delta^{13}C$ excursion. Nannoconid abundance resumes during the C-isotope recovery starting within magnetochron CM10N. The “nannoconid decline” interval is also characterised by higher abundance of *Diazomatolithus* throughout the entire Weissert-OAE interval. Absolute abundances of *Diazomatolithus* (Erba & Tremolada, 2004) show a symmetric increase and decrease specular to the relative decrease and increase in abundance of nannoconids. In Italian pelagic sections, the onset of the “nannoconid decline” is also marked by a peak in abundance of pentaliths (Bersezio et al., 2002; Erba & Tremolada, 2004) (Fig. 7).

The “nannoconid decline” depicted in the Tethyan sections (Channell et al., 1993; Bersezio et al., 2002;

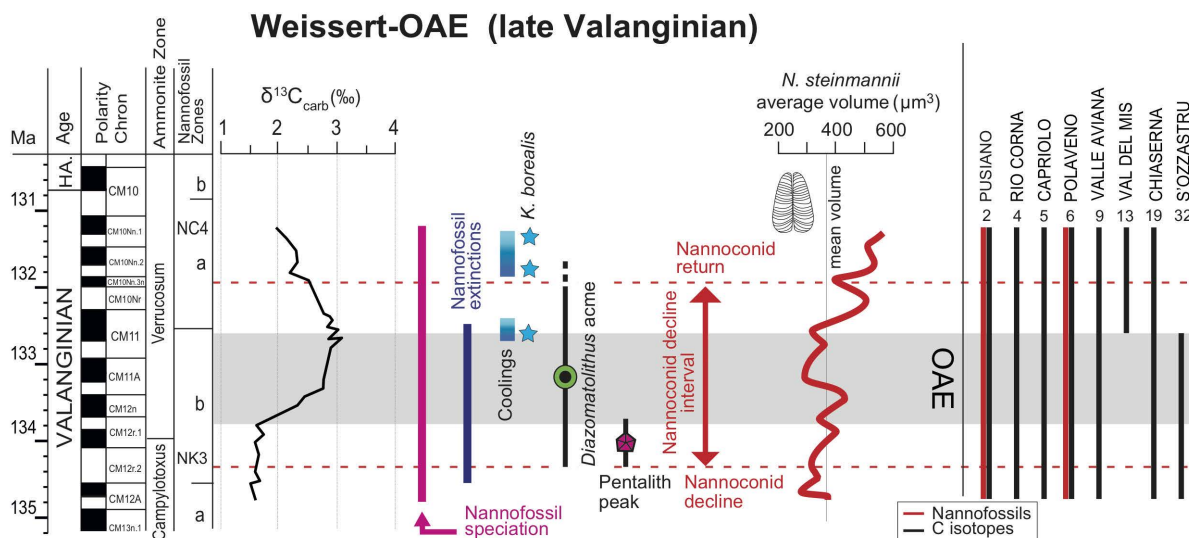


Fig. 7 - On the left: synthesis of calcareous nannofossil changes through the Weissert-OAE (ca. 134 Ma). Nannofossil origination and extinction intervals are reported as pink and blue bars, respectively. The nannoconid variations in abundance (Erba & Tremolada, 2004) and the volume of *N. steinmannii* (three point moving average of the volume, this study) are reported. The extent of the *Diazomatolithus* acme, the pentalith abundance peak and the presence of *Kokia borealis* are also represented (Bersezio et al., 2002; Erba & Tremolada, 2004). On the right: the stratigraphic extent of published (semi)quantitative nannofossil data (red bar) and available inorganic and/or organic stable carbon isotope record (black bar) is reported for each section. Section numbering as in Fig. 3. The Weissert-OAE is indicated with a grey band. The time scale is from Channell et al. (1995). Carbon isotope curve is modified after Channell et al. (1993) (Capriolo section).

Erba & Tremolada, 2004; Bottini et al., 2018) has been later documented as a global shift in the composition of nannofloral assemblages (Erba et al., 2004; Bornemann & Mutterlose, 2008; Greselle et al., 2011; Barbarin et al., 2012; Duchamp-Alphonse et al., 2014; Mattioli et al., 2014).

Morphometric analyses of *N. steinmannii* were performed for the Polaveno section (Fig. 8) to test a possible size reduction associated to the “nannoconid decline”. Collected data show that the base width and the height fluctuate independently ($R^2 = 0.31$), but that the volume is highly correlated with the base width ($R^2 = 0.81$) and to a minor extent with the height ($R^2 = 0.66$). In Fig. 7, we illustrate the volume fluctuations as the three-point moving average of the volume curve. Average volume values of ca. $300 \mu\text{m}^3$ are recorded in the interval preceding the Weissert-OAE and a moderate increase is observed at the onset of the OAE, followed by a decrease (to ca. $250 \mu\text{m}^3$) in correspondence of the climax of the $\delta^{13}\text{C}$ excursion. The interval following the Weissert-OAE is marked by a large increase in the average volume (to ca. $500 \mu\text{m}^3$) during the recovery phase. The size variations of *N. steinmannii* do not show any correspondence with fluctuations in nannoconid total abundance, indicating that these two parameters were independent and that the factor/s that caused the “nannoconid decline” did not affect the size of *N. steinmannii*, although larger specimens are observed in the recovery phase of the C-isotope curve at supraregional scale (Barbarin et al., 2012; this study).

The Italian pelagic record of the Weissert-OAE shows changes in nannofossil abundance and composition that have been also documented in France (Barbarin et al., 2012; Duchamp et al., 2014), in the Atlantic (Bornemann & Mutterlose, 2008) and in the Pacific (Erba et al., 2004) Oceans, thus demonstrating the supra-regional nature of the nannoplankton response. The Weissert-OAE differs from other Cretaceous OAEs since it was characterised by relatively cooler conditions, as for example documented by the occurrence of the nannofossil boreal species *Kokia borealis* Perch-Nielsen, 1988 at low latitudes in Romania (Melinte & Mutterlose, 2001) and in the tropical Pacific Ocean (Erba et al., 2004). Therefore, the palaeoenvironmental perturbations across the Weissert-OAE cannot be ascribed to global warming. The biocalcification crisis expressed by the “nannoconid decline” has been linked to excess CO_2 and concurrent higher fertility (Bersezio et al., 2002; Erba & Tremolada, 2004; Erba et al., 2004; Weissert & Erba, 2004). Although ocean acidification as the triggering factor of the major decrease in abundance of the heavily calcified nannoconids has been disputed (Duchamp-Alphonse et al., 2007, 2014; Barbarin et al., 2012), there is a general consensus on the

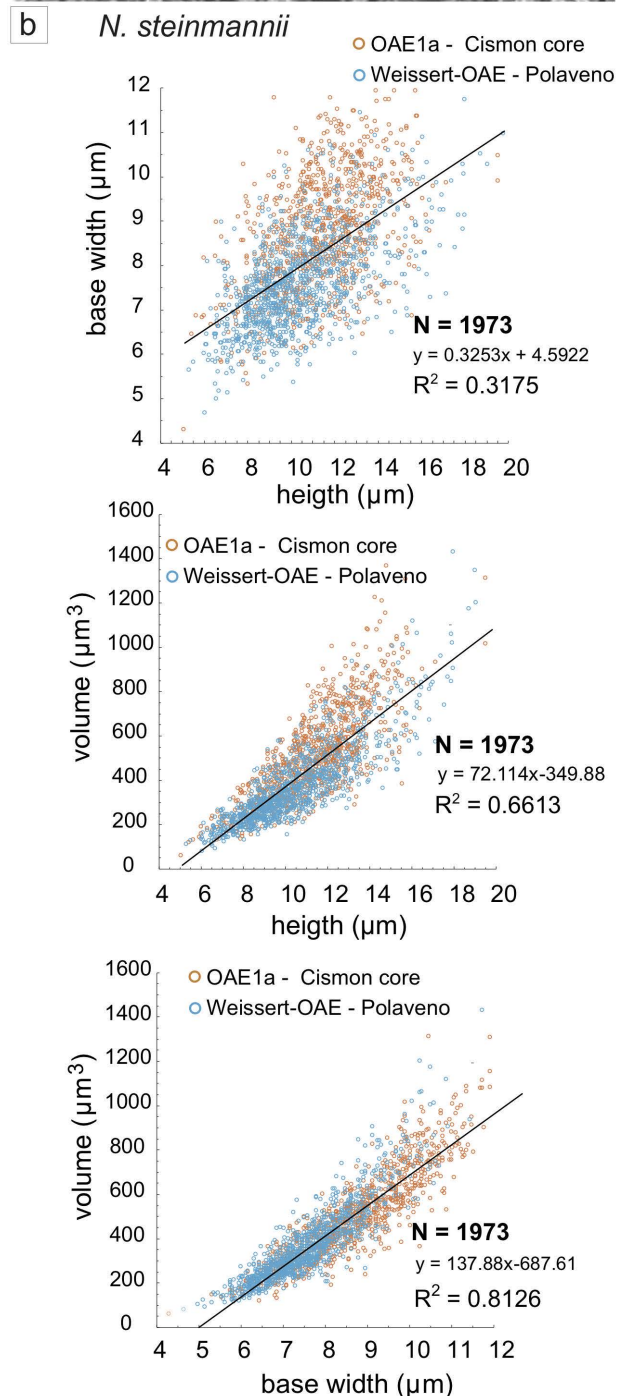
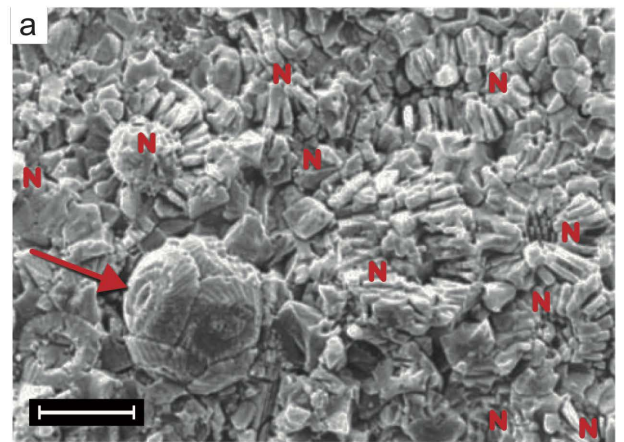


Fig. 8 - a) Scanning electron microscope image of a nannoconid-micrite from the Maiolica limestone of the Gorgo a Cerbara section. Nannoconids are marked by “N”, on the left side, indicated by the arrow, there is a coccosphere of *Watznaueria barnesiae* (Black in Black & Barnes, 1959) (after Erba, 1994); scale bar = $10 \mu\text{m}$. b) Scatter plots of *N. steinmannii* base width, height and volume with Pearson correlation coefficient (r) and the number of measurements (N). Blue circles refer to the Polaveno section (Valanginian Weissert-OAE), orange circles refer to the Cison Core (early Aptian OAE1a).

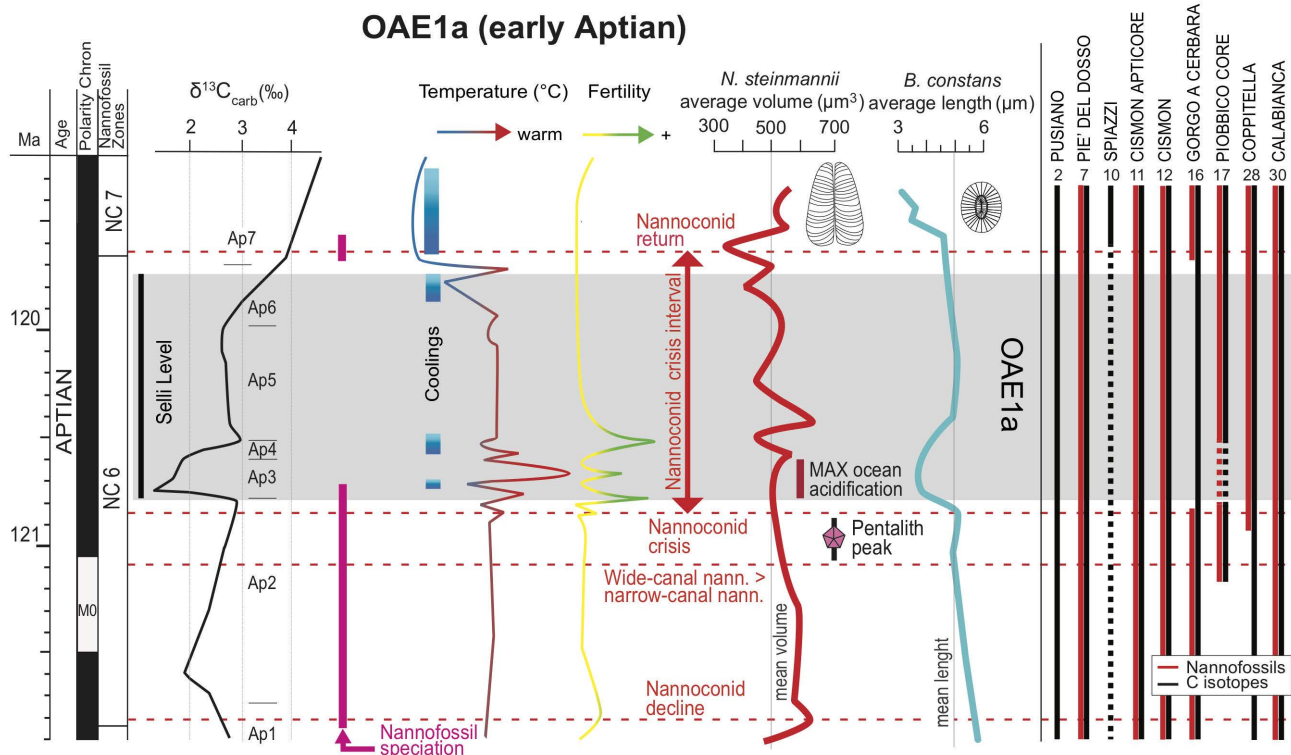


Fig. 9 - On the left: synthesis of calcareous nannofossil changes through the early Aptian OAE1a (ca. 120 Ma). Nannofossil origination intervals are reported as pink bars. The nannoconid variations in abundance (Erba & Tremolada, 2004; Bottini et al., 2015), the volume of *N. steinmannii* (three point moving average of the volume, this study) and the length of *B. constans* (three point moving average of the length; Erba et al., 2010) are reported. The pentalith abundance peak is also represented (Erba & Tremolada, 2004). Nannofossil-based temperature and nutrient indices are after Bottini et al. (2015). On the right: the stratigraphic extent of published (semi)quantitative nannofossil data (red bar) and available inorganic and/or organic stable carbon isotope record (black bar) is reported for each section. The occurrence of a hiatus is indicated with a dashed line. Section numbering as in Fig. 3. The OAE1a is indicated with a grey band. The time scale is from Malinverno et al. (2010, 2012). Carbon isotope curve is modified after Bottini et al. (2015), Cismón Core (Italy). Identification of segments of the carbon isotopic anomaly across OAE1a follows Bottini et al. (2015).

role of enhanced fertility (Bersezio et al., 2002; Erba et al., 2004; Duchamp-Alphonse et al., 2007, 2014; Bornemann & Mutterlose, 2008; Barbarin et al., 2012).

The early Aptian OAE1a

Nine Italian sections record the occurrence of OAE1a as traced by carbon isotope data (Fig. 9). In particular, the Pusiano and Piè del Dosso sections in the Lombardy Basin, the Spiazzi section on the Trento Plateau, the Cismón Core and outcrop in the Belluno Basin, the Gorgo a Cerbara section and the Piobbico Core in the Umbria-Marche Basin, the Coppitella section in Gargano (Puglia, southern Italy) and the Calabianca section in Sicily. The Cismón APTICORE is the most studied record for OAE1a in Italy (Tab. 3). In fact, following the first work of Erba et al. (1999), a large amount of published literature has continuously extended and/or refined the C_{carb} and C_{org} chemostratigraphy, highlighting the importance of this core as a fundamental reference for the OAE1a interval. The distribution of the various sections allows for comparisons of the occurrence and extent of OAE1a in different basins. However, it must be noticed that not all the published records are complete, in particular the Spiazzi section documents only a small portion of the event, as it preserves just the uppermost part of the carbon isotopic anomaly, while a hiatus corresponds to the Ap3

and Ap4 intervals of the carbon excursion in the Piobbico Core (Bottini et al., 2015).

Quantitative abundance data of nannofossil assemblages of the upper Barremian-lower Aptian are available for the Piè del Dosso, Cismón outcrop and Core, Gorgo a Cerbara, Piobbico Core, Coppitella and Calabianca (Erba, 1994; Luciani et al., 2001; Bellanca et al., 2002; Erba & Tremolada, 2004; Bottini et al., 2015). Slightly before the onset of OAE1a, the “nannoconid crisis” documents a major decrease of nannofossil calcite production. It represents the culmination of a trend initiated close to the Barremian/Aptian boundary with the “nannoconid decline” associated with the appearance of small taxa. Together these changes seem to testify the response of calcareous nannoplankton to increased CO_2 and metal enrichment (Erba et al., 2015). The “nannoconid crisis” corresponds to a more severe biocalcification failure, with a drop in pelagic biogenic calcite production of ~80% under excess CO_2 , enhanced nutrient availability, global warming and possibly ocean acidification (Erba et al., 2010). Despite the major temporary crisis during OAE1a, the nannoconids were able to survive, presumably in sufficiently shielded ecological niches, and to partially recover to pre-crisis abundance and palaeofluxes when palaeoenvironmental conditions ameliorated (Erba et al., 2015).

ITALIAN PELAGIC SECTIONS WITH NANNOFOSSIL AND CARBON ISOTOPIC DATA FOR OAE1a				
n.	Locality	Reference	Nannofossils	$\delta^{13}\text{C}$
2.	Pusiano (Lombardy Basin, northeastern Italy)	Keller et al., 2011		•
7.	Piè del Dosso (Lombardy Basin, northeastern Italy)	Erba, 1994	•	
		Giorgioni et al., 2015		•
10.	Spiazzi (Trento Plateau, northeastern Italy)	Weissert et al., 1985		•
11.	Cismon APTICORE (Belluno Basin, northeastern Italy)	Premoli Silva et al., 1999	•	
		Erba et al., 1999		•
		Tremolada & Erba, 2002	•	
		van Breugel et al., 2007		•
		Erba & Tremolada, 2004	•	
		Mehay et al., 2009	•	•
		Erba et al., 2010	•	•
		Giorgioni et al., 2015		•
		Bottini et al., 2015	•	
		This work	•	
12.	Cismon (Belluno Basin, northeastern Italy)	Weissert et al., 1985		•
		Erba, 1994	•	
		Menegatti et al., 1998		•
16.	Gorgo a Cerbara (Umbria-Marche, central Italy)	Coccioni et al., 1992	•	
		Erba, 1994	•	
		Erbacher et al., 1996		•
		Tejada et al., 2009		•
		Stein et al., 2011		•
17.	Piobbico Core (Umbria-Marche, central Italy)	Premoli Silva et al., 1989	•	
		Erba, 1994	•	
		Erba et al., 2015		•
		Bottini et al., 2015	•	
28.	Coppitella (Gargano, southern Italy)	Luciani et al., 2001	•	•
30.	Calabianca (Sicily, southern Italy)	Bellanca et al., 2002	•	•

Tab. 3 - Compilation of papers documenting quantitative nannofossil and carbon isotope data for the OAE1a interval.

Morphometric data of *B. constans*, obtained for the uppermost Barremian through Cenomanian interval of Italian sections (Erba et al., 2010; Faucher et al., 2017; this work), show that coccolith length and width are directly correlated ($R^2 = 0.80$) (Fig. 10), thus we only comment the fluctuations of the mean length, reported as the three-point moving average of the mean length curve. In the Cismon Core the coccolith length/width Pearson correlation is very high ($R^2 = 0.90$); *B. constans* shows a marked reduction in size in correspondence of the onset of the OAE1a and minimum average size (ca. 3 μm) was reached in the core of the negative $\delta^{13}\text{C}$ segment Ap3 (Fig. 9). The mean *B.*

constans length increases across segments Ap4 to Ap6 and remains relatively stable up to the end of OAE1a. A minor decrease in the average coccolith size is detected in segment Ap7.

Morphometric analyses of *N. steinmannii* performed in the Cismon Core (this study) highlight rather stable sizes through OAE1a. As for the Weissert-OAE, the base width and height are not correlated but there is a correlation between the base width and the height with the volume (Fig. 8). The average volume is above 500 μm^3 prior to OAE1a and shows a minor decrease during the event. The only interval characterised by relatively smaller specimens

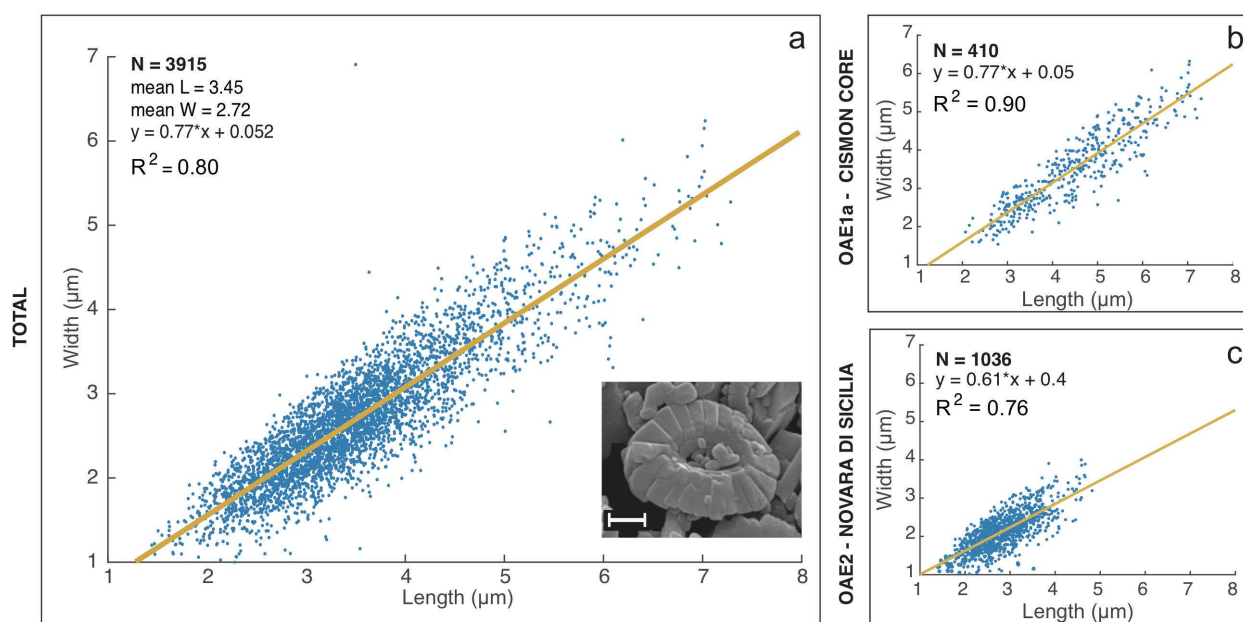


Fig. 10 - Scatter plots of *B. constans* length and width with Pearson correlation coefficient (r) and the number of measurements (N). a) Scatter plots of *B. constans* length and width measured in uppermost Barremian-Cenomanian Italian sections (Erba et al., 2010; Faucher et al., 2017; this work); scale bar = 1 μ m. b) Scatter plots of *B. constans* length and width measured across the early Aptian OAE1a in the Cismone Core (Erba et al., 2010). c) Scatter plots of *B. constans* across the Cenomanian/Turonian OAE2 from Novara di Sicilia section (Faucher et al., 2017).

(average volume comprised between 300 and 400 mm^3) coincides with the end of OAE1a (segments Ap6-base Ap7) (Fig. 9) which is followed by an interval of increased sizes during $\delta^{13}\text{C}$ segment Ap7 (Fig. 9). The average volume of *N. steinmannii* in the early Aptian (500 mm^3) is relatively higher compared to the Weissert-OAE (380 mm^3). But, similarly to the Valanginian Weissert-OAE, the *N. steinmannii* mean size does not show correlation with the nannoconid total abundance. In the specific case of OAE1a, the volume fluctuations of *N. steinmannii* do not follow the size variations displayed by *B. constans* coccoliths.

The latest Barremian “nannoconid decline” and early Aptian “nannoconid crisis” have been documented at global scale (Erba, 1994, 2004; Erba et al., 2015) and are interpreted as the result of concurrent higher fertility and excess CO_2 that would have negatively affected the biocalcification process in calcareous nannoplankton (Erba & Tremolada, 2004; Erba et al., 2010, 2015). The coincidence of the “nannoconid decline” and “nannoconid crisis” with trace metal enrichments was further explained by hydrothermal activity releasing large quantities of biolimiting and/or toxic trace elements (Erba et al., 2015). The maximum perturbation was reached in the core of the negative $\delta^{13}\text{C}$ anomaly, when the highest temperatures, highest surface water fertility, the maximum ocean acidification and the maximum reduction of coccolith size occurred. The nannoconids responded to these perturbations with a severe reduction in the total abundance, but not with significant size variations.

The latest Cenomanian OAE2

Ten sections reporting the carbon isotope excursion for the OAE2 in Italy are described in the literature (Fig. 11). Most sections are located in the Umbria-

Marche Basin (Furlo, Gorgo a Cerbara, Monte Petrano, Bottaccione, Contessa sections, and Gubbio S2 Core), but other outcrops document the OAE2 positive C-isotope excursion in the Belluno Basin (Cismone section) and in Sicily (Novara di Sicilia, Calabianca and Guidaloca sections). Among all, the Bottaccione area represents a cornerstone for OAE2 C-isotope chemostratigraphy in Italy (Tab. 4). In fact, following the seminal work of Scholle & Arthur (1980), many papers in the past 40 years have continuously documented the occurrence of the $\delta^{13}\text{C}$ positive anomaly characterising OAE2 in the Gubbio succession. Even if the Umbria-Marche Basin remains a key-area for the stratigraphy of OAE2, recent advances in the $\delta^{13}\text{C}$ chemostratigraphy (Gambacorta et al., 2015, 2016), suggest that in the Furlo, Contessa-Gubbio S2 Core, Monte Petrano and Gorgo a Cerbara sections a regional hiatus elides most of the C-isotope anomaly, namely the “plateau”, the “c” peak and the first part of the recovery. Therefore, the OAE2 stratigraphic record in these sections was proved incomplete (Fig. 11). In Sicily, just the Calabianca section contains the entire $\delta^{13}\text{C}$ excursion, as the Novara di Sicilia and Guidaloca sections cover only the lower and uppermost part of the event, respectively.

Quantitative analyses of calcareous nannofloras are scanty for Italian sections, because the Bonarelli Level is typically barren of calcareous nannofossils. Changes in abundance across OAE2 were obtained for the Bottaccione section (Erba, 2004) and morphometric data were documented by Faucher et al. (2017) for the Novara di Sicilia section. In addition, quantitative nannofossil data are available for the intervals below and above the Bonarelli Level of the Furlo and Monte Petrano sections. The absence or extremely rareness of calcareous nannofossils across the OAE2 black shales of the Bonarelli Level is attributed to extreme acidification

ITALIAN PELAGIC SECTIONS WITH NANNOFOSSIL AND CARBON ISOTOPIC DATA FOR OAE2			
n.	Locality	Reference	$\delta^{13}\text{C}$
12.	Cismon (Belluno Basin, northeastern Italy)	Gambacorta et al., 2015	•
15.	Furlo (Umbria-Marche, central Italy)	Mort et al., 2007 Jenkyns et al., 2007 Gambacorta et al., 2015 Bottini & Erba, 2018	• • • •
16.	Gorgo a Cerbara (Umbria-Marche, central Italy)	Kuroda et al., 2007	•
18.	Monte Petrano (Umbria-Marche, central Italy)	Erbacher et al., 1996 Gambacorta et al., 2015 Bottini & Erba, 2018	• • •
22.	Bottaccione Gorge (Umbria-Marche, central Italy)	Scholle & Arthur, 1980 Renard, 1986 Arthur et al., 1988 Corfield et al., 1991 Erba, 1994 Jenkyns et al., 1994 Scopelliti et al., 2008 Sprovieri et al., 2013	• • • • • • • •
23.	Gubbio - S2 Core (Umbria-Marche, central Italy)	Tsikos et al., 2004	•
24.	Contessa (Umbria-Marche, central Italy)	Stoll & Schrag, 2000	•
29.	Novara di Sicilia (northwestern Sicily, southern Italy)	Scopelliti et al., 2008 Faucher et al., 2017	• •
30.	Calabianca (northwestern Sicily, southern Italy)	Scopelliti et al., 2004 Scopelliti et al., 2008	• •
31.	Guidaloca (northwestern Sicily, southern Italy)	Scopelliti et al., 2004	•

Tab. 4 - Compilation of papers documenting quantitative nannofossil and carbon isotope data for the OAE2 interval.

conditions (Erba, 2004). A drop in nannofossil abundance and species richness has been documented worldwide (Nederbragt & Fiorentino, 1999; Hardas & Mutterlose, 2007; Linnert et al., 2010, 2011; Corbett & Watkins, 2013) and interpreted as the result of eutrophic conditions, perhaps combined with trace metal enrichments in surface water. These factors of palaeoenvironmental stress could have favored phytoplanktonic group other than calcareous nannoplankton (Erba, 2004; Lignum et al., 2007; Linnert et al., 2010; Faucher et al., 2017). Indeed, *Biscutum* is interpreted as a higher fertility taxon, but its drop in abundance might be evidence of trophic conditions above threshold values for calcareous nannoplankton during OAE2 (Erba, 2004).

Morphometric data of *B. constans* across the latest Cenomanian OAE2 in the Novara di Sicilia section, integrated with those gathered for the Eastbourne section (Faucher et al., 2017), are represented in Fig. 11. Coccoliths of *B. constans* show significant variations in

size as traced by length and width. These two parameters are directly correlated ($R^2 = 0.76$) (Fig. 10), thus we only comment the fluctuations of the mean length, as represented in the smoothed curve of Fig. 11. At the OAE2 onset, *B. constans* shows a first decrease in size, followed by an increase of coccolith size in $\delta^{13}\text{C}$ peak "a". A further size decrease culminates with dwarfism around $\delta^{13}\text{C}$ peak "b", where the smallest coccoliths are recorded (ca. 1.5 mm). Similar and coeval trends have been documented in a variety of settings as a biocalcification response to palaeoenvironmental global stress. However, at Novara di Sicilia, *B. constans* coccoliths have the most reduced sizes compared to other sections: this seems to depict a trend of declining average coccolith size with decreasing latitude (Faucher et al., 2017).

Fluctuations of calcareous nannofossil abundance and size of selected taxa across the latest Cenomanian OAE2 are interpreted as caused by global warming, interrupted by the cooling interlude of the Plenus Cold

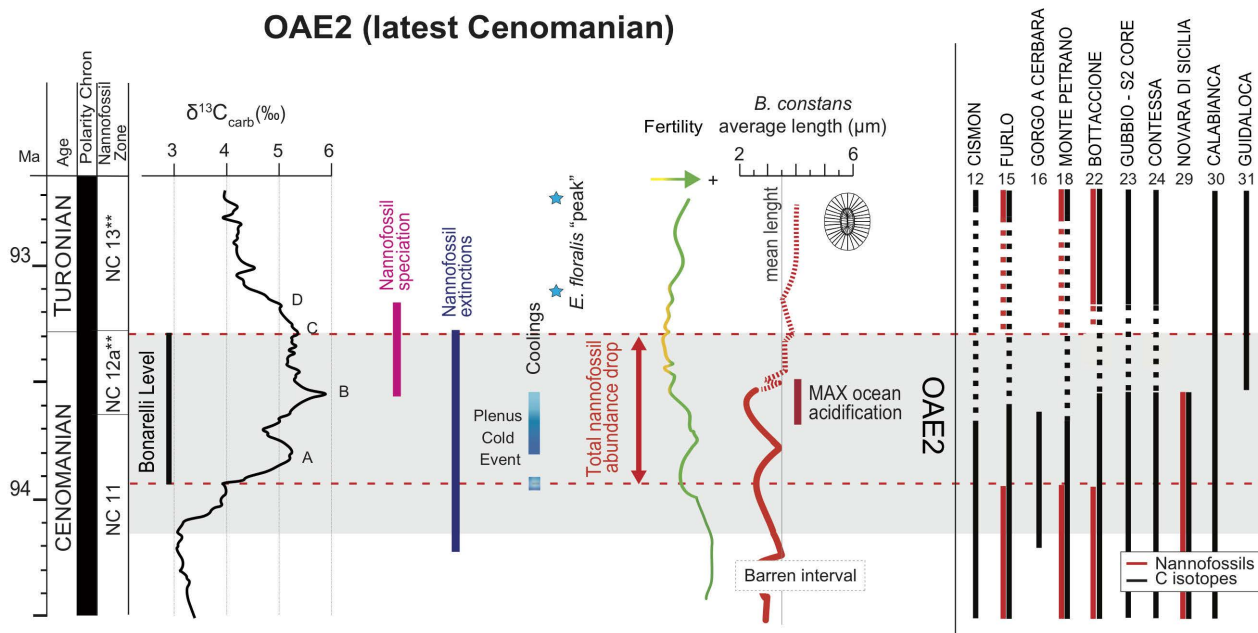


Fig. 11 - On the left: synthesis of calcareous nannofossil changes through the latest Cenomanian OAE2 (ca. 94 Ma). Nannofossil origination and extinction intervals are reported as pink and blue bars, respectively. The total nannofossil abundance variations (from Gubbio section, Erba, 2004) and the length of *B. constans* (three point moving average of the mean length, Faucher et al., 2017) are reported. Nannofossil based-nutrient index and peaks of *Eprolithus floralis* (Stradner, 1962) are from Erba (2004). Cooling intervals are from Jenkyns et al. (2017). On the right: the stratigraphic extent of published (semi)quantitative nannofossil data (red bar) and available inorganic and/or organic stable carbon isotope record (black bar) is reported for each section. The occurrence of a hiatus is indicated with a dashed line. Considering the proximity of the sites, we assume an extent of the hiatus for the Contessa and Bottaccione Gorge sections equal to that observed in the Gubbio S2 Core. Section numbering as in Fig. 3. The OAE2 is indicated with a grey band. The time scale is modified after Gradstein et al. (2012). Carbon isotope curve is modified after Tsikos et al. (2004), Eastbourne section (UK). Identification of individual peaks of the carbon isotopic anomaly across OAE2 follows Voigt et al. (2007).

Event (Gale & Christensen, 1996; Gale et al., 2019), changes in ocean fertility and chemistry. The short return to larger *B. constans* coccoliths around $\delta^{13}\text{C}$ peak "a" occurs in the Plenus Cold Event: a cool-water preference was implied for *B. constans* (Lees et al., 2005) and may explain its increase in size during the cooling interval. The subsequent *B. constans* dwarfism correlates with the maximum ocean perturbation with metal enrichments, temperature rise and probably ocean acidification due to excess CO_2 (Erba, 2004; Snow et al., 2005; Jarvis et al., 2011; Du Vivier et al., 2015; Faucher et al., 2017). Only a partial return to pre-OAE2 sizes was observed in *B. constans* coccoliths during the C-isotope recovery phase following $\delta^{13}\text{C}$ peak "d", suggesting the persistence of stressing conditions in the earliest Turonian.

CONCLUDING REMARKS

Our synthesis points out that Italian pelagic sections are key to quantify changes in calcareous nannoplankton during times of highly perturbed conditions associated with OAEs, as evidenced by $\delta^{13}\text{C}$ anomalies testifying discrete global alterations of the C cycle. Indeed, in addition to extreme climatic conditions and oceanic fertilisation, OAEs were also times of altered chemistry making calcification difficult. It is possible that volcanically driven excess CO_2 in the ocean/atmosphere system (Jenkyns, 2010) induced ocean acidification (Erba et al., 2010) and caused crises of the dominant rock-forming

calcareous nannoplankton forms. This seems the case for the "*Schizosphaerella* crisis", the "nannoconid decline" and the "nannoconid crisis" during the early Toarcian T-OAE, the late Valanginian Weissert-OAE and the early Aptian OAE1a, respectively. An even more dramatic drop in nannofossil abundance characterises the latest Cenomanian OAE2, marked by a widespread biocalcification failure of calcareous nannoplankton taxa.

In addition to major changes in nannofossil abundance, a species-specific decrease in size has been detected for most OAEs, specifically for *Schizosphaerella* across the T-OAE and *B. constans* in the interval of maximum perturbation of both OAE1a and OAE2. Size of *N. steimannii*, instead, does not show significant variations across the Weissert-OAE and OAE1a. We underline that none of the taxa experiencing a calcification crisis and/or showing a size decrease got extinct: they recovered when the palaeoenvironment returned to a pre-perturbation state, although the calcareous nannoplankton return to normal conditions occurred much slower than their response to environmental stress at the beginning of the OAE disturbance. After the T-OAE and OAE1a, schizosphaerellids and nannoconids resumed in abundance, although nannofossil assemblages changed to a different composition. This was also due to originations of new species starting some one million years before the onset of the T-OAE and OAE1a and continuing through the events (Figs 5 and 9), indicating that some calcareous nannoplankton taxa could overcome the stressing phase, perhaps by resorting to innovative pathways of

calcification. These speciation episodes developed quickly, at an average rate of one first occurrence every 100–200 k years, with no accompanying increase in extinction rate, suggesting resilience of this phytoplankton group.

The Italian pelagic record shows that the response of calcareous nannoplankton to palaeoenvironmental perturbations of the Weissert-OAE and OAE2 was significantly different. The Valanginian “nannoconid decline” was gradual and less pronounced, as it was the recovery phase, while in the late Cenomanian the dramatic reduction in nannofossil total abundance is as sudden as the recovery after OAE2. As far as nannoplankton evolutionary patterns and rates are concerned, the response to the Weissert-OAE and OAE2 was different between the two events and also with respect to the T-OAE and OAE1a. During the late Valanginian-early Hauterivian (Fig. 7), a few first occurrences followed each other slowly, about one every million years. Across OAE2, instead, extinctions occurred with a rate of one every 100–200 k years at the onset or at the end of the event, while some originations are recorded from the middle part of OAE2 and continued afterwards (Fig. 11).

In conclusion, OAEs perturbations are fully recorded in pelagic micrites by shifts in abundance of calcareous nannofossils and specifically of rock-forming taxa. The same taxa partly and gradually resumed when palaeoecosystem conditions ameliorated. Changes in biocalcification are further documented by species-specific reduction in size under maximum stress during OAEs. The role of palaeoenvironmental pressure on calcareous nannoplankton evolution during the early Toarcian T-OAE, late Valanginian Weissert-OAE, early Aptian OAE1a and latest Cenomanian OAE2, if any, was not univocal, but in general resulted in the origination of new taxa.

ACKNOWLEDGEMENTS

We thank our Colleagues that contributed with thoughtful discussions to the comprehension of Jurassic and Cretaceous OAEs, particularly J.E.T. Channell, H. Jenkyns, I. Premoli Silva, and H. Weissert: with them we shared field work, especially in Italy, and scientific debates. M. Parente and I. Premoli Silva provided insightful reviews complementing the Editors’ criticism. This synthesis benefitted, at various stages, of the financial support by MIUR-PRIN2011(2010X3PP8J) awarded to E.E. and SIR-2014 (MIUR-Scientific Independence of young Researchers) to C.B.

REFERENCES

- Abramovich S., Keller G., Stüben D. & Berner Z. (2003). Characterization of late Campanian and Maastrichtian planktonic foraminiferal depth habitats and vital activities based on stable isotopes. *Palaeogeography, Palaeoclimatology, Palaeoecology*, 202: 1–29.
- Arthur M.A., Dean W.E. & Pratt L.M. (1988). Geochemical and climatic effects of increased marine organic carbon burial at the Cenomanian/Turonian boundary. *Nature*, 335: 714–717.
- Arthur M.A., Jenkyns H.C., Brumsack H.-J. & Schlanger S.O. (1990). Stratigraphy, geochemistry, and paleoceanography of organic-carbon-rich Cretaceous sequences. In Ginsburg R.N. & Beaudoin B. (eds), *Cretaceous Resources, Events and Rhythms*, NATO ASI Series, 304: 75–119.
- Arthur M.A. & Schlanger S.O. (1979). Cretaceous “oceanic anoxic events” as causal factors in development of reef-reservoired giant oil fields. *AAPG Bulletin*, 63: 870–885.
- Barbarin N., Bonin A., Mattioli E., Pucéat E., Cappetta H., Gréselle B., Pittet B., Vennin E. & Joachimski M. (2012). Evidence for a complex Valanginian nannoconid decline in the Vocontian basin (South East France). *Marine Micropaleontology*, 84: 37–53.
- Bellanca A., Erba E., Neri R., Premoli Silva I., Sprovieri M., Tremolada F. & Verga D. (2002). Paleocyanographic significance of the Tethyan “Livello Selli” (Early Aptian) from the Hybla Formation, northwestern Sicily: biostratigraphy and high-resolution chemostratigraphic records. *Palaeogeography, Palaeoclimatology, Palaeoecology*, 185: 175–196.
- Bersezio R., Erba E., Gorza M. & Riva A. (2002). Berriasian-Aptian black shales of the Maiolica Formation (Lombardian Basin, Southern Alps, northern Italy): Local to global events: *Palaeogeography, Palaeoclimatology, Palaeoecology*, 180: 253–275.
- Black M. & Barnes B. (1959). The structure of Coccoliths from the English Chalk. *Geological Magazine*, 96: 321–328.
- Bornemann A. & Mutterlose J. (2008). Calcareous nannofossil and $\delta^{13}\text{C}$ records from the Early Cretaceous of the Western Atlantic Ocean: evidence for enhanced fertilization across the Berriasian-Valanginian transition. *Palaios*, 23: 821–832.
- Bottini C., Dieni I., Erba E. & Massari F. (2018). The Valanginian Weissert Oceanic Anoxic Event Recorded in Central-Eastern Sardinia (Italy). *Rivista Italiana di Paleontologia e Stratigrafia*, 124: 617–637.
- Bottini C. & Erba E. (2018). Mid-Cretaceous paleoenvironmental changes in the western Tethys. *Climate of the Past*, 14: 1147–1163.
- Bottini C., Erba E., Tiraboschi D., Jenkyns H.C., Schouten S. & Sinninghe Damsté J.S. (2015). Climate variability and ocean fertility during the Aptian Stage. *Climate of the Past*, 11: 383–402.
- Bown P.R., Lees J.A. & Young J.R. (2004). Calcareous nannoplankton evolution and diversity through time. In Winter A. & Siesser W.G. (eds), *Coccolithophores*: 481–508.
- Breheret I.G. (1983). Sur des niveaux de black shales dans l’Albien inférieur et moyen du domaine vocontien (sud-est de la France): étude de nanofacies et signification des palaeoenvironnements. *Bulletin du Muséum National d’Histoire Naturelle, Paris*, 5: 113–159.
- Bucefalo Palliani R., Cirilli S. & Mattioli E. (1998). Phytoplankton response and geochemical evidence of the lower Toarcian relative sea level rise in the Umbria-Marche basin (Central Italy). *Palaeogeography, Palaeoclimatology, Palaeoecology*, 142: 33–50.
- Casellato C.E. & Erba E. (2015). Calcareous nannofossil biostratigraphy and paleoceanography of the Toarcian Oceanic Anoxic Event at Colle di Sogno section (Southern Alps, Italy). *Rivista Italiana di Paleontologia e Stratigrafia*, 105: 343–376.
- Channell J.E.T., Erba E. & Lini A. (1993). Magnetostratigraphic calibration of the Late Valanginian carbon isotope event in pelagic limestones from Northern Italy and Switzerland. *Earth Planetary Science Letters*, 118: 145–166.
- Channell J.E.T., Erba E., Nakanishi M. & Tamaki K. (1995). Late Jurassic–Early Cretaceous time scales and oceanic magnetic anomaly block models. In Berggren W.A. et al. (eds), *Geochronology, time scales and global stratigraphic correlation. SEPM (Society for Sedimentary Geology) Special Publication*, 54: 51–63.
- Claps M., Erba E., Masetti D. & Melchiorri F. (1995). Milankovitch-type cycles recorded in Toarcian black shales from the Belluno Trough (Southern Alps, Italy). *Memorie di Scienze Geologiche*, 47: 179–188.
- Clémence M.E., Gardin S. & Bartolini A. (2015). New insights in the pattern and timing of the Early Jurassic calcareous nannofossil crisis. *Palaeogeography, Palaeoclimatology, Palaeoecology*, 427: 100–108.

- Cobianchi M. & Picotti V. (2001). Sedimentary and biological response to sea-level and palaeoceanographic changes of a Lower-Middle Jurassic Tethyan platform margin (Southern Alps, Italy). *Palaeogeography, Palaeoclimatology, Palaeoecology*, 169: 219-244.
- Coccioni R., Erba E. & Premoli Silva I. (1992). Barremian–Aptian calcareous plankton biostratigraphy from the Gorgo a Cerbara section (Marche, Central Italy) and implications for plankton evolution. *Cretaceous Research*, 13: 517-537.
- Coccioni R., Nesci O., Tramontana M., Wezel F.C. & Moretti E. (1987). Descrizione di un livello-guida “radiolaritico-bituminoso-ittiolitico” alla base delle Marne a Fucoidi nell’Appennino Umbro-Marchigiano. *Bollettino della Società Geologica Italiana*, 106: 183-192.
- Corbett M.J. & Watkins D.K. (2013). Calcareous nannofossil paleoecology of the mid-Cretaceous Western Interior Seaway and evidence of oligotrophic surface waters during OAE2. *Palaeogeography, Palaeoclimatology, Palaeoecology*, 392: 510-523.
- Corfield R.M., Cartlidge J.E., Premoli-Silva I. & Housley R.A. (1991). Oxygen and carbon isotope stratigraphy of the Palaeogene and Cretaceous limestones in the Bottaccione Gorge and the Contessa Highway sections, Umbria, Italy. *Terra Nova*, 3: 414-422.
- Dal Piaz G. (1907). Le Alpi Feltrine. *Memorie del Reale Istituto Veneto di Scienze Lettere ed Arti*, 27: 1-176.
- Deflandre G. & Dangeard L. (1938). *Schizosphaerella*, un nouveau microfossile méconnu du Jurassique moyen et supérieur. *Comptes Rendus (Hebdomadaires des Séances) de l’Académie des Sciences Paris*, 207: 1115-1117.
- Dromart G., Garcia J.-P., Gaumet F., Picard S., Rousseau M., Atrops F., Lecuyer C. & Sheppard S.M.F. (2003). Perturbation of the carbon cycle at the Middle/Late Jurassic transition: geological and geochemical evidence. *American Journal of Science*, 303: 667-707.
- Du Vivier A.D., Jacobson A.D., Lehn G.O., Selby D., Hurtgen M.T. & Sageman B.B. (2015). Ca isotope stratigraphy across the Cenomanian–Turonian OAE 2: links between volcanism, seawater geochemistry, and the carbonate fractionation factor. *Earth and Planetary Science Letters*, 416: 121-131.
- Duchamp-Alphonse S., Gardin S. & Bartolini A. (2014). Calcareous nannofossil response to the Weissert episode (Early Cretaceous): Implications for palaeoecological and palaeoceanographic reconstructions. *Marine Micropaleontology*, 113: 65-78.
- Duchamp-Alphonse S., Gardin S., Fiet N., Bartolini A., Blamart D. & Pagel M. (2007). Fertilization of the northwestern Tethys (Vocontian basin, SE France) during the Valanginian carbon isotope perturbation: evidence from calcareous nannofossils and trace element data. *Palaeogeography, Palaeoclimatology, Palaeoecology*, 243: 132-151.
- Erba E. (1994). Nannofossils and superplumes: the early Aptian nannoconid crisis. *Paleoceanography*, 9: 483-501.
- Erba E. (2004). Calcareous nannofossils and Mesozoic oceanic anoxic events. *Marine Micropaleontology*, 52: 85-106.
- Erba E. (2006). The first 150 million years history of calcareous nannoplankton: biosphere–geosphere interactions. *Palaeogeography, Palaeoclimatology, Palaeoecology*, 232: 237-250.
- Erba E., Bartolini A. & Larson R.L. (2004). Valanginian Weissert oceanic anoxic event. *Geology*, 32: 149-152.
- Erba E., Bottini C., Weissert H.J. & Keller C.E. (2010). Calcareous nannoplankton response to surface-water acidification around Oceanic Anoxic Event 1a. *Science*, 329: 428-432.
- Erba E., Channell J.E.T., Claps M., Jones C., Larson R.L., Opdyke B., Premoli Silva I., Riva A., Salvini G. & Torricelli S. (1999). Integrated stratigraphy of the Cismon Apticore (Southern Alps, Italy): A “reference section” for the Barremian–Aptian interval at low latitudes. *Journal of Foraminiferal Research*, 29: 371-391.
- Erba E., Duncan R.A., Bottini C., Tiraboschi D., Weissert H., Jenkyns H.C. & Malinverno A. (2015). Environmental consequences of Ontong Java Plateau and Kerguelen Plateau volcanism. *Geological Society of America Special Papers*, 511: 271-303.
- Erba E. & Tremolada F. (2004). Nannofossil carbonate fluxes during the Early Cretaceous: phytoplankton response to nutrification episodes, atmospheric CO₂ and anoxia. *Paleoceanography*, 19: 1-18.
- Erbacher J., Thurow J. & Littke R. (1996). Evolution patterns of radiolaria and organic matter variations: A new approach to identify sea-level changes in mid-Cretaceous pelagic environments. *Geology*, 24: 499-502.
- Farinacci A. (1964). Microrganismi dei calcari ‘Maiolica’ e ‘Scaglia’ osservati al microscopio elettronico (nannoconi e coccolithophoridi). *Bollettino della Società Paleontologica Italiana*, 3: 172-181.
- Faucher G., Erba E., Bottini C. & Gambacorta G. (2017). Calcareous nannoplankton response to the latest Cenomanian Oceanic Anoxic Event 2 perturbation. *Rivista Italiana di Paleontologia e Stratigrafia*, 123: 159-176.
- Fraguas Á., Comas-Rengifo M.J., Gómez J.J. & Goy A. (2012). The calcareous nannofossil crisis in Northern Spain (Asturias province) linked to the Early Toarcian warming-driven mass extinction. *Marine Micropaleontology*, 94: 58-71.
- Gaetani M. & Poliani G. (1978). Il Toarciano ed il Giurassico medio in Albenza. *Rivista Italiana di Paleontologia e Stratigrafia*, 91: 295-320.
- Gale A.S. & Christensen W.K. (1996). Occurrence of the belemnite *Actinocamax plenus* in the Cenomanian of SE France and its significance. *Bulletin of the Geological Society of Denmark*, 43: 68-77.
- Gale A.S., Jenkyns H.C., Tsikos H., van Breugel Y., Sinnighe Damste J.S., Bottini C., Erba E., Russo F., Falzoni F., Petrizzo M.R., Dickson A.J. & Wray D.S. (2019). High-resolution bio- and chemostratigraphy of an expanded record of Oceanic Anoxic Event 2 (Late Cenomanian–Early Turonian) at Clot Chevalier, near Barrême, SE France (Vocontian Basin, SE France). *Newsletters on Stratigraphy*, 52: 97-129.
- Gambacorta G., Bersezio R., Weissert H. & Erba E. (2016). Onset and demise of Cretaceous oceanic anoxic events: The coupling of surface and bottom oceanic processes in two pelagic basins of the western Tethys. *Paleoceanography*, 31: 732-757.
- Gambacorta G., Jenkyns H.C., Russo F., Tsikos H., Wilson P.A., Faucher G. & Erba E. (2015). Carbon- and oxygen-isotope records of mid-Cretaceous Tethyan pelagic sequences from the Umbria-Marche and Belluno Basins (Italy). *Newsletters on Stratigraphy*, 48: 299-323.
- Giorgioni M., Keller C.E., Weissert H., Hochuli P.A. & Bernasconi S.M. (2015). Black shales—from coolhouse to greenhouse (early Aptian). *Cretaceous Research*, 56: 716-731.
- Górka H. (1957). Les Coccolithophoridés du Maestrichtien supérieur de Pologne. *Acta Palaeontologica Polonica*, 2: 239-284.
- Gradstein F.M., Ogg J.G., Schmitz M.D. & Ogg G.M. (2012). The Geologic Time Scale 2012. 1176 pp. Elsevier B.V., Amsterdam.
- Gréselle B., Pittet B., Mattioli E., Joachimski M., Barbarin N., Riquier L., Reboulet S. & Pucéat E. (2011). The Valanginian isotope event: a complex suite of palaeoenvironmental perturbations. *Palaeogeography, Palaeoclimatology, Palaeoecology*, 306: 41-57.
- Hardas P. & Mutterlose J. (2007). Calcareous nannofossil assemblages of Oceanic Anoxic Event 2 in the equatorial Atlantic: Evidence of an eutrophication event. *Marine Micropaleontology*, 66: 52-69.
- Hermoso M., Minoletti F., Rickaby R.E., Hesselbo S.P., Baudin F. & Jenkyns H.C. (2012). Dynamics of a stepped carbon isotope excursion: Ultra high-resolution study of Early Toarcian environmental change. *Earth and Planetary Science Letters*, 319: 45-54.
- Hesselbo S.P., Gröcke D., Jenkyns H.C., Bjerrum C.J., Farrimond P., Bell H.S.M. & Green O.R. (2000). Massive dissociation of gas hydrate during a Jurassic oceanic anoxic event. *Nature*, 406: 392-395.

- Hesselbo S.P., Jenkyns H.C., Duarte L.V. & Oliveira L.C.V. (2007). Carbon-isotope record of the Early Jurassic (Toarcian) Oceanic Anoxic Event from fossil wood and marine carbonate (Lusitanian Basin, Portugal). *Earth and Planetary Science Letters*, 253: 455-470.
- Jarvis I., Gale A.S., Jenkyns H.C. & Pearce M.A. (2006). Secular variation in Late Cretaceous carbon isotopes: a new $\delta^{13}\text{C}$ carbonate reference curve for the Cenomanian–Campanian (99.6–70.6 Ma). *Geological Magazine*, 143: 561-608.
- Jarvis I., Lignum J.S., Gröcke D.R., Jenkyns H.C. & Pearce M.A. (2011). Black shale deposition, atmospheric CO_2 drawdown, and cooling during the Cenomanian–Turonian Oceanic Anoxic Event. *Paleoceanography*, 26: PA3201.
- Jarvis I., Mabrouk A., Moody R.T.J. & Cabrera S.D. (2002). Late Cretaceous (Campanian) carbon isotope events, sea-level change and correlation of the Tethyan and Boreal realms. *Palaeogeography, Palaeoclimatology, Palaeoecology*, 188: 215-248.
- Jenkyns H.C. (1980). Cretaceous anoxic events: From continents to oceans. *Journal of the Geological Society of London*, 137: 171-188.
- Jenkyns H.C. (1985). The Early Toarcian and Cenomanian–Turonian anoxic events in Europe: Comparisons and contrasts. *Geologische Rundschau*, 74: 505-518.
- Jenkyns H.C. (1988). The Early Toarcian (Jurassic) anoxic event: stratigraphic, sedimentary, and geochemical evidence. *The American Journal of Science*, 288: 101-151.
- Jenkyns H.C. (2010). Geochemistry of oceanic anoxic events. *Geochemistry, Geophysics, Geosystems*, 11: Q03004.
- Jenkyns H.C. & Clayton C.C. (1986). Black shales and carbon isotopes in pelagic sediments from the Tethyan Lower Jurassic. *Sedimentology*, 33: 87-106.
- Jenkyns H.C., Dickson A.J., Ruhl M. & Van den Boom S.H. (2017). Basalt-seawater interaction, the Plenius Cold Event, enhanced weathering and geochemical change: deconstructing Oceanic Anoxic Event 2 (Cenomanian–Turonian, Late Cretaceous). *Sedimentology*, 64: 16-43.
- Jenkyns H.C., Gale A.S. & Corfield R.M. (1994). Carbon- and oxygen-isotope stratigraphy of the English Chalk and Italian Scaglia and its palaeoclimatic significance. *Geological Magazine*, 131: 1-34.
- Jenkyns H.C., Gröcke D.R. & Hesselbo S.P. (2001). Nitrogen isotope evidence for water mass denitrification during the early Toarcian (Jurassic) oceanic anoxic event. *Paleoceanography*, 16: 593-603.
- Jenkyns H.C., Matthews A., Tsikos H. & Erel Y. (2007). Nitrate reduction, sulfate reduction, and sedimentary iron isotope evolution during the Cenomanian–Turonian oceanic anoxic event. *Paleoceanography*, 22: PA3208.
- Kálin O. & Bernoulli D. (1984). *Schizosphaerella* Deflandre and Dangeard in Jurassic deeper-water carbonate sediments, Mazagan Continental Margin (Hole 547b) and Mesozoic Tethys In Hinz K., Winterer E.L. et al., *Initial Reports of the Deep-Sea Drilling Project*, 79: U.S. Government Printing Office, Washington, 79: 411-435.
- Kamptner E. (1931). *Nannoconus steinmanni* nov. gen., nov. spec., ein merkwürdiges gesteinsbildendes Mikrofossil aus dem jüngeren Mesozoikum der Alpen. *Paläontologische Zeitschrift*, 13: 288-298.
- Keller C.E., Hochuli P.A., Weissert H., Bernasconi S.M., Giorgioni M. & Garcia T.I. (2011). A volcanically induced climate warming and floral change preceded the onset of OAE1a (Early Cretaceous). *Palaeogeography, Palaeoclimatology, Palaeoecology*, 305: 43-49.
- Kuroda J., Ogawa N.O., Tanimizu M., Coffin M., Tokuyama H., Kitazato H. & Ohkouchi N. (2007). Contemporaneous massive subaerial volcanism and late Cretaceous Oceanic Anoxic Event 2. *Earth and Planetary Science Letters*, 256: 211-223.
- Leckie R.M., Bralower T.J. & Cashman R. (2002). Oceanic anoxic events and plankton evolution: Biotic response to tectonic forcing during the mid-Cretaceous. *Paleoceanography*, 17: PA000623.
- Lees J.A., Bown P.R., & Mattioli E. (2005). Problems with proxies? Cautionary tales of calcareous nannofossil paleoenvironmental indicators. *Micropaleontology*, 51: 333-343.
- Lignum J., Jarvis I. & Pearce M. (2007). The dinoflagellate cyst record of the Cenomanian–Turonian boundary (OAE 2): Data from a newly cored black shale succession, Wunstorf, northern Germany. *Geophysical Research Abstracts*, 9: 3854.
- Lini A., Weissert H. & Erba E. (1992). The Valanginian carbon isotope event: a first episode of greenhouse climate conditions during the Cretaceous. *Terra Nova*: 4: 374-384.
- Linnert C., Mutterlose J. & Erbacher J. (2010). Calcareous nannofossils of the Cenomanian/Turonian boundary interval from the Boreal Realm (Wunstorf, northwest Germany). *Marine Micropaleontology*, 74: 38-58.
- Linnert C., Mutterlose J., & Mortimore R. (2011). Calcareous nannofossils from Eastbourne (southeastern England) and the paleoceanography of the Cenomanian–Turonian boundary interval. *Palaios*, 26: 298-313.
- Lohmann H. (1902). Die Coccolithophoridae, eine Monographie der Coccolithen bildenden Flagellaten, zugleich ein Beitrag zur Kenntnis des Mittelmeerauftriebs. *Archiv für Protistenkunde*, 1: 89-165.
- Luciani V., Cobianchi M. & Jenkyns H.C. (2001). Biotic and geochemical response to anoxic events: the Aptian pelagic succession of the Gargano Promontory (southern Italy). *Geological Magazine*, 138: 277-298.
- Malinverno A., Erba E. & Herbert T.D. (2010). Orbital tuning as an inverse problem: Chronology of the early Aptian oceanic anoxic event 1a (Selli Level) in the Cismonte APTICORE. *Paleoceanography*, 25: PA2203.
- Malinverno A., Hildebrandt J., Tominaga M. & Channell J.E.T. (2012). M-sequence geomagnetic polarity time scale (MHTC12) that steadies global spreading rates and incorporates astrochronology constraints. *Journal of Geophysical Research*, 117: B06104.
- Mattioli E. (1997). Nannoplankton productivity and diagenesis in the rhythmically bedded Toarcian–Aalenian Fiuminata section (Umbria–Marche Apennine, central Italy). *Palaeogeography, Palaeoclimatology, Palaeoecology*, 130: 113-133.
- Mattioli E. & Pittet B. (2002). The contribution of calcareous nannoplankton to the carbonate production in the Early Jurassic. *Marine Micropaleontology*, 45: 175-190.
- Mattioli E. & Pittet B. (2004). Spatial and temporal distribution of calcareous nannofossils along a proximal–distal transect in the Umbria–Marche basin (Lower Jurassic; Italy). *Palaeogeography, Palaeoclimatology, Palaeoecology*, 205: 295-316.
- Mattioli E., Pittet B., Bucefalo Palliani R., Röhl H.J., Schmid-Röhl A. & Moretini E. (2004b). Phytoplankton evidence for the timing and correlation of palaeoceanographical changes during the early Toarcian oceanic anoxic event (Early Jurassic). *Journal of the Geological Society*, 161: 685-693.
- Mattioli E., Pittet B., Petitpierre L. & Mailliot S. (2009). Dramatic decrease of pelagic carbonate production by nannoplankton across the early Toarcian anoxic event (T-OAE). *Global Planetary Change*, 65: 134-145.
- Mattioli E., Pittet B., Riquier L. & Grossi V. (2014). The mid-Valanginian Weissert Event as recorded by calcareous nannoplankton in the Vocontian Basin. *Palaeogeography, Palaeoclimatology, Palaeoecology*, 414: 472-485.
- Mattioli E., Pittet B., Suan G. & Mailliot S. (2008). Calcareous nannoplankton changes across the early Toarcian oceanic anoxic event in the western Tethys. *Paleoceanography and Palaeoclimatology*, 23: PA3208.
- Mattioli E., Pittet B., Young J.R. & Bown P.R. (2004a). Biometric analysis of Pliensbachian–Toarcian (Lower Jurassic) coccoliths of the family Biscutaceae: Intra- and interspecific variability versus palaeoenvironmental influence. *Marine Micropaleontology*, 52: 5-27.

- Méhay S., Keller C.E., Bernasconi S.M., Weissert H., Erba E., Bottini C. & Hochuli P.A. (2009). A volcanic CO₂ pulse triggered the Cretaceous Oceanic Anoxic Event 1a and a biocalcification crisis: *Geology*, 37: 819-822.
- Melinte M. & Mutterlose J. (2001). A Valanginian (Early Cretaceous) 'boreal nannoplankton excursion' in sections from Romania. *Marine Micropaleontology*, 43: 1-25.
- Menegatti A.P., Weissert H., Brown R.S., Tyson R.V., Farrimond P., Strasser A. & Caron M. (1998). High resolution δ¹³C stratigraphy through the early Aptian "Livello Selli" of the Alpine Tethys. *Paleoceanography*, 13: 530-545.
- Moretini E., Santantonio M., Bartolini A., Cecca F., Baumgartner P.O. & Hunziker, J.C. (2002). Carbon isotope stratigraphy and carbonate production during the Early-Middle Jurassic: examples from the Umbria-Marche-Sabina Apennines (central Italy). *Palaeogeography, Palaeoclimatology, Palaeoecology*, 184: 251-273.
- Mort H., Jacquat O., Adatte T., Steinmann P., Föllmi K., Matera V., Berner Z. & Stüben D. (2007). The Cenomanian/Turonian anoxic event at the Bonarelli level in Italy and Spain: enhanced productivity and/or better preservation? *Cretaceous Research*, 28: 597-612.
- Nederbragt A.J. & Fiorentino A. (1999). Stratigraphy and palaeoceanography of the Cenomanian-Turonian boundary event in Oued Mellegue, north-western Tunisia. *Cretaceous Research*, 20: 47-62.
- Noël D. & Busson G. (1990). L'importance des schizosphères, stomiosphères, Conusphaera et Nannoconus dans la genèse des calcaires fins pélagiques du Jurassique et du Crétacé inférieur/ Importance of schizospheres, stomiospheres, Conusphaera and Nannoconus in the genesis of Jurassic and Early Cretaceous fine-grained pelagic limestones. *Sciences Géologiques, Bulletin*, 43: 63-93.
- Perch-Nielsen K. (1988). New Lower Cretaceous calcareous nanofossil species from England. *Newsletter of the International Nannoplankton Association*, 10: 30-37.
- Peti L., Thibault N., Clémence M.E., Korte C., Dommergues J.L., Bougeault C., Pellenard P., Jelby M.E. & Ullmann C.V. (2017). Sinemurian–Pliensbachian calcareous nanofossil biostratigraphy and organic carbon isotope stratigraphy in the Paris Basin: Calibration to the ammonite biozonation of NW Europe. *Palaeogeography, Palaeoclimatology, Palaeoecology*, 468: 142-161.
- Premoli Silva I., Erba E., Salvini G., Verga D. & Locatelli C. (1999). Biotic changes in Cretaceous anoxic events. *Journal of Foraminiferal Research*, 29: 352-370.
- Premoli Silva I., Erba E. & Tornaghi M.E. (1989). Palaeoenvironmental signals and changes in surface fertility in mid Cretaceous Corg-rich pelagic facies of the Fucoid Marls (central Italy). *Geobios*, 22: 225-236.
- Renard M. (1986). Pelagic carbonate chemostratigraphy (Sr, Mg, ¹⁸O, ¹³C). *Marine Micropaleontology*, 10: 117-164.
- Reolid M., Mattioli E., Nieto L.M. & Rodríguez-Tovar F. (2014). The Early Toarcian oceanic anoxic event in the external subbetic (Southiberian Palaeomargin, Westernmost Tethys): geochemistry, nanofossils and ichnology. *Palaeogeography, Palaeoclimatology, Palaeoecology*, 411: 79-94.
- Robinson S.A., Heimhofer U., Hesselbo S.P. & Petrizzo M.R. (2017). Mesozoic climates and oceans – a tribute to Hugh Jenkyns and Helmut Weissert. *Sedimentology*, 64: 1-15.
- Sabatino N., Neri R., Bellanca A., Jenkyns H.C., Baudin F., Parisi G. & Masetti D. (2009). Carbon-isotope records of the Early Jurassic (Toarcian) oceanic anoxic event from the Valdorbica (Umbria–Marche Apennines) and Monte Mangart (Julian Alps) sections: palaeoceanographic and stratigraphic implications. *Sedimentology*, 56: 1307-1328.
- Schindelin J., Arganda-Carreras I., Frise E., Kaynig V., Longair M., Pietzsch T., Preibisch S., Rueden C., Saalfeld S., Schmid B., Tinevez J.Y., White D.J., Hartenstein V., Eliceiri K., Tomancak P. & Cardona A. (2012). Fiji: an open-source platform for biological-image analysis. *Nature Methods*, 9: 676.
- Schlanger S.O. & Jenkyns H.C. (1976). Cretaceous oceanic anoxic events: Causes and consequences. *Geologie en Mijnbouw*, 55: 179-184.
- Scholle P.A. & Arthur M.A. (1980). Carbon isotope fluctuations in Cretaceous pelagic limestones: potential stratigraphic and petroleum exploration tool. *American Association of Petroleum Geologists Bulletin*, 64: 67-87.
- Scopelliti G., Bellanca A., Coccioni R., Luciani V., Neri R., Baudin F., Chiari M. & Marcucci M. (2004). High-resolution geochemical and biotic records of the Tethyan 'Bonarelli Level' (OAE2, latest Cenomanian) from the Calabianca–Guidaloca composite section, northwestern Sicily, Italy. *Palaeogeography, Palaeoclimatology, Palaeoecology*, 208: 293-317.
- Scopelliti G., Bellanca A., Erba E., Jenkyns H.C., Neri R., Tamagnini P., Luciani V. & Masetti D. (2008). Cenomanian–Turonian carbonate and organic-carbon isotope records, biostratigraphy and provenance of a key section in NE Sicily, Italy: Palaeoceanographic and palaeogeographic implications. *Palaeogeography, Palaeoclimatology, Palaeoecology*, 265: 59-77.
- Scotese C.R. (ed.) (2014). Atlas of Plate Tectonic Reconstructions (Mollweide Projection), Volumes 1-6, *PALEOMAP Project PaleoAtlas for ArcGIS*, PALEOMAP Project, Evanston, IL.
- Snow L.J., Duncan R.A. & Bralower T.J. (2005). Trace element abundances in the Rock Canyon Anticline, Pueblo, Colorado, marine sedimentary section and their relationship to Caribbean plateau construction and oxygen anoxic event 2. *Palaeogeography*, 20: PA3005.
- Sprovieri M., Coccioni R., Lirer F., Pelosi N. & Lozar F. (2006). Orbital tuning of a lower Cretaceous composite record (Maiolica Formation, central Italy). *Palaeoceanography*, 21: PA4212.
- Sprovieri M., Sabatino N., Pelosi N., Batenburg S.J., Coccioni R., Iavarone M. & Mazzola S. (2013). Late Cretaceous orbitally-paced carbon isotope stratigraphy from the Bottaccione Gorge (Italy). *Palaeogeography, Palaeoclimatology, Palaeoecology*, 379-380: 81-94.
- Stein M., Föllmi K.B., Westermann S., Godet A., Adatte T., Matera V., Fleitmann D. & Berner Z. (2011). Progressive palaeoenvironmental change during the Late Barremian–Early Aptian as prelude to Oceanic Anoxic Event 1a: Evidence from the Gorgo a Cerbara section (Umbria-Marche basin, central Italy). *Palaeogeography, Palaeoclimatology, Palaeoecology*, 302: 396-406.
- Stoll H.M. & Schrag D.P. (2000). High-resolution stable isotope records from the Upper Cretaceous rocks of Italy and Spain: glacial episodes in a greenhouse planet? *Geological Society of America Bulletin*, 112: 308-319.
- Stradner H. (1962). Über neue und wenig bekannte Nanofossilien aus Kreide und Alttertiär. *Sonderabdruck aus den Verhandlungen der Geologischen Bundesanstalt*, 2: 363-377.
- Suan G., Mattioli E., Pittet B., Lecuyer C., Sucheras-Marx B., Duarte L.V., Philippe M., Reggiani L. & Martineau F. (2010). Secular environmental precursors to Early Toarcian (Jurassic) extreme climate changes. *Earth and Planetary Science Letters*, 290: 448-458.
- Suan G., Mattioli E., Pittet B., Maillot S. & Lécuyer C. (2008). Evidence for major environmental perturbation prior to and during the Toarcian (Early Jurassic) oceanic anoxic event from the Lusitanian Basin, Portugal. *Paleoceanography* 23: PA1202.
- Tejada M.L.G., Katsuhiko S., Kuroda J., Coccioni R., Mahoney J.J., Ohkouchi N., Sakamoto T. & Tatsumi Y. (2009). Ontong Java Plateau eruption as a trigger for the early Aptian oceanic anoxic event. *Geology*, 37: 855-858.
- Tremolada F. & Erba E. (2002). Morphometric analysis of the Aptian *Rucinolithus terebrodentarius* and *Assipetra infracretacea* nannoliths: Implications for taxonomy, biostratigraphy and Palaeoceanography. *Marine Micropaleontology*, 44: 77-92.

- Tremolada F., Van de Schootbrugge B. & Erba E. (2005). Early Jurassic schizosphaerellid crisis in Cantabria, Spain: implications for calcification rates and phytoplankton evolution across the Toarcian oceanic anoxic event. *Paleoceanography*, 20: PA2011.
- Tsikos H., Jenkyns H.C., Walsworth-Bell B., Petrizzo M.R., Forster A., Kolonic S., Erba E., Premoli Silva I., Baas M., Wagner T. & Sinninghe Damsté J.S. (2004). Carbon-isotope stratigraphy recorded by the Cenomanian–Turonian Oceanic Anoxic Event: correlation and implications based on three key localities. *Journal of the Geological Society*, London, 161: 711-719.
- van Breugel Y., Schouten S., Tsikos H., Erba E., Price G.D. & Sinninghe Damsté J.S. (2007). Synchronous negative carbon isotope shifts in marine and terrestrial biomarkers at the onset of the early Aptian oceanic anoxic event 1a: Evidence for the release of ^{13}C -depleted carbon into the atmosphere. *Paleoceanography*, 22: PA1210.
- Van de Schootbrugge B., Bailey T.R., Rosenthal Y., Katz M.E., Wright J.D., Miller K.G., Feist-Burkhardt S. & Falkowski P.G. (2005). Early Jurassic climate change and the radiation of organic-walled phytoplankton in the Tethys Ocean. *Paleobiology*, 31: 73-97.
- Voigt S., Aurag A., Leis F. & Kaplan U. (2007). Late Cenomanian to Middle Turonian high-resolution carbon isotope stratigraphy: New data from the Münsterland Cretaceous Basin, Germany. *Earth and Planetary Science Letters*, 253: 196-210.
- Weissert H. (1989). C-isotope stratigraphy, a monitor of paleoenvironmental change: a case study from the Early Cretaceous. *Surveys in Geophysics*, 10: 1-61.
- Weissert H. & Erba E. (2004). Volcanism, CO_2 and palaeoclimate: a Late Jurassic–Early Cretaceous carbon and oxygen isotope record. *Journal of the Geological Society*, 161: 695-702.
- Weissert H., Lini A., Föllmi K.B. & Kuhn O. (1998). Correlation of Early Cretaceous carbon isotope stratigraphy and platform drowning events: a possible link? *Palaeogeography, Palaeoclimatology, Palaeoecology*, 137: 189-203.
- Weissert H., McKenzie J.A. & Channell J.E.T. (1985). Natural variations in the carbon cycle during the Early Cretaceous. In Sundquist E.T. & Broecker W.S. (eds), *The Carbon Cycle and Atmospheric CO_2 : Natural variations Archean to the Present. Geophysical Monographs*, 32: 531-545.
- Wiegand G.E. (1984). Two New Genera of Calcareous Nannofossils from the Lower Jurassic. *Journal of Paleontology*, 58: 1151-1155.

Manuscript received 20 March 2019

Revised manuscript accepted 2 April 2019

Published online 30 April 2019

Guest Editors Massimo Bernardi & Giorgio Carnevale

Appendix G

Erba et al. 2019b

Coring the sedimentary expression of the early Toarcian Oceanic Anoxic Event: new stratigraphic records from the Tethys Ocean

Elisabetta ERBA, Gabriele GAMBACORTA, **Stefano VISENTIN**,
Liyenne CHAVALHEIRO, Dario REOLON, Giulia FAUCHER
& Matteo PEGORARO



Coring the sedimentary expression of the early Toarcian Oceanic Anoxic Event: new stratigraphic records from the Tethys Ocean

Elisabetta Erba, Gabriele Gambacorta, Stefano Visentin, Liyenne Chavalheiro, Dario Reolon, Giulia Faucher, and Matteo Pegoraro

Dipartimento di Science della Terra, Università degli Studi di Milano, Milano, Italy

Correspondence: Elisabetta Erba (elisabetta.erba@unimi.it)

Received: 14 June 2019 – Revised: 2 September 2019 – Accepted: 4 September 2019 – Published:

Abstract. **ISI** The Toarcian Oceanic Anoxic Event (T-OAE) interval was cored at Colle di Sogno and Gajum in the Lombardy Basin (Southern Alps, northern Italy). The Sogno and Gajum cores recovered 26.83 and 31.18 stratigraphic metres, respectively, of pelagic sediments consisting of marly limestones, marlstone, marly claystone, and black shale. Drilling at both sites resulted in 100 % recovery of unweathered material. The pelagic succession comprises a relatively expanded black shale interval of 4.98 m in the Sogno core and 15.35 m in the Gajum core, with lower and upper boundaries without evidence of hiatuses. The Sogno and Gajum cores can be considered reference sections for the pelagic lower Toarcian interval of the western Tethys and will provide high-resolution micropaleontological, inorganic and organic geochemical, isotopic multiproxy data. Integrated stratigraphy and cyclostratigraphy are predicted to result in estimates of durations and rates to model the ecosystem resilience to the extreme perturbations of the T-OAE and gain a better understanding of current global changes and help provide better projections of future scenarios.

1 Introduction

The emergence of climate change as a crucial issue for society has urged the understanding of the future state of the planet within the context of increasing carbon dioxide concentrations. The ocean is the oldest ecosystem and the largest on Earth by volume and best records global changes in climate and atmospheric composition. Marine ecosystems are inextricably involved in the physical, chemical, biological processes of global change. In the near future, the ocean's uptake of CO₂ is expected to rapidly decline because of surface water warming, decreasing pH (acidification), increased vertical stratification, and slowed thermohaline circulation (Solomon et al., 2009). Consequently, a very rapid “in and out” from icehouse to greenhouse state – and vice versa – urges comprehension of positive and negative feedbacks on the biosphere.

Understanding of the Earth system at timescales longer than human observations has become imperative, because anthropogenic activities are likely to increase by orders of mag-

nitude the rates of climatic change that usually result from natural processes. The Earth's ecosystems, thus, should be scrutinized on the medium- and long-term scales using geological records of past extreme environmental disturbances that exemplify varied tempos and modes of resilience, occasionally reaching tipping points that triggered permanent modifications **CEI**.

The Toarcian Oceanic Anoxic Event (T-OAE) is the oldest Mesozoic case of global anoxia with widespread deposition of organic matter-rich sediments in a variety of depositional settings from continental to shallow- and deep-marine (Jenkyns, 1985, 1988, 2010). Available evidence suggests that at ~ 183 Ma the atmosphere and oceans experienced high CO₂, possibly due to the degassing of lava fields in the Karoo–Ferrar large igneous province and/or from dissociation and oxidation of methane hydrates in continental-margin sediments (Jenkyns, 2010) and/or terrestrial environments (Them et al., 2017). High atmospheric carbon dioxide possibly initiated greenhouse conditions that accelerated

weathering and the hydrological cycle, increasing nutrient recycling into the oceans.

Although the original definition of the T-OAE was based on the presence of a lithostratigraphic marker (Jenkyns, 1985), the development of chemostratigraphy demonstrated that the T-OAE is associated with a negative C isotopic anomaly documented in marine carbonates and organic matter as well as in terrestrial organic matter including fossil wood and specific organic compounds (Jenkyns and Clayton, 1986; Hesselbo et al., 2000, 2007; Schouten et al., 2000; Jenkyns et al., 2002; Emmanuel et al., 2006; Van Breugel et al., 2006; Al-Suwaidi et al., 2010; Caruthers et al., 2011; Izumi et al., 2012; Kafousia et al., 2014; Reolid, 2014; Xu et al., 2017; Them et al., 2017; Fantasia et al., 2018). As shown by Fantasia et al. (2018), such a negative C isotopic anomaly might have resulted from volcanogenic CO₂, thermogenic methane associated with metamorphism, and dissociation of marine or terrestrial clathrates.

The T-OAE is further marked by an Os anomaly (Cohen et al., 2004; Percival et al., 2016; Them et al., 2017), biocalcification crisis (Erba, 2004; Mattioli et al., 2004; Casellato and Erba, 2015; Erba et al., 2019), increased primary productivity (Jenkyns, 2010; Erba, 2004), and ocean acidification (Erba, 2004; Trecalli et al., 2012; Casellato and Erba, 2015; Posenato et al., 2018), which occurred during an exceptional warming phase (Dera et al., 2011; Korte and Hesselbo, 2011; Gómez et al., 2016) and a major transgression (e.g. Haq et al., 1987; Hardenbol et al., 1998).

Jurassic pelagic successions in the Southern Alps have been extensively investigated for stratigraphy, sedimentology, paleontology, and geochemistry (Bernoulli and Jenkyns, 2009; Erba et al., 2019). In particular, multi- and interdisciplinary studies have demonstrated that the Jurassic pelagic successions of the Lombardy Basin represent “type-sections” of the Tethyan southern margin (Gaetani, 2010). Indeed, the Lombardy Basin is part of the relatively undeformed portion of Adria interpreted as an African “promontory” or as a microplate (Fig. 1). In the latest Triassic–earliest Jurassic a rifting phase caused the breakup of carbonate platforms into a series of “horst and graben” that exerted a physiographic control on sediment type and distribution for most of the Jurassic (Bernoulli and Jenkyns, 1974, 2009; Bosence et al., 2009; Santantonio and Carminati, 2011). As a consequence, sedimentation was differentiated with the deposition of thick complete pelagic successions in the deeper zones, while sedimentation was typically condensed and incomplete in correspondence of the structural highs.

During the Jurassic the Lombardy Basin was globally a deep area between the Lugano High to the west and the Trento Plateau to the east (Fig. 1). However, the latest Triassic–earliest Jurassic rifting disentangled a number of troughs and paleohighs that are as follows, from west to east: Monte Nudo Trough, Lugano High, Generoso Trough, Corni di Canzo High, Albenza Plateau, Monte Cavallo High, Sebino Trough, Botticino High (Gaetani, 1975, 2010). In the

troughs, partially resedimented Lower Jurassic marlstone–limestone sequences may reach a non-decompacted thickness of 3000 m (e.g. in the Generoso Trough), but condensation and hiatuses characterize the paleohigh sections with reddish nodular facies. Along slopes connecting structural highs to the troughs, sedimentation was marked by slumps, resedimented bodies, and, locally, megabreccias within condensed and occasionally incomplete facies (Gaetani and Erba, 1990; Gaetani, 2010) (Fig. 1). In addition to regional tectonics, the Lombardy Basin successions record global climatic and oceanographic changes, including the T-OAE (Erba et al., 2019). In fact, lower Toarcian black shales have been documented in various sections, offering the opportunity to investigate the consequences of the T-OAE global changes on marine biota in the Tethys Ocean (Erba et al., 2019).

After close investigations of section outcropping in the Lombardy Basin, the Colle di Sogno and Gajum sites were selected as the most promising locations for continuous coring of pelagic records (Gaetani and Erba, 1990; Casellato and Erba, 2015) for continuous coring. In this paper, we document coring operations and lithostratigraphic characterization of both the Sogno and Gajum cores and outline ongoing multidisciplinary research.

2 Coring through the sedimentary record of the early Toarcian Oceanic Anoxic Event

The T-OAE is considered a natural Earth system experiment, which allows us to (a) detect and quantify processes associated with emissions of greenhouse gases and natural atmospheric pollutants; (b) understand the role of greenhouse gases on climate dynamics and its influence on the hydrological cycle; (c) characterize changes in ocean and atmospheric chemistry and their interactions; (d) assess changes in biodiversity and dynamics of ecosystems and understand the functioning of biotic sinks; and (e) quantify biosphere–geosphere–atmosphere interactions and their timings or rates.

Analysis of past global change requires the collection of high-resolution data from continuous and ideally unweathered sequences. In surface outcrops, sedimentary rocks and particularly black shales are commonly badly degraded and, consequently, drilling is crucial to ensure the recovery of high-quality fresh cored material. In this paper we identify the T-OAE adopting the original definition by Jenkyns (1985) based on lithostratigraphy. Therefore, the T-OAE in the Lombardy Basin corresponds to the Livello a Pesci (Tintori, 1977; Gaetani and Poliani, 1978; Erba and Casellato, 2010; Erba et al., 2019). This interval has an average thickness of 0.5 to 5 m, but reaches a few tens of metres in the most expanded sections. Black shales are rarely recorded on paleohighs, whereas they are ubiquitous in deeper basins. As the T-OAE occurred at a global scale, the local lack of black shales

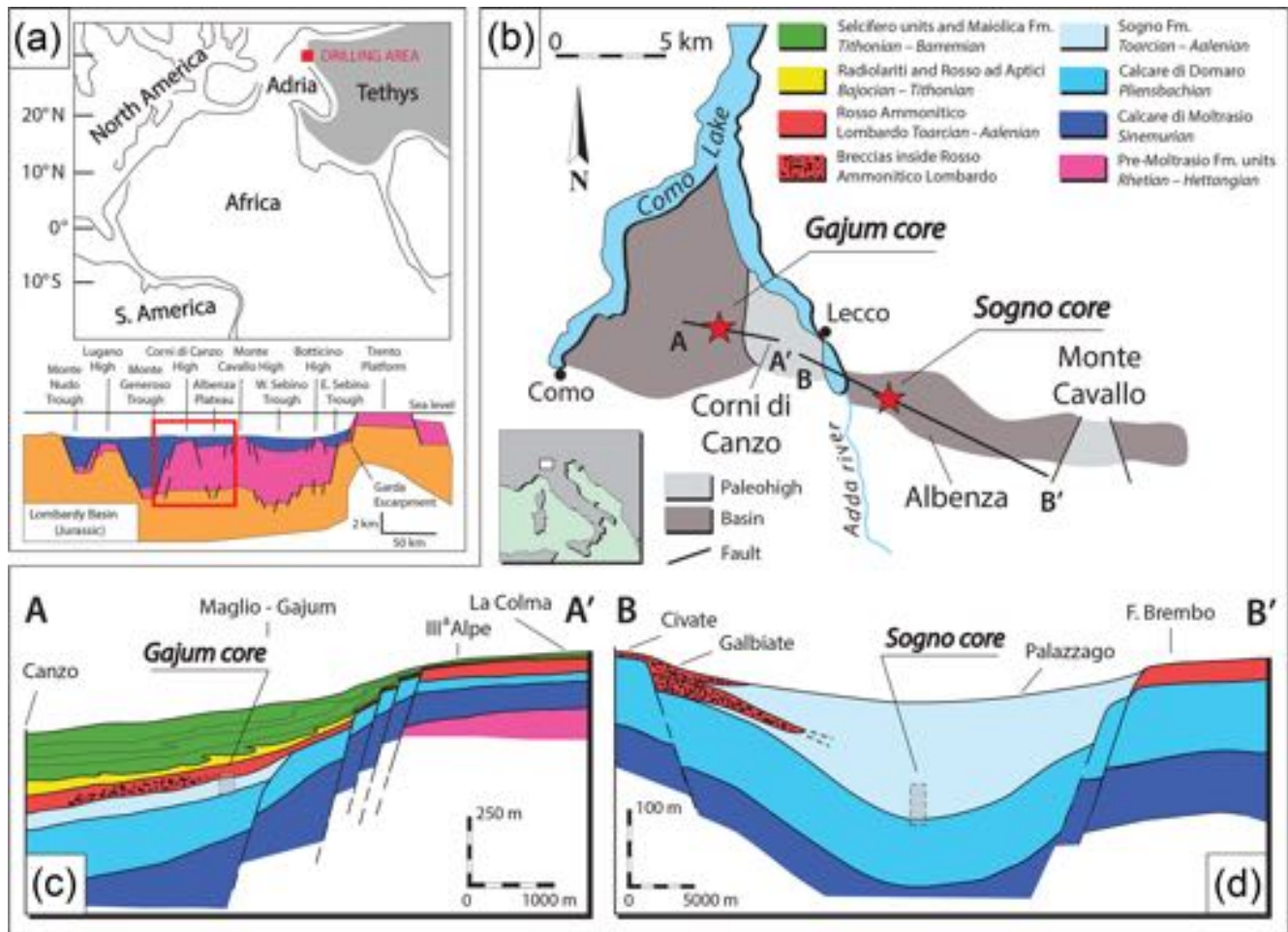


Figure 1. Location of the Sogno and Gajum drilling sites relative to (a) paleogeography and (b) current geography. The drilling area was part of the Lombardy Basin (Southern Alps). (c) The Gajum core is sited in an inner basin along the western slope of the Corni di Canzo High while (d) the Sogno core was drilled on the Albenza Plateau as detailed in the geological sections in the lower part of the figure (modified after Gaetani and Poliani, 1978 and Gaetani and Erba, 1990).

in the Lombardy Basin is usually the result of condensation and/or stratigraphic gaps.

Location of the drill sites and justification for coring

TS2 Two Lower Jurassic sections at Colle di Sogno and Gajum, respectively, were selected for continuous coring through the Toarcian organic-rich black shale interval (Fig. 1). Within the Lombardy Basin, these sections represent significantly different geological settings on a pelagic structural high, namely the Albenza Plateau (Colle di Sogno) and in an inner basin along the slope of the Mt Corni di Canzo structural high (Gajum) (Gaetani and Erba, 1990; Gaetani, 2010). Both successions are relatively expanded and lack the diagenetic manganese–carbonate horizons (present in the Toarcian black shales of the Belluno Basin, Southern Alps, for example) that would compromise primary geochemical

signatures (Farrimond et al., 1988; Jenkyns, 1988; Jenkyns et al., 1991; Bellanca et al., 1999).

The Colle di Sogno site (Fig. 1) was selected because the Jurassic sequence exposed is pelagic, stratigraphically continuous and relatively expanded (Gaetani and Erba, 1990; Muttoni et al., 2005; Channell et al., 2010; Casellato and Erba, 2015). It consists of limestone and marlstone, with chert and marly claystone as minor lithologies. The T-OAE is here represented by ~ 5 m of dark grey to black marly claystones of the Livello a Pesci. At Colle di Sogno, the type-section of the Sogno Formation (Gaetani and Poliani, 1978), located along the road SP 179 on the northern slope of Mt Brughetto, was proved to be suitable for high-resolution multidisciplinary studies of litho-, bio-, chemo-, magneto-, and cyclo-stratigraphy (Gaetani and Poliani, 1978; Jenkyns and Clayton, 1986; Gaetani and Erba, 1990; Hinnov et al., 2000; Channell et al., 2010; Casellato and Erba, 2015).

The Gajum succession crops out in a small lateral cut of the Ravella valley (Fig. 1), where the basal lithofacies of the Moltrasio Limestone Formation suggests sedimentation in shallower water than on the Albenza Plateau (Gaetani and Poliani, 1978; Gaetani and Erba, 1990; Pasquini and Vercesi, 2002). In particular, slumps and resedimented bodies with an eastward-sliding direction document a constant instability of the ramp, indicating that the succession developed in a small inner basin separated by a sill from a deeper basin to W (CE7) (Pasquini and Vercesi, 2002). A sharp lithological change marks the boundary between the carbonate-rich lithologies of the Domaro Limestone Formation and the overlying clay-rich lithologies of the lower Sogno Formation consisting of marlstones and marly limestones followed by reddish nodular limestones of the Rosso Ammonitico Lombardo. At Gajum the expanded nature of the black shale interval (~ 15 m) offers the opportunity for studying the inception, evolution, and termination of the T-OAE in great detail.

3 Drilling operations and lab core preparation

The Sogno drilling campaign took place in June 2013, while the Gajum core was drilled in February 2016 (Fig. 2). At both Sogno and Gajum sites, drilling operations were performed with the DELTABASE 520 Modular Hydraulic Rotary Drill. The Sogno coring was accomplished with a T2 double corer, using narrow-kerf, sawtoothed drill bits that cut a 101 mm diameter borehole and 84 mm diameter cores. The Gajum core was obtained using a modified T6 triplex corer, including a plastic liner for the best recovery, using narrow-kerf, sawtoothed drill bits that cut a 131 mm diameter borehole and 101 mm diameter cores. At Gajum, after coring, the borehole was logged using a QL40-OBI optical televiewer to obtain high-resolution images of the borehole wall, together with a total gamma radiation tool (Fig. 3).

All cores were initially described on site and a preliminary log was produced. Then, cores were packed, labelled, and put in PVC plastic boxes to prevent contamination and transported to the Department of Earth Sciences in Milan where they are archived. Here, during lab preparation, all cores were longitudinally split along the dip and divided into an archive half and a sampling half, both marked at centimetre scale. The archive half was photographed in high resolution and composite photologs were produced for each site.

4 Preliminary results

4.1 Lithostratigraphy of the Sogno core

Four distinct boreholes (S1, S2, S3, and S4) were drilled at Colle di Sogno along the SP 179 road (45°47'20.5" N, 9°28'30.0" E). The outcropping beds show a strike of 150° and a dip of 68° to the southwest (240°).

Initially, a single borehole was planned to penetrate the lower Toarcian–uppermost Pliensbachian interval and reach

the base of the Sogno Formation at ~ 35 m penetration depth. However, at ~ 25 m penetration depth (core S1-27) a sharp dip increase to 88° revealed the occurrence of a fold, partially faulted and reversed, persisting for ~ 4 m (cores S1-27, S1-28, and S1-29). Indeed, core S1-30 perfectly correlates with the lower part of core S1-26 and two black shales were used as lithostratigraphic markers. Coring was extended for ~ 2 m (cores S1-31 and S1-32) penetrating the top of the black shale interval and then operations were interrupted to shift drilling to borehole S2 (Fig. 4). Due to the steep dip, it was decided to perform a 10° inclined coring to decrease the total penetration depth down into the Domaro Limestone Formation. Borehole S2 started just above the top of the black shale interval of the Livello a Pesci, perfectly duplicating core S1-32. However, technical problems prevented coring below a few metres and operations stopped after recovery of core S2-3. The third borehole (S3) was moved 0.5 m relative to S2 and was cored vertically. Again, the recovered succession started from just above the top of the black shale interval with core S3-1 triplicating cores S1-32 and S2-1. Coring was extended to 40 m penetration depth, reaching the uppermost part of the Domaro Limestone Formation (Fig. 4). A fourth borehole (S4) was performed to duplicate the middle and lower portion of the black shale interval to ensure material for multidisciplinary investigations. The recovery percentage for the four boreholes is 99.9 %.

Lithostratigraphic units were defined on the basis of lithological features (i.e. lithology and colours determined with the Munsell Rock Color Chart) and sedimentary structures (i.e. presence or lack of bioturbation and/or lamination). For each core at least four dip measurements were taken during lab preparation to calculate the stratigraphic thickness of the drilled section as 25.33 m under CE10 1.5 m of rubble at the top. A complete composite section, representing the upper Pliensbachian–lower Toarcian interval, was created by combining the data obtained from the S1 and S3 boreholes (Fig. 5). The following key observations were derived:

1. The first 1.5 m of the S1 borehole are represented by soil cover and rubble.
2. The S1 core, despite the occurrence of a faulted fold disturbing the succession, recovered a complete section above the Livello a Pesci. The bottommost part of the well reached the uppermost part of the black shale interval. This correlates with the top black shale interval recovered in the upper part of the S3 core.
3. The upper limit of the black shale interval was cored both at S1 and S3 sites.
4. The S3 core recovered a few metres CE11 of succession above the black shale interval, the entire Livello a Pesci, and the lower portion of the Sogno Formation, in addition to the topmost part of the Domaro limestone CE12. In particular, at 25.47 m, the lithostratigraphic boundary

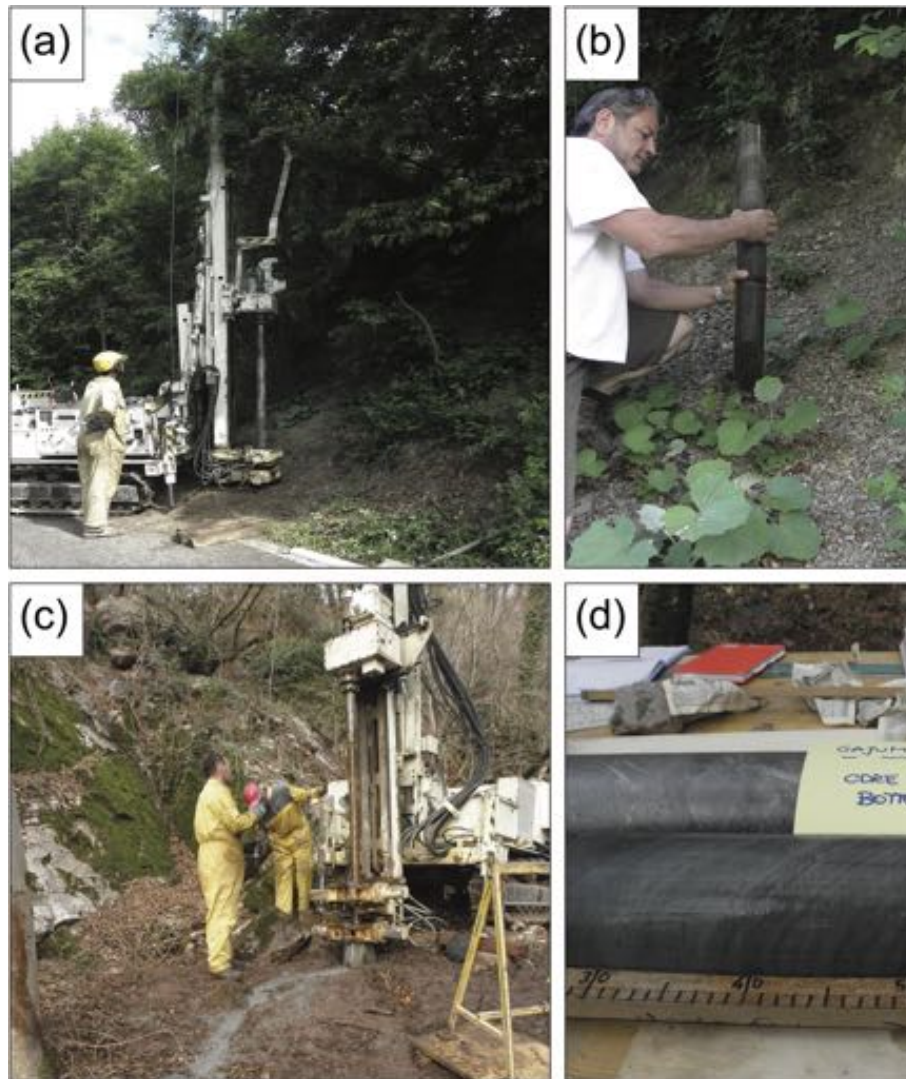


Figure 2. Coring operations and results at Sogno and Gajum sites. (a) Coring Sogno Site 4. (b) Livello a Pesci in the Sogno core compared to the equivalent outcropping lithostratigraphic interval. (c) Coring at Gajum. (d) Black shale interval recovered in core 10 of the Gajum core.

between the Sogno Formation and Domaro Limestone Formation was recovered.

Combining the above information and considering the dip measured in individual cores (variable in the range of 60 to 87°), the “stratigraphic thickness” of each lithostratigraphic unit was calculated. The overlapping intervals (i.e. U1-5 and U3-1) were matched and duplications were eliminated. The lithologic log of the composite S1–S3 Sogno core, in stratigraphic depths (from 1.5 to 26.83 m), is illustrated in Fig. 5. The composite S1–S3 Sogno core section recovered a complete upper Pliensbachian–lower Toarcian interval, with the S1 core representing its upper portion, and the S3 core the lower part.

The following lithostratigraphic units (U1-1 to U1-5, and U3-2 to U3-11, of the S1 and S3 cores, respectively) are described, from the topmost to the bottommost:

- Unit 1 (1.50 to 4.82 m): marly limestones, olive-grey in colour. In the upper and lowermost parts of the unit, high concentrations of reddish mottles and sporadic bioturbation are documented.
- Unit 2 (4.82 to 9.54 m): marly limestones, olive-grey in colour, characterized by intense bioturbation. In particular, the uppermost part of the unit documents the presence of frequent *Planolites*.
- Unit 3 (9.54 to 10.52 m): marly limestones, grey in colour, characterized by intense bioturbation. Locally, faintly laminated intervals are observed.

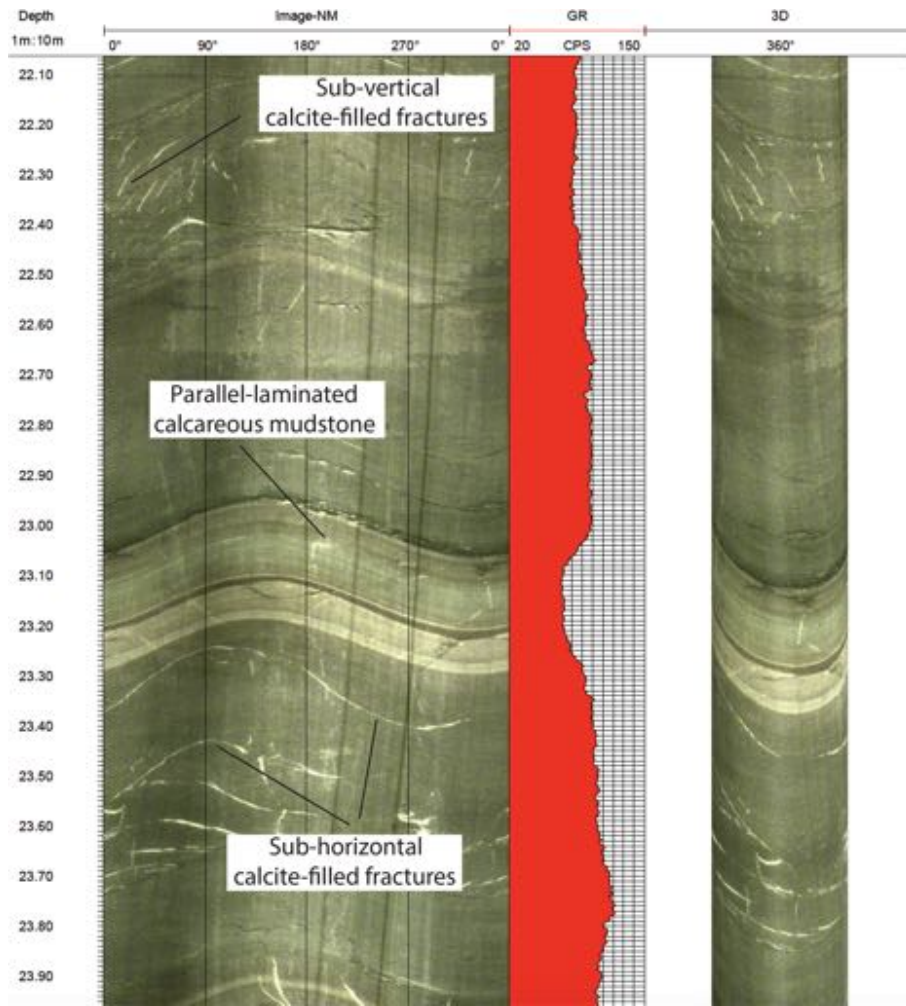


Figure 3. Example of Gajum borehole wall image recorded with a QL40-OBI optical televiewer. From left to right: borehole depth, 360° continuous upwrapped digital image of the borehole wall, total natural gamma ray, 3-D log visualization reproducing a virtual core of the borehole.

- Unit 4 (10.52 to 11.87 m): marly limestones with evident and widespread bioturbation. locally, 1 cm thick black shales **CE14** and laminated intervals are present.
- Unit 5 (11.87 to 14.55 m): black shales characterized by well-developed lamination, especially in the uppermost part, in addition to pyrite nodules. In the lower portion, very little bioturbation is documented.
- Unit 6 (14.55 to 15.93 m): marly limestones, grey to very dark-grey in colour, with reddish to greyish spots. Bioturbation (burrow) dimensions increase within this unit and thin emerald-green laminae are documented.
- Unit 7 (15.93 to 16.86 m): marly limestones, with variations in colour from grey, to very dark-grey and dark-red. In the lowermost portion, bioturbation and lamination are observed.
- Unit 8 (16.86 to 19.10 m): marly limestones, dark-red in colour, with sporadic greyish spots.
- Unit 9 (19.10 to 19.45 m): marly limestones, grey in colour.
- Unit 10 (19.45 to 21.35 m): marly limestones, grey-brown in colour. This is a disturbed interval comprising a level of pebbly marlstones (between 19.45 and 20.03 m), with minor slump structures. Sporadic stylolites are present.
- Unit 11 (21.35 to 22.92 m): marly limestones, grey in colour, characterized by frequent stylolite structures. In addition, 2 cm thick black shale intervals are documented at ~ 21.8 and 22 m, respectively.
- Unit 12 (22.92 to 24.35 m): marly limestones, alternating in colour from reddish to olive-grey. Sporadic bioturbation and lamination can be observed **CE15**.

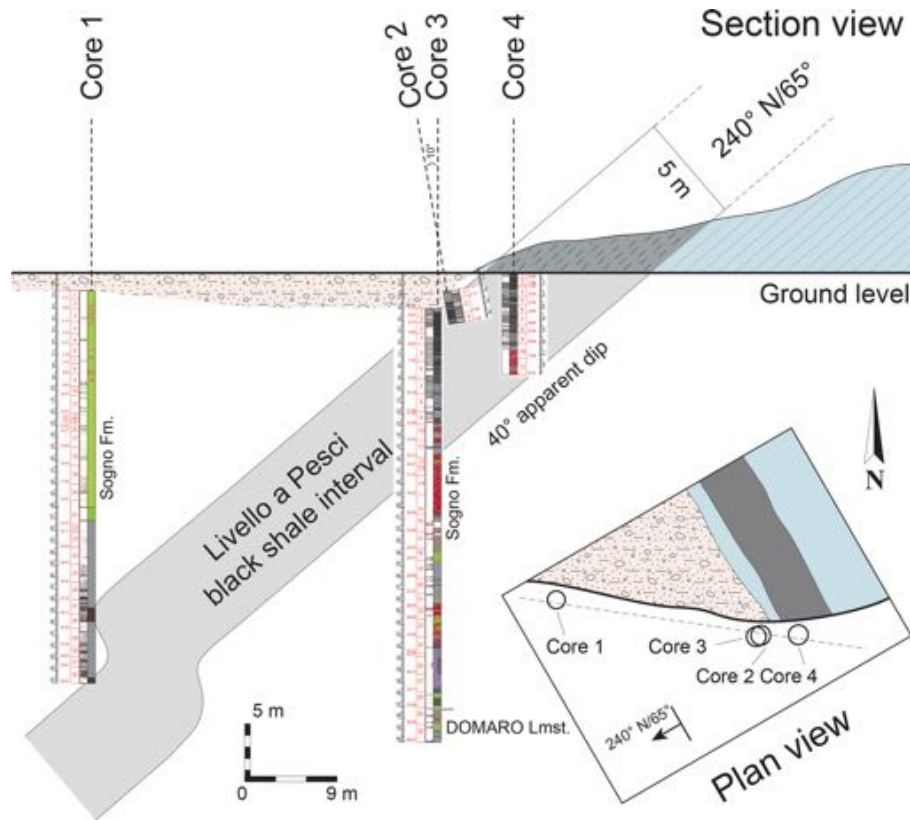


Figure 4. Section and plan view of the relative positions of the four boreholes drilled at Colle di Sogno. A pronounced fold was encountered at ~ 25 m penetration depth in Sogno borehole 1 that was abandoned after reaching the topmost part of the black shale interval. Three additional boreholes were cored as explained in the text.

- Unit 13 (24.35 to 24.99 m): marly limestones, reddish-greyish in colour.

Unit 14 (24.99 to 25.47 m): marly limestones, light-brown to grey-brown in colour. Small and large (1 cm thick) burrows are documented. The base of this unit corresponds to the base of the Sogno Formation.

- Unit 15 (25.47 to 26.83 m): marly limestones, olive-grey to dark-grey in colour. Little bioturbations and frequent stylolite structures are observed. This unit corresponds to the uppermost part of the Domaro Limestone Formation.

with four measurements on average, and used to calculate the corrected thickness of the drilled section as 28.18 m after removal of 3 m of rubble at the top. As for the Sogno core, lithostratigraphic units were defined based on lithological features and sedimentary structures. The dip measured in individual cores (variable in the range of 40 to 50°) was used to calculate the “stratigraphic thickness” of each lithostratigraphic unit described below, from the topmost to the bottommost:

- Unit 1 (3.00 to 4.35 m): dark brown to dusky red nodular limestone. nodules are 3–5 cm in size and light grey in colour. A resedimented level, consisting of a microbreccia, is detected at 3.92–3.96 m. This unit corresponds to the lower part of the Rosso Ammonitico Lombardo.

- Unit 2 (4.35 to 7.60 m): marly limestone, grey to olive grey in colour, with dark grey laminated intervals. Three cm-thick black shale intervals occur at 5.24–5.35, 6.26–6.43, and 6.70–6.81 m.

- Unit 3 (7.60 to 10.60 m): grey to dark grey marly limestone, with heavily bioturbated levels alternating with

4.2 Lithostratigraphy of the Gajum core

The Gajum core (45°51′03.2″ N, 09°17′19.5″ E, at 555 m slm) was drilled close to “Fonte Gajum” – Canzo (CO), in the Ravella valley next to the trail named Via delle Alpi (Fig. 1). The outcropping beds show a strike of 245° and a dip of 46° to the northwest (335°).

A single borehole was drilled at Gajum to a total penetration depth of 42.37 m, with 100 % recovery of excellent-quality material throughout drilling operation. For each core a set of dip measurements was taken during lab preparation,

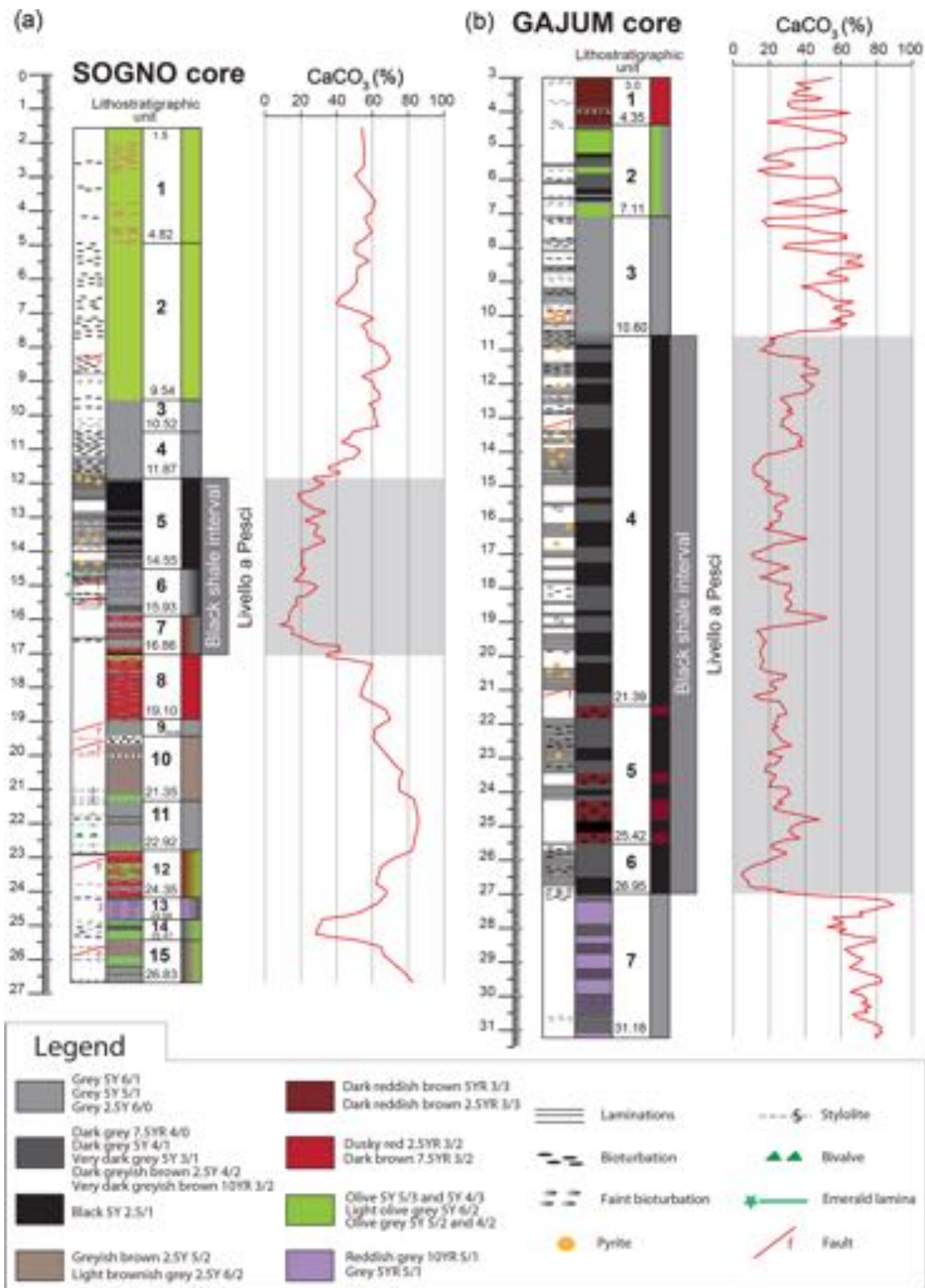


Figure 5. Lithostratigraphy and calcium carbonate content of the Sogno (a) and Gajum (b) cores. The grey pattern highlights the Livello a Pesci black shale interval that is the lithostratigraphic record of the T-OAE in the Lombardy Basin. The CaCO₃ content was detected using the Dietrich-Frühling gas volumetric method by measuring evolved CO₂ after acidification of the bulk sample with HCl.

intervals characterized by faint lamination. Some pyrite nodules are observed in the lowermost part of the unit.

- Unit 4 (10.60 to 21.39 m): dark to very dark grey to black marly claystones. This “black shale” interval is characterized by well-developed lamination and frequent pyrite nodules. In the upper and middle portion, discrete intervals with faint bioturbation are observed.
- Unit 5 (21.39 to 25.42 m): dark to very dark grey to black marly claystones characterized by well-developed lamination and a few pyrite nodules. Three intervals of dusky red limy cherts are identified at 21.39–21.87, 23.52–23.81, and 24.30–25.52 m. The highest and lowest cherty reddish levels delimit the top and bottom of this unit, respectively.
- Unit 6 (25.42 to 26.95 m): dark grey to very dark grey to black marly claystones, with evident laminations and sporadic faint bioturbations. The base is undulated.
- Unit 7 (26.95 to 31.18 m): grey to reddish grey marly limestones, with fractures filled by diagenetic calcite.

In Fig. 5 the Sogno and Gajum cores are correlated: the T-OAE black shale interval is represented in both sections, but with significantly different thicknesses, namely 4.98 m in the Sogno core and 15.35 m in the Gajum core. The lithostratigraphic onset and termination of the Livello a Pesci black shale interval, based on the lowest and highest black marly claystones, are nicely preserved in both cores, without lithologic evidence of hiatus or disturbance. In the Gajum core the beginning of the anoxic interval is quite abrupt and represented by the change from a few centimetres thick, grey, pseudonodular, and heavily bioturbated marly limestone to black shales with an irregular base mimicking nodularity of the underlying interval: this lithostratigraphic boundary is very similar to the onset of the early Aptian OAE1a in the Cismon core (Erba et al., 2010^{TS4}). The upper boundary is, conversely, relatively transitional from laminated black shales to dark grey marly limestones. In the Sogno core, instead, both the base and top of the black shale interval are sharp.

The Livello a Pesci is not homogeneous in the Sogno and Gajum cores: in both records, the lower part is characterized by the occurrence of a few reddish levels. These are cherty in the Gajum core (Unit 5) and clayey in the Sogno core (Unit 7). Also, black shales are dominant in the upper part of the Livello a Pesci in both cores (Unit 4 of the Gajum core and Unit 5 of the Sogno core).

As far as the calcium carbonate content is concerned (Fig. 5) in the Sogno and Gajum cores, the interval below the Livello a Pesci is characterized by values of around 60 % and 60 %–80 % CaCO₃, respectively. A drop in calcium carbonate content to an average of 20 % is recorded within the black shale interval in both cores, with lowermost values of 5 % (Gajum core) to 10 % (Sogno core) in the lowermost part.

Above the Livello a Pesci, the calcium carbonate content reverts [CB19](#) to 40 %–60 %, with frequent fluctuations.

5 Future objectives

The fresh material recovered with the Sogno and Gajum cores provide complete and relatively expanded pelagic records from the western Tethys Ocean. Detailed multidisciplinary investigations are in progress to collect multi-proxy records for building a high-resolution dataset prodromic for modelling the nature and significance of the T-OAE. The specific objectives are as follows:

1. *High-resolution integrated stratigraphy.* This is based on nannofossil biostratigraphy, magnetostratigraphy, chemostratigraphy, and cyclostratigraphy. Milankovitch cycles will be used to estimate durations of the T-OAE.
2. *Detailed studies of critical paleoceanographic parameters.* This includes total organic carbon; isotopic anomalies; and major, minor and trace elements that will be used to assess changes in surface and bottom water mass characteristics.
3. *Identification and quantification of the response of the biosphere.* This is based on quantitative and high-resolution investigation of calcareous phytoplankton assemblages. In particular, we will focus on the relative timing and possible phase-lag of the response to the overwhelming forcing function/s. These relationships will be used to model the resilience of the oceanic biosphere.
4. *Characterization of the Early Jurassic climate, ocean dynamics, and their response to orbital cyclicity.* In particular, we plan to decipher local from regional and global changes across the paleoenvironmental perturbation. Also, the cyclostratigraphy will allow for the assessment of the influence of eccentricity, obliquity, and precession cycles before, during, and after the T-OAE.

Data availability. The Sogno and Gajum cores are stored at the Department of Earth Sciences “Ardito Desio” of the University of Milan (Italy). [ITSS](#)

Author contributions. EE conceived and executed the Sogno and Gajum coring. She coordinated the lab core work and prepared the paper. GG co-supervised the core description and contributed to the paper. Other co-authors (SV, LC, DR, GF, MP) contributed to core splitting, archiving, and sampling.

Competing interests. The authors declare that they have no conflict of interest.

Acknowledgements. The T-OAE coring project derived from fieldwork and in-depth discussions with Maurizio Gaetani on Jurassic stratigraphy of the Lombardy Basin. We acknowledge the editor Thomas Wiersberg, and the two reviewers Alicia Fantasia and Stephen Hesselbo, who greatly improved the quality of the paper with their constructive comments. The Sogno and Gajum coring campaign was funded by MIUR-PRIN2011 (2010X3PP8J) awarded to Elisabetta Erba.

Financial support. This research has been supported by the MIUR (MIUR-PRIN2011 (grant no. 2010X3PP8J)) [TS6](#)

Review statement. This paper was edited by Thomas Wiersberg and reviewed by Stephen Hesselbo and Alicia Fantasia.

References

- Al-Suwaidi A. H., Angelozzi, G. N., Baudin F., Damborenea, S. E., Hesselbo, S. P., Jenkyns, H. C., Manceñido M. O., and Riccardi A. C.: First record of the Early Toarcian Oceanic Anoxic Event from the Southern Hemisphere, Neuquén Basin, Argentina, *J. Geol. Soc. London*, 167, 633–636, 2010.
- Bellanca, A., Masetti, D., Neri, R., and Venezia, F.: Geochemical and sedimentological evidence of productivity cycles recorded in Toarcian black shales from the Belluno Basin, Southern Alps, northern Italy, *J. Sediment. Res.*, 69B, 466–476, 1999.
- Bernoulli, D. and Jenkyns, H. C.: Alpine, Mediterranean, and Central Atlantic Mesozoic facies in relation to the early evolution of the Tethys, in: *Modern and Ancient Geosynclinal Sedimentation*, edited by: Dott, R. H. and Shaver R. H., *Soc. Econ. Paleont. Mineral., Spec. Publ.*, 19, 129–160, 1974.
- Bernoulli, D. and Jenkyns, H. C.: Ancient oceans and continental margins of the Alpine-Mediterranean Tethys: Deciphering clues from Mesozoic pelagic sediments and ophiolites, *Sedimentology*, 56, 149–190, 2009.
- Bosence, D., Procter, E., Aurell, M., Kahla, A. B., Boudagher-Fadel, M., Casaglia, F., Cirilli, S., Mehdie, M., Nieto, L., Rey, J., Scherreiks, R., Soussi, M., and Waltham, D.: A Dominant Tectonic Signal in High-Frequency, Peritidal Carbonate Cycles? A Regional Analysis of Liassic Platforms from Western Tethys, *J. Sediment. Res.*, 79, 389–415, 2009.
- Caruthers, A. H., Gröcke, D. R., and Smith, P. L.: The significance of an Early Jurassic (Toarcian) carbon-isotope excursion in Haida Gwaii (Queen Charlotte Islands), British Columbia, Canada, *Earth Planet. Sc. Lett.*, 307, 19–26, 2011.
- Casellato, C. E. and Erba, E.: Calcareous nannofossil biostratigraphy and paleoceanography of the Toarcian Oceanic Anoxic Event at Colle di Sogno section (Southern Alps, Italy), *Riv. Ital. Paleontol. S.*, 105, 343–376, 2015.
- Channell, J. E. T., Erba, E., Muttoni, G., and Tremolada, F.: Early Cretaceous magnetic stratigraphy in the APTICORE drill core and adjacent outcrop at Cismon (Southern Alps, Italy), and correlation to the proposed Barremian/Aptian boundary stratotype, *Geol. Soc. Am. Bull.*, 112, 1430–1443, 2000. [TS7](#)
- Channell, J. E. T., Casellato, C. E., Muttoni, G., and Erba, E.: Magnetostatigraphy, nannofossil stratigraphy and apparent polar wander for Adria-Africa in the Jurassic–Cretaceous boundary interval, *Palaeogeogr. Palaeoclimatol.*, 293, 51–75, 2010.
- Cohen, A. S., Coe, A. L., Harding, S. M., and Schwark, L.: Osmium isotope evidence for the regulation of atmospheric CO₂ by continental weathering, *Geology*, 32, 157–160, 2004.
- Dera, G., Brigaud, B., Monna, F., Laffont, R., Pucéat, E., Deconinck, J.-F., Pellenard, P., Joachimski, M. M., and Durlet, C.: Climatic ups and downs in a disturbed Jurassic world, *Geology*, 39, 215–218, 2011.
- Emmanuel, L., Renard, M., Cubaynes, R., De Rafelis, M., Hermoso, M., Lecallonnec, L., Le Solleuz, A., and Rey, J.: The “Schistes Carton” of Quercy (Tarn, France): a lithological signature of a methane hydrate dissociation event in the early Toarcian. Implications for correlations between Boreal and Tethyan realms, *Bull. Soc. Géol. Fr.*, 177, 239–249, 2006.
- Erba, E.: Calcareous nannofossil distribution in pelagic rhythmic sediments (Aptian-Albian Piobbico core, Central Italy), *Riv. Ital. Paleontol. S.*, 97, 455–484, 1992. [TS8](#)
- Erba, E.: Calcareous nannofossils and Mesozoic oceanic anoxic events, *Mar. Micropaleontol.*, 52, 85–106, 2004.
- Erba, E. and Casellato C. E.: Paleoceanografia del Giurassico nella Tetide occidentale: l’archivio geologico del Bacino Lombardo, *Rendiconti dell’Istituto Lombardo, Accademia di Scienze e Lettere, Special Publication on “Una nuova Geologia per la Lombardia”*, 447, 115–140, 2010.
- Erba, E. and Larson, R. L.: The Cismon APTICORE (Southern Alps, Italy): a “reference section” for the Lower Cretaceous at low latitudes, *Riv. Ital. Paleontol. S.*, 104, 181–192, 1998. [TS9](#)
- Erba, E., Channell, J. E. T., Claps, M., Jones, C., Larson, R. L., Opdyke, B., Premoli Silva, I., Riva, A., Salvini, G., and Torricelli, S.: Integrated stratigraphy of the Cismon Apticore (Southern Alps, Italy): a “reference section” for the Huterivian-Aptian interval at low latitudes, *J. Foramin. Res.*, 29, 371–391, 1999. [TS10](#)
- Erba, E., Premoli Silva, I., Sinninghe Damste, J., Jenkyns, H., Farrimond, P., Boettcher, M., Brumsack, H., and Kuhnt, W.: Multi-disciplinary study of the Cenomanian/Turonian Oceanic Anoxic Event 2: preliminary results from the Gubbio Core (central Italy), *Journal of Conference (EUG XI)*, 199, 2000. [TS11](#) [TS12](#)
- Erba, E., Bottini, C., Faucher, G., Gambacorta, G., and Visentin, S.: The response of calcareous nannoplankton to Oceanic Anoxic Events: The Italian pelagic record, *B. Soc. Paleontol. Ital.*, 58, 51–71, 2019.
- Fantasia, A., Föllmi, K. B., Adatte, T., Bernàirdez, E., Spangenberg, J. E., and Mattioli, E.: The Toarcian Oceanic Anoxic Event in southwestern Gondwana: an example from the Andean Basin, northern Chile, *J. Geol. Soc.*, 175, 883–902, 2018.
- Farrimond, P., Englinton, G., Brassell, S. C., and Jenkyns, H. C.: The Toarcian black shale event in northern Italy, *Org. Geochem.*, 13, 823–832, 1988.
- Fischer, A. G., Herbert, T. D., Napoleone, G., Premoli Silva, I., and Ripepe, M.: Albian pelagic rhythms (Piobbico core), *J. Sediment. Petrol.*, 61, 1164–1172, 1991. [TS13](#)
- Gaetani, M.: Jurassic stratigraphy of the Southern Alps: a review, *Geology of Italy*, 1, 377–402, 1975.
- Gaetani, M.: From Permian to Cretaceous: Adria as pivotal between extensions and rotations of Tethys and Atlantic Oceans, in: *The Geology of Italy*, edited by: Beltrando, M., Peccerillo, A., Mattei,

- M., Conticelli, S., and Doglioni, C., *J. Virt. Expl.*, 36, paper 5.a, 2010. [TS14](#)
- Gaetani, M. and Erba, E.: Il bacino Lombardo: un sistema paleoalto/fossa in un margine continentale passivo durante il Giurassico, 75° Congresso Soc. Geol. It., Guida all'escursione A3, 1990. [TS15](#)
- Gaetani, M. and Poliani, G.: Il Toarciano e il Giurassico medio in Albenza (Bergamo), *Riv. Ital. Paleontol. S.*, 84, 349–382, 1978.
- Gómez, J. J., Comas-Rengifo, M. J., and Goy, A.: Palaeoclimatic oscillations in the Pliensbachian (Early Jurassic) of the Asturian Basin (Northern Spain), *Clim. Past*, 12, 1199–1214, <https://doi.org/10.5194/cp-12-1199-2016>, 2016.
- Hardenbol, J., Thierry, J., Farley, M. B., Jacquin, T., de Graciansky, P.-C., and Vail, P. R.: Mesozoic and Cenozoic sequence chronostratigraphic framework of European basins, in: Mesozoic and Cenozoic sequence stratigraphy of European basins, edited by: de Graciansky, P.-C., Hardenbol, J., Jacquin T., and Vail, P. R., *SEPM Special Publication*, 60, 3–13, charts 1–8, 1998. [TS16](#)
- Haq, B. U., Hardenbol, J., and Vail, P. R.: Chronology of fluctuating sea-levels since the Triassic, *Nature*, 235, 1156–1167, 1987.
- Herbert, T. D. and Fischer, A.G.: Milankovitch climate origin of mid-Cretaceous black shale rhythms in central Italy, *Nature*, 321, 739–743, 1986. [TS17](#)
- Hesselbo, S. P., Gröcke, D. R., Jenkyns, H. C., Bjerrum, C. J., Farinon, P., Morgans Bell, H. S., and Green, O. R.: Massive dissociation of gas hydrate during a Jurassic Oceanic Anoxic Event, *Nature*, 406, 392–395, 2000.
- Hesselbo, S. P., Jenkyns, H. C., Duarte, L. V., and Oliveira, L. C. V.: Carbon-isotope record of the Early Jurassic (Toarcian) Oceanic Anoxic Event from fossil wood and marine carbonate (Lusitanian Basin, Portugal), *Earth Planet. Sc. Lett.*, 253, 455–470, 2007.
- Hinnov, L. A. Park, J., and Erba E.: Lower-Middle Jurassic rhythmites from the Lombard Basin, Italy: a record of orbitally forced carbonate cycles modulated by secular environmental changes in West Tethys, in: *Advances in Jurassic Research*, edited by: Hall R. L. and Smith P. L., *Trans Tech Publications*, 437–454, 2000. [TS18](#)
- Izumi, K., Miyaji, T., and Tanabe, K.: Early Toarcian (Early Jurassic) oceanic anoxic event recorded in the shelf deposits in the northwestern Panthalassa: evidence from the Nishinakayama formation in the Toyora area, west Japan, *Palaeogeogr. Palaeocl.*, 315–316, 100–108, 2012.
- Jenkyns, H. C.: The Early Toarcian and Cenomanian-Turonian anoxic events in Europe: comparisons and contrasts, *Geol. Rundsch.*, 74, 505–518, 1985.
- Jenkyns, H. C.: The Early Toarcian (Jurassic) Anoxic Event: stratigraphic, sedimentary and geochemical evidence, *Am. J. Sci.*, 288, 101–151, 1988.
- Jenkyns, H. C.: Mesozoic anoxic events and palaeoclimate, *Zbl. Geo. Pal.*, 1997, 943–949, 1999. [TS19](#)
- Jenkyns, H. C.: Geochemistry of oceanic anoxic events, *Geochem. Geophys. Geosy.*, 11, Q03004, 2010. [TS20](#)
- Jenkyns, H. C. and Clayton, C. J.: Black shales and carbon isotopes in pelagic sediments from the Tethyan Lower Jurassic, *Sedimentology*, 33, 87–106, 1986.
- Jenkyns, H. C. and Clayton, C. J.: Lower Jurassic epicontinental carbonates and mudstones from England and Wales: chemostratigraphic signals and the early Toarcian anoxic event., *Sedimentology*, 44, 687–706, 1997. [TS21](#)
- Jenkyns, H. C., Géczy, B., and Marshall, J. D.: Jurassic manganese carbonates of central Europe and the early Toarcian anoxic event, *J. Geol.*, 99, 137–149, 1991.
- Jenkyns, H. C., Gröcke, D. R., and Hesselbo, S. P.: Nitrogen-isotope evidence for watermass denitrification during the Early Toarcian (Jurassic) Oceanic Anoxic Event, *Paleoceanography*, 16, 593–603, 2001. [TS22](#)
- Jenkyns, H. C., Jones, C. E., Gröcke, D. R., Hesselbo, S. P., and Parkinson, D. N.: Chemostratigraphy of the Jurassic System: applications, limitations and implications for palaeoecology, *J. Geol. Soc.*, 159, 351–378, 2002.
- Jones, C. E. and Jenkyns, H. C.: Seawater strontium isotopes, oceanic anoxic events, and seafloor hydrothermal activity in the Jurassic and Cretaceous, *Am. J. Sci.*, 301, 112–149, 2001. [TS23](#)
- Kafousia, N., Karakitsios, V., Mattioli, E., Kenjo, S., and Jenkyns H. C.: The Toarcian Oceanic Anoxic Event in the Ionian Zone, Greece, *Palaeogeogr. Palaeocl.*, 393, 135–145, 2014.
- Korte, C. and Hesselbo, S. P.: Shallow marine carbon and oxygen isotope and elemental records indicate icehouse-greenhouse cycles during the early Jurassic, *Paleoceanography*, 26, PA4219, <https://doi.org/10.1029/2011PA002160>, 2011.
- Larson, R. L. and Erba, E.: Onset of the mid-Cretaceous greenhouse in the Barremian-Aptian: Igneous events and the biological, sedimentary and geochemical responses, *Paleoceanography*, 14, 663–678, 1999. [TS24](#)
- Little, C. T. S. and Benton, M. J.: Early Jurassic mass extinction: a global long-term event, *Geology*, 23, 495–498, 1995. [TS25](#)
- Mattioli, E. and Erba, E.: Synthesis of calcareous nannofossil events in Tethyan Lower and Middle Jurassic successions, *Riv. Ital. Paleontol. S.*, 105, 343–376, 1999. [TS26](#)
- Mattioli, E., Pittet, B., Bucefalo Palliani, R., Rohl, H.-J., Schmid-Rohl, A., and Morettini, E.: Phytoplankton evidence for timing and correlation of palaeoceanographical changes during the Early Toarcian oceanic anoxic event (Early Jurassic), *J. Geol. Soc. London*, 161, 685–693, 2004.
- McArthur, J. M., Donovan, D. T., Thirlwall, M. F., Fouke, B. W., and Matthey, D.: Strontium isotope profile of the early Toarcian (Jurassic) oceanic anoxic event, the duration of ammonite biozones, and belemnite palaeotemperatures, *Earth Planet. Sc. Lett.*, 179, 269–285, 2000. [TS27](#)
- Muttoni, G., Erba, E., Kent, D. V., and Bachtadse, V.: Mesozoic Alpine facies deposition as a result of past latitudinal plate motion, *Nature*, 434, 59–63, 2005.
- Pálffy, J. and Smith, P. L.: Synchrony between Early Jurassic extinction, oceanic anoxic event, and the Karoo-Ferrar flood basalt volcanism, *Geology*, 28, 747–750, 2000. [TS28](#)
- Pasquini, C. and Vercesi, P. L.: Tettonica sinsedimentaria e ricostruzione paleogeografica del margine occidentale dell'Alto dei Corni di Canzo nel Lias inferiore, *Memorie della Società Geologica Italiana*, 57, 107–114, 2002.
- Percival, L. M. E., Cohen, A. S., Davies, M. K., Dickson, A. J., Hesselbo, S. P., Jenkyns, H. C., Leng, M. J., Mather, T. A., Storm, M. S., and Xu, W.: Osmium isotope evidence for two pulses of increased continental weathering linked to Early Jurassic volcanism and climate change, *Geology*, 44, 759–762, 2016.
- Posenato, R., Bassi, D., Trecalli, A., and Parente, M.: Taphonomy and evolution of Lower Jurassic lithotid bivalve accumulations

- in the Apennine Carbonate Platform (southern Italy), *Palaeogeogr. Palaeoclimatol.*, 489, 261–271, 2018.
- Premoli Silva, I., Erba, E., and Tornaghi, M. E.: Paleoenvironmental signals and changes in surface fertility in Mid Cretaceous Corg-rich pelagic facies of the Fucoïd Marls (Central Italy), *Geobios*, 11, 225–236, 1989. [TS29](#)
- Premoli Silva, I., Erba, E., Salvini, G., Verga, D., and Locatelli C.: Biotic changes in Cretaceous Anoxic Events, *J. Foramin. Res.*, 29, 352–370, 1999. [TS30](#)
- 10 Reolid, M.: Stable isotopes on foraminifera and ostracods for interpreting incidence of the Toarcian Oceanic Anoxic Event in Westernmost Tethys: role of water stagnation and productivity, *Palaeogeogr. Palaeoclimatol.*, 395, 77–91, 2014.
- Rosales, I., Quesada, S., and Robles, S.: Primary and diagenetic isotopic signals in fossils and hemipelagic carbonates: the Lower Jurassic of northern Spain, *Sedimentology*, 48, 1149–1169, 2001. [TS31](#)
- Santantonio, M. and Carminati, E.: The Jurassic rifting evolution of the Apennines and Southern Alps (Italy): Parallels and differences, *Bull. Geol. Soc. Am.*, 124, 468–484, 2011.
- 20 Schouten, S., van Kaam-Peters, H. M. E., Rijpstra, W. I. C., Schoell, M., and Sinninghe Damsté, J. S.: Effects of an oceanic anoxic event on the stable carbon isotopic composition of early Toarcian carbon, *Am. J. Sci.*, 300, 1–22, 2000.
- 25 Solomon, S., Plattner, G.-K., Knutti, R., and Friedlingstein, P.: Irreversible climate change due to carbon dioxide emissions, *P. Natl. Acad. Sci. USA*, 106, 1704–1709, 2009.
- Them, T. R., Gill, B. C., Selby, D., Gröcke, D. R., Friedman, R. M., and Owens, J. D.: Evidence for rapid weathering response to climatic warming during the Toarcian Oceanic Anoxic Event, *Sci. Rep.*, 7, 5003, <https://doi.org/10.1038/s41598-017-05307-y>, 2017. 30
- Tintori, A.: Toarcian fishes from the Lombardy Basin, *B. Soc. Paleontol. Ital.*, 16, 143–152, 1977.
- Trecalli, A., Spangenberg, J., Adatte, T., Föllmi, K. B., and Parente, M.: Carbonate platform evidence of ocean acidification at the onset of the early Toarcian oceanic anoxic event, *Earth Planet. Sc. Lett.*, 357–358, 214–225, 2012. 35
- Vakhrameyev, V. A.: *Classopolis* pollen as an indicator of Jurassic and Cretaceous climate, *Int. Geol. Rev.*, 24, 1190–1196, 1982. [TS32](#) 40
- van Breugel, Y., Baas, M., Schouten, S., Mattioli, E., and Damsté, J. S. S.: Isorenieratane record in black shales from the Paris Basin, France: Constraints on recycling of respired CO₂ as a mechanism for negative carbon isotope shifts during the Toarcian oceanic anoxic event, *Paleoceanography*, 21, <https://doi.org/10.1029/2006PA001305>, 2006. [TS33](#) 45
- Xu, W., Ruhl, M., Jenkyns, H. C., Hesselbo, S. P., Riding, J. B., Selby, D., Naafs, B. D. A., Weijers, J. W. H., Pancost, R. D., Tegelaar, E., and Idiz, E.: Carbon sequestration in an expanded lake system during the Toarcian oceanic anoxic event, *Nat. Geosci.*, 10, 129–134, 2017. 50

Appendix H

Abstracts presented at international congresses

1. **Visentin S.**, Reolon D., Faucher G., Erba E., (2017) - Calcareous nannofossil biostratigraphy and paleoceanography across the Toarcian Oceanic Anoxic Event cored at Colle di Sogno (Lombardy Basin, northern Italy), *16th INA MEETING, abstract book*, 164. **Athens, Greece (September 24th – 28th 2017)**
2. **Visentin S.**, Reolon D., Faucher G., Erba E., (2017) - Calcareous nannofossil biostratigraphy and paleoceanography across the Toarcian Oceanic Anoxic Event cored at Colle di Sogno (Lombardy Basin, Northern Italy), *1st IW-T-OAE, abstract book*, 125. **Jaen, Spain (October 4th – 7th 2017)**
3. **Visentin S.**, Reolon D., Faucher G., Erba E., (2018) – Calcareous nannofossil paleoceanography across the Toarcian Oceanic Anoxic Event: a story of fertility and acidification (Sogno Core, Lombardy Basin, Northern Italy), *Congresso SGI-SIMP, abstract book*, 21. **Catania, Italy (September 12th – 14th 2018)**
4. **Visentin S.**, Mutterlose J., Erba E., (2019) - Calcareous nannofossil biostratigraphy as a tool to better constrain the Toarcian Oceanic Anoxic Event: a comparison between Tethyan and Boreal sections, *3rd International Congress on Stratigraphy (STRATI), abstract book*, 426. **Milan, Italy (July 2nd – 5th 2019)**
5. **Visentin S.**, Mutterlose J., Erba E., (2019) – Biostratigraphic constraints of the Early Toarcian Oceanic Anoxic Event: new data from calcareous nannofossil investigations from Boreal and Tethyan sections, *3rd IW-T-OAE, abstract book (in press)*. **Erlangen, Germany (September 2nd – 5th)**
6. **Visentin S.**, Faucher G., Erba E., (2019) - Taxonomic revision of the genus *Carinolithus* (Early-Middle Jurassic) based on morphometric analyses and diagenesis observations: Implications for biostratigraphy and evolutionary trends, *17th INA MEETING, abstract book*, 109. **Santos, Brazil (September 15th – 19th).**

Calcareous nannofossil biostratigraphy and paleoceanography across the Toarcian Oceanic Anoxic Event cored at Colle di Sogno (Lombardy Basin, northern Italy)

Stefano Visentin

Università degli studi di Milano, Dipartimento di Scienze della Terra, 20133 Milano, Italy; stefano.visentin@unimi.it

Dario Reolon

Università degli studi di Milano, Dipartimento di Scienze della Terra, 20133 Milano, Italy; dario.reolon@studenti.unimi.it

Giulia Faucher

Università degli studi di Milano, Dipartimento di Scienze della Terra, 20133 Milano, Italy; giulia.faucher@unimi.it

Elisabetta Erba

Università degli studi di Milano, Dipartimento di Scienze della Terra, 20133 Milano, Italy; elisabetta.erba@unimi.it

Calcareous nannofossil biostratigraphy was carried out in the upper Pliensbachian-lower Toarcian interval cored at Colle di Sogno (northern Italy). Semiquantitative analyses were performed on ~160 samples across the Domaro Limestone-Sogno Formation boundary that was recovered in two different boreholes (S1 and S3). Geochemistry evidenced the presence of the negative C isotopic excursion across the “fish level” black shale interval representative of the Toarcian Oceanic Anoxic Event (T-OAE).

Main and secondary events of the Tethyan zonation (Mattioli & Erba, 1999) were recognized, allowing the identification of Zones NJT 5 and NJT 6. The T-OAE C isotopic anomaly was constrained by the FO of *Carinolithus superbis* at the onset and the LO of *Mitrolithus jansae* at the end. Our results confirmed that the latter biohorizon is a primary stratigraphic event.

Semiquantitative and morphometric analyses were performed on *Schizosphaerella punctulata* and *M. jansae* to assess potential changes in abundance, size, and/or morphologies relative to the T-OAE. Both taxa displayed a major decrease in abundance at the onset of T-OAE and remained rare through the interval of perturbed conditions. Only *S. punctulata* showed a recovery at the end of the

T-OAE, while *M. jansae* barely survived the paleoenvironmental stress and disappeared soon after its termination.

Our results confirm that calcareous nannoplankton were influenced by paleoenvironmental changes associated with the T-OAE when increased nutrient availability, warming, and excess CO₂ led to a dramatic shift in assemblage composition. After a period of prolonged stability and oligotrophy that promoted a diversified calcareous phytoplankton community with abundant k-selected deep- and intermediate-dwellers, meso- to eutrophic conditions occurred that were locally associated with accelerated runoff and favored opportunistic taxa. After the T-OAE, paleoceanographic conditions, at least as far as the photic zone was concerned, only partially and gradually returned to a pre-perturbation state, suggesting that the deepening of the nutricline and re-establishment of stability required a long period after anoxia terminated.

References

- Mattioli, E. & Erba, E. 1999. Synthesis of calcareous nannofossil events in the Tethyan Lower and Middle Jurassic successions. *Rivista Italiana di Paleontologia e Stratigrafia*, **105**(3): 343–376.

**CALCAREOUS NANNOFOSSIL BIOSTRATIGRAPHY AND PALEOCEANOGRAPHY
ACROSS THE TOARCIAN OCEANIC ANOXIC EVENT CORED AT COLLE DI
SOGNO (LOMBARDY BASIN, NORTHERN ITALY)**

Visentin, Stefano; Reolon, Dario; Faucher, Giulia; Erba, Elisabetta
*Dipartimento di Scienze della Terra, Università degli Studi di Milano, Via Mangiagalli 34,
20133 Milano, Italy, e-mail: stefano.visentin@unimi.it*

Calcareous nannofossil biostratigraphy was carried out in the Upper Pliensbachian – Lower Toarcian interval cored at Colle di Sogno (N Italy). Semiquantitative analyses were performed on ~ 160 samples across the Domaro Lmst./Sogno Fm. boundary recovered with two different boreholes (S1 and S3) with a total stratigraphic thickness of 40 m. Geochemistry evidenced the presence of the negative C isotopic excursion across the “Fish Level” black shale interval representative of the Toarcian Oceanic Anoxic Event (T-OAE).

Nannofossil main and secondary events of the Tethyan zonation were recognized allowing the identification of the NJT 5 and NJT 6 Zones. The T-OAE C isotopic anomaly is constrained by the FO of *Carinolithus superbis* at the onset and the LO of *Mitrolithus jansae* at the end: our results, in particular, confirm that the latter biohorizon is a primary stratigraphic event.

Semiquantitative and morphometric analyses were performed on *Schizosphaerella punctulata* and *Mitrolithus jansae* to assess potential changes in abundance, size and/or morphologies relative to the T-OAE. Both taxa display a major decrease in abundance at the onset of T-OAE and remain rare through the interval of perturbed conditions. Only *S. punctulata* shows a recovery at the end of the T-OAE, while *M. jansae* barely survived the palaeoenvironmental stress and disappeared soon after its termination. As previously found, *S. punctulata* shows a decrease in size across the T-OAE possibly as a result of higher fertility combined with some acidification. Contrarily, *M. jansae* does not show significant size decrease across the T-OAE.

Our results confirm that calcareous nannoplankton were influenced by paleoenvironmental changes associated with the T-OAE: increased nutrient availability, warming and excess CO₂ concurred to the dramatic shift in assemblage composition. Complex global changes contributed to the establishment and maintenance of very stressing surface waters favouring opportunistic taxa. The period preceding T-OAE was a time of prolonged stability and oligotrophy promoting a diversified calcareous phytoplankton community with abundant

k-selected deep- and intermediate-dwellers. Then, T-OAE was marked by meso- to eutrophic conditions, locally associated to accelerated run-off favoured opportunistic taxa: both heavily calcified *S. punctulata* and *M. jansae* experienced a major decrease in abundance and the former taxon also underwent reduction in size while taxa producing smaller and less calcified coccoliths were favoured. Stressing conditions started in the latest Pliensbachian and triggered subsequent changes in nannofloral composition and structure recorded worldwide suggest that the environmental perturbations preceding and accompanying the T-OAE possibly stimulated biomineralization of new coccolith morphologies. After the T-OAE, palaeoceanographic conditions, at least as far as the photic zone is concerned, only partly and gradually returned to a pre-perturbation state suggesting that the deepening of the nutricline and re-establishment of stability required a long period after anoxia terminated.

Calcareous nannofossil paleoceanography across the Toarcian Oceanic Anoxic Event: a story of fertility and acidification (Sogno Core, Lombardy Basin, Northern Italy)

Visentin S., Reolon D., Faucher G. & Erba E.*

Dipartimento di Scienze della Terra "Ardito Desio", Università degli Studi di Milano

* Corresponding email: elisabetta.erba@unimi.it

Keywords: Toarcian Oceanic Anoxic Event, global change, nannoplankton resilience.

The Toarcian Oceanic Anoxic Event (T-OAE) represents a global extreme perturbation of the ocean-atmosphere system evidenced by geochemical anomalies, severe changes in the chemistry of the ocean and largest response of marine biota. In Western Tethys the T-OAE is represented by a black shale interval (locally named Fish Level) associated to a carbonate crisis. In the Early Jurassic, calcareous nannoplankton were already a main producer of pelagic micrites and, consequently, changes in nannofossil assemblages can help disentangle surface water conditions relative to global to local perturbations. Nannofossil investigations were performed on the Sogno Core that recovered a 27 meter-thick stratigraphic section (upper Pliensbachian-lower Toarcian): excellent quality of cores allowed a high-resolution sampling for multidisciplinary characterization of changes prior to, during and after the T-OAE.

Quantitative and morphometric analyses of *Schizosphaerella punctulata* and *Mitrolithus jansae* identified changes in abundance, size and/or morphologies: both taxa display a major decrease in abundance at the onset of T-OAE and remain rare through the interval of perturbed conditions. Only *S. punctulata* shows a recovery at the end of the T-OAE, while *M. jansae* barely survived the paleoenvironmental stress and disappeared soon after its termination. *S. punctulata* shows a decrease in size across the T-OAE possibly as a result of higher fertility combined with some acidification. Contrarily, *M. jansae* does not show significant size decrease across the T-OAE. Calcareous nannoplankton were influenced by increased nutrient availability, warming and excess CO₂ that concurred to the dramatic shift in assemblage composition. Complex global changes contributed to the establishment and maintenance of very stressing surface waters favouring opportunistic taxa. The period preceding T-OAE was a time of prolonged stability and oligotrophy promoting a diversified calcareous phytoplankton community with abundant k-selected deep- and intermediate-dwellers. Then, the T-OAE was marked by meso-eutrophic conditions, locally associated to accelerated run-off favoured opportunistic taxa: both heavily calcified *S. punctulata* and *M. jansae* experienced a major decrease in abundance and the former taxon also underwent reduction in size while taxa producing smaller and less calcified coccoliths were favoured. Stressing conditions started in the latest Pliensbachian and triggered subsequent changes in nannofloral composition and structure recorded worldwide suggest that the environmental perturbations preceding and accompanying the T-OAE possibly stimulated biomineralization of new coccolith morphologies. After the T-OAE, paleoceanographic conditions, at least as far as the photic zone is concerned, only partly and gradually returned to a pre-perturbation state suggesting that the deepening of the nutricline and re-establishment of stability required a long period after anoxia terminated.

Calcareous nannofossil biostratigraphy as a tool to better constrain the Toarcian Oceanic Anoxic Event: a comparison between Tethyan and Boreal sections

Visentin S.*¹, Erba E.¹ & Mutterlose J.²

¹ Dipartimento di Scienze della Terra, Università degli Studi di Milano, Italy. ² Institut für Geologie, Mineralogie und Geophysik, Ruhr-Universität Bochum, Germany.

Corresponding author email: stefano.visentin@unimi.it

Keywords: Nannofossil biostratigraphy, C isotope excursion, Pliensbachian-Toarcian.

Calcareous nannofossil biostratigraphy was carried out in the Upper Pliensbachian – Lower Toarcian containing the Toarcian Oceanic Anoxic Event (T-OAE) interval. In particular, semiquantitative analyses were performed: (a) on a total of 158 samples in the composite Sogno Core (Lombardy Basin, Southern Alps) representing a pelagic Tethyan section, and (b) on a total of 334 samples across the Amaltheenton Fm. and Posidonienschiefer Fm., in three cores and a section from the Boreal realm, in the Lower Saxony Basin (Northern Germany). Primary and secondary events of the Tethyan (Mattioli & Erba, 1999) and Boreal zonations (Bown et al., 1988; Bown & Cooper 1998) were recognized allowing the identifications of the NJT5, NJT6 for the Sogno Core and NJ5, NJ6, NJ7 Zones for the German cores/sections, respectively. The sequence of nannofossil biohorizons is generally consistent with data available for various areas at lower and higher latitudes, confirming their reproducibility and reliability for intra and inter-regional correlations. Geochemistry evidences the presence of the negative C isotopic excursion across the “Fish Level” black shale interval expression of the T-OAE in the Sogno Core. The same anomaly is recorded in the German successions at the base of the Posidonia Shale witnessing the passage from well oxygenated to predominantly anoxic conditions. Our results show that the T-OAE C isotopic excursion recorded in the Sogno Core is excellently constrained by the FO of *Carinolithus superbus* at the onset and the LO of *Mitrolithus jansae* at the end. Moreover, a significant decrease in abundance and size of *Schizosphaerella punctulata* (the so called “*S. punctulata* crisis”) and a *M. jansae* abundance drop further characterise the T-OAE perturbation. Only *S. punctulata* shows a recovery at the end of the T-OAE, while *M. jansae* barely survived the palaeoenvironmental stress and disappeared soon after its termination. The extreme rareness of *S. punctulata* and the absence of *M. jansae* in the Boreal domain prevent the recognition of the “*S. punctulata* crisis” and *M. jansae* decline. Nevertheless, our preliminary study reveals the LOs of *Crepidolithus granulatus* and *Parabdolithus liasicus* together with the FO of *C. superbus* as additional events marking the onset of the C isotopic excursion exclusively in the German cores/sections. Nannofossil biostratigraphy permits the effective dating and correlating of Lower Jurassic major palaeoceanographic events and particularly of the T-OAE which are of a great importance to derive a definitive model for the Posidonia Shale deposition.

Bown P.R., Cooper M.K.E. & Lord A.R. (1988) - A Calcareous Nannofossil Biozonation Scheme for the early to mid-Mesozoic. *Newsl. Stratigr.*, 20, 91-114.

Bown P.R. & Cooper M.K.E. (1998) - Jurassic. In: Bown P.R. (Ed.). *Calcareous nannofossil biostratigraphy*. British Micropaleontol. Soc. Pub. Series: 34-85. Kluwer Academic Publishers, London.

Mattioli E. & Erba E. (1999) - Synthesis of calcareous nannofossil events in Tethyan Lower and Middle Jurassic successions. *Riv. It. Paleontol. Strat.*, 105(3), 343-376.

Biostratigraphic constraints of the Early Toarcian Oceanic Anoxic Event: new data from calcareous nannofossil investigations of Boreal and Tethyan sections.

Stefano Visentin^a, Elisabetta Erba^a, Jörg Mutterlose^b

^a*Dipartimento di Scienze della Terra, Università degli Studi di Milano, Via Mangiagalli 34, 20133 Milano, Italy, e-mail: stefano.visentin@unimi.it, elisabetta.erba@unimi.it*

^b*Institut für Geologie, Mineralogie und Geophysik, Ruhr-Universität Bochum, 44801 Bochum, Germany, e-mail: joerg.mutterlose@rub.de*

Calcareous nannofossil biostratigraphy was carried out in Upper Pliensbachian – Lower Toarcian sediments, which cover the Toarcian Oceanic Anoxic Event (T-OAE) interval. In particular, semiquantitative analyses were performed on a total of 158 samples in the composite Sogno Core (Lombardy Basin, Southern Alps) representing a pelagic Tethyan section whereas quantitative investigations were applied to a total of 168 samples across the Amaltheenton Fm. and Posidonienschiefer Fm., from two cores belonging to the Boreal Realm (Lower Saxony Basin, northern Germany). Primary and secondary events of the Tethyan and Boreal zonations were recognized, allowing the identifications of the NJT5, NJT6 nannofossil Zones for the Sogno Core and the NJ5, NJ6, NJ7 Zones for the German sections, respectively. The sequence of nannofossil biohorizons is generally consistent with data available for various areas at lower and higher latitudes, confirming their reproducibility and reliability for intra and inter-regional correlations. Geochemistry evidences the presence of the negative C isotopic excursion across the “Fish Level” black shale interval expression of the T-OAE in the Sogno Core. The same anomaly is recorded in the German successions at the base of the Posidonia Shale witnessing the passage from well oxygenated to predominantly anoxic conditions.

Our results show that the T-OAE C isotopic excursion recorded in the Sogno Core is excellently constrained by the first occurrence (FO) of *Carinolithus superbus* at the onset and the last occurrence (LO) of *Mitrolithus jansae* at the end. A significant decrease in abundance and size of *Schizosphaerella punctulata* (the “*S. punctulata* crisis”) and an abundance drop of *M. jansae* further characterise the T-OAE perturbation. Only *S. punctulata* shows a recovery at the end of the T-OAE, while *M. jansae* barely survived the palaeoenvironmental stress and disappeared soon after its termination. The extreme rareness of *S. punctulata* and the absence of *M. jansae* in the Boreal Realm prevent the recognition of the “*S. punctulata* crisis” and the *M. jansae* decline. Our study reveals the LO of *Biscutum finchii* together with the FO of *C. superbus* as an additional event approximating the onset of the C isotopic excursion exclusively in the German successions. Further events, such as the LOs of *Biscutum grandis*, *Crepidolithus granulatus* and *Parhabdolithus liasicus* are detected within the C isotopic anomaly exclusively in the German sections. Nannofossil biostratigraphy permits the effective dating and correlating of Lower Jurassic major palaeoceanographic events and particularly of the T-OAE which are of a great importance to derive a definitive model for the Posidonia Shale deposition.

Taxonomic revision of the genus *Carinolithus* (Early–Middle Jurassic) based on morphometric analyses and diagenesis observations: Implications for biostratigraphy and evolutionary trends

Stefano Visentin, Giulia Faucher, Elisabetta Erba

University of Milan, Department of Earth Science, 20133 Milan, Italy; stefano.visentin@unimi.it, giulia.faucher@unimi.it, elisabetta.erba@unimi.it

A total of 100 specimens of the genus *Carinolithus* were selected from published papers and new sampling of sections in the Tethys Ocean (Sogno Core and Breggia sections, Lombardy Basin). The species *C. poulabronei* and *C. cantaluppii* have diagnostic characters that cannot be confused with other those of species and, consequently, were not considered for morphometric analysis. Size measurements were performed for the following parameters: total height, height without proximal and distal shields, stem width (SW), proximal shield width, distal shield width (DS) and thickness of the distal shield (TDS). Only three (DS, TDS and SW) were diagnostic for taxon discrimination. Based on the DS, two groups were distinguished – $>7.8 \mu\text{m}$ and $<6.8 \mu\text{m}$. Two groups were distinguished based on the TDS – $>1.8 \mu\text{m}$ and $<1.5 \mu\text{m}$. Analogously, based on the SW, two groups of specimens were identified – $>1.3 \mu\text{m}$ and $<1.0 \mu\text{m}$.

Our results provide a revised subdivision of *C. superbus* and *C. magharensis* based on a simple, but effective, morphometry that can be seen with a polarising-light microscope. An additional 50 specimens of *C. cantaluppii* were qualitatively investigated to assess the potential role of diagenesis on its morphology. Four pictures were taken for each specimen – with and without a quartz-plate, and at 0° and 45° to the polarisers. All investigated specimens revealed that *C. cantaluppii* is a diagenetic artifact that is produced through different degrees of overgrowth on specimens of *C. poulabronei*, *C. superbus* and *C. magharensis*. Using a quartz-plate at 45° to the polarisers allows: 1) recognition of the species that have undergone the diagenetic modification; and 2) the degree of diagenetic change. This impacts the taxonomy and correct identification of this species, and suggests a method for the evaluation of nanofossil/sediment preservation. The morphometry-based revised taxonomy of the genus *Carinolithus* has the potential for improving the biostratigraphic resolution of the Toarcian–Aalenian interval, and has implications for the reconstruction of evolutionary trends.

Acknowledgements

“Things dealing with science should be written in English, but things dealing with hearth must be written with your native language: in my case, that’s Italian”.

Ed è per questo che mi accingo a ringraziare in italiano tutte quelle persone che hanno contribuito in maniera determinante al mio dottorato.

In primo luogo, ci tengo a ringraziare il mio leader, Elisabetta, per tutto ciò che mi ha insegnato. Oltre al bagaglio scientifico, mi ha trasmesso molto anche a livello umano. Mi ha insegnato quanto è importante procedere con ordine e metodo nel nostro lavoro, ad avere rispetto anche per i più piccoli dettagli e come questi possano influire sul risultato finale. Cosa ancora più grande, è riuscita a comprendere a fondo le mie notevoli energie e dirigerle sempre verso un obiettivo preciso e concreto, riducendone al minimo lo spreco e mantenendo solido il mio entusiasmo. A lei devo veramente molto e sono certo che continuerò a fare tesoro dei suoi insegnamenti anche dopo la fine del dottorato.

Un ringraziamento speciale è rivolto ad Emanuela che mi ha trasmesso il suo sapere sulla tassonomia dei nannofossili del Giurassico. Sempre molto gentile e disponibile, mi ha permesso di trascorrere una piacevolissima esperienza durante il mio soggiorno di tre mesi a Lione.

Allo stesso modo ringrazio Joerg, con cui ho trascorso ben sei mesi a Bochum, donandomi la possibilità di espandere la mia passione campionando e studiando carote del Boreale. L’esperienza fatta in Germania è stata di grande utilità anche per imparare nuove tecniche di analisi e diversi metodi di fare ricerca.

Sono tutt’ora in debito con Giulia, a cui devo ancora una pizza, per avermi sostenuto e fornito suggerimenti durante la stesura del mio primo articolo scientifico, che verrà sottomesso a breve. Un grazie speciale va di dovere anche a Victor che mi ha sempre aiutato e saputo consigliare al meglio, contribuendo a far fiorire la mia passione per la ricerca scientifica.

Ringrazio tutti gli altri miei colleghi di lavoro, tra cui Anna, Francesco, Gaia, Liyenne, Claudia, Matteo, Francesca e Silvia per tutte le bellissime risate fatte in questi anni e le esperienze condivise. Ovviamente, tutto ciò non sarebbe stato possibile senza aver avuto a fianco una fantastica famiglia ed ottimi amici. Quindi ancora una volta, grazie a tutti voi, di cuore.